DESIGN AND SYNTHESIS OF NEW TYPE I BICONTINUOUS CUBIC LYOTROPIC LIQUID CRYSTAL MONOMERS BASED ON THE GEMINI FRAMEWORK FOR MOLECULAR-SIZE SEPARATION APPLICATIONS

By

Brian R. Wiesenauer

B.S., Saginaw Valley State University, University Center, MI, 2007

A thesis submitted to the

Faculty of the Graduate School of the

University of Colorado in partial fulfillment

of the requirements of the degree of

Doctor of Philosophy

Department of Chemistry and Biochemistry

2013

This thesis entitled:

"DESIGN AND SYNTHESIS OF NEW TYPE I BICONTINUOUS CUBIC LYOTROPIC LIQUID CRYSTAL MONOMERS BASED ON THE GEMINI FRAMEWORK FOR MOLECULAR-SIZE SEPARATION APPLICATIONS"

Written by Brian R. Wiesenauer

has been approved for the Department of Chemistry and Biochemistry

_____

Douglas L. Gin, Ph.D.

_____

Wei Zhang, Ph.D.

Date _____

The final copy of this thesis has been examined by the signatories and we find that both the content and the form meet acceptable presentation standards of scholarly work in the above mentioned discipline.

ABSTRACT

Wiesenauer, Brian R.

(Ph.D., Chemistry, Department of Chemistry and Biochemistry)

Design and synthesis of new type I bicontinuous cubic lyotropic liquid crystal monomers based on the gemini framework for molecular-size separation applications

Thesis directed by Prof. Douglas L. Gin

The overall objective of this thesis research was the design and synthesis of new type I bicontinuous cubic (Q_I) phase-forming, gemini-shaped lyotropic liquid crystal (LLC) monomers for the preparation of nanoporous polymer membrane materials. These new Q_I-phase LLC monomers were designed to overcome several shortcomings of previously developed Q_I-phase LLC monomers in the Gin research group that include expensive and difficult synthesis, poor film processibility, and limited blendability with additives. The first method for obtaining this objective was the synthesis of six homologues of a new gemini ammonium LLC monomer, two of which exhibit a Q_I phase with water. Both of these LLCs form a robust Q_I phase such that a gel of these materials can be fully infused into a microporous support membrane and then cross-linked to maintain the LLC phase structure. The resulting Q_I-phase polymer film showed a uniform pore size of 0.86 nm in water nanofiltration and desalination experiments. This Q_I monomer platform is less costly and less rigorous to synthesize than previously synthesized phosphonium-based gemini Q_I LLC monomers. These new LLC monomers also have the ability to blend with the hydrophobic, commercially available cross-linkable elastomer vinyl-EPDM (v-EPDM) to form breathable composite barrier materials. In the appropriate composition, melt-infused gemini ammonium monomer/v-EPDM polymer membranes exhibit extremely high pure

water vapor fluxes, and high rejection of toxic industrial chemical vapors. A new cross-linkable gemini LLC monomer based on charged imidazolium units was also developed that forms a Q_I phase with glycerol. This new LLC monomer can be solution-cast from MeOH and UV-irradiated to form cross-linked thin-film composite Q_I membranes with slightly larger effective pore size (0.96 nm) than the previous systems. A related goal of this thesis research was to develop methods for systematically tuning the effective pore size of nanoporous Q_I polymer-based materials by using glycerol-based LLC monomer/monomer blends. While a number of these LLC monomer/monomer blends exhibited potential Q_I phases in glycerol, the Q_I LLC phases formed were only relatively stable in the bulk state. Unfortunately, attempts to cross-link these Q_I phase monomer/monomer blends resulted in a small degree of phase disruption and phase separation.

ACKNOWLEDGMENTS

The thesis was put together as a collaborative work between some wonderful researchers, lab mates, and friends. I want to first and foremost thank Professor Douglas Gin. His guidance, tutelage, expertise, and confidence in me as a researcher are the reasons I am at this point in my career. I would be remiss if I did not sincerely thank Professor Richard Noble for all of his knowledge and advice along the way.

I would like to thank Dr. Brian J. Elliott and Vinh Nguyen at TDA Research, Inc. for all of their assistance with finishing up this work. Their experimental knowledge and know-how were invaluable to me throughout my thesis research. Thanks to Curt Theriault at The Dow Chemical Company for suggesting I look into CU for graduate school, and for being a great friend and mentor throughout the years.

I must thank the Gin group members that were there for me through thick and thin and enhanced my experiences at CU. I am indebted to Evan Hatakeyama, Jason Bara, Chris Gabriel, and Rob Kerr for mentoring me when I came into the group and had little idea what was in store for me. I need to give a very special thank you to Blaine Carter, whose engineering expertise and membrane fabrication abilities were crucial to my thesis coming together the way it has. I want to thank my hard-working undergraduate research assistant, Erik Wislinsky. I owe all of you a ton. I also want to thank former lab mates like Andy LaFrate, Sean Crawford, Julian Edwards, Nate Urban, Bret Voss, Phuc Tien Nguyen, Lee Miller, and Andrew Allen for their support. I would like to thank current members of the Gin group like Maggie Reynolds, Josh Sloan, Zhangxing Shi, Rhia Martin, Lily Robertson, Will McDanel, Matt Cowan, and Trevor

Carlisle for being a sounding-board for research ideas and providing constructive criticism when I needed it.

On a personal note, I would like to thank the people that kept me sane throughout the process. Thanks to Kyle Schnitzenbaumer, Tao Gong, Jon Langberg, Tim Rochelle, and Mark Moran for the Monday Poker Nights that were greatly needed. I want to thank my parents for their love and support throughout my extended educational experiences. You guys were always just a phone call away, and I can't tell you how important that was to me. Lastly, I want to thank my beautiful wife Erin for everything. I could not have done it without your love and encouragement throughout the years.

Thank you.

TABLE OF CONTENTS

CHAPTER PAGE

LIST OF TABLES

TABLE **PAGE**

LIST OF FIGURES

FIGURE **PAGE**

LIST OF EQUATIONS

CHAPTER 1

Introduction

Nanoporous polymer materials based on self-organized, bicontinuous cubic lyotropic liquid crystal assemblies and their applications

(Manuscript published under the same title in *Polymer Journal* **2012**, *44*, 461–468, co-authored with Gin, D. L.)

Abstract

The bicontinuous cubic (Q) lyotropic liquid crystal (LLC) phases formed by the phase-separation and self-organization of amphiphilic molecules in water are intriguing structures for a number of transport-related applications because they possess ordered, uniform, 3D-interconnected water channels on the size of single molecules. Polymeric materials formed from either the templated polymerization or cross-linking of conventional monomers around Q phases, or the direct polymerization or cross-linking of Q phases formed by reactive amphiphiles retain the desired LLC nanostructure but are more robust for true application development. The structures of Q LLC phases were only elucidated in the late 1980s, and the first successful preparation of polymers based on Q phases was reported soon after. However, the development and demonstration of these nanoporous polymers for material applications were not realized until the first decade of the twenty-first century. This focus review provides an overview of work in the area of Q LLC phase-based polymer materials, with a focus on the work of our research group and that of our collaborators on polymer networks prepared by the direct polymerization

of reactive Q phases and their development as functional materials for several engineering applications.

1.1 Introduction

Lyotropic liquid crystals (LLCs) are amphiphilic molecules typically composed of a hydrophilic headgroup section and a hydrophobic tail section that have the ability to phase-separate and self-organize into nanostructured assemblies in the presence of water. The resulting fluid, ordered LLC phases have varying degrees of average order, different levels of hydrophilic and hydrophobic domain interconnectivity, and uniform periodic features in the circa 1–10 nm size range (For general reviews on LLC phases and their classifications, see: refs 1–3). LLC phases have recently attracted a great deal of attention because of their benefits as a versatile platform for the design of functional, nanoporous polymer materials. For example, by employing reactive LLCs (that is, monomers), the desired phase can be locked-in directly via chemical cross-linking to afford robust, nanoporous polymer networks (For reviews on the synthesis and applications of nanostructured polymers made from polymerizable LLCs, see: refs 4–6). LLC networks made by this approach have been used for applications such as templated nanocomposite synthesis, drug delivery, molecular transport/separation and heterogeneous catalysis.[7,8] Alternatively, non-polymerizable LLC phases have been used as nanostructured templates for the polymerization of conventional monomers dissolved in either the hydrophilic or hydrophobic domains. Subsequent extraction of the LLC components affords nanoporous polymer ‘replicas’ of the original LLC phases that can also be used for a number of material applications.[9]

In both approaches, much of the utility stems from the ability to vary the LLC phase over a wide range of architectures via amphiphile design and composition control.[1–3] (For overviews of how amphiphile shape/packing and system composition can determine the type of LLC phase formed, see: refs 10,11). These architectures range from ordered, 1D-hexagonal (H) and 2D-lamellar (L) phases to 3D-bicontinuous cubic (Q) phases with ordered, interconnected pores in all directions (Figure 1.1).[1–3] Within each of these LLC phase designations are more specific classifications (Type I or II) that relate to the mean curvature of the hydrophobic/hydrophilic interface. Type I (that is, normal) phases curve around the hydrophobic domains and Type II (that is, inverted) phases curve around the aqueous domains, with the L phase (zero mean curvature) serving as the central point of an ideal LLC phase progression. Consequently, Type I and II LLC phases of the same geometry can be considered reflections across the L phase and 'inside-out' with respect to one another. Q phases exist between the low-curvature L and the high-curvature H phases, and are also classified as Type I or II (For a review on bicontinuous Q LLC phases, see: ref. 12). Q phases are deemed bicontinuous because they consist of two non-

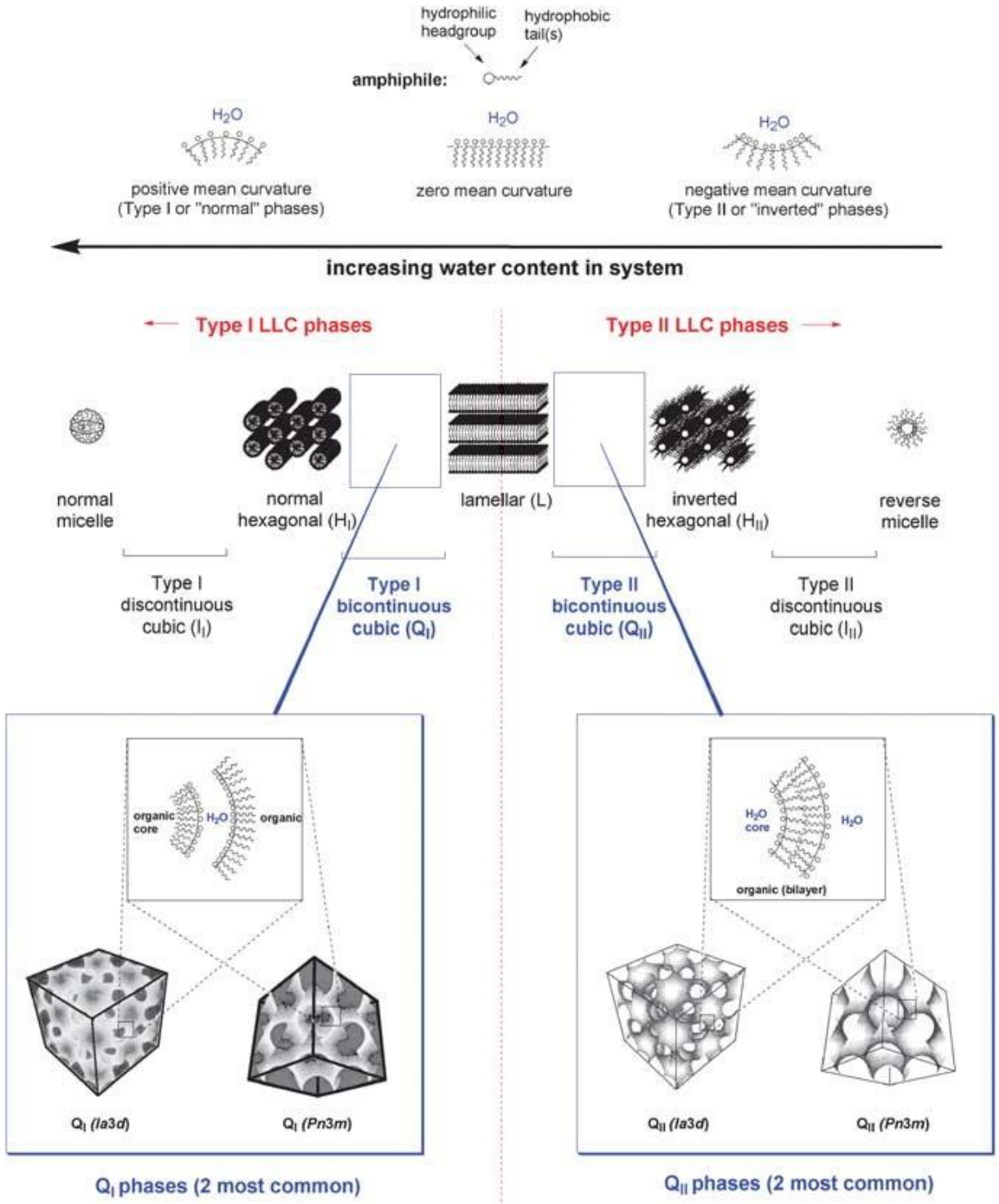

Figure 1.1. Schematic representations of the LLC phases formed by amphiphiles in water in an ideal phase progression, with a focus on the Type I and II Q phases. In the Q-phase representations, the gray/shaded areas represent the hydrophobic domains formed by the tails of the amphiphiles, and the open/white areas represent the water domains. Partially reproduced from ref. 34 with permission. Copyright (2003) American Chemical Society.

connected but intertwined hydrophobic and hydrophilic regimes that exist with overall Q symmetry.[12] There are believed to be six different Q-phase geometries possible from X-ray diffraction studies,[13] with the *Ia*3*d* and *Pn*3*m* architectures (Figure 1.1) being the most common.

Polymeric materials derived from LLC phases provide several distinct benefits for material applications. The ordered, open nanochannels can provide directionality for enhanced molecular transport or for molecular size discrimination. In addition, they can also provide confinement and access to interior reactive sites for catalysis. However, creating robust, polymer materials via LLC assemblies in an efficient manner can be problematic. In the direct polymerization approach, the LLC monomers must be connected quickly before disruption of the desired phase occurs, as the degree of entropy of the initial monomeric LLC phase (at equilibrium) drastically changes upon polymerization. Likewise, the LLC phase-templated polymerization of included monomers requires rapid polymerization to retain the desired phase. This latter approach is more forgiving because the non-LLC monomers being polymerized are not bonded to the amphiphiles making up the LLC phase template, thereby allowing the entropy decrease upon polymerization to have less impact on the 'decoupled' LLC phase. Nanoporous polymers have also been synthesized via the selective domain etching of stabilized phase separated block copolymers or via templated monomer polymerization in the domains of these copolymer assemblies (For examples of nanoporous polymers formed by phase-separated block copolymer nanostructures, see: refs 14,15). However, the materials derived from block copolymer nanostructures have much larger pores (10–50nm).

The Q phases (Figure 1.1) are a particularly intriguing subset of LLC phases that are highly desirable for nanomaterial applications because they can assuage some of the issues that lower-

dimensionality LLC phases have with respect to internal access and transport. The interpenetrating water channels within the Q phases provide better access to interior reactive sites compared with H and L phases, which is important for catalysis and drug-delivery applications. The interconnectivity of the Q-phase nanopores also affords a pore system that is difficult to completely block. Finally, the 3D-interconnected nature of the nanopores alleviates the need for bulk alignment of the material to obtain high throughput for transport applications. These features make polymers based on Q phases much more amenable to transport and membrane applications. The only drawback to Q-phase polymers is that travel through the pores is more tortuous for molecular transport applications.

Surprisingly, although Q phases have been recognized to exist for many decades, their detailed structures were only postulated and confirmed experimentally within the last 25 years.[13] Despite the attractiveness and potential benefits of Q LLC phase-based polymers for engineering applications, these materials have only been realized within the last circa 20 years. Moreover, the material properties and performance benefits of Q-phase polymers have only been demonstrated within the last 10 years. In this 'focus review', we provide an overview of work in the area of Q LLC phase-based nanoporous polymer materials, with a specific focus on the work of our group and that of our collaborators in the direct polymerization of Q-phase assemblies and their development for specific applications.

1.2. History of Q-phase materials

1.2.1. Nanoporous polymer materials via template polymerization of non-LLC monomers in Q-phase assemblies

In 1991, Anderson and Ström were the first researchers to demonstrate that nanoporous polymers based on Q LLC phases could be formed. They showed that methyl methacrylate can be radically polymerized within the organic regions of a Q_{II} (*Pn*3*m*) phase based on a didodecyldimethylammonium bromide/decane mixture, in order to form a polymeric replica of the initial LLC phase.[16,17] They proposed that the resulting Q_{II}-phase polymer replicas may be useful for applications such as bioseparations or use as soft-tissue substitutes, burn dressing, suture coatings, and drug-delivery patches.[17]

Another reported attempt at Q-phase-templated polymerization involved the polymerization of the reactive organic anions (for example, acrylates) of pre-formed H- and Q-phase LLC systems formed by modified dodecylammonium surfactants.[18] In this work, Hartmann and Sanderson observed that the polyacrylate and polymethacrylate formed from the templated Q phases changed into the L phase following polymerization, implying that a change in the packing parameter of the surfactant upon oligomer formation early in the polymerization can lead to LLC phase disruption.

In the past decade, much of the work in Q-phase-templated polymerization of conventional monomers has been performed by Guymon and co-workers. One of their primary goals was to investigate the effects of LLC-phase order on the photopolymerization kinetics of incorporated conventional monomers. In 2001, they demonstrated that upon photopolymerization of acrylamide within a template Q_{II}-phase architecture of the commercial non-ionic surfactant Brij 58 (Figure 1.2) and water, the polymerization rate doubled compared with a micelle-templated

system, and a 10-fold increase was observed over the original isotropic homogeneous mixture.[19] These results were replicated 2 years later with Brij 56 surfactant system (Figure 1.2).[20] It was

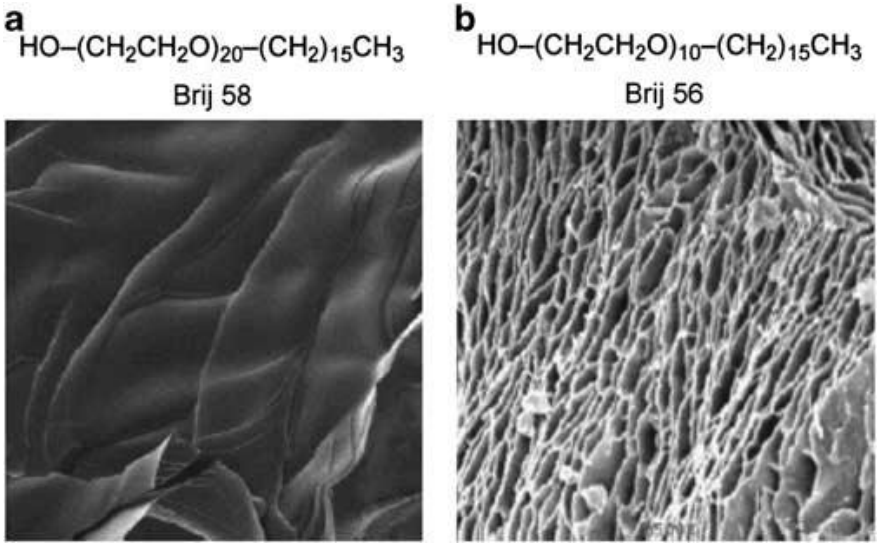

Figure 1.2. Structures of the surfactants used for Q_{II}-phase-templated polymerization of conventional monomers by Guymon and co-workers, along with SEM images of the polyacrylamide formed in their (a) isotropic Brij 56, and (b) Q_{II}-phase Brij 56 mixtures. Partially reproduced from ref. 22 with permission. Copyright (2006) American Chemical Society.

theorized that such LLC phase-templated polymerizations could lead to enhanced polymer-based separation materials. Related work performed by the Guymon group[21–23] has centered around determining to what extent polymerization conditions and LLC phase architecture influence the nanostructure and the physical properties of the templated linear polymers and cross-linked hydrogels formed by different included monomers. In general, they found that the polymerization rate in the Q-phase-templated systems,[22] as well as the mechanical strength and diffusive transport properties of the resulting polymers,[23] were significantly higher than those in corresponding isotropic, homogeneous surfactant/water mixtures. These Q_{II}-templated polymers were proposed to be useful for fabrication of advanced hydrogel materials and synthetic biomaterials, but these applications have not been realized yet.

1.2.2. Nanoporous polymer materials via the direct polymerization or cross-linking of reactive Q-phase materials

Although polymers fabricated via templated polymerization of monomers within Q phases present intriguing properties, nanoporous polymers prepared via the direct polymerization or cross-linking of reactive Q phases have been highly sought-after because they have several unique features. Compared with templated polymer replicas, one of the advantages of directly polymerized or cross-linked Q phases is that the hydrophilic headgroups of the LLC monomers are all localized in the walls of the water channels. This feature allows for better control over nanopore environment and incorporation of specific functional groups in the pores if they are present in the LLC monomers. Unfortunately, one of the biggest challenges in this approach is the design of Q-phase-forming monomers that can be rapidly polymerized with retention of the phase structure. Because Q phases are considered saddle points between L and H phases,[1,12] LLC shape- and packing parameter-based approaches[10,11] have not been very reliable in designing amphiphiles that predictably form Q phases. The most successful approaches to designing Q-phase LLC monomers have been (1) preparing reactive variants of non-polymerizable surfactants known to form Q phases, and (2) using mixtures of LLC monomers and temperature variations to fine-tune system curvature and interfacial energy. Only a very limited number of LLC monomer platforms have been designed that reliably form Q phases.

Pioneering work in the synthesis of directly polymerizable Q phases was performed by O'Brien and co-workers in 1995.[24] They developed the first example of an LLC monomer system (**1a**+**1b**) that could assemble into Q_{II} phases and then be polymerized with retention of the desired nanostructures (Figure 1.3). Monomers **1a** and **1b** were synthesized from natural phospholipids and cross-linked by thermally-initiated radical polymerization.[24] Unfortunately,

this monomer design approach required small-scale, elaborate syntheses and expensive starting materials.[24] Subsequent work resulted in two glycerol-based Q_{II}-phase LLC monomer systems (**2a**+**2b**) and **2c** (Figure 1.3) that are more economical and easier to produce in larger quantities than **1a** and **1b**.[25–27] However, as for (**1a**+**1b**), careful blending of **2a** and **2b** is required to obtain

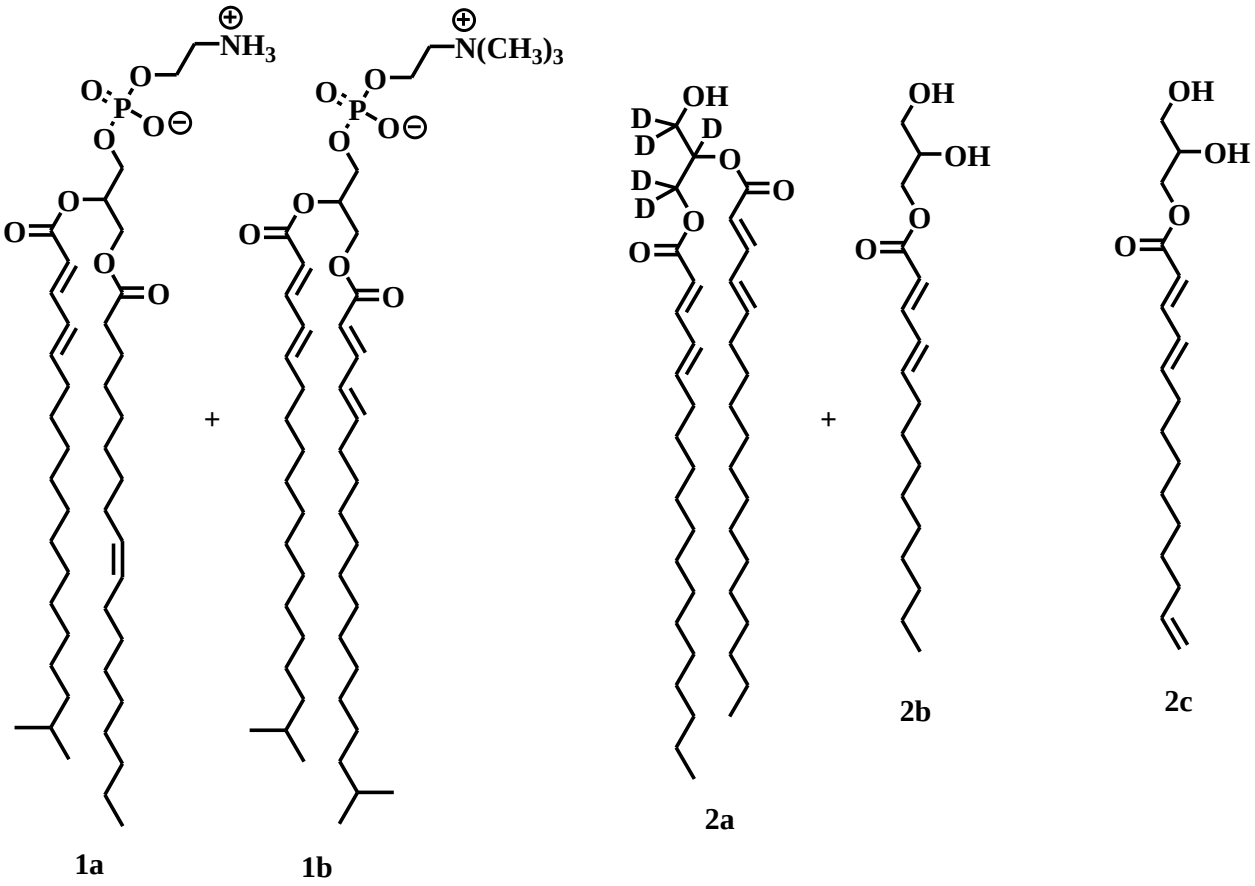

Figure 1.3. Structures of LLC monomer systems designed and used by O'Brien and co-workers that form Q_{II} phases in water.

the desired Q_{II} phases. Monomer **2c** can form a Q_{II} phase without co-monomers and is intrinsically cross-linkable, but the doubly-reactive single tail is synthetically complex to produce.[25] These papers, as well as other papers by O'Brien and co-workers on these polymerizable Q_{II}-phase systems,[28–31] focused mostly on fundamental studies of chain-addition polymerization in Q phases. They also studied the diffusion of dendrimers in the water channels

of the cross-linked Q_{II}-phase mixed-lipid systems and found that it was sufficiently rapid for the materials to be potentially useful for controlled release applications of encapsulated large drugs and macromolecules.[32]

1.3. Design and development of directly cross-linked Q-phase LLC assemblies as functional polymer materials for engineering applications

Over the last 10 years, the Gin group has performed extensive work on the design and synthesis of directly cross-linkable Q-phase LLC assemblies. With the aid of collaborators, we have also demonstrated that the resulting nanoporous polymers can be employed in a number of transport-related applications with performance benefits. The distinguishing features of most of this work are the use of 'gemini' LLC monomer platforms and the formation and cross-linking of Q_I LLC phases. The gemini surfactant platform consists of two hydrophilic headgroups tethered by a spacer, and attached to each headgroup unit is a flexible hydrophobic tail. In terms of surfactant behavior, gemini amphiphiles are theorized to have lower critical micelle concentrations, and therefore, a wider range of more attainable phase-separated architectures.[33] In terms of monomer design, this motif allows for two chain-polymerizable tails to be placed within the same monomer unit (that is, intrinsically cross-linkable), thereby allowing rapid formation of robust networks at fairly low degrees of conversion without the need for added cross-linkers. These LLC monomers (monomer platforms **3** and **4**) and the resulting cross-linked

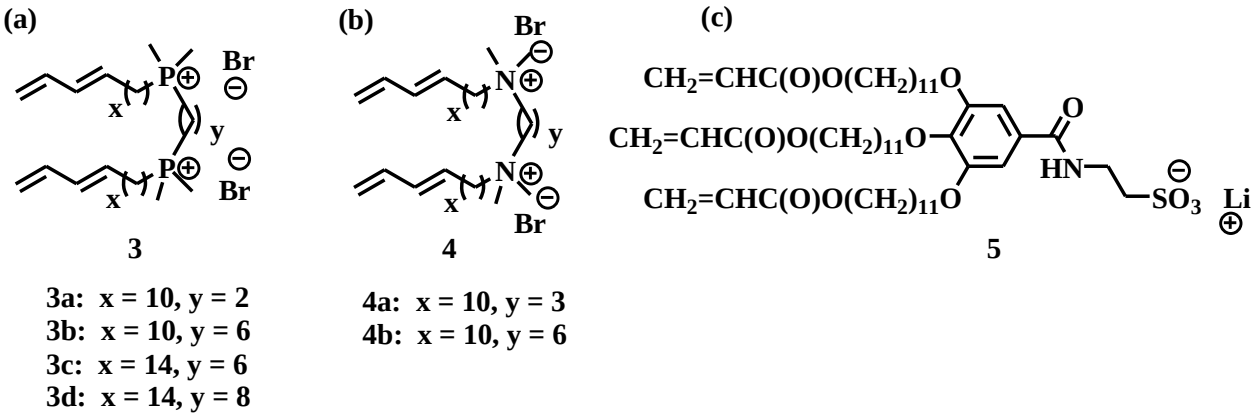

Figure 1.4. Structures of LLC monomers developed by the Gin group that form and can be cross-linked in Q phases: (a) gemini phosphonium monomers **3a–d** that form Q_I phases in water, (b) gemini ammonium monomers **4a** and **4b** that form Q_I phases in water, and (c) taper-shaped Li-sulfonate salt monomer **5** that forms a Q_{II} phase in propylene carbonate (PC).

polymers set themselves apart from the host of Q-phase monomers and polymers previously reported because of their ability to form Q_I phases rather than the more common Q_{II} phases. The Gin group also developed a new subclass of cross-linkable LLC monomers (**5**) that forms Q_{II} phases in non-aqueous polar solvents and can be cross-linked with retention of the phase structure. The structures of these LLC monomers are all shown in Figure 1.4. Initial work in the area of Q_I-phase-forming gemini LLC monomers was performed by Pindzola et al.[34] It was the first example of a cross-linkable, Q_I-phase LLC system. In this work, a series of nine different gemini phosphonium monomers with alkyl-1,3-diene tails were synthesized and their LLC phase behavior with water was examined. Of the nine homologous monomers synthesized, eight were found to exhibit diverse LLC-phase behavior with water, and four of them (**3a–d**) displayed a Q_I phase in water somewhere between 55 and 90 wt% monomer over a range of temperatures. They also were able to retain their Q_I nanostructure after photo-initiated radical cross-linking, as confirmed by both polarized light microscopy and powder X-ray diffraction.[34] No applications were initially proposed for these rather exotic materials.

The first application explored for these polymers was their use as a selectively permeable membrane material that allows water vapor transport but blocks the passage of chemical warfare agent (CWA) simulants in the vapor phase.[35] The impetus for this work was to develop a new type of protective garment material for military personnel and first-responders that allows water vapor 'breathability' for effective personal cooling while completely blocking toxic CWAs (For a review of CWAs and their chemistry, see: ref. 36). Currently, only a very limited number of examples of 'breathable' CWA barrier materials are known. Most economical CWA barrier materials are based on dense polymers, such as crosslinked butyl rubber (BR), that block the passage of all vapors (For a recent review of CWA- and biological warfare agent-protective garment materials and needs, see: ref. 37). The lack of water-vapor breathability can quickly lead to heat exhaustion for the wearer. The Gin group and collaborators believed that a Q_I-phase LLC polymer-BR blend with hydrophilic nanopores would allow good water-vapor transport while being able to size-reject larger, more hydrophobic CWA molecules and related molecules (Figure 1.5).

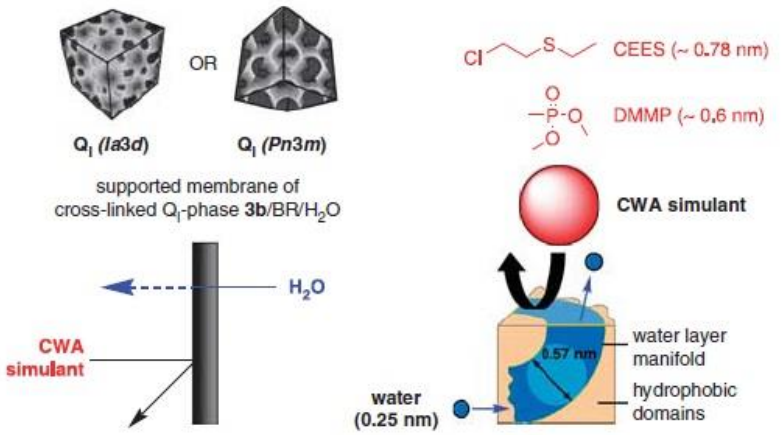

Figure 1.5. Schematic representation of selective 2-chloroethyl ethyl sulfide and DMMP vapor rejection and water-vapor transport through a supported, Q_I-phase, cross-linked **3b**/BR/H_2O composite membrane.

Lu et al.[35] found that when monomer **3b** was blended with commercial-grade BR in the presence of water, a surprisingly broad Q_I-phase region was observed at 65 °C in a **3b**/BR/H_2O-phase diagram. In order to test the water vs. CWA vapor-permeation selectivity of this LLC-BR composite material, a method was developed for making melt-infused, supported Q_I-phase membrane films of photo-cross-linked **3b**/BR/H_2O on a 25–30-mm thick microporous polymer support. In cross-flow vapor transport studies, these supported membranes exhibited a substantial thickness-normalized water-vapor flux of (5.9 ± 0.3) x 10^3 g m^{-2} day^{-1} μm.[35] Thus for a 4-mm thick film of this material, the water-vapor flux exceeds the generally accepted military breathability requirement of 1500 gm^{-2} day^{-1}, and is almost 300 times more permeable to water vapor than pure, vulcanized BR on the same support material. In contrast, the thickness-normalized vapor flux of 2-chloroethyl ethyl sulfide, a sulfur mustard (that is, blister agent) CWA simulant, through this material was observed to be (2.86 ± 0.05) x 10^2 g m^{-2} day^{-1} μm. These permeation values represent a vapor molar selectivity for H_2O/2-chloroethyl ethyl sulfide of 150, which is 500 times higher than the H_2O/2-chloroethyl ethyl sulfide selectivity seen through pure, vulcanized BR on the same support.[35]

This same Q_I-phase cross-linked **3b**/BR/H_2O polymer material was later examined as a breathable barrier for protection against nerve agent CWAs (that is, highly toxic, reactive organophosphorus esters that disrupt neurochemical pathways and cause the loss of autonomic functions[36]).[38] Using dimethyl methylphosphonate (DMMP) as a nerve agent simulant, it was found that the cross-linked, Q_I-phase **3b**/BR/H_2O composite worked extraordinarily well for the rejection of DMMP while maintaining high water-vapor breathability. This barrier membrane rejected 99.91% of the DMMP vapor while allowing a thickness-normalized water vapor

permeability of circa 5900 $gm^{-2}day^{-1}$ μm, giving a H_2O/DMMP molar selectivity of 1600.[38] Because DMMP is very water soluble, the mechanism for rejection of DMMP through the Q_I-phase composite cannot occur by solubility-based rejection from the water pores, but rather must proceed by a molecular size-exclusion mechanism via the nanopores. From estimates of DMMP molecular size and its observed percent rejection, it was inferred that this cross-linked Q_I-phase LLC-BR membrane has an effective water nanopore size of circa 0.57 nm (Figure 1.5).[38] As discussed in the following sections, separate liquid phase molecular-sieving filtration studies on the cross-linked Q_I-phase of **3b**/H_2O revealed that it has a uniform, effective water nanopore size of circa 0.75 nm, thereby corroborating a molecular-sieving mechanism for the selective CWA vapor rejections.

The Q_I phase of **3b**/H_2O (no BR) has also been extensively studied as a platform for synthesizing a new type of liquid water-desalination and purification membrane. Current water-purification membranes are either dense, reverse osmosis (RO) polymer membranes with circa 0.5 nm inter-chain voids that completely size-exclude larger hydrated salt ions or dissolved molecules from water molecules (0.25 nm) (For an overview of RO membranes, see: ref. 39), or nanoporous nanofiltration (NF) membranes that have non-uniform pores on the 1–10 nm scale (For a recent review on NF membranes, see: ref. 40). The lack of selectivity control in the former type of membrane and the compromises in molecular selectivity in the latter type of membrane mean that there is room for improvement. Polymers with uniform, interconnected molecular-size pores, such as those in Q-phase LLC networks, may be able to function as molecular-sieving membranes that have most of the capabilities of RO and NF membranes but none of their liabilities. To this end, water NF and desalination studies on the cross-linked Q_I phase of **3b**/H_2O were first examined in the Gin group by Zhou et al.[41] In this study, **3b** was found to form a Q_I

phase with water at ratios between 80 and 90 wt% monomer and temperatures up to 85 °C. Supported, 35–40-mm thick, Q_I-phase membranes of cross-linked **3b**/H_2O were prepared by heating and pressing the initial monomer mixture into a hydrophilic, microporous support and then photo-cross-linking the Q_I phase in place. Dead-end water NF and desalination studies (400 psi pressure, 2000 p.p.m aq. feed solutions) showed that the resulting supported Q_I-phase polymer membranes can almost completely (95 to 99.9%) reject dissolved salt ions and neutral

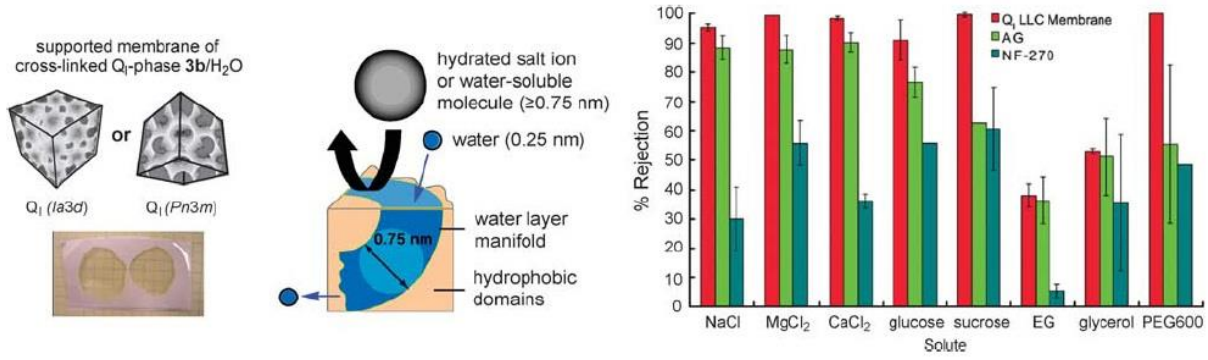

Figure 1.6. Mechanism of water NF/desalination through a supported Q_I- phase of cross-linked **3b**/H_2O and comparison of its solute rejection vs. those of two commercial RO and NF membranes. Partially reproduced from ref. 41 with permission. Copyright (2007) American Chemical Society.

molecules in the 0.7–1.2-nm size range in one pass. They exhibited solute rejections comparable to a commercial RO membrane (AG membrane produced by the General Electric Company) and better than a commercial NF membrane (NF-270 membrane produced by the Dow Chemical Company) (Figure 1.6).[41] From the rejection performance of different-size neutral solutes, the effective 'pore' or water layer gap size of the cross-linked Q_I phase of **3b**/H_2O was calculated to be 0.75 nm using a modified Ferry equation model.[41] The thickness-normalized water permeability of these Q_I membranes was found to be similar to that reported for the active layer of commercial RO membranes. Having high solute rejections, as well as permeation performance

comparable to that of a commercial RO membrane, means that this nanoporous Q_I-phase polymer shows promise as a new type of water purification membrane.

More detail on the nanopore size and water NF performance of this material was further elucidated by Hatakeyama et al.[42] in 2011 via more extensive water filtration studies using a wider range of test solutes, a more appropriate pore model, static aqueous chlorine and protein fouling analysis, and comparisons against other commercial RO membranes. Membrane preparation for these more extensive experiments was the same as previously described, but a new set of small, non-charged organic molecules and more environmentally-relevant inorganic salts (including borates and arsenates) were used in the rejection studies. Two different Donnan-steric pore models were used to estimate the pore radius based on rejection values for this new set of solutes. The initial Ferry equation pore model adapted to this work was based on a lateral ensemble of uniform cylinders, whereas the new pore model was based on uniform, straight slit pores that more closely resembles the annulus channels of the Q_I phase but without the curvature. Results from these more detailed studies provided support that this Q_I-phase polymer membrane material has uniform-size nanopores and a water NF performance that is slightly below that of commercial RO membranes but substantially better than that of current NF membranes.[42] This phosphonium-based Q_I-phase polymer was also found to be tolerant to aq. ClO^- and fairly resistant to nonspecific protein adsorption, making it an intriguing candidate as a new type of chlorine- and protein-resistant water filtration membrane material.

One more research goal pursued by the Gin group in the gemini LLC monomer area was the development of cheaper, more easily synthesized Q_I-phase-forming LLC monomers for polymer membrane applications. Gemini phosphonium monomer **3b** worked exceptionally for its desired applications, however, there were several drawbacks to this initial monomer system, one being

the rigorousness of the synthesis and the other was the cost of synthesis. The synthesis of **3b** requires expensive phosphorus-based reagents and involves pyrophoric intermediates, as well as a Na metal/liquid NH_3-reduction step, thus limiting it to small-scale laboratory preparations. The cost for starting materials alone (excluding solvents and chromatographic supplies) is also upwards of $79/g.[43] Consequently, **3b** is not viable for scale-up or potential industrial production, and only serves as a proof-of-concept prototype. These problems need to be solved if a Q_I-phase monomer system is to be scalable, easily modifiable and potentially commercially viable. Recent work by Hatakeyama et al.[43] resulted in the successful development of a new ammonium-based gemini LLC monomer platform **4** (Figure 1.4b) that is significantly cheaper, easier to synthesize and more scalable compared with phosphonium platform **3**. The synthesis of these gemini ammonium monomers is much simpler, involves non-air-sensitive intermediates and reagents, and relies on commercially available, inexpensive tetramethyl alkylamines to form the cationic gemini headgroup. A set of six homologs were generated, and two of them, **4a** and **4b** (Figure 1.4b), were found to form Q_I phases with water above 55 °C. Dead-end water NF studies on supported, melt-infused, Q_I-phase membranes made from cross-linked **4a**/H_2O showed that they also afford high salt and organic solute rejections. From the rejection data, it was calculated that the effective pore size of this material is 0.86 nm.[43] The cost to synthesize **4a** in terms of starting materials and reagents is roughly $13/g,[43] which is a significant cost reduction compared with **3b**, and with only a slight penalty in membrane performance. This new gemini monomer system represents a promising new design for Q_I-phase monomers.

One other piece of Q-phase polymer research that has come out of the Gin group is the synthesis of a new type of LLC monomer (**5**) that forms a Q_{II} phase with a Li salt-doped organic liquid electrolyte, propylene carbonate.[44] It has been shown that nanostructured LC-based ionic

materials can be used to enhance and even direct ion conductivity for potential device applications (For a recent review of LC-based ion-conducting materials, see: ref. 45). Monomer **5** is a taper-shaped molecule containing three long acrylate tails at one end and a hydrophilic lithium sulfonate ionic headgroup at the other (Figure 1.4c). After photo-initiated radical cross-linking, the resulting flexible Q_{II}-phase network contains 3D-interconnected, liquid propylene carbonate/Li salt nanochannels for enhanced Li^+ conductivity, allowing it to function as a new type of separator membrane for Li batteries. Room-temperature ion conductivities measured for freestanding Q_{II}-phase films of cross-linked **5** containing 15 wt% (0.245M $LiClO_4$ in propylene carbonate) were (9 ± 4) x 10^{-3} S cm^{-1}, as determined by AC impedance studies.[44] Control experiments showed that the $LiClO_4$ dopant was necessary to provide adequate room-temperature Li^+ conductivity. An interesting observation is that this material displays significant liquid-like mobility in the nanochannels even at low temperatures. It only loses an order of magnitude of ion conductivity when cooled from room temperature to -65 °C (Figure 1.7)

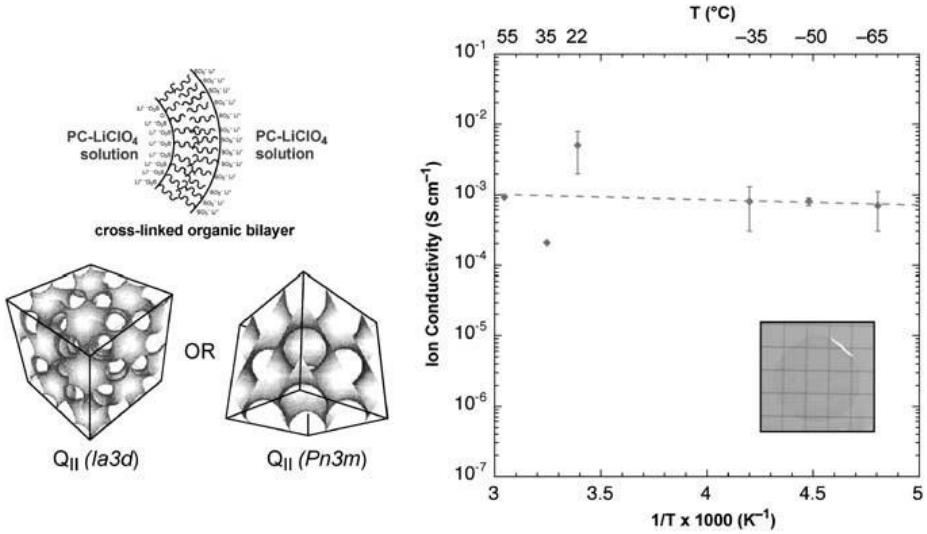

Figure 1.7. Structure of a cross-linked Q_{II} phase of **5** containing 15 wt% (0.245M $LiClO_4$ in PC) and its ion conductivity performance as a function of temperature. Partially reproduced from ref. 44 with permission. Copyright (2009) American Chemical Society. A full color version of this figure is available at *Polymer Journal* online.

leading to the possibility of good Li battery performance even at very low temperatures. This relatively 'flat' ion conductivity with decreasing temperature is very rare in conventional polymer and gelled-polymer electrolytes but is highly desired for low-temperature Li battery operation. Optimization of these new polymer/liquid electrolyte composites and demonstration of their effectiveness in working Li-metal batteries are in progress. Recently, cross-linked bicontinuous cubic Li^+-conducting materials based on thermotropic (that is, solvent-free) LC monomers have been developed by researchers in Japan as a complementary approach to the use of polymerizable Q-phase LLC assemblies.[46]

1.4. Summary

Robust, nanoporous polymer materials with 3D-interconnected, molecular-size pores can be formed via the direct cross-linking of Q phases formed by reactive LLCs or via the templated polymerization of conventional monomers included in Q phases. These materials have exceptional potential for use in a number of transport applications. Our research group has primarily focused on the design of gemini LLC monomers to form directly cross-linked Q_I-phases with sub-1-nm pores as a new material-development direction. We have shown that these new Q_I-phase networks can be used for a wide array of membrane-based molecular-sieving applications, including water NF, desalination, and selective vapor transport. We have also made initial inroads into the design of LLC monomers that can form Q_{II} phases with non-aqueous polar organic solvents instead of water as the LLC solvent. Li salt-doped versions of these latter Q_{II}-phase polymer/liquid nanocomposites show enhanced ion conductivity properties, making them potentially useful for better-performing Li batteries. Current research directions in our group include developing methods for controlling the effective size of the nanopores in these Q-phase

polymer materials and developing processing techniques for fabricating high-quality, thin (~5-μm thick) films of the Q-phase monomer mixtures to make superior, high-throughput membranes.

1.5. References

1. Tate, M. W., Eikenberry, E. F., Turner, D. C., Shyamsunder, E.; Gruner, S. M. *Chem. Phys. Lipids* **1991,** *57*, 147.

2. Seddon, J. M. *Biochim. Biophys. Acta* **1990**, *1031*, 1.

3. Tiddy, G. J. T. *Phys. Rep.* **1980**, *57*, 1.

4. Gin, D. L., Gu, W., Pindzola, B. P.; Zhou, W. J. *Acc. Chem. Res.* **2001**, *34*, 973.

5. Miller, S. A., Ding, J. H.; Gin, D. L. *Curr. Opin. Colloid Interface Sci.* **1999**, *4*, 338.

6. Mueller, A.; O'Brien, D. F. *Chem. Rev.* **2002**, *102*, 727.

7. Gin, D. L., Pecinovsky, C. S., Bara, J. E.; Kerr, R. L. *Struct. Bonding* **2008**, *128*, 181.

8. Gin, D. L., Lu, X., Nemade, P. R., Pecinovsky, C. S., Xu, Y.; Zhou, M. *Adv. Funct. Mater.* **2006**, *16*, 865.

9. Hentze, H. P.; Kaler, E. W. *Curr. Opin. Colloid Interface Sci.* **2003**, *8*, 164.

10. Israelachvili, J. N. *Intermolecular and surface forces* Academic Press: Boston, 1992; pp 291.

11. Israelachvili, J. N., Mitchell, D. J.; Ninham, B. W. *J. Chem. Soc. Faraday Trans. II* **1975**, *72*, 1525.

12. Fontell, K. *Colloid Polym. Sci*. **1990**, *268*, 264.

13. Mariana, P., Luzzati, V.; Delacroix, H. *J. Mol. Biol.* **1988**, *204*, 165.

14. Chen, L., Phillip, W. A., Cussler, E. L.; Hillmyer, M. A. *J. Am. Chem. Soc.* **2007**, *129*, 13786.

15. Ndoni, S., Vigild, M. E.; Berg, R. H. *J. Am. Chem. Soc.* **2003**, *125*, 13366.

16. Anderson, D. M.; Ström, P. in *Polymer Association Structures*. El–Nokaly, M. A., Eds.; ACS Symposium Series 384; American Chemical Society: Washington, DC, 1989, pp 204–224.

17. Anderson, D. M.; Ström, P. *Physica A* **1991**, *176*, 151.

18. Hartmann, P. C.; Sanderson, R. S. *Macromol. Symp*. **2005**, *225*, 229.

19. Lester, C. L, Smith, S. M.; Guymon, C. A. *Macromolecules* **2001**, *34*, 8587.

20. Lester, C. L., Smith, S. M., Jarrett, W. L.; Guymon, C. A. *Langmuir* **2003**, *19*, 9466.

21. Forney, B. S.; Guymon, C. A. *Macromol. Rapid Commun.* **2011**, *32*, 765.

22. DePierro, M. A., Carpenter, K. G.; Guymon, C. A. *Chem. Mater.* **2006**, *18*, 5609.

23. Clapper, J. D.; Guymon, C. A. *Macromolecules* **2007**, *40*, 1101.

24. Lee, Y. S., Yang, J. Z., Sisson, T. M., Frankel, D. A., Gleeson, J. T., Aksay, E., Keller, S. L., Gruner, S. M.; O'Brien, D. F. *J. Am. Chem. Soc*. **1995**, *117*, 5573.

25. Yang, D., O'Brien, D. F.; Marder, S. R. *J. Am. Chem. Soc.* **2002**, *124*, 13388.

26. Srisiri, W., Lamparski, H. G.; O'Brien, D. F. Synthesis of polymerizable monoacylglycerols and 1,2-diacyl-sn-glycerols. *J. Org. Chem.* **1996**, *61*, 5911.

27. Srisiri, W., Benedicto, A.; O'Brien, D. F. *Langmuir* **1998**, *14*, 1921.

28. Sisson, T. M., Srisiri, W.; O'Brien, D. F. *J. Am. Chem. Soc.* **1998**, *120*, 2322.

29. Liu, S.; O'Brien, D. F. *Macromolecules* **1999**, *32*, 5519.

30. Liu, S., Sisson, T. M.; O'Brien, D. F. *Macromolecules* **2001**, *34*, 465.

31. O'Brien, D. F., Armitage, B., Benedicto, A., Bennett, D. E., Lamparski, H. G., Lee, Y.-S., Srisiri, W.; Sisson, T. M. *Acc. Chem. Res.* **1998**, *31*, 861.

32. Jeong, S. W.; O'Brien, D. F. *Langmuir* **2002**, *18*, 1073.

33. Zana, R. Dimeric (gemini) surfactants: *J. Colloid Interface Sci.* **2002**, *248*, 203.

34. Pindzola, B. A., Jin, J.; Gin, D. L. *J. Am. Chem. Soc.* **2003**, *125*, 2940.

35. Lu, X., Nguyen, V., Zhou, M., Zeng, X., Jin, J., Elliott, B. J.; Gin, D. L. *Adv. Mater.* **2006**, *18*, 3294.

36. Talmage, S. S., Watson, A. P., Hauschild, V., Munro, N. B.; King, J. *Curr. Org. Chem.* **2007**, *11*, 285.

37. Schreuder-Gibson, H. L., Truong, Q., Walker, J. E., Owens, J. R., Wander, J. D.; Jones, Jr. W. E. *Mater. Res. Soc. Bull.* **2003**, *28*, 574.

38. Lu, X., Nguyen, V., Zeng, X., Elliott, B. J.; Gin, D. L. *J. Mem. Sci*. **2008**, *318*, 397.

39. Fell, C. J. D. "Reverse Osmosis," *Membrane Separations Technology. Principles and Applications*; Noble, R. D.; Stern, A. S.; Eds.; Elsevier Science: Amsterdam, 1995; Chapter 4.

40. Bhattacharya, A.; Ghosh, P. *Rev. Chem. Eng.* **2004**, *20*, 111.

41. Zhou, M., Nemade, P. R., Lu, X., Zeng, X., Hatakeyama, E. S., Noble, R. D.; Gin, D. L. *J. Am. Chem. Soc.* **2007**, *129*, 9574.

42. Hatakeyama, E. S., Gabriel, C. J., Wiesenauer, B. R., Lohr, J. L., Zhou, M., Noble, R. D.; Gin, D. L. *J. Mem. Sci.* **2011**, *366*, 62.

43. Hatakeyama, E. S., Wiesenauer, B. R., Gabriel, C. J., Noble, R. D.; Gin, D. L. *Chem. Mater.* **2010**, *22*, 4525.

44. Kerr, R. L., Miller, S. A., Shoemaker, R. K., Elliott, B. J.; Gin, D. L. *J. Am. Chem. Soc.* **2009**, *131*, 15972.

45. Kato, T. *Angew. Chem. Int. Ed.* **2010**, *49*, 7847.

46. Ichikawa, T., Yoshio, M., Hamasaki, A., Kagimoto, J., Ohno, H.; Kato, T. *J. Am. Chem. Soc.* **2011**, *133*, 2163.

Chapter 2

Research Goals: Design of new Q_I-phase lyotropic liquid crystal monomers for molecular-size separation membranes

2.1. Introduction

As described in Chapter 1, bicontinuous cubic (Q) lyotropic liquid crystal (LLC) systems are intriguing for materials applications involving molecular-level transport or separation because they have discreet, ordered, uniform nanopores on the size range of ca. 0.7-10 nm. Polymerizable versions of these LLC systems can be fabricated into neat polymer membranes that utilize only the intrinsic properties of the LLC ordered arrays, or blended polymer systems that incorporate the utility of a co-polymer with the directed transport properties of LLC nanostructures. When fabricated into neat membranes or polymer blends, these Q-phase LLC systems have interconnected nanochannels that facilitate molecular transport across the membrane. Production of LLC systems in a cost-effective, systematic fashion is highly desired if they are to be generated at a large scale for any type of commercial application. Despite the interest shown in Q-phase LLC materials, there are many drawbacks that need to be overcome if they are to be developed into a commercially viable and effective new class of transport or separation material.

Previous polymerizable type II bicontinuous cubic (i.e., Q_{II}) phase LLC systems (monomers **1a** and **1b**) developed by the O'Brien research group[1-4] were generated synthetically from rather expensive natural phospholipid starting materials (Figure 2.1). These led to small-scale, elaborate syntheses that were not amenable to large industrial-scale production. Likewise, the first generations of gemini surfactant monomers that form type I bicontinuous cubic (i.e., Q_I) phases in the Gin research group[5-6] provided their own unique set of drawbacks. Monomer **3b**

(Figure 2.1) involved a synthetic route that was complex, expensive, and problematic.[5-6] The first step in the synthesis of **3b** involves a $Na^0/NH_{3(l)}$ reduction, and the second synthetic step affords a pyrophoric diphosphine intermediate, neither of which are amenable to industrial scale-up. In the same vein, the tetramethyldiphosphine disulfide precursor required for the synthesis of **3b** costs ca. $36/g, which is prohibitive when considering larger-scale production. These monomer synthesis hurdles need to be overcome before commercial development can be realized.

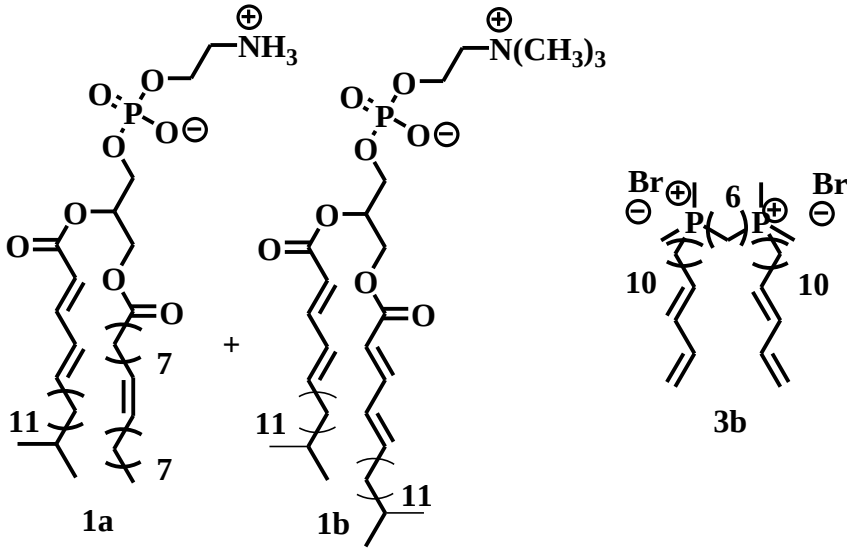

Figure 2.1. Compounds **1a** and **1b** that are synthesized from expensive natural phospholipids. Compounds **3b** is synthesized from a pyrophoric intermediate, as well as very expensive tetramethyldiphosphine disulfide precursor.

In addition to current Q LLC monomer synthesis complexity and cost, another hurdle to the development of these materials for applications is their blendability with other polymers and monomers. As mentioned in Chapter 1, some membrane/barrier material applications involving Q-phase LLC monomer systems involve successfully blending them with other reactive polymers (or monomers) with retention of the Q phase architecture. For example, Q_I-phase LLC

monomer/co-polymer composites are one approach that have been explored to produce the more desirable selectively permeable personal protective garments. The issues that arise when trying to fabricate co-polymer blended LLC membranes stems from (a) finding a commercially available elastomer that can cross-link to your LLC system, (b) finding a system that is highly breathable, (c) finding a co-polymer system that is tolerated by the nanostructure of the desired LLC material, and (d) allows for the dexterity needed for performing sensitive work. We plan to discuss work toward new elastomeric materials for a selectively permeable toxic chemical vapor protective membrane material.

One other consideration in the materials development of Q-phase LLC polymers is their processibility, especially into supported, defect-free thin films containing a very thin (sub-1-μm-thick) active layer with retention of the desired Q phase. The thicker a membrane is fabricated, the more material is wasted and the lower the water flux because thicker films inherently show higher resistance to flow through the material. This thin-film composite (TFC) configuration is necessary because it provides the highest possible water flux, while utilizing the least material and providing the durability and mechanical strength needed for a membrane that will be subjected to high filtration pressures. State-of-the-art commercial technology provides TFC reverse osmosis (RO)[7] and nanofiltration (NF)[8] membranes with an active layer that is $\leq$0.1 μm thick. Currently, the fabrication of liquid crystals into TFC membranes is an emerging field. Q-phase thermotropic (i.e., solvent-free) LC monomers have recently been fabricated into a TFC architecture,[9] while the lone example of a LLC system fabricated into a TFC configuration involved non-aligned cylindrical pores (H_{II} phase) that exhibits very low flux.[10] In order to make Q-phase LLC thin-film fabrication more efficient, a solvent-casting process must be developed utilizing a low-volatility solvent such that heated processing does not disrupt the LLC phase

composition window. Likewise, new LLC monomers need to be designed and synthesized such that they provide cost-effective materials that can be produced at large scale. Herein, we explore the design and synthesis of new, more economical, more easily scalable LLC monomer systems that can be used for water desalination and nanofiltration applications.

2.2. Goals of this thesis research

The goals of my Ph.D. research were to design and synthesize new Q_I-phase forming monomers that have (1) less elaborate and more scalable synthetic routes, (2) provide potentially better blendability with cross-linkable commercial polymers with Q_I-phase retention, and (3) allow for facile thin-film processing with retention of the desired LLC phase. In addition to these three major research goals, my thesis research also examined preliminary approaches to modifying the effective pore size of cross-linked Q_I-phase polymers.

Chapter 3 describes the process of making the synthesis of Q_I-phase LLC monomers more cost-effective, avoiding pyrophoric intermediates in the process, and making the general synthetic scheme more facile. The new synthetic route will require accounting for all of these considerations. In order to improve on Q_I-phase LLC monomer **3b**, special consideration had to be given to designing a synthetic scheme in such a way that it would not only lower the cost of the end-product, but would simplify the process to get to several key intermediates.

In Chapter 4, a method for alleviating the problems (i.e., expensive LLC monomers, poor material tactility, inadequate water flux) that arise when using previous LLC/BR blended systems was evaluated. The previously discussed cost-effective monomer system **4** was utilized and blended with v-EPDM, a developmental variation of the commercially-produced cross-linkable elastomer EPDM, for the design of a selectively permeable toxic chemical agent barrier

material. This melt-infused membrane exhibited enhanced water vapor flux and high toxic vapor rejection, as compared to the previous system analyzed in the Gin research group, and met or exceeded relevant military standards.

Chapter 5 will detail how we set out to improve the processibility of water desalination membranes by (1) switching over to a third generation LLC monomer system that is even more cost-effective than previous iterations; (2) analyzing the ability of these systems to form LLC phases in non-aqueous, low-volatility systems; and (3) fabricating TFC membranes. This new monomer and solvent system produces the optimal membrane architecture that allows for higher pure water flux, while exhibiting a similar solute rejection performance compared to previous melt-infused membrane systems. The TFC membrane system affords the durability and mechanical strength to survive high-pressure industrial processes and the economy-of-scale that utilizes the minimal amount of LLC monomer to coat the largest possible support surface.

Chapter 6 discusses the exploration of a method to potentially impart pore size control to our water nanofiltration membranes. By utilizing blends of polymerizable LLC monomers, we discovered that Q phases could be formed in the presence of glycerol in the bulk state. Of the 13 different monomer blends analyzed, six blends showed evidence of Q phase formation with glycerol upon initial PLM penetration scan analysis. Unfortunately, all attempts so far to polymerize these LLC monomer blends with retention of the Q phase have failed. Future work should focus on investigating the reason for the LLC phase changes observed upon photo-cross-linking, as well as methods for altering the blend composition to help better stabilize the Q phases.

In Chapter 7, the future directions of this thesis work will be recommended. A very promising new set of gemini imidazolium LLC monomers, utilizing very economical and

modular acrylate and methacrylate polymerizable tails, has been synthesized and qualitatively screened for their Q_I phase formation with glycerol via polarized light microscopy. Initial results show that several of these new monomers form potential Q phases with glycerol, but no full phase diagrams have yet been elucidated, and no membrane fabrication has been attempted thus far. Several other directions for this work will be outlined, such as using solvent additives and atomic layer deposition to tune LLC-based membrane effective pore size

2.3. References

1. Lee, Y. S., Yang, J. Z., Sisson, T. M., Frankel, D. A., Gleeson, J. T., Aksay, E., Keller, S. L., Gruner, S. M.; O'Brien, D. F. *J. Am. Chem. Soc*. **1995**, *117*, 5573.

2. Yang, D., O'Brien, D. F.; Marder, S. R. *J. Am. Chem. Soc.* **2002**, *124*, 13388.

3. Srisiri, W., Lamparski, H. G.; O'Brien, D. F. *J. Org. Chem.* **1996**, *61*, 5911.

4. Srisiri, W., Benedicto, A.; O'Brien, D. F. *Langmuir* **1998**, *14*, 1921.

5. Pindzola, B. A., Jin, J.; Gin, D. L. *J. Am. Chem. Soc.* **2003**, *125*, 2940.

6. Zhou, M., Nemade, P. R., Lu, X., Zeng, X., Hatakeyama, E. S., Noble, R. D.; Gin, D. L. *J. Am. Chem. Soc.* **2007**, *129*, 9574.

7. Fell, C. J. D. "Reverse Osmosis," *Membrane Separations Technology. Principles and Applications*; Noble, R. D.; Stern, A. S.; Eds.; Elsevier Science: Amsterdam, 1995; Chapter 4.

8. Bhattacharya, A.; Ghosh, P. *Rev. Chem. Eng.* **2004**, *20*, 111.

9. Henmi, M.; Nakatsuji, K; Ichikawa, T.; Tomioka, H.; Sakamoto, T.; Yoshio, M.; Kato, T. *Adv. Mater*. **2012**, *24*, 2238.

10. Zhou, M.; Kidd, T. J.; Noble, R. D.; Gin. D. L. *Adv. Mater.* **2005**, *17*, 1850.

CHAPTER 3

Nanoporous, bicontinuous cubic lyotropic liquid crystal networks via polymerizable gemini ammonium surfactants

(Manuscript published under the same title in *Chemistry of Materials* **2010**, *22*, 4525-4527, co-authored with Hatakeyama, E. S.; Gabriel, C. J.; Noble, R. D.; Gin, D. L.)

3.1. Introduction

Cross-linked lyotropic liquid crystal (LLC) assemblies are a class of ordered, nanoporous polymer materials that have been shown to be useful for a number of important applications.[1] These polymer materials are formed by the in situ cross-linking of reactive amphiphiles (i.e., surfactants) that self-organize in water (or other polar solvents) into micro-phase-separated, liquid-crystalline assemblies containing periodic, nanometer-scale, aqueous regions/pores filled with mobile water molecules. The water regions can range in shape from closed spheres to 1D cylinders and 2D lamellae, to 3D interconnected networks.[1] Unlike similar nanoporous polymers made via direct cross-linking of[2] or replica-synthesis using[3] phase-separated block copolymers, LLC networks have pores that are significantly smaller (i.e., ≤1 to 10 nm) and are lined with the headgroups of the amphiphiles.[1] This latter feature allows for convenient pore functionalization and tuning.[1b,c] Because of these features, LLC networks have been used in nanocomposite synthesis,[1a,c] heterogeneous catalysis,[1a,c] molecular-size-based membrane separations,[4] and enhanced ion transport.[5]

One of the most important and sought-after types of cross-linked LLC assemblies are those with a bicontinuous cubic (Q) structure.[1c,4,5] Q phases (like other LLC phases) are classified as

type I (i.e., normal or water-rich) or type II (i.e., inverted or water-poor) depending on whether the hydrophilic-hydrophobic interface curves away from or towards the water regions, respectively.[1] In Q-phase systems, the open-framework and 3D interconnected pores provide better accessibility for catalysis and transport compared to lower-dimensionality LLC phases such as the 1D cylindrical hexagonal (H) and 2D lamellar (L) phases.[1c,4,5] Also, there is no need for pore alignment in these systems for transport applications because of their cubic symmetry.[1c,4,5] Recent work with Q_I-phase LLC-based polymer membranes[4] and cubic phase LLC[5] and thermotropic LC[6] ion-conducting materials have verified these statements. Another interesting feature of certain cross-linked Q_I phases is that uniform sub-1-nm pore sizes have been achieved, making them valuable for molecular sieving applications.[7,8]

Unfortunately, only a handful of LLC monomer systems are known to form polymerizable Q phases. O'Brien and co-workers pioneered two Q_{II}-phase LLC monomer platforms based on singly- and doubly-reactive derivatives of natural phosholipids[9] and glycerol amphiphiles.[10–12] Unfortunately, the phospholipid-based systems involve fairly demanding syntheses that limit the scale of production.[9] In the case of the glycerol-based monomers, the syntheses are less demanding and use more available starting materials.[10–12] However, in both cases, mixtures of monopolymerizable and cross-linkable surfactants are typically required to obtain the desired Q_{II} phases and cross-linked networks.[9–11] Our research group pioneered Q_I-phase LLC monomers based on a cross-linkable gemini phosphonium surfactant (**3**) (Figure 3.1).[13] This 1st-generation

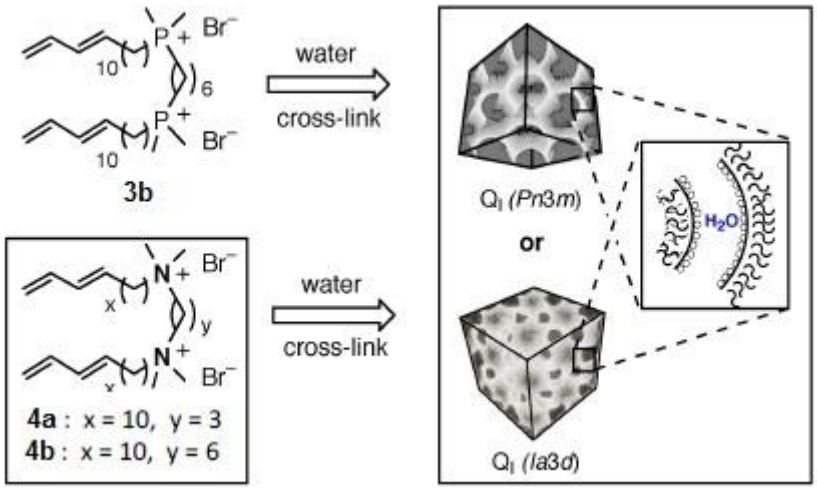

Figure 3.1. Structures of 1st- and 2nd-generation Q_I-phase LLC monomers based on gemini phosphonium and ammonium platforms, respectively.

gemini LLC Q_I monomer can be photopolymerized into polymer membranes containing a Q_I network. However, its synthesis requires an expensive phosphine-sulfide starting material, pyrophoric phosphine intermediates, and a $Na/NH_{3\ (l)}$ reduction step to make the gemini head unit.[13] In addition, the Q_I phase of **3b** requires processing at elevated temperatures (70 °C) to generate films for applications such as molecular-size-based water nanofiltration (NF) and desalination.[7] These features put severe limitations on the amount, cost, and scalability of this 1st-generation Q_I-phase material for applications.

Herein, we present a more facile route to nanoporous Q_I-phase networks using a new *ammonium*-based cross-linkable gemini LLC platform (**4**) that utilizes inexpensive starting materials and less demanding synthetic procedures (Figure 3.1). Two homologues of **4** (i.e., **4a** and **4b**) formed Q_I phases with water at ≥50 °C under atmospheric pressure. Processing these monomers into supported Q_I-phase polymer membranes requires milder processing conditions than the 1st-generation monomer **3**. Preliminary water NF and desalination studies on supported

cross-linked Q_I-phase polymer membranes of **4a** show that they are able to purify water similar to Q_I membranes based on **3**.

3.2. Results and Discussion

Designing a new Q_I-phase monomer based on a gemini ammonium platform was chosen for several reasons: First, this platform is similar to the gemini phosphonium platform (**3**) that has produced several Q phases.[13] Also, several non-polymerizable gemini ammonium surfactants in the literature exhibit a wide variety of LLC phases, including Q phases.[14–16] However, only a very small number of polymerizable gemini ammonium amphiphiles have been reported,[17,18] and polymerizable versions that afford Q (and other LLC) phases are unprecedented.

As shown in Figure 3.2, the synthesis of **4** utilizes a single high-yield reaction between commercially available and relatively inexpensive alkyl-bridged tetramethyldiamines with 2 equivalents of the polymerizable ω-bromoalkyl-1,3-diene tail units. In contrast, the synthesis of phosphonium monomer **3b** involves multiple steps requiring high and low temperatures and expensive and/or pyrophoric phosphine reagents to make the intermediate gemini head unit, followed by the same diene tail attachment step (see Supp. Info.).[13] This new procedure represents a significant reduction in cost, effort, and synthetic complexity for Q-phase LLC monomer production compared to prior approaches.[9–13]

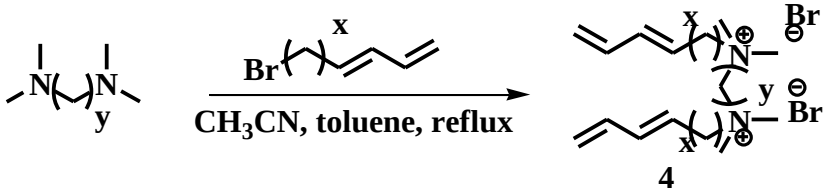

4

4a: x = 10 , y = 3 **4b: x = 10 , y = 6**
4c: x = 8 , y = 3 **4d: x = 8 , y = 6**
4e: x = 6 , y = 3 **4f: x = 6 , y = 6**

Figure 3.2. General synthesis scheme for homologues of monomer **4**.

Six homologues of **4** were initially synthesized to investigate their LLC phase behavior with water (Figure 2). Monomers **4a–f** were constructed using three different length 1,3-diene-terminated tails (x = 6, 8, 10) and two different head unit spacer lengths (y = 3, 6) (see Supp. Info. for details). The phase diagrams of **4a–f** as a function of composition with water were mapped out over a range of temperatures using variable-temperature polarized light microscopy (PLM). The structure of each LLC phase was identified by its PLM optical texture and powder X-ray diffraction (XRD) pattern. Specifically, the desired Q phases are characterized by having completely black PLM optical textures and powder XRD pattern that typically have two prominent *d*-spacing peaks with the ratio $1/\sqrt{6} : 1/\sqrt{8}$.[13]

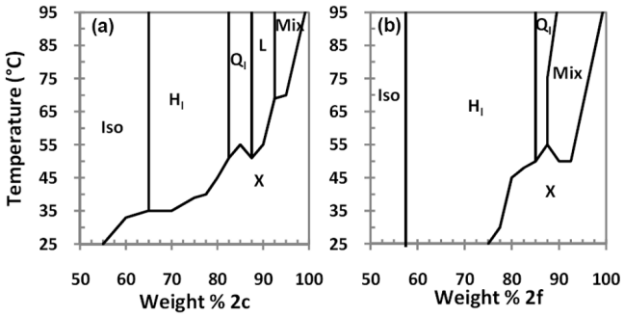

Figure 3.3. LLC phase diagrams of (a) **4a**, and (b) **4b** with water. Iso = micellar or non-ordered, H_I = type I hexagonal, Q_I = type I bicontinuous cubic, L = lamellar, Mix = LLC + crystalline, X = crystalline.

Q phases were not found for four of the gemini ammonium homologues. The two compounds with the shortest tails (**4e** and **4f**) did not exhibit any LLC behavior. The two compounds with the medium length tails (**4c** and **4d**) were found to form H phases, but no Q phases were observed (see Supp. Info.). However, the two homologues of **4** with the longer tails (**4a** and **4b**) were found to form Q phases. The phase diagrams for **4a** and **4b** (Figure 3.3) show that a Q_I phase forms with 12.5–17.5 wt % and 12.5–15 wt % water, respectively, at temperatures of ≥50 °C. Figure 3.4 shows that mixtures of **4a** and **4b** with 15 wt % water have the characteristic Q-phase XRD *d*-spacing ratio of $1/\sqrt{6} : 1/\sqrt{8}$, plus black PLM textures.[13] Since this Q phase appears on the water-rich side of a L phase on the phase diagram (and before a H phase), it was identified as a type I phase.[1,13]

The stabilization of the Q_I-phases of **4a** and **4b** into robust polymer networks was examined by photo-initiated radical cross-linking. In order to do this, films of the Q_I-phase mixtures containing a photo-initiator (PI) (84.2/14.8/1.0 (w/w/w) (**4a** or **4b**)/H_2O/PI) were heated to 60 °C to form the Q_I phase, and subsequently irradiated with a 365 nm UV light (8.5 mW cm^{-2}) for 1 h. The resulting materials are transparent, free-standing polymer films. FT-IR analysis of the polymerized samples showed a diene conversion of >95% (see Supp. Info.).[13] Retention of the Q_I-phase after cross-linking was verified by retention of the original PLM texture and XRD pattern (Figure 3.4). After cross-linking, a weak, broad peak sometimes appears that corresponds to the $1/\sqrt{22}$ *d*-spacing of a Q phase.[13] This peak does not correspond to a H or L phase XRD peak.

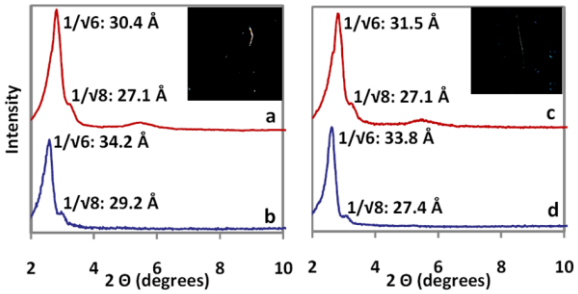

Figure 3.4. Powder XRD spectra of Q_I-phase mixtures of: (a) **4a** polymerized at 60 °C, (b) unpolymerized **4a** at 60 °C, (c) **4b** polymerized at 60 °C, and (d) unpolymerized **4b** at 60 °C. In all cases, the composition was 84.2/14.8/1.0 (w/w/w) monomer/H_2O/PI. Insets: PLM images of each cross-linked Q_I phase.

Previous studies showed that supported membranes of the cross-linked Q_I phase of phosphonium monomer **3b** have uniform 0.75 nm pores and can be used as an effective water NF membrane.[7] These 1st-generation Q_I-phase membranes can almost completely remove small organic solutes and inorganic salts from water via a molecular-size-exclusion mechanism (Table 3.1).[7] In order to demonstrate that the Q_I networks formed by the new gemini ammonium monomers afford similar size nanopores and are useful for similar separations, initial water NF tests were conducted on supported Q_I membranes of cross-linked **4a**. To do this, supported cross-linked Q_I membranes of **4a** were made by melt-pressing and photopolymerizing a Q_I-phase LLC mixture containing 84.2/14.8/1.0 (w/w/w) **4a**/H_2O/PI onto the same membrane support as in prior studies.[7] However, this processing can be accomplished at lower temperatures (55–60 °C) because of the slightly different properties of the respective Q_I phase.[19] This allows for easier processing since water loss, which can disrupt the Q_I phase, is less of a factor.

Table 3.1 shows that the initial water NF rejection performance of supported Q_I-phase membranes of **4a** compared to that of **3b** under the same test conditions (see Supp. Info.).[7] The Q_I-phase membranes of **4a** reject organic solutes and inorganic salts almost as well as the 1st-generation Q_I membranes based on **3**. The Q_I membranes of **4a** have a slightly larger nanopore

width of 0.86 nm, according to modeling of the neutral solute rejection behavior using the modified Ferry Equation (see Supp. Info.).[7] These 2nd-generation Q_I membranes also afford a similar level of throughput, with a thickness-normalized pure water permeance at 400 psi (27.6 bar) of 0.054 ± 0.003 L m^{-2} h^{-1} bar^{-1} μm, which is slightly lower than that of Q_I membranes of **3b** (0.086 ± 0.001 L m^{-2} h^{-1} bar^{-1} μm) under the same conditions.[20] However, the **4a** membranes are much easier and less expensive to make in terms of the monomer.

Table 3.1. Comparision of dead-end water NF performance of cross-linked Q_I-phase membranes prepared from **3b** and **4a**.

Test Solute	Hydrated Diameter (nm)[a]	Rejection (%)[b] Q_I Membrane	Rejection (%)[b] Q_I Membrane
NaCl	0.72 ($Na^+_{(aq)}$)	95 ± 1	94 ± 2
KCl	0.66 ($K^+_{(aq)}$)	91 ± 3	92 ± 2
MgCl2	0.86 ($Mg^{2+}_{(aq)}$)	>99.3	95 ± 2
CaCl2	0.82 ($Ca^{2+}_{(aq)}$)	>99.3	96.9 ± 0.2
Sucrose	0.94	>99	97.9 ± 0.2
Glucose	0.73	96 ± 2	94 ± 1
Glycerol	0.36	53 ± 1	45 ± 11
Ethylene glycol	0.32	38 ± 4	38 ± 3

(a) Previously published data from reference 7 and references therein.
(b) All filtrations were conducted with 2000 ppm aqueous test solutions in a stirred, dead-end filtration cell with a pressure of 400 psi.

3.3. Conclusion

In summary, a new Q_I-phase gemini LLC monomer system has been developed that is more easily and economically synthesized than prior examples. Two homologues of this gemini ammonium-based monomer system exhibit Q_I phases that can be cross-linked with retention of the structure. Supported membranes of these materials can be used for aqueous molecular size

separations and exhibit uniform, sub-1-nm size pores. We are currently exploring systematic structural modification of the monomer **4** platform to reduce and control the effective Q_I nanopore size for targeted molecular-size separations. We are also exploring Q_I phase formation of **4** homologues with solvents other than pure water (e.g., non-aqueous solvents and ionic solutions) to see if pore size can be manipulated by solvent environment. We are also examining methods to prepare thinner films of the cross-linked Q_I phases on membrane supports to increase their flux. The more facile and scalable synthesis afforded by this new monomer platform makes these and other optimization studies viable. Finally, we are determining if these new Q_I-phase monomers can be copolymerized with commercial elastomers to make nanoporous, selective vapor barrier materials[8] in a more facile and economical fashion.

3.4. Supporting information

3.4.1. Materials and General Procedures

Chromium (IV) oxide, pyridine, 9-bromo-1-nonanol, allyltrimethylsilane, *sec*-butyl lithium (1.4 M in cyclohexane), aluminum oxide (activated, basic), 2-isopropoxy-4,4,5,5-tetramethyl-1,3,2-dioxaborolane, *N,N,N',N'*-tetramethylethylene-1,2-diamine, *N,N,N',N'*-tetramethylpropane-1,3-diamine, *N,N,N',N'*-tetramethylhexane-1,6-diamine, and 2-hydroxy-2-methylpropiophenone were obtained from Sigma-Aldrich Co. and used as purchased. 7-Bromo-1-heptanol was purchased from TCI America and used as received. 11-Bromo-1-undecanol was obtained from Fluka and used as purchased. All solvents were purchased from Sigma-Aldrich or Fisher Scientific, and purified/dehydrated via N_2-pressurized activated alumina columns, unless otherwise noted. All chemical syntheses were carried out under a dry argon atmosphere using standard Schlenk line techniques, unless otherwise noted. Filtration through silica gel was

performed using 230–400 mesh, normal-phase silica gel purchased from Sorbent Technologies. The water used in LLC phase formulation and water filtration experiments was de-ionized, and had a resistivity of >12 MΩ cm^{-1}. Solupor E075-9H01A microporous support membrane (made from hydrophilically treated, ultrahigh-molecular-weight polyethylene (PE) fiber matte) was provided by DSM Solutech (Geleen, The Netherlands). Mylar sheets were purchased from American Micro Industry, Inc.

3.4.2. Instrumentation

^{1}H NMR spectra were obtained using a Bruker 300 Ultrashield™ (300 MHz) spectrometer, Varian Inova 500 (500 MHz), or Inova 400 (400 MHz) spectrometers. Chemical shifts are reported in ppm relative to deuterated solvent. Fourier-transform infrared spectroscopy (FT-IR) measurements were performed using a Matteson Satellite series spectrometer, as thin films on Ge crystals. HRMS analysis was performed by the Central Analytical Facility in the Dept. of Chemistry and Biochemistry at the University of Colorado, Boulder. LLC mixtures were homogenized using an IEC Centra-CL2 centrifuge. Powder X-ray diffraction (XRD) spectra were obtained with an Inel CPS 120 diffraction system using a monochromated Cu K_α radiation source. The apparatus was equipped with a film holder and temperature-programmable heating stage to analyze samples. All powder XRD spectra were calibrated against a silver behenate diffraction standard (d_{100} = 58.4 ± 0.1 Å).[21] Powder XRD measurements were all performed at ambient temperature (21 ± 1 °C). Variable temperature polarized light microscopy (PLM) studies were performed using a Leica DMRXP polarizing light microscope equipped with a Q-Imaging MicroPublisher 3.3 RTV digital camera, a Linkam LTS 350 thermal stage, and a Linkam CI 94 temperature controller. Automatic temperature profiles and image captures were

performed using Linkam Linksys32 software. Images were captured at 125x magnification. Photopolymerizations were conducted using a Spectroline XX-15A 365 nm UV lamp (8.5 mW cm^{-2} at the sample surface). UV light fluxes at the sample surface were measured using a Spectroline DCR-100X digital radiometer equipped with a DIX-365 UV-A sensor. Photopolymerizations were conducted on a custom-made temperature-controlled hot stage. Filtration studies were performed using custom designed, stainless steel, stirred, dead-end filtration cells that can accommodate 2.5 cm diameter membrane test samples. The ion conductivity of permeate solutions was measured using a VWR International electrical conductivity meter model 2052-B. Total organic carbon (TOC) analysis of permeate solutions containing organic solutes was conducted using a Test N Tube TOC kit (Hach), a COD reactor (DRM 200, Hach), and an Agilent 9453 UV-visible spectrophotometer. A Carver model C manual press equipped with a digitally temperature-controlled Carver 3796 heated platen set was used to manufacture membrane samples.

3.4.3. Synthesis

3.4.3.1. 10-Bromodeca-1,3-diene

Pyridinium chlorochromate (PCC) on alumina (78.6 g, 91.2 mmol, 178 mol %) was added to a solution of 7-bromo-1-heptanol (10.0 g, 51.3 mmol, 100 mol %) in CH_2Cl_2 (250 mL). The reaction mixture was stirred at room temperature for 16 h, and then the solvent was removed under reduced pressure (35 mm Hg). The brown residue was stirred in diethyl ether (100 mL), filtered through a pad of SiO_2, and washed with diethyl ether (5 x 50 mL). The solvent was removed under reduced pressure (35 mm Hg) to afford 7-bromo-1-heptanal as a light yellow oil (10 g, 97%) that was used without further purification. Matteson's reagent (10.4 g, 43.1 mmol,

120 mol%) was added to a solution of 7-bromo-1-heptanal (6.94 g, 35.9 mmol, 100 mol %) in diethyl ether (125 mL). The reaction was stirred at room temperature for 24 h and then triethanolamine (8.58 g, 57.5 mmol, 160 mol %) was added and the reaction was stirred for an additional 6 h. During this time a white precipitate formed. The reaction mixture was then washed with saturated aq. $NaHCO_3$ (2 x 100 mL), dried using anhydrous $MgSO_4$, filtered, and the solvent was removed under reduced pressure (35 mm Hg). The resulting oil was dissolved in diethyl ether (100 mL), H_2SO_4 (0.1 mL) was added, and the reaction was stirred at room temperature for 16 h. The reaction mixture was then poured into a separatory funnel, diluted with diethyl ether (100 mL), and washed with saturated aq. $NaHCO_3$ (2 x 100 mL). The organic layer was dried (anh. $MgSO_4$), filtered, and the solvent was removed under reduced pressure (35 mm Hg) to afford the crude product as a light yellow oil. Purification by filtration through a pad of SiO_2 with 6:1 (v/v) hexanes / CH_2Cl_2 (1 L) gave the product as a clear, colorless oil (5.0 g, 66%). ^{1}H NMR (400 MHz, $CDCl_3$): δ 6.34 (ddd, *J* = 17.0, 10.4, 10.1Hz, 1H), 6.09 (dd, *J* = 15.2, 10.4 Hz, 1H), 5.72 (dt, *J* = 15.2, 7.0 Hz, 1H), 5.11 (d, *J* = 17.0 Hz, 1H), 4.94 (d, *J* = 10.1 Hz, 1H), 3.42 (t, *J* = 6.8 Hz, 2H), 2.12 (m, 2H), 1.83 (m, 2H), 1.41 (m, 6H). ^{13}C NMR (400 MHz, $CDCl_3$): δ 137.66, 135.58, 131.38, 115.52, 35.56, 32.65, 32.26, 28.93, 28.15, 27.82. IR (neat): 3082, 3010, 2937, 2845, 1792, 1642, 1459, 1350, 1301, 1260, 1197, 1003, 951, 899, 729. cm^{-1}.

3.4.3.2. 12-Bromododeca-1,3-diene

Synthesized as described in the literature.[22] Chemical characterization data for the synthesized monomer were consistent with those reported in the literature.[22]

3.4.3.3. 14-Bromotetradeca-1,3-diene

Synthesized as described in the literature.[22] Chemical characterization data for the synthesized monomer were consistent with those reported in the literature.[22]

3.4.3.4. 1,3-Bis(deca-7,9-dienyl-*N*,*N*,*N*',*N*'-tetramethylammonium)propane dibromide (4e)

N,*N*,*N*',*N*'-Tetramethyl-1,3-propanediamine (0.150 g, 1.15 mmol, 100 mol %) and 10-bromodeca-1,3-diene (0.512 g, 2.36 mmol, 210 mol %) were dissolved in toluene (10 mL) and acetonitrile (10 mL) in a 50-mL round-bottom flask equipped with a stir bar and a reflux condenser. The clear, colorless solution was heated with stirring to 82 °C for 15 h. The white precipitate that formed after cooling to 0 °C using an ice water bath was filtered and washed with hexanes (2 x 50 mL), affording a white powder (0.5 g, 85%). ^{1}H NMR (400 MHz, $CDCl_3$): δ 6.31 (dt, *J* = 10.4, 6.4 Hz, 2H), 6.05 (dd, *J* = 10.4, 4.4 Hz, 2H), 5.68 (dd, *J* = 14.6, 7.6 Hz, 2H), 5.10 (d, *J* = 16.8 Hz, 2H), 4.98 (d, *J* = 10.8 Hz, 2H), 3.93 (t, J = 8.0 Hz, 4H), 3.50 (m, 4H), 3.36 (s, 12H), 2.78 (dt, 2H), 2.08 (m, 4H), 1.77 (m, 8H), 1.39 (m, 8H). ^{13}C NMR (100 MHz, DMSO-d_6): δ 17.09, 22.19, 26.09, 28.62, 28.87, 32.27, 50.70, 59.88, 63.95, 115.71, 131.48, 135.56, 137.65. IR (thin film, MeOH): 3417, 2926, 2854, 2056, 1649, 1483, 1464, 1003, 949, 897, 588 cm^{-1}. HRMS (ES) calcd. for $C_{27}H_{52}BrN_2$ ($M^+ M^+ Br^-$): 483.3308; observed: 483.3303.

3.4.3.5. 1,3-Bis(dodeca-9,11-dienyl-*N*,*N*,*N*',*N*'-tetramethylammonium)propane dibromide (4c).

N,*N*,*N*',*N*'-Tetramethyl-1,3-propanediamine (0.521 g, 4.00 mmol, 100 mol %) and 12-bromododeca-1,3-diene (2.05 g, 8.37 mmol, 209 mol %) were dissolved in toluene (10 mL) and acetonitrile (10 mL) in a 50-mL round-bottom flask equipped with a stir bar and a reflux

condenser. The clear, colorless solution was heated with stirring to 82 °C for 15 h. The white precipitate that formed after cooling to 0 °C using an ice water bath was filtered and washed with hexanes (2 x 50 mL), affording a white powder (2.0 g, 89%). ^{1}H NMR (300 MHz, $CDCl_3$): δ 6.32 (dt, *J* = 10.3, 17.1, 2H), 6.05 (dd, 2H), 5.71 (dd, 2H), 5.10 (d, 2H), 4.96 (d, 2H), 3.96 (t, 4H), 3.57 – 3.42 (m, 4H), 3.35 (s, 12H), 2.81 (dt, 2H), 2.07 (t, 4H), 1.82 (m, 4H), 1.68 (m, 8H), 1.34 (m, 12H). ^{13}C NMR (400MHz, $CDCl_3$): δ 137.332, 135.398, 130.999, 114.798, 66.501, 60.983, 51.267, 32.521, 29.305, 29.218, 29.112, 29.047, 26.332, 22.979, 18.986. IR (thin film, MeOH): 3437, 2933, 2856, 2094, 1801, 1604, 1651, 1487, 1470, 1003, 951, 899, 723, 650 cm^{-1}. HRMS (ES) calcd. for $C_{31}H_{60}BrN_2$ ($M^+ M^+ Br^-$): 539.3934; observed: 539.3913.

3.4.3.6. 1,3-Bis(tetradeca-11,13-dienyl-*N*,*N*,*N*',*N*'-tetramethylammonium)propane dibromide (4a).

N,*N*,*N*',*N*'-tetramethyl-1,3-propanediamine (1.62 g, 12.4 mmol, 100 mol %) and 14-bromotetradeca-1,3-diene (7.16 g, 26.2 mmol, 211 mol%) were dissolved in toluene (10 mL) and acetonitrile (10 mL) in a 50-mL round-bottom flask equipped with a stir bar and a reflux condenser. The clear, colorless solution was heated with stirring to 82 °C for 15 h. The white precipitate that formed after cooling to 0 °C using an ice water bath was filtered and washed with hexanes (2 x 50 mL), affording a white powder (7.0 g, 87%). ^{1}H NMR (300 MHz, $CDCl_3$): δ 6.32 (dt, *J* = 10.2, 17.2, 2H), 6.03 (dd, 2H), 5.72 (dd, *J* = 7.2, 14.8, 2H), 5.09 (d, *J* = 0.6, 2H), 4.96 (d, 2H), 3.96 (t, 4H), 3.56 – 3.43 (m, 4H), 3.36 (s, 12H), 2.81 (t, 2H), 2.07 (m, 4H), 1.75 (m, 8H), 1.32 (m, 24H). ^{13}C NMR (75 MHz, $CDCl_3$): δ 137.48, 135.67, 131.00, 114.75, 66.88, 61.19, 51.42, 32.67, 29.54, 29.42, 29.36, 29.30, 26.45, 23.11, 19.12. IR (thin film, MeOH):

3437, 2933, 2856, 2094, 1801, 1604, 1651, 1487, 1470, 1003, 951, 899, 723, 650 cm^{-1}. HRMS (ES) calcd. for $C_{35}H_{68}BrN_2$ ($M^+ M^+ Br^-$): 595.4560; observed: 595.4547.

3.4.3.7. 1,6-Bis(deca-7,9-dienyl-*N*,*N*,*N*',*N*'-tetramethylammonium)hexane dibromide (4f).

N,*N*,*N*',*N*'-Tetramethyl-1,6-hexanediamine (0.222 g, 1.29 mmol, 100 mol %) and 10-bromodeca-1,3-diene (0.588 g, 2.71 mmol, 210 mol %) were dissolved in toluene (10 mL) and acetonitrile (10 mL) in a 50-mL round-bottom flask equipped with a stir bar and a reflux condenser. The clear, colorless solution was heated with stirring to 82 °C for 15 h. The white precipitate that formed upon cooling to 0 °C using an ice water bath was filtered and washed with hexanes (2 x 50 mL), affording a white powder (0.7 g, 84%). ^{1}H NMR (300 MHz, $CDCl_3$): δ 6.33 (dt, 2H), 6.05 (dd, *J* = 10.4, 14.5, 2H), 5.69 (dd, *J* = 7.3, 14.9, 2H), 5.10 (d, *J* = 16.9, 2H), 4.97 (d, *J* = 10.2, 2H), 3.78 (t, 4H), 3.46 (m, 4H), 3.39 (s, 12 H), 2.25 – 1.93 (m, 8H), 1.67 (m, 8H), 1.39 (m, 12H). ^{13}C NMR (75 MHz, $CDCl_3$): δ 137.35, 135.02, 131.40, 115.11, 64.90, 64.35, 51.20, 32.42, 29.01, 28.89, 26.33, 24.40, 23.00, 21.76. IR (thin film, MeOH): 3012, 2931, 2858, 1934, 1716, 1651, 1474, 1398, 1160, 907 cm^{-1}. HRMS (ES) calcd. for $C_{30}H_{58}BrN_2$ ($M^+ M^+ Br^-$): 527.3753; observed: 527.3762.

3.4.3.8. 1,6-Bis(dodeca-9,11-dienyl-*N*,*N*,*N*',*N*'-tetramethylammonium)hexane dibromide (4d).

N,*N*,*N*',*N*'-Tetramethyl-1,6-hexanediamine (0.467 g, 2.71 mmol, 100 mol %) and 12-bromododeca-1,3-diene (1.40 g, 5.71 mmol, 210 mol %) were dissolved in toluene (10 mL) and acetonitrile (10 mL) in a 50-mL round-bottom flask equipped with a stir bar and a reflux condenser. The clear, colorless solution was heated with stirring to 82 °C for 15 h. The white

precipitate that formed upon cooling to 0 °C using an ice water bath was filtered and washed with hexanes (2 x 50 mL), affording a white powder (2.0 g, 86%). ^{1}H NMR (400 MHz, $CDCl_3$): δ 6.31 (dt, 2H), 6.05 (dd, 2H), 5.70 (dd, 2H), 5.09 (d, 2H), 4.95 (d, 2H), 3.75 (m, 4H), 3.45 (m, 4H), 3.38 (s, 12H), 2.07 (m, 8H), 1.67 (m, 8H), 1.33 (m, 20H). ^{13}C NMR (400 MHz, $CDCl_3$): δ 137.386, 135.509, 131.011, 114.795, 64.738, 64.177, 51.086, 32.556, 29.310, 29.283, 29.139, 29.067, 26.367, 24.565, 22.950, 21.755. IR (thin film, MeOH): 3012, 2927, 2858, 2072, 1716, 1655, 1486, 1471, 1156, 1007, 903, 727 cm^{-1}. HRMS (ES) calcd. for $C_{31}H_{60}BrN_2$ (M^+ M^+ Br^-): 581.4405; observed: 581.4404.

3.4.3.9. 1,6-Bis(tetradeca-11,13-dienyl-*N*,*N*,*N*',*N*'tetramethylammonium)hexane dibromide (4b).

N,*N*,*N*',*N*'-Tetramethyl-1,6-hexanediamine (0.401 g, 2.32 mmol, 100 mol %) and 14-bromotetradeca-1,3-diene (1.29 g, 4.72 mmol, 203 mol%) were dissolved in toluene (10 mL) and acetonitrile (10 mL) in a 50-mL round-bottom flask equipped with a stir bar and a reflux condenser. The clear, colorless solution was heated with stirring to 82 °C for 15 h. The white precipitate that formed upon cooling to 0 °C using an ice water bath was filtered and washed with hexanes (2 x 50 mL), affording a white powder (1.0 g, 83%). ^{1}H NMR (300 MHz, $CDCl_3$): δ 6.31 (dt, *J* = 10.2, 16.9, 2H), 6.04 (dd, *J* = 10.3, 15.2, 2H), 5.71 (dd, 2H), 5.08 (d, *J* = 16.9, 2H), 4.95 (d, *J* = 10.2, 2H), 3.75 (m, 4H), 3.46 (m, 4H), 3.39 (s, 12H), 2.06 (m, 8H), 1.66 (m, 8H), 1.31 (m, 28H). ^{13}C NMR (75 MHz, $CDCl_3$): δ 137.53, 135.75, 131.02, 114.77, 77.62, 77.20, 76.78, 65.06, 64.37, 51.23, 32.71, 29.56, 29.55, 29.52, 29.41, 29.33, 26.48, 24.21, 23.05, 21.67. IR (thin film, MeOH): 3008, 2923, 2854, 1651, 1601, 1490, 1471, 1064, 1026, 957, 907, 727 cm^{-1}. HRMS (ES) calcd. for $C_{31}H_{60}BrN_2$ (M^+ M^+ Br^-): 637.5010; observed: 637.5030.

3.4.4. Determination of LLC phase behavior and LLC phase diagrams.

Previously published methods were used to examine the LLC phase behavior.[7,13] LLC samples of specific composition were made by adding an appropriate amount of monomer, water, and 2-hydroxy-2-methylpropiophenone (HMP), a photo-initiator (PI), to custom made glass vials, and sealed with Teflon tape and Parafilm. LLC samples were mixed by alternately hand-mixing and centrifuging (3500 rpm) until completely homogenous. It should be noted that the LLC samples are sensitive to evaporative water loss. Special attention was taken to keep the samples sealed as much as possible during sample mixing and transferring to minimize water loss.

The range of each LLC phase was determined using variable-temperature PLM. Specimens were prepared by pressing samples between a microscope slide and microscope cover-slip. The assembly was then placed on the PLM thermal stage and annealed past its isotropic temperature or up to 85 °C (whichever came first). The sample was slowly cooled and allowed to come back to its room temperature phase. The sample was then heated to 95 °C at a rate of 5 °C/min with digital image capture every 1.25 °C and continuous recording of the light intensity. Images were captured at 125x magnification. Changes in optical texture and light intensity were used to determine changes in the LLC phase of the mixture.

The identity of each observed phase was then confirmed by XRD by analyzing a point in each distinct phase region as elucidated by PLM. XRD spectra of the samples were taken either by using a film holder apparatus for room temperature spectra or a heated stage for higher temperature spectra. In the film holder, a sample was placed between Mylar sheets with an appropriate spacer, annealed, placed in the film holder, and then examined. On the heated stage,

a sample was placed in an aluminum XRD pan and a piece of Mylar was used to cover the sample to prevent evaporation. The spacing of the XRD peaks is used to determine the LLC phase. Using the combined PLM and XRD data, phase diagrams were plotted for each LLC monomer as a function of composition and temperature.

Phase diagrams of the LLC behavior for gemini ammonium monomers **4c, 4d, 4e,** and **4f** are shown in Figure 3.S1. The LLC phase behavior of the monomers **4a** and **4b** are shown in the main body of the manuscript (Figure 3.3). Compositions, temperatures, and powder XRD data for representative LLC samples are tabulated in Table 3.S1. Representative PLM images of each phase are shown in Figures 3.S2–3S5.

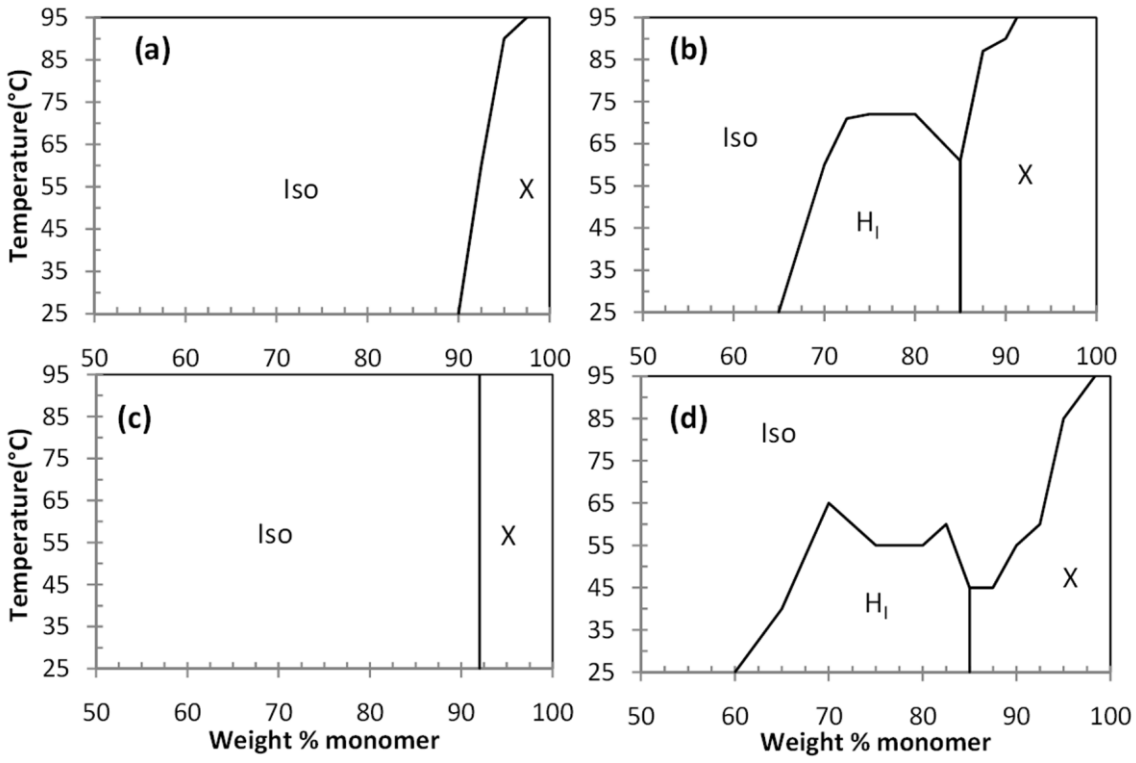

Figure 3.S1. Phase diagrams of (a) monomer **4e** (x = 6, y = 3), (b) monomer **4c** (x = 8, y = 3), (c) monomer **4f** (x = 6, y = 6), and (d) monomer **4d** (x = 8, y = 6) with water. Iso = an isotropic or pseudo-isotropic phase (e.g., micelles, a discontinuous cubic phase, or a non-ordered phase); H_I = normal hexagonal phase; Q_I = normal bicontinuous cubic phase; X = crystalline phase.

Table 3.S1. Compositions, temperatures, and powder XRD peak data for unpolymerized and polymerized gemini ammonium monomer LLC mixtures with water. The temperature refers to the approximate temperature of the LLC mixture during XRD for unpolymerized samples. For polymerized samples (denoted by "polymer" next to the compound label), the temperature refers to the temperature of the sample during polymerization. XRDs were taken at R.T. for polymerized samples. The LLC phases listed were determined by XRD pattern and PLM texture analysis.

Compound	x	Y	Composition (wt % monomer)	Temp. (°C)	Powder XRD *d*-spacing (Å)			LLC phase
4c	8	3	70	R.T.	33.6	19.6		H_I
4c– cross-linked	8	3	70	R.T.	29.8			H_I
4a	10	3	75	40	36.9			H_I
4a – cross-linked	10	3	75	40	31.9	18.6	16.3	H_I
4a	10	3	85	60	34.2	27.1		Q_I
4a – cross-linked	10	3	85	60	30.4	27.1		Q_I
4a	10	3	90	80	31.0			L
4a – cross-linked	10	3	90	80	31.3	15.5		L
4d	8	6	70	R.T.	31.6			H_I
4d – cross-linked	8	6	70	R.T.	31.6			H_I
4d	8	6	80	R.T.	29.9			H_I
4d – cross-linked	8	6	80	R.T.	30.1	18.1		H_I
4b– cross-linked	10	6	75	60	30.8	18.2	15.5	H_I
4b	10	6	85	60	33.8	28.4		Q_I
4b– cross-linked	10	6	85	60	31.5	27.1		Q_I
4b	10	6	90	90	30.0			L
4b – cross-linked	10	6	90	90	31.7	16.1		L

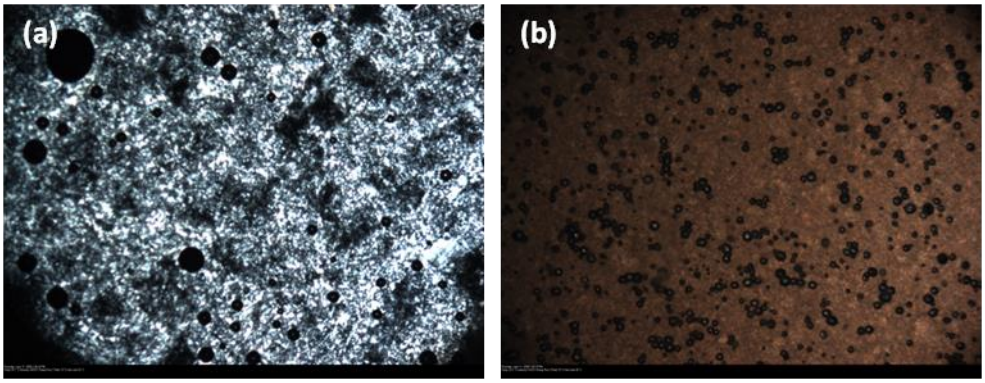

Figure 3.S2. Representative PLM optical textures of LLC mixtures of **4c** (x = 8, y = 3): (a) a H_I phase consisting of 75/25 (w/w) **4c** / water at 30 °C, (b) a crystalline phase consisting of 85/15 (w/w) **4c** / water at 30 °C.

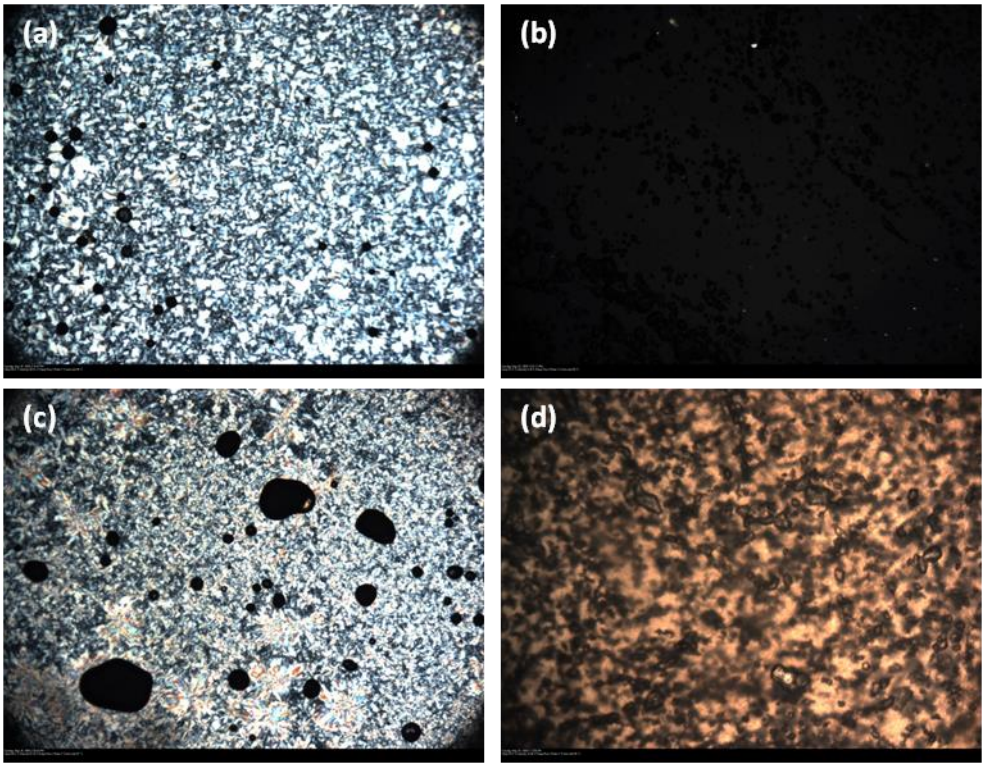

Figure 3.S3. Representative PLM optical textures of LLC mixtures of **4a** (x =10, y = 3): (a) a H_I phase consisting of 65/35 (w/w) **4a** / water at 60 °C, (b) a Q_I phase consisting of 85/15 (w/w) **4a** / water at 60 °C, (c) a L phase consisting of 90/10 (w/w) **4a** / water at 60 °C, and (d) a crystalline phase consisting of 95/5 (w/w) 4a / water at 60 °C.

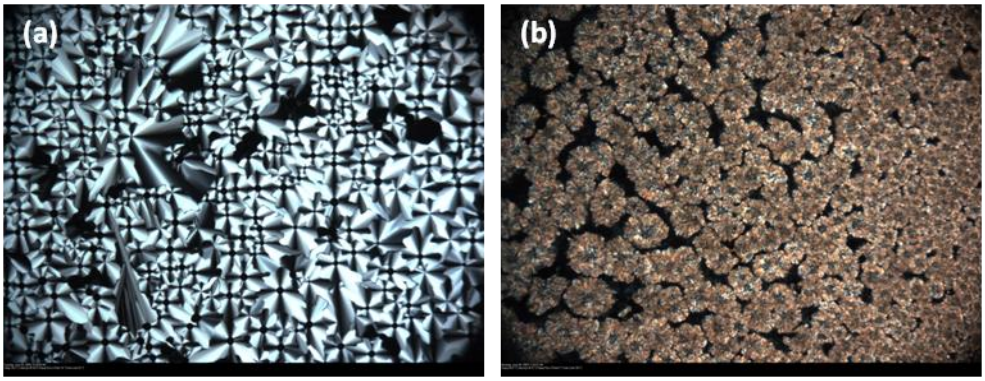

Figure 3.S4. Representative PLM optical textures of LLC mixtures of **4d** (x = 8, y = 6): (a) a H_I phase consisting of 72.5/27.5 (w/w) **4d** / water at 50 °C, and (b) a crystalline phase consisting of 90/10 (w/w) **4d** / water at 50 °C.

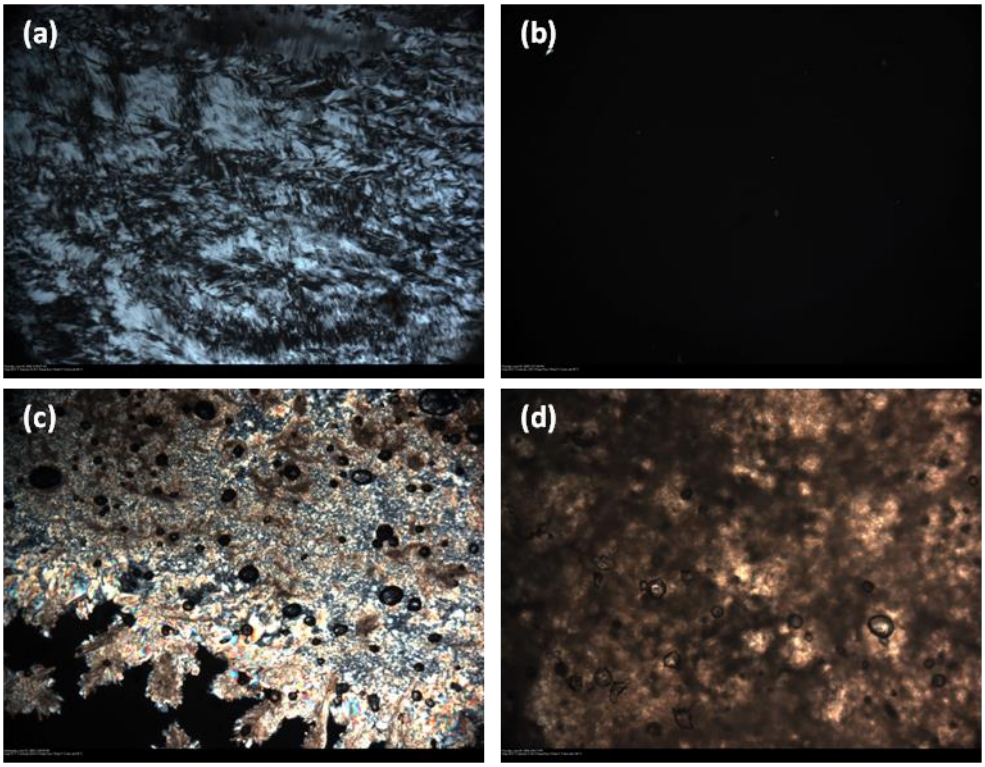

Figure 3.S5. Representative PLM optical textures of LLC mixtures of **4b** (x = 10, y = 6): (a) a H_I phase consisting of 75/25 (w/w) **4b** / water at 60 °C, (b) a Q_I phase consisting of 85/15 (w/w) **4b** /water at 60 °C, (c) a mixed crystalline/LLC phase consisting of 90/10 (w/w) **4b** / water at 60 °C, and (d) a crystalline phase consisting of 95/5 (w/w) **4b** / water at 60 °C.

3.4.5. Determination of the degree of diene polymerization of bicontinuous cubic (Q_I) phases.

LLC samples of 84.2/14.8/1.0 (w/w/w) **4a**/H_2O/HMP and **4b**/H_2O/HMP were made. This specific composition forms a Q_I phase when heated above 50 °C and 55 °C, respectively. Samples were prepared for FT-IR analysis by placing a small amount of LLC sample between two Ge plates with an appropriate spacer and heated to 60 °C to form a Q_I phase. The mixtures between the two Ge plates were then examined using a FT-IR spectrometer to obtain pre-polymerization spectra of the mixtures. Using the same LLC mixtures, a small amount was placed between a Ge crystal plate and quartz plate with the same spacer. The quartz plate minimizes the loss of water in the LLC sample while being transparent to UV light for photopolymerization. Samples were then heated and held at 60 °C to form the Q_I phase and then irradiated with 365 nm light (8.5 mW cm^{-2}) for 1 h. The quartz plate was then carefully removed leaving the polymerized LLC sample on the Ge plate. The polymerized sample was then examined using a FT-IR spectrometer to obtain post-polymerization spectra of the mixtures. The 1004 cm^{-1} absorbance peak in the pre-polymerized samples comes from the C–H out of plane wagging from the –$CH=CH_2$ located at the end of the diene terminated tails of the monomer.[7,13] The disappearance of the 1004 cm^{-1} in the post-polymerized samples suggest >95% degree of 1,3-diene conversion for the Q_I-phase LLC sample.[7,13] This is more than sufficient to create a highly cross-linked polymer network. Subsequently, PLM and XRD analysis of the polymerized samples showed that it still retained the Q_I-phase nanostructure. The resulting Q_I-phase material is highly stabilized due to the high degree of cross-linking. The FT-IR spectra showing the pre-polymerized and post-polymerized samples of the two Q_I phases are shown in Figures 3.S6 and 3.S7.

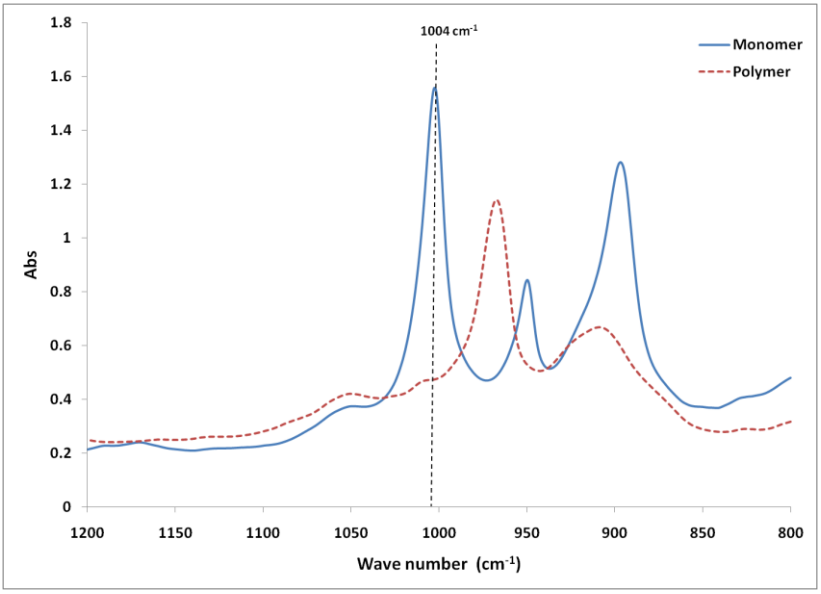

Figure 3.S6. FT-IR spectra of 84.2/14.8/1.0 (w/w/w) **4a**/H_2O/HMP heated to 60 °C before polymerization (monomer mixture) and after 1 h of 365 nm UV light exposure (8.5 mW cm^{-2}) at 60 °C (cross-linked polymer). Disappearance of the 1004 cm^{-1} FT-IR band suggests >95% conversion of the 1,3-diene functional group while in the Q_I phase.[7,13]

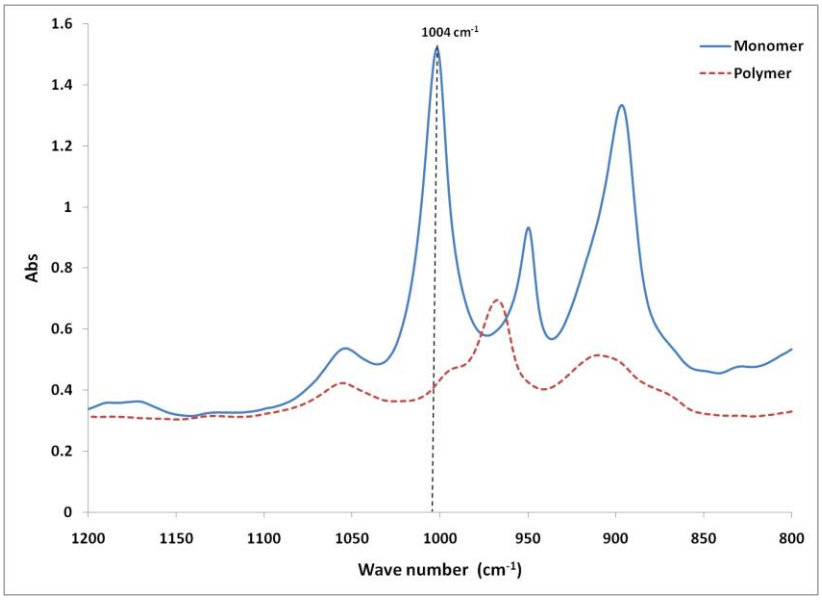

Figure 3.S7. FT-IR spectra of 84.2/14.8/1.0 (w/w/w) **4b**/H_2O/HMP heated to 60 °C before polymerization (monomer mixture) and after 1 h of 365 nm UV light exposure (8.5 mW cm^{-2}) at 75 °C (cross-linked polymer). Disappearance of the 1004 cm^{-1} FT-IR band suggests >95% conversion of the 1,3diene functional group while in the Q_I phase.[7,13]

3.4.6. Fabrication of supported Q_I-phase membranes of 4a.

Supported membranes of the cross-linked Q_I-phase of monomer **4a** were made using a modified hot-pressing method previously published.[7] In this process, a Q_I-phase monomer gel mixture containing 84.2/14.8/1.0 (w/w/w) **4a**/H_2O/HMP was prepared. A small amount of the LLC monomer mixture (50–100 mg) was then placed on a piece of Solupor E075-9H01A support membrane. This was then placed between two Mylar sheets to prevent water evaporation. The membrane sample between Mylar sheets was then placed between two mirror-like, polished aluminum plates. The aluminum plates provide a smooth, heat conductive surface for hot-pressing of the membrane assembly. The membrane assembly was then pressed using a Carver manual press equipped with temperature controlled heated platens pre-heated to 60 °C. An applied force of 1–8 tons for 10 min was used to infuse the Q_I-phase monomer mixture completely through the entire depth of the Solupor E075-9H01A support. The membrane sample removed from the press and aluminum plates. It was then clamped between two quartz plates pre-heated to 60 °C and photo-polymerized at 60 °C with a 365 nm UV light source (ca. 8.5 mW cm^{-2}) for 1 h to radically photo-cross-link the Q_I-phase nanostructure. The quartz plates help minimize water loss during photopolymerization. Cross-linking and stabilization of the Q_I-phase nanostructure in the Solupor E075-9H01A support membrane was verified by powder XRD analysis. Figure 3.S8 shows the Q_I phase was maintained after polymerization in the Solupor E075-9H01A support. The resulting supported membrane appears optically transparent (Figure 3.S9).

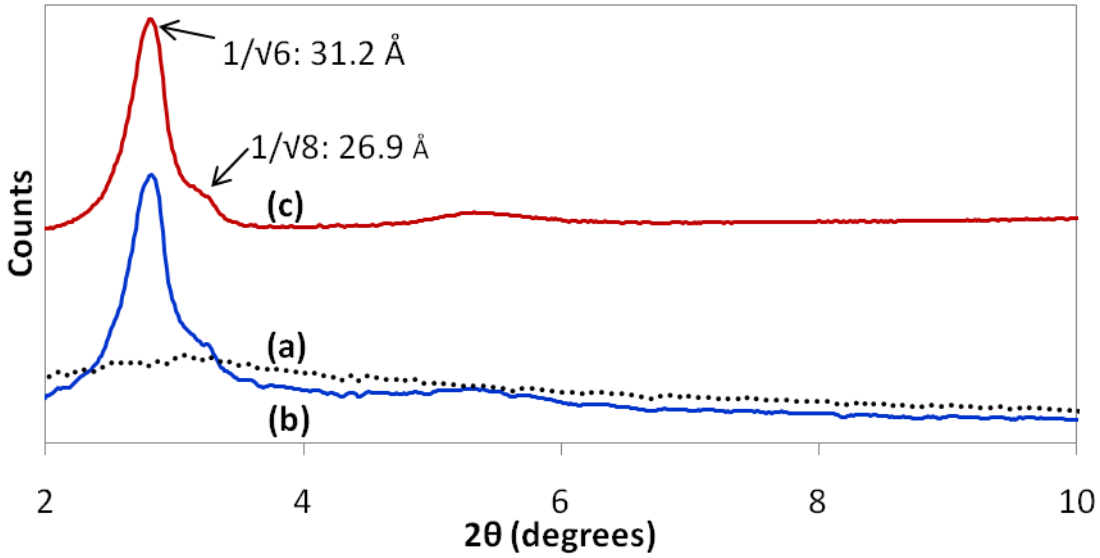

Figure 3.S8. XRD spectra of (a) the Solupor PE support material, (b) the cross-linked Q_I phase of **4a** fully infused in the Solupor PE support material, and (c) the subtraction of the powder XRD profiles of (a) from (b) to give the structure of just the cross-linked Q_I phase of **4a**. The XRD spectrum (c) suggests that the Q_I phase nanostructure is maintained in the polymerized supported membrane.

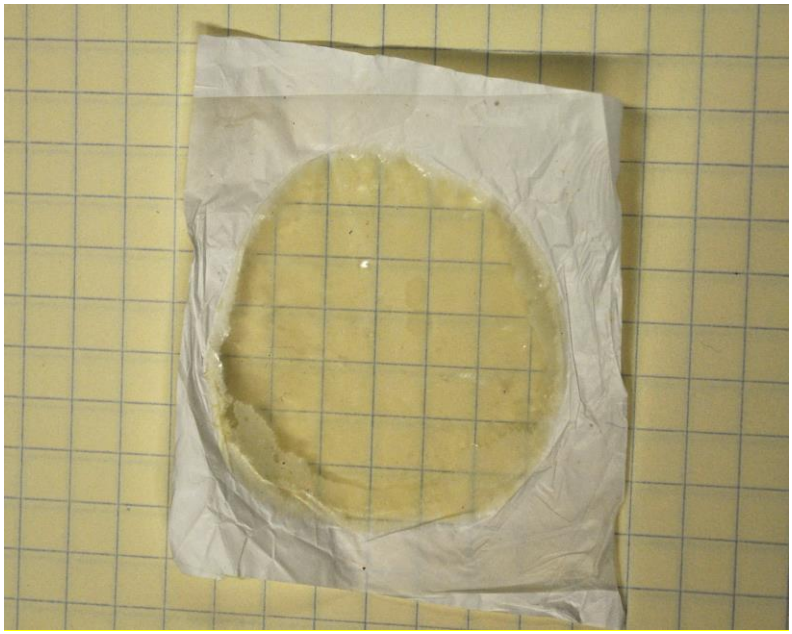

Figure 3.S9. Picture of a supported cross-linked Q_I-phase membrane of **4a**. Scale: Each grid division is 0.25 of an inch. The polymerized Q_I-phase of **4a** infused into the Solupor support is visually transparent, while the surrounding pristine Solupor support material is not.

3.4.7. Water nanofiltration testing of supported Q_I-phase membranes of 4a.

Membrane discs of the supported Q_I-phase membranes of **4a** (2.5 cm in diameter) were cut from sheets using a sharpened circular punch die. The membrane discs were installed into custom-made, stainless steel, stirred dead-end filtration cells (Figure 4.S10). The membrane holder has a 2.5 cm outer diameter and an effective filtration area of 3.8 cm^2. Deionized water was filtered through the membrane using 2.76 x 10^6 Pa (400 psi) of N_2 pressure as the driving force. The deionized water was filtered at ambient temperature (21 ± 1 °C) until at least 5 mL of permeate was collected. The first filtration with deionized water is to ensure the integrity of the membrane and also to clean out any unpolymerized monomer or other contaminates that might remain in the membrane after processing.

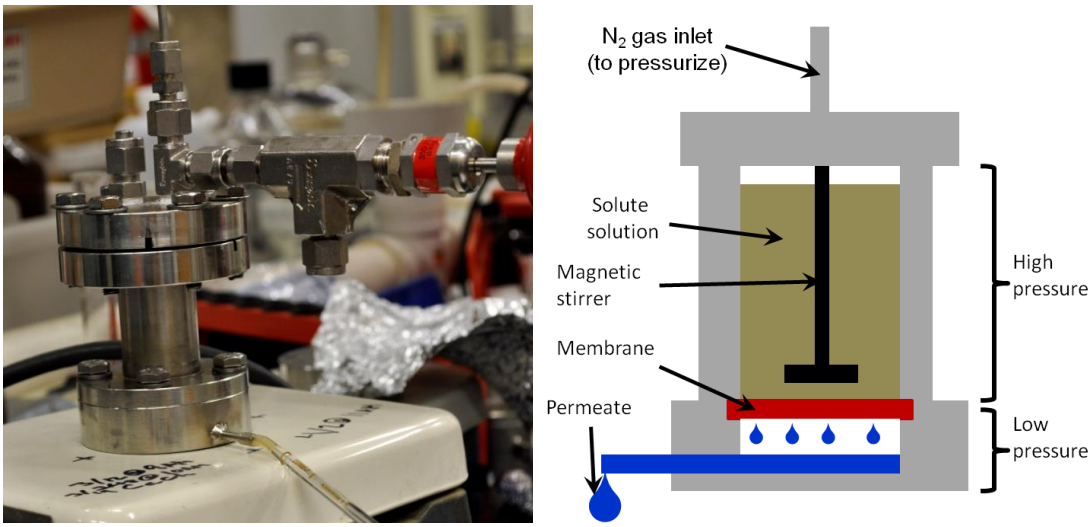

Figure 3.S10. Image and schematic representation of the custom-made, stirred dead-end water filtration cells used in this study.

All filtration experiments were then carried out using aqueous feed solutions containing a single solute at 2000 ppm concentration. Each stirred dead-end filtration cell was loaded with 25 mL of the feed solution and pressurized to 2.76 x 10^6 Pa (400 psi) of N_2 pressure. The first 1–2

mL of permeate were discarded. The next 2–4 mL of permeate were then collected and examined to determine thickness-normalized permeance and rejection.

For all filtration studies, the thickness-normalized permeance (P') was calculated as follows using Eq. 3.S1:

$$P' = \frac{\Delta V}{A \Delta t} \frac{1}{\Delta p} \Delta x \qquad \text{(Equation 3.S1)}$$

where A is the surface area of the membrane (3.8 cm^2), ΔV is the permeate volume, and Δt is the time needed to collect the permeate, ΔP is the transmembrane pressure, and Δx is the membrane thickness. The rejection (R) was calculated as follows using Eq. 3.S2:

$$R = \left(1 - \frac{C_{permeate}}{C_{feed}}\right) \cdot 100 \qquad \text{(Equation 3.S2)}$$

where $C_{permeate}$ and C_{feed} are the concentration of solute in the permeate and feed, respectively. All reported permeances and rejections are averages of three different membrane samples in separated experiments. Reported errors are standard deviations calculated using three different membranes in separate experiments.

3.4.8. Permeate analysis.

The concentration of NaCl, KCl, $MgCl_2$, and $CaCl_2$ in the permeate solution were determined using an electrical conductivity meter. The conductivity meter was calibrated for each salt using standard aqueous solutions of each salt. The concentrations of all the neutral organic solutions were determined using TOC digestion kit with a modified procedure based on

Hach method 10173 and subsequent UV-visible analysis. Calibration plots made with standard solutions prior to each study to ensure accuracy.

3.4.9. Estimation of the effective pore size using the Ferry equation.

The Ferry equation (eqn. 3.S3) describes rejection as a function of effective solute size and effect pore size.[23] This simple steric pore model assumes that the solutes are spherical and the membrane pores are uniform cylinders. The Ferry equation has been used to describe a variety of porous membranes.[7,23-25] The Ferry equation is shown as follows in Eq. 3.S3:

$$R' = \left[1 - \left(1 - \frac{r_{solute}}{r_{pore}}\right)^2\right]^2 \cdot 100 \qquad \text{(Equation 3.S3)}$$

where *R'* is the rejection in percent based on pore size exclusion, r_{solute} is the solute diameter, and r_{pore} is the pore diameter. The observed rejection data of the Q_I-membrane of **4a** for the non-charged solutes (i.e., sucrose, glucose, glycerol, and ethylene glycol) were fitted to the Ferry equation to estimate the effective pore size in the absence of charge-charge effects. The solute diameters used in this study are the same as the values used in a previous study with **3**.[7] After fitting the rejection data to the Ferry model, it was determined that the effective pore size of the supported Q_I-phase membranes of **4a** is ca. 0.86 nm. This is slightly larger than the ca. 0.75 nm pores found in the 1st-generation Q_I-phase membranes of **3**.[7] Figure 3.S11 shows that the Ferry equation with a uniform pore size of 0.86 nm is in good agreement with the observed rejection data for the neutral solutes.

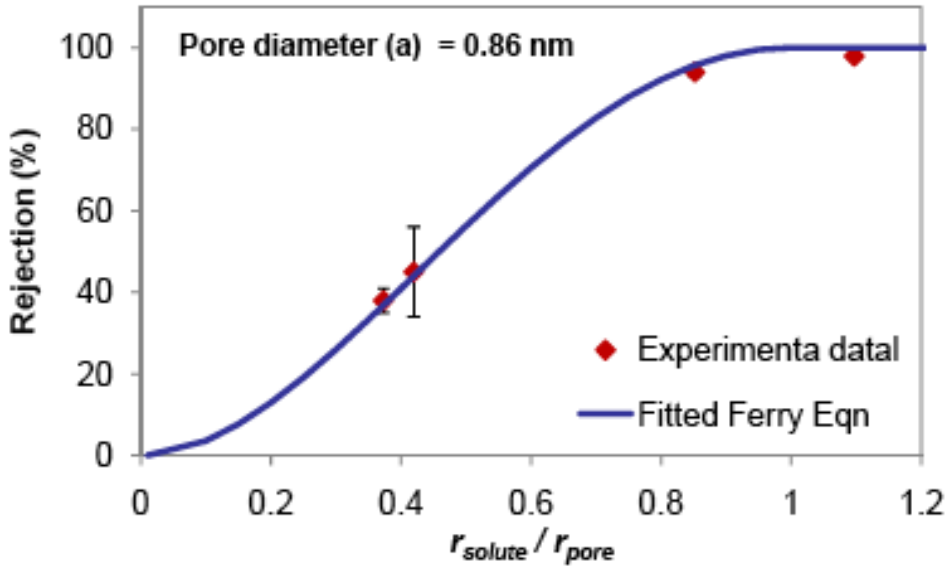

Figure 3.S11. Calculated (Ferry Equation with r_{pore} = 0.86 nm) and experimentally measured rejections for the neutral solute molecules. Water filtrations were performed in stirred, dead-end filtration cells with a differential pressure of 2.76 x 10^6 Pa (400 psi) and a solute concentration of 2000 ppm.

3.4.10. Reagent cost analysis of 4a vs. the gemini phosphonium monomer (3)

The cost analysis of the reagents needed to make **4a** and the previously published gemini phosphonium LLC material[7] are shown in Tables 3.S2–S4. The synthesis schemes are shown in Figure 3.S12 and 3.S13. Only the reagent costs purchased on the laboratory scale are considered, with observed laboratory scale yields for each reaction. No solvent, purification materials, energy, or time considerations are calculated in these cost estimates for LLC monomer synthesis. Table 3.S2 describes the cost of the intermediate 14-bromotetradeca-1,3-diene. It is an intermediate used in both final products. Table S3 and S4 show that the overall cost of **4a** is much lower than the original gemini phosphonium LLC monomer **3**. The reagents cost of **4a** is approximately $14.38/g while that of the original gemini phosphonium LLC monomer **3b** is $78.45/g.

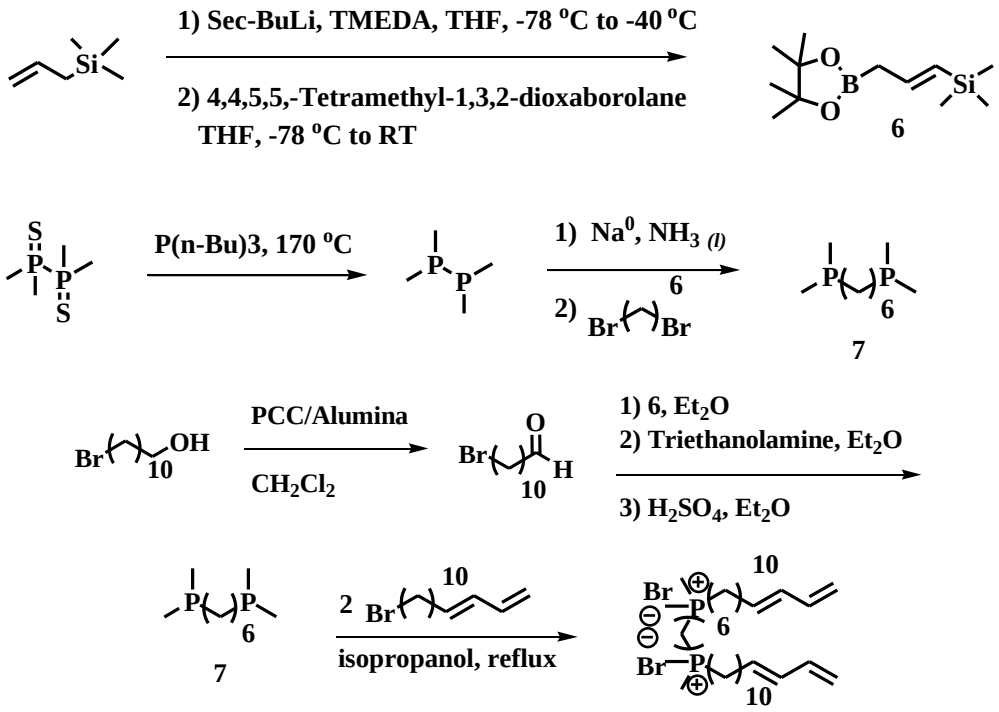

Figuree 3.S12: Synthesis scheme for gemini phosphonium LLC monomer **3b**.[7]

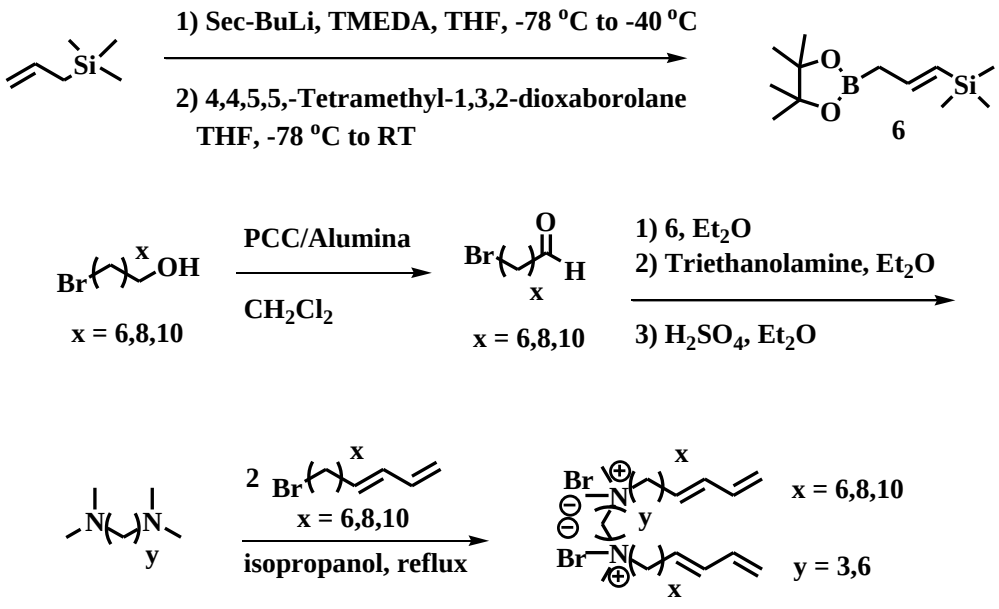

Figure 3.S13: General synthesis scheme for homologues of new gemini ammonium LLC monomer **4.**

Table 3.S2. Reagent costs for synthesizing the 14-bromotetradeca-1,3-diene tail. It is subsequently used in the synthesis of **4a,** and the previously published gemini phosphonium LLC monomer. The costs listed do not consider solvent, purification materials, energy, or labor.

Compound	**Mass**	**Cost**	**$/g**	**Scale of Reaction**	**Cost in reaction**	**Overall $/g**
Chromium (IV) oxide	500 g	$174.00	$0.35	30 g	$10.50	
Brockman Basic Alumina	5 kg	$287.00	$0.06	250 g	$15.00	
Pyridine	982 g	$141.50	$0.14	23.8 g	$3.33	
$/gram for PCC synthesis				369.75 g	$28.83	$0.08
11-bromo-1-undecanol	50 g	$155.00	$3.10	16g	$49.60	
PCC			$0.08	83 g	$6.64	
$/gram for PCC oxidation of aldehyde				14.3 g	$56.24	$3.93
N,*N*,*N*',*N*'-tetramethylethylenediamine	77.5 g	$106.00	$1.37	18.6 g	$25.48	
sec-Butyl lithium, 1.4 M in cyclohexane	71.7 g	$144.80	$2.02	10.2 g	$20.60	
Allytrimethylsilane	50g	$91.60	$1.83	18.3 g	$33.49	
2-Isoproxy-4,4,5,5-tetramethyl-1,3,2-dioxaborolane	91.2g	$145	$1.59	27.0 g	$42.93	
$/gram for synthesis of Matteson's Reagent [2]				27.7 g	$122.50	$4.42
11-bromo-1-undecanal			$3.93	22.5 g	$88.43	
Matteson's Reagent			$4.42	26.8 g	$118.46	
Triethanolamine	1124 g	$84.30	$0.08	21.6 g	$1.73	
$/gram of 14-bromotetradeca-1,3-diene				**16.3 g**	**$208.62**	**$12.80**

Table 3.S3. Reagent cost of synthesizing the final product **4a**. The listed costs do not include solvent, purification materials, energy, or labor.

Compound	Mass	Cost	$/g	Scale of Reaction	Cost in reaction	Overall $/g
14-bromotetradeca-1,3-diene			$12.80	5.39 g	$68.99	
N,*N*,*N*',*N*'-tetramethylpropanediamine	77.9 g	$29.40	$0.38	1.22 g	$0.46	
$/gram of 4a				4.83 g	$69.45	**$14.38**

Table 3.S4. Reagent costs of synthesizing the original gemini phosphonium LLC monomer previously used to make nanostructured polymer membranes for water nanofiltration.[7,13] The listed costs do not include solvent, purification materials, energy, or labor.

Compound	Mass	Cost	$/g	Scale of Reaction	Cost in reaction	Overall $/g
tetramethyldiphosphine disulfide	5 g	$123.70	$24.74	25.0 g	$618.50	
tributyl phosphine	100 g	$25.00	$0.25	58.2 g	$14.55	
$/g of tetramethyldiphosphine				14.9 g	$633.05	$42.49
Tetramethyldiphosphine			$42.49	14.9 g	$633.05	
sodium (metal)	100 g	$48.40	$0.48	2.85 g	$1.37	
ammonia (liquid)	170 g	$435.00	$2.56	68.2 g	$174.59	
1,6-dibromohexane	500 g	$76.50	$0.15	15.68 g	$2.35	
$/g of 1,6-bis(dimethylphosphino)hexane[7]				4.840 g	$811.36	$167.63
1,6-bis(dimethylphosphino)hexane			$167.63	4.840 g	$811.36	
14-bromotetradeca-1,3-diene			$12.80	13.47 g	$172.42	
$/g of gemini phosphonium (3)				12.54 g	$983.78	**$78.45**

3.5. References

1. For reviews of cross-linked LLC phases and their applications, see: (a) Gin, D. L.; Gu, W.; Pindzola, B. A.; Zhou, W.-J. *Acc. Chem. Res.* **2001**, *34*, 973. (b) Mueller, A.; O'Brien, D. F. *Chem. Rev.* **2002**, *102*, 727. (c) Gin, D. L.; Lu, X.; Nemade, P. R.; Pecinovsky, C. S.; Xu, Y.; Zhou, M. *Adv. Funct. Mater.* **2006**, *16*, 865.

2. Liu, G.; Ding, J. *Adv. Mater.* **1998**, *10*, 69. (b) Urbas, A. M.; Maldovan, M.; DeRege, P.; Thomas, E. L. *Adv. Mater.* **2002**, *14*, 1850. (c) Wolf, J. H.; Hillmyer, M. A. *Langmuir* **2003**, *19*, 6553. (d) Yang, S. Y.; Ryu, I.; Kim, H. Y.; Kim, J. K.; Jang, S. K.; Russell, T. P. *Adv. Mater.* **2006**, *18*, 709.

3. Meng, Y.; Gu, D.; Zhang, F.; Shi, Y.; Yang, H.; Li, Z.; Tu, B.; Zhao, D. *Angew. Chem. Int. Ed.* **2005**, *44*, 7053. (b) Zhang, F.; Meng, Y.; Gu, D.; Yan, Y.; Yu, C.; Tu, B.; Zhao, D. *J. Am. Chem. Soc.* **2005**, *127*, 13508. (c) Xing, R.; Liu, N.; Liu, Y.; Wu, H.; Jiang, Y.; Chen, L.; He, M.; Wu, P. *Adv. Funct. Mater.* **2007**, *17*, 2455.

4. For a review of cross-linked LLC membranes, see: Gin, D. L.; Bara, J. E.; Noble, R. D.; Elliott, B. J. *Macromol. Rapid Commun.* **2008**, *29*, 367.

5. Kerr, R. L.; Miller, S. A.; Shoemaker, R. K.; Elliott, B. J.; Gin, D. L. *J. Am. Chem. Soc.* **2009**, *131*, 15972.

6. Ichikawa, T.; Yoshio, M.; Hamasaki, A.; Mukai, T.; Ohno, H.; Kato, T. *J. Am. Chem. Soc.* **2007**, *129*, 10662.

7. Zhou, M.; Nemade, P. R.; Lu, X.; Zeng, X.; Hatakeyama, E. S.; Noble, R. D.; Gin, D. L. *J. Am. Chem. Soc.* **2007**, *129*, 9574.

8. Lu, X.; Nguyen, V.; Zeng, X.; Elliott, B. J.; Gin, D. L. *J. Mem. Sci.* **2008**, *318*, 397.

9. Lee, Y.-S.; Yang, J.-Z.; Sisson, T. M.; Frankel, D. A.; Gleeson, J. T.; Aksay, E.; Keller, S. L.; Gruner, S. M.; O'Brien, D. F. *J. Am. Chem. Soc.* **1995**, *117*, 5573.

10. Srisiri, W.; Benedicto, A.; O'Brien D. F.; Trouard; T. P. *Langmuir* **1998**, *14*, 1921.

11. Jeong, S. W.; O'Brien, D. F.; Orädd, G.; Lindblom, G. *Langmuir* **2002**, *18*, 1073.

12. Yang, D.; O'Brien, D. F.; Marder, S. R. *J. Am. Chem. Soc.* **2002**, *124*, 13388.

13. Pindzola, B. A.; Jin, J.; Gin, D. L. *J. Am. Chem. Soc.* **2003**, *125*, 2940.

14. For a review of gemini surfactants, see: Menger, F. M.; Keiper, J. S. *Angew. Chem. Int. Ed.* **2000**, *39*, 1906..

15. Fuller, S.; Shinde, N. N.; Tiddy, G. J. T.; Attard, G. S.; Howell, O. *Langmuir* **1996**, *12*, 1117.

16. In, M.; Zana, R. *J. Dispersion Sci. Techno.* **2007**, *28*, 143.

17. Abe, M.; Tsubone, K.; Koike, T.; Tsuchiya, K.; Ohkubo, T.; Sakai, H. *Langmuir* **2006**, *22*, 8293.

18. Caillier, L.; Taffin de Given, E.; Levy, R.; Vandenberghe, Y.; Geribaldi, S.; Guittard, F. *J. Colloid Interfac. Sci.* **2009**, *332*, 201.

19. The fact that the ammonium monomers **2c** and **2f** form Q_I phases at lower temperatures compared to **1** is entirely serendipitous, but beneficial for processing.

20. The lower permeance may be due to the lower water content of the new membranes (15% vs. 20%), different possible surface effects, and/or lower water diffusivity due to different pore surface chemistry (N^+ vs. P^+).

21. Blanton, T. N.; Huang, T. C.; Toraya, H.; Hubbard, C. R.; Robie, S. B.; Louer, D.; Gobel, H. E.; Will, G.; Gilles, R.; Raftery, T. *Powder Diffr.* **1995**, *10*, 91–95.

22. Hoag, B. P.; Gin, D. L. *Macromolecules* **2000**, *33*, 8549-8558.

23. Ferry, J. D. *Chem. Rev.* **1936**, *18*, 373–455.

24. Gibbins, E.; D' Antonio, M.; Nair, D.; White, L. S.; Freitas dos Santos, L. M.; Vankelecom, I. F. J.; Livingston, A. G. *Desalination* **2002**, *147*, 307–313.

25. Geens, J.; Boussu, K.; Vandecasteele, C.; Van der Bruggen, B. *J. Mem. Sci.* **2006**, *281*, 139–148.

CHAPTER 4

Design of a new, breathable nanoporous barrier material for organic vapor protection via the use of gemini surfactant monomers and cross-linkable v-EPDM blends

4.1. Introduction

Effective personal protection against vapor-phase toxic industrial chemicals (TICs) is of grave importance to workers in industry. One example of a highly effective personal protective barrier material is butyl rubber (BR), which can be cross-linked through the process of vulcanization of the residual alkene units of the polymers.[1,2] Cross-linked shows amazing durability and a high degree of resistance to toxic chemical vapor permeation due to its high degree of interlink density within polymer chains.[2-4] The main drawback to using cross-linked BR for protective garments is the near impermeability of such materials toward respiratory gases and water vapor.[4] The resulting highly ineffective cooling, coupled with excessive workload and warm temperatures, can place the wearer under a heavy thermal burden, leading to heat exhaustion.[4,5] For the outlined application, the ideal characteristics shown by a personal protective garment would be the ability to selectively block toxic agents in the vapor phase, while allowing transport of water and air across the membrane, along with being tactile enough to perform delicate operations when used in hand coverings.[4,5] Recent advances in personal protective garments have utilized functional materials systems, including selectively permeable membranes, as well as reagents or catalysts that break down and neutralize toxic agents.[5]

Two recent approaches toward realizing this type of selectively permeable but tactile material have utilized polymerizable lyotropic liquid crystal (LLC) monomers blended with BR. The first approach utilized a wedge-shaped surfactant monomer with acrylate-terminated tails (**8**) that forms ordered, inverted cylindrical (H_{II}) nanopores in the presence of H_2O and can be

radically cross-linked with BR.[6,7] The resulting H_{II}-phase cross-linked **8**-BR composite exhibited good water vapor transport and high rejections of toxic chemical agents. The nanoporous, aqueous domains of this **8**/BR/H_2O system allowed for enhanced transport of hydrophilic agents across the membrane via the water nanopores, while inhibiting the transport of hydrophobic toxic agents. Supported films of this cross-linked **8**-BR composite with the H_{II} morphology were tested for pure water vapor flux and exhibited a value of 204 g m^{-2} day^{-1}, while similarly treated cross-linked BR showed almost no water flux.[6] Additionally, the **8**-BR composite material afforded a molar selectivity of water vapor to 2-chloroethyl ethyl sulfide (CEES, a toxic organic chemical) that was 20 times greater than that of a neat BR membrane.[6] Despite these positive trends, the absolute water vapor flux for the composite material was still far below the generally accepted value that serves as the standard military requirement.[4] Likewise, the absolute CEES (see Figure 4.8) transport across the membrane was somewhat higher than that observed for pure cross-linked BR.[6] In order to alleviate the issues with water transport across the composite membrane, it was hypothesized that the film should contain bicontinuous morphology with pores aligned uniformly and perpendicular to the surface.[8] The issue with using a H_{II} material for this application is the inability of such material that assumes a polydomain nature to uniformly align along the direction of molecular transport.[8] The ideal morphology would be a 3D-interconnected bicontinuous cubic (Q) phase, which provides optimal pore access, continuity, and does not require physical pore alignment.[9,10] To satisfy this requirement, a 2nd-generation composite membrane based on co-cross-linked **3b**-BR was developed.[11]

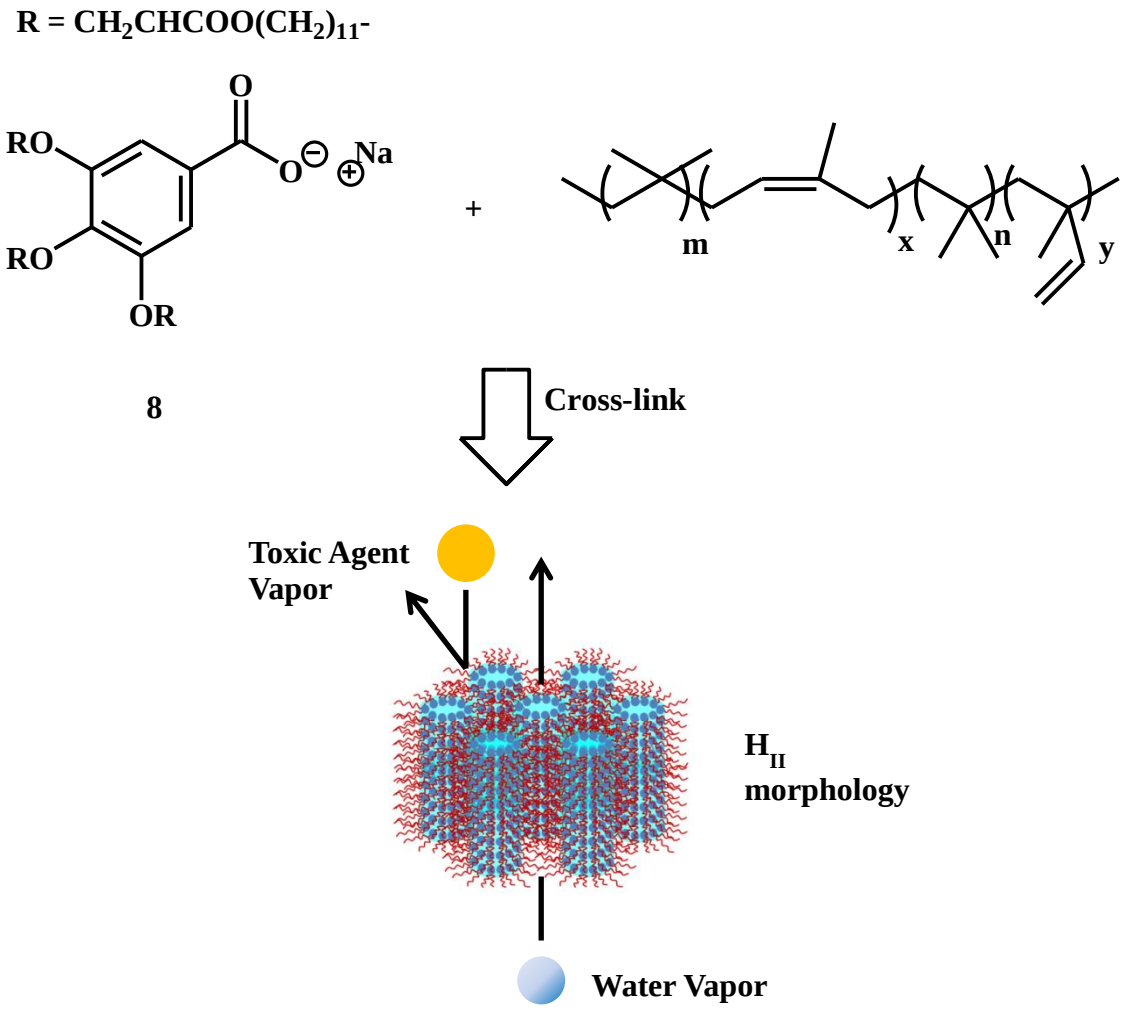

Figure 4.1. Wedge-shaped monomer **8** that forms H_{II}-phase with BR in the presence of water.

The second LLC-based approach took advantage of an inherently cross-linkable gemini phosphonium LLC monomer that was capable of forming a normal (i.e., type I) bicontinuous cubic (Q_I) morphology in the presence of H_2O and could be cross-linked to BR through radical photo-polymerization.[12] This Q_I architecture means that there should always be a continuous pathway from one side of the membrane to the other, without the need for alignment of the material. In order to homogenize a composite blend of surfactant **3b** in water and hydrophobic

BR as a 9.1 wt% mixture in hexanes, alternating hand-mixing and centrifuging was required, while allowing the hexanes to evaporate upon mixing.[12] While initial morphological tests were performed at ambient temperatures using PLM and XRD, the composite material tended to form a lamellar (L) LLC phase.[12] However, subsequent testing at elevated temperatures proved the material to exhibit a broad Q_I phase above 55 °C, as was indicated by the characteristic black optical textures under PLM and a $1/\sqrt{6} : 1/\sqrt{8}$ *d*-spacing ratio observed by powder XRD analysis.[12] An interesting feature observed in this morphological study was that the composition range at which **3b** can form a Q phase with BR and H_2O is much wider (44.7 -76.4 wt%) than in the initial **3b**/H_2O (82–88 wt%).[12] Also, it could tolerate up to 35 wt% of BR at 70 °C before the nanostructure was perturbed. In order to prove homogeneity in these composite samples, films were cross-linked and subjected to testing under an electron microprobe analyzer to determine the distribution of elemental phosphorous, which appeared to be evenly distributed down to at least the 1 μm resolution level.[12]

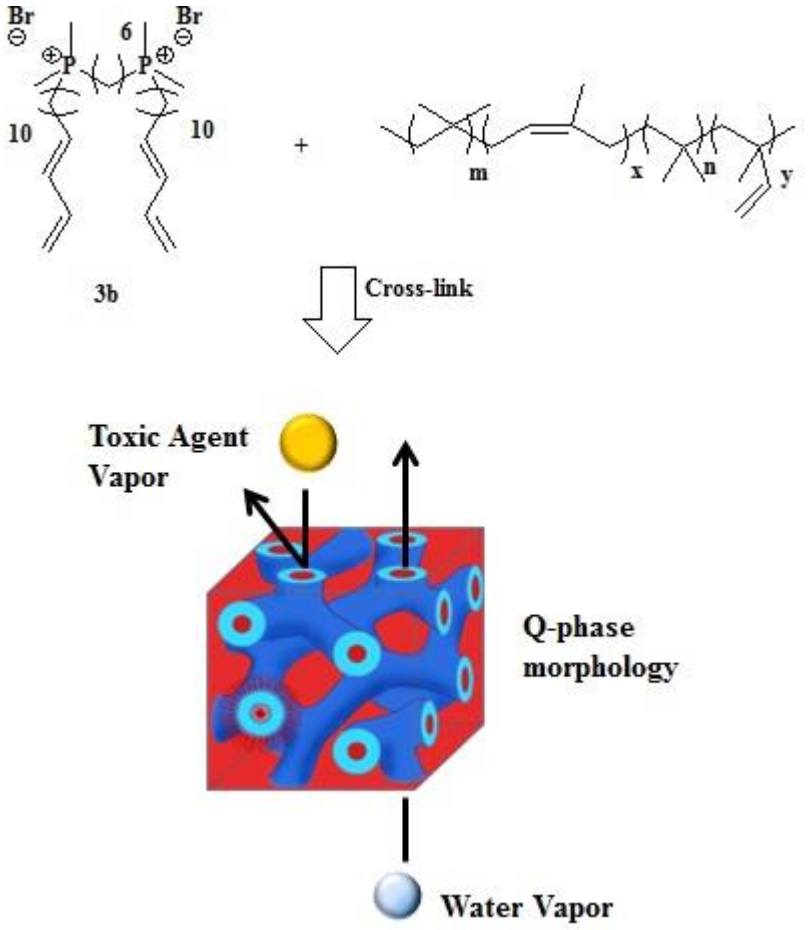

Figure 4.2. Gemini phosphonium LLC monomer **3b** that forms a Q_I phase with BR in the presence of water.

Testing of this composite material for water vapor versus chemical agent vapor permeation required the fabrication of thin films that were devoid of even the smallest defects. In order to attain these types of membranes, a heated hydraulic press was used to fully impregnate the homogenous **3b**/BR/H_2O mixture into a microporous polyethylene support. The melt-infused thin film was then cross-linked, before utilization of PLM and XRD to ensure that the Q phase structure was retained after processing. A summary of the selective vapor transport properties of the supported Q_I-phase membrane formed from 73.9/9.0/16.2/0.9 (w/w/w/w) **3b**/BR/H_2O/photo-

initiator can be found in Table 4.1.[12] In general, the resulting cross-linked composite membrane exhibits a thickness-normalized water vapor flux of (5.9 ± 0.3) x 10^3 g m^{-2} day^{-1}, which meets military specifications,[4] and is nearly 300 times higher than the thickness-normalized water vapor flux of vulcanized BR fabricated on the same support. Similarly, the absolute CEES vapor penetration was measured to be (2 ± 1) x 10^1 g m^{-2} day^{-1} μm, which is slightly lower than that observed for cross-linked BR.[12] Putting this data together affords a vapor-phase H_2O/CEES molar selectivity of (1.5 ± 0.1) × 10^2, showing a 500 times increase over the molar selectivity observed for cross-linked BR.[12] These values represent vast improvements over the commercial BR gloves that are currently employed for chemical protection at the U.S. Army Research Laboratories.[4]

Table 4.1. The thickness-normalized water vapor flux, thickness-normalized CEES vapor flux, and molar selectivity results for a supported Q-phase **3b**/BR/H_20/photo-initiator membrane compared to pure cross-linked BR, a H_{II} **8**-BR membrane, and **3b**-BR membrane formed at RT, all generated at the same 73.9/9.0/16.2/0.9 (w/w/w/w) composition.[12]

Membrane	**Morphology**	**Thickness-normalized Water Vapor Flux (g m^{-2} day^{-1} μm)**	**Thickness-normalized CEES Vapor Flux (g m^{-2} day^{-1} μm)**	**Molar Selectivity (H_2O/CEES)**
3b/BR	Q_I phase	(5.9 ± 0.3) x 10^3	(2.86 ± 0.05) x 10^2	(1.5 ± 0.1) x 10^2
Pure BR	Amorphous	(0.2 ± 0.1) x 10^2	(4.2 ± 0.6) x 10^2	0.3 ± 0.2
8/BR	H_{II} phase	(3.5 ± 0.4) x 10^2	(2.5 ± 0.3) x 10^2	9 ± 2
3b/BR	L phase	(4.5 ± 0.1) x 10^3	(8.8 ± 0.2) x 10^2	37 ± 6

Despite the advances made by this 2nd-generation Q_I-phase material based on **3b**-BR over the previous H_{II}–phase **8**-BR-based material, several improvements need to be made before this can be developed into a potentially viable toxic chemical agent protective garment. Due to the fact that cross-linked LLC-BR blends form a dense, non-tactile material, the choice of cross-

linkable co-polymer and LLC monomer needs to be analyzed so that it yields a flexible membrane that affords the wearer a higher level of dexterity. Using a gemini phosphonium monomer such as **3b** for the LLC monomer for this application provides a very expensive, synthetically demanding target that cannot be scaled up industrially. The ideal LLC monomer for this application should be synthesized in a more facile fashion from precursors that are most cost-effective than those used to synthesized the gemini phosphonium derivative. Herein, we explore the use of two new, more easily synthesized, more economical Q_I-phase-forming gemini LLC monomers to blend and cross-link with commercial polymerized vinyl-(ethylene-propylene-diene monomer) (i.e., v-EPDM polymer) a radically cross-linkable hydrocarbon polymer that can be generated with tailored amounts of vinyl side-chains for different degrees of cross-linking. Using these new Q_I-phase LLC monomers with v-EPDM offered the possibility for generating a nanoporous composite with the desired membrane properties and more tactile mechanical properties

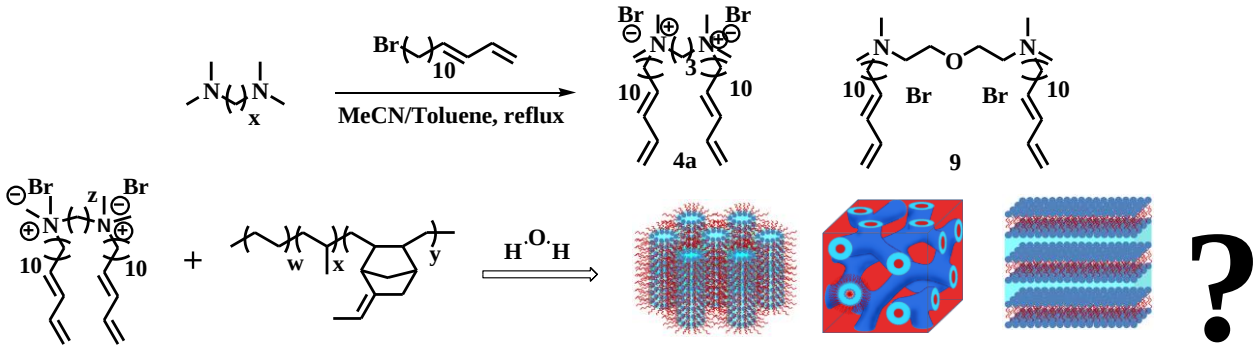

Figure 4.3. Synthesis of monomers used in LLC-EPDM blending study, as well as the general structure of v-EPDM. The goal of this project is to blend gemini ammonium monomers **4a** and **9** with EPDM polymer, in the presence of water, and induce LLC phase formation.

4.2. Experimental

4.2.1. Materials

Chromium (IV) oxide, pyridine, allyltrimethylsilane, *sec*-butyl lithium (1.4 M in cyclohexane), aluminum oxide (activated, basic), 2-isopropoxy-4,4,5,5-tetramethyl-1,3,2-dioxaborolane, *N,N,N',N'*-tetramethylpropane-1,3-diamine, *N,N,N',N'*-tetramethylhexane-1,6-diamine, bis[2-(*N*,*N*-dimethylamino)-ethyl] ether, and 2-hydroxy-2-methylpropiophenone were obtained from Sigma-Aldrich Co. and used as purchased. 11-Bromo-1-undecanol was obtained from Fluka and used as purchased. All solvents were purchased from Sigma-Aldrich or Fisher Scientific, and purified/dehydrated via N_2-pressurized activated alumina columns, unless otherwise noted. All chemical syntheses were carried out under a dry argon atmosphere using standard Schlenk line techniques, unless otherwise noted. Filtration through silica gel was performed using 230–400 mesh, normal-phase silica gel purchased from Sorbent Technologies. The water used in LLC phase formulation and water filtration experiments was de-ionized, and had a resistivity of >12 MΩ cm^{-1}. Solupor E075-9H01A microporous support membrane (made from hydrophilically treated, ultrahigh-molecular-weight polyethylene (PE) fiber matte) was provided by DSM Solutech (Geleen, The Netherlands). Mylar sheets were purchased from American Micro Industry, Inc. v-EPDM (Batch No: DE82700C, stabilized with 750 ppm octadecyl-3,5-di-(*tert*)-butyl-4-hydroxyhydrocinnamate) was purchased from Royal DSM and purified to eliminate the particulates in the polymer prior to use.

4.2.2. Instrumentation

^{1}H NMR spectra were obtained using a Bruker 300 Ultrashield^{TM} (300 MHz) spectrometer, Varian Inova 500 (500 MHz), or Inova 400 (400 MHz) spectrometers. Chemical shifts are

reported in parts per million, relative to deuterated solvent. Fourier-transform infrared spectroscopy (FT-IR) measurements were performed using a Matteson Satellite series spectrometer, as thin films on Ge crystals. HRMS analysis was performed by the Central Analytical Facility in the Dept. of Chemistry and Biochemistry at the University of Colorado, Boulder. LLC mixtures were homogenized using an IEC Centra-CL2 centrifuge. Powder X-ray diffraction (XRD) spectra were obtained with an Inel CPS 120 diffraction system using a monochromated Cu K_α radiation source. The apparatus was equipped with a film holder and temperature-programmable heating stage to analyze samples. All powder XRD spectra were calibrated against a silver behenate diffraction standard (d_{100} = 58.4 ± 0.1 Å).[1] Powder XRD measurements were all performed at ambient temperature (22 ± 1 °C). Variable temperature polarized light microscopy (PLM) studies were performed using a Leica DMRXP polarizing light microscope equipped with a Q-Imaging MicroPublisher 3.3 RTV digital camera, a Linkam LTS 350 thermal stage, and a Linkam CI 94 temperature controller. Automatic temperature profiles and image captures were performed using Linkam Linksys32 software. Images were captured at 125x magnification. Photopolymerization of membranes was conducted using a Spectroline XX-15A 365 nm UV lamp (8.5 mW cm^{-2} at the sample surface) and a custom-made temperature controlled hot stage. UV light fluxes at the sample surface were measured using a Spectroline DCR-100X digital radiometer equipped with a DIX-365 UV-A sensor. A Carver model C manual press equipped with a digitally temperature-controlled Carver 3796 heated platen set was used to manufacture membrane samples.

4.2.3. Synthesis

4.2.3.1 14-Bromotetradeca-1,3-diene[13]

Synthesized as described in the literature.[13] Spectroscopic characterization and purity data for this compound matched published data.[13]

4.2.3.2. 1,3-Bis(tetradeca-11,13-dienyl-*N*,*N*,*N*',*N*'-tetramethylammonium)propane dibromide (4a)

N,*N*,*N*',*N*'-Tetramethyl-1,3-propanediamine (1.62 g, 12.4 mmol, 100 mol%) and 14-bromotetradeca-1,3-diene (7.16 g, 26.2 mmol, 211 mol%) were dissolved in toluene (10 mL) and acetonitrile (10 mL) in a 50-mL round-bottom flask equipped with a stir bar and a reflux condenser. The clear, colorless solution was heated with stirring to 82 °C for 15 h. The white precipitate that formed after cooling to 0 °C using an ice water bath was filtered and washed with hexanes (2 x 50 mL), affording a white powder (7.0 g, 87%). 1H NMR (300 MHz, $CDCl_3$): δ 6.32 (dt, *J* = 10.2, 17.2, 2H), 6.03 (dd, 2H), 5.72 (dd, *J* = 7.2, 14.8, 2H), 5.09 (d, *J* = 0.6, 2H), 4.96 (d, 2H), 3.96 (t, 4H), 3.56 – 3.43 (m, 4H), 3.36 (s, 12H), 2.81 (t, 2H), 2.07 (m,4H), 1.75 (m, 8H), 1.32 (m, 24H). 13C NMR (75 MHz, CDCl3): δ 137.48, 135.67, 131.00, 114.75, 66.88, 61.19, 51.42, 32.67, 29.54, 29.42, 29.36, 29.30, 26.45, 23.11, 19.12. IR (thin film, MeOH): 3437, 2933, 2856, 2094, 1801, 1604, 1651, 1487, 1470, 1003, 951, 899, 723, 650 cm^{-1}. HRMS (ES) calcd. for $C_{35}H_{68}BrN_2$ (M+ M+ Br–): 595.4560; observed: 595.4547.

4.2.3.3. 1,1'-(Oxydi-2,1-ethanediyl)bis[3-(tetradeca-11,13-dienyl)*N*,*N*,*N'N'*-tetramethylammonium] dibromide (9)

Bis[2-(*N*,*N*-dimethylamino)-ethyl] ether (0.88 g, 5.49 mmol, 100 mol%) and 14-bromotetradeca-1,3-diene (3.30 g, 12.1 mmol, 218 mol%) were dissolved in toluene (20 mL) and

acetonitrile (20 mL) in a 50-mL round-bottom flask equipped with a stir bar and a reflux condenser. The clear, colorless solution was heated with stirring to 82 °C for 66 h. The white precipitate that formed after cooling to -40 °C was filtered and washed with hexanes (2 x 50 mL), affording a white powder (4.9 g, 90%). ^{1}H NMR (300 MHz, $CDCl_3$) δ 6.42 – 6.18 (m, 2H), 6.12 – 5.93 (m, 2H), 5.70 (dd, *J* = 14.8, 7.3 Hz, 2H), 5.15 – 5.00 (m, 2H), 4.93 (dd, *J* = 10.1, 1.8 Hz, 2H), 4.47 – 4.25 (m, 4H), 4.16 – 3.88 (m, 4H), 3.75 – 3.55 (m, 4H), 3.45 (s, 12H), 2.14 – 1.95 (m, 4H), 1.70 (s, 4H), 1.50 – 0.97 (m, 28H). ^{13}C NMR (300 MHz, $CDCl_3$) δ 137.45, 135.67, 130.97, 114.72, 66.03, 64.75, 64.17, 51.81, 32.65, 29.55, 29.53, 29.44, 29.28, 26.44, 23.05. IR (neat powder): 3020, 2953, 2921, 2852, 1600, 1467, 1357, 1131, 1004, 950 cm^{-1}. HRMS (ES) calcd. for $C_{36}H_{70}Br_2N_2O$ $(MBr)^+$: 625.4667; observed: 625.4678.

4.2.4. Preparation of v-EPDM/hexanes solution

v-EPDM) (17.01 g) was weighted out into a 250-mL Erlenmeyer flask equipped with a stir bar. The structure of v-EPDM can be found in Figure 4.4. Hexanes (153.1 g) was added to the flask, and the solution was stirred with gentle heating (35 °C) for 16 h., affording a suspension that was optically opaque and in which visible particulates were suspended. This ~ 10 wt% mixture of v-EPDM/hexanes was then diluted to ~ 2 wt% using excess hexanes, and the resulting liquid suspension was filtered through a piece of Whatman qualitative filter paper. The still opaque filtrate was collected and run through a fresh piece of Whatman qualitative filter paper 3 more times. The resulting filtrate was visibly clear and free of residual particulates. The clear, colorless filtrate was then transferred to a 500 mL round-bottom flask and concentrated until the solution was determined to be 9.44 wt% EPDM in hexanes. This solution was used for all phase diagram work reported on monomers **4a** and **9**. Due to the high volatility of hexanes, the

concentration of v-EPDM in solution was calculated every morning that LLC/v-EPDM samples were evaluated via polarized light microscopy (PLM), to ensure that the appropriate amount of v-EPDM was added to each LLC-water sample.

4.2.5. Preparation and characterization of LLC/v-EPDM mixtures and phase diagram analysis

4a/v-EPDM/H_2O and **9**/v-EPDM/H_2O composites were prepared by initially homogenizing the LLC monomers in water. This procedure involved weighing out the appropriate masses of monomer and water into a custom-made glass vial, sealing the vial with Parafilm, and centrifuging (3500 rpm, 15 min). The LLC/water sample was then fully homogenized through a process of hand-mixing for ca. 5 min at ambient temperature. At that point, the appropriate volume of a 9.44 wt% v-EPDM/hexanes solution was added to the LLC mixture contained in the glass vial. Hand-mixing utilizing a metal spatula commenced, allowing the hexanes to evaporate throughout the mixing process. LLC/water mixture was incorporated into the aforementioned v-EPDM/hexanes solution, until the solution began to appear opaque and stiffen. Mixing was considered thorough when the vapors of hexanes no longer wafted out of the glass vial. It was found very difficult to homogenize samples under these conditions. Most samples exhibited phase separation upon visual inspection. There was much difficulty found incorporating the v-EPDM polymer into the LLC/water matrix, due to the inherent immiscibility of an extremely hydrophobic polymer and a water-based surfactant matrix.

The LLC phase morphology of each LLC/v-EPDM/H_2O mixture was determined using PLM analysis followed by structure confirmation of each identified separate phase region using powder XRD. In this process, PLM samples were first prepared by pressing specimens of each

different composition between microscope cover-slips. All phase diagram work was performed at ambient temperature, after annealing each sample to 85 °C, then cooling to room temperature. The optical texture and phase of each specimen was recorded, and the identity of each homogeneously mixed sample was then confirmed by XRD through analysis of one composition point sample in each distinct phase region that was observed using PLM. Specimens that were analyzed using XRD were prepared by mixing the appropriate composition of LLC/v-EPDM with 1 wt% photo-initiator (PI), and polymerizing the sample between the glass cover-slips that were used for PLM analysis using 365 nm UV light. The polymerized sample was then extracted from the cover-slips and analyzed using XRD. A few representative PLM images, as well as the XRD profile and PLM image for a L phase blend are shown in Figure 4.4. This L phase was isolated only on one occasion, and could not be reproduced upon further analysis. The ternary phase diagrams of the LLC behavior of **4a**/v-EPDM/H_2O and **9**/v-EPDM/H_2O are shown in Figure 4.5. A poly-crystalline phase was seen for all EPDM compositions in all samples mixed with monomer compositions higher than 95/5 (w/w) **4a**/H_2O. All samples containing **4a**/H_2O at a lower monomer concentration than 65/35 (w/w) were seen as fluid isotropic materials at ambient conditions. The crystalline phase was observed for all specimens with monomer concentrations higher than 92.5/7.5 (w/w) **9**/H_2O. All samples of **9**/H_2O mixed with a lower monomer composition than 61/39 (w/w) were determined to be a fluid isotropic phase at ambient conditions.

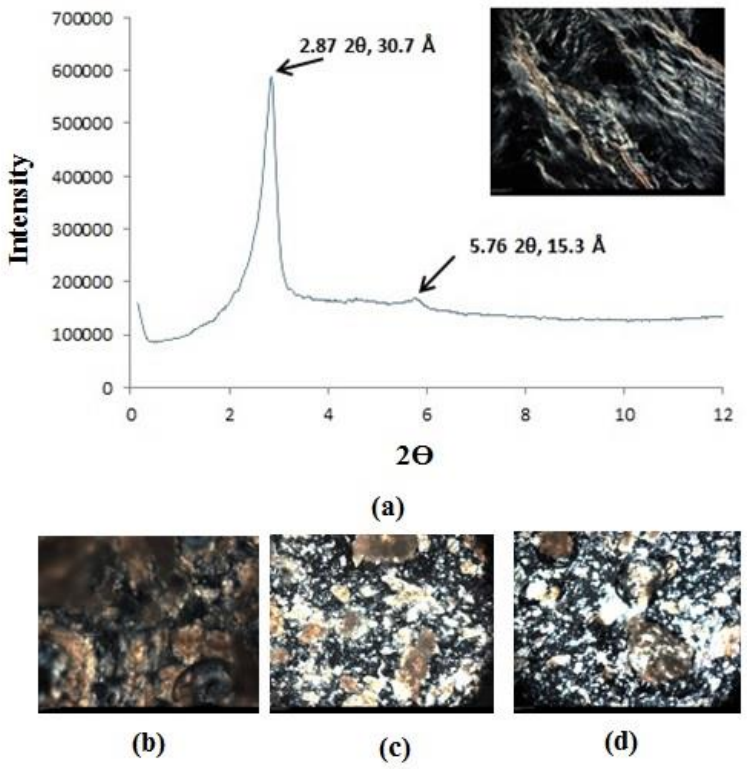

Figure 4.4. (a) PLM image and powder XRD profile of a sample containing 60.3/10.6/28.4/0.7 (w/w/w/w) **4a**/H_2O/v-EPDM/photo-initiator that exhibited a L phase. This was isolated only once, and could not be reproduced. (b) PLM image showing inhomogeneity in a sample containing 58.1/6.5/35.4 (w/w/w) **4a**/H_2O/v-EPDM. (c) PLM image showing inhomogeneity in a sample containing 47.4/5.3/47.3 (w/w/w) **9**/H_2O/v-EPDM. (d) PLM image showing sample inhomogeneity for a specimen containing 43.4/9.2/47.4 (w/w/w) **9**/H_2O/v-EPDM.

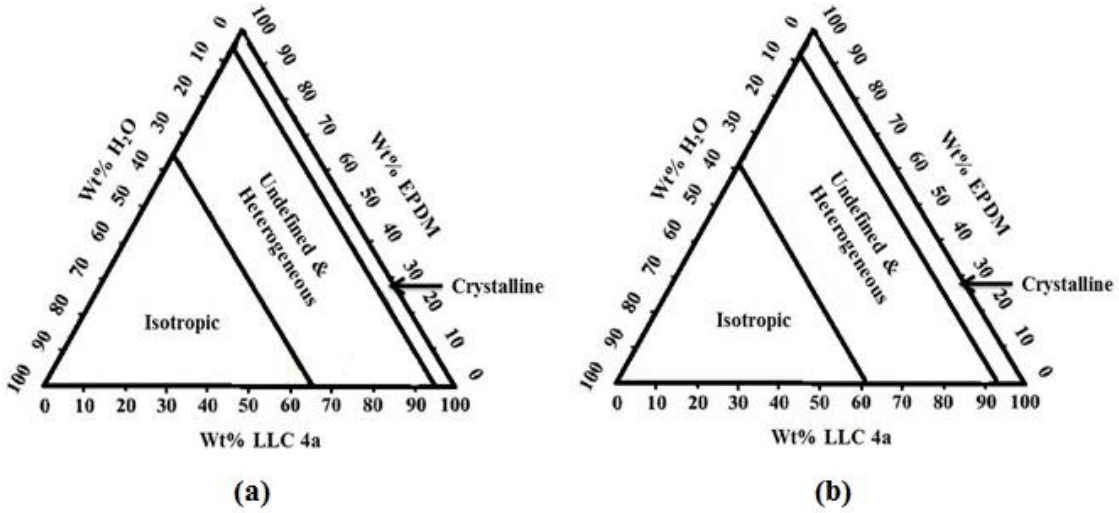

Figure 4.5. (a) Ternary phase diagram for **4a**/H_2O/v-EPDM. (b) Ternary phase diagram for **9**/H_2O/v-EPDM. Both of these were recorded at ca. 620 mm Hg and 22 ± 2 °C.

4.2.6. Fabrication of supported membrane of 4a/v-EPDM/H_2O.

All supported test membrane fabrication and TICs vapor permeation analysis work was performed at TDA Research, Inc., located in Wheat Ridge, CO. A small amount of LLC/v-EPDM (unidentified phase) sample containing 42/7.5/50/0.5 (w/w/w/w) **4a**/H_2O/v-EPDM/photo-initiator was first placed on a swatch of Solupor® E075-9H01A polymer support membrane. This specimen was then sandwiched between Mylar sheets and placed between two aluminum platens. The full set-up was placed onto a hydraulic press assembly at room temperature (24 ± 1 °C). Pressure on the hydraulic press was held at 3 tons force for 2 min, allowing the specimen to soak slowly into the pores of the support material before increasing the pressure to 12 tons of force, and holding for 10 min. This high pressure processing afforded a supported LLC/v-EPDM/H_2O membrane that was fully infused throughout the thickness of the Solupor® support. The resulting fully infused membrane (still kept between Mylar sheets to help minimize water

vapor loss) was then irradiated with 365 nm UV light (ca. 200 mW cm^{-2} at the sample surface) for 1 hr. to fully cross-link the membrane, and fix the ordered architecture. The LLC character of this cross-linked, supported film was confirmed using XRD. A picture of a representative membrane can be seen in Figure 4.6 below. The LLC/v-EPDM/H_2O blend is seen as the circular discoloration in the middle of the square support. Several membranes were fabricated for the water permeation testing, each of which kept the relative concentrations of LLC/H_2O (85/15) (w/w) consistent, while varying the percentage of added v-EPDM polymer. All samples membranes were generated using 1 wt% (compared to mass of total LLC/H_2O/v-EPDM mixture) of 2-hydroxy-2-methylpropiophenone as photo-initiator.

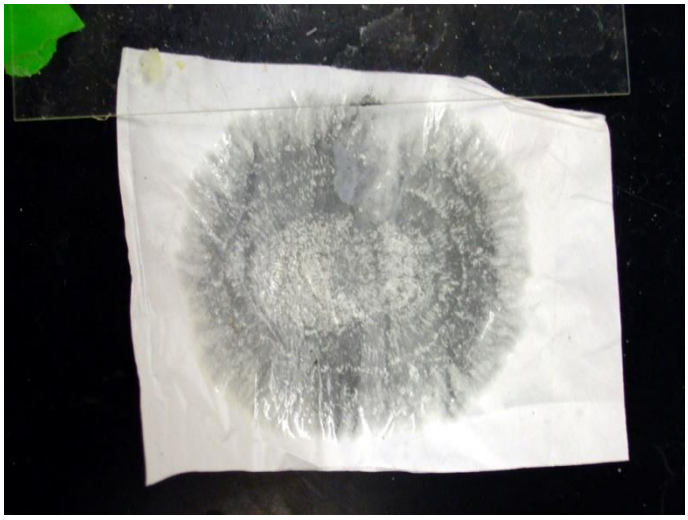

Figure 4.6. LLC/v-EPDM/H_2O blend that has been fully infused into a Solupor® support membrane. The sample shows some inhomogeneity from visual inspection, as well as no discernible LLC phase via XRD characterization.

4.2.7. Fabrication of supported membrane consisting of neat v-EPDM

All membrane fabrication work was performed at TDA Research, Inc., located in Wheat Ridge, CO. EPDM/hexanes solution was prepared via the method described above. An aliquot

of this solution containing about 200 mg of EPDM was dried by hand stirring in air and placed on a piece of Solupor® support membrane. The Solupor® support was then place between two Mylar sheets and sandwiched between aluminum plates, then placed on a hydraulic hot press. The plates were pre-heated to 60 °C, before application of 5 tons of force for 20 minutes, which infused the polymer completely throughout the entire Solupor® support.

4.2.8. Fabrication of supported membrane consisting of neat LLC

All membrane fabrication work was performed at TDA Research, Inc., located in Wheat Ridge, CO. A supported Q_I-phase polymer membrane of **4a** was fabricated using a hot-pressing method. A monomer gel was prepared containing a 84/15/1 (w/w/w) composition of **4a**/H2O/photo-initiator and a small aliquot (100 mg) was place on a swatch of Solupor® support membrane, before sandwiching between Mylar sheets to prevent evaporation. The sample was then transferred between two aluminum platens, then transferred to a heated hydraulic press. The hot press was heated to 60 °C prior to applying 5 tons of force for 10 minutes, which infused the monomer gel throughout the entire depth of the Solupor® support. After it was fully infused into the support, the LLC sample was transferred to a hot-stage equipped with a 365 nm UV light source, and irradiated for 1 hour to radically photo-cross-link the Q_I architecture.

4.2.9. Water permeation testing and analysis of fabricated supported v-EPDM, supported LLC, and LLC/v-EPDM blend membranes

All water permeation testing and analysis performed at TDA Research, Inc., located in Wheat Ridge, CO. All fabricated membranes were tested in a custom-made stainless steel test cell with inlet and outlet gas ports on each side of the sample. This set-up utilized both a feed

gas stream containing the chemical contaminant of interest, and a sweep stream. Both of these streams were humidified with water ranging from 0 to 100% relative humidity (R.H.) at room temperature. Water vapor and the chemical contaminant were introduced into the stream by bubbling pure, dry air through liquid columns of the contaminant or water. The R.H. was controlled by mixing a 100% R.H. air stream with a 0% R.H. air stream until the appropriate humidity was reached. The pressure across the test sample membrane was measured and controlled by adjusting gas flow rates using flow controllers. Activated carbon traps were used to absorb chemical contaminant and water vapors. Humidity probes were used to measure the water vapor going into and out of the test cell on both the feed and sweep sides, while chloroform was used to extract the adsorbed chemical contaminant, before quantification via gas chromatography.

4.3. Results and discussion

For this project, the important issues from the previous gemini phosphonium LLC monomer/BR system that need to be overcome are (1) design of a new monomer system that can form LLC phases in the presence of v-EPDM and is less costly and more easily synthesized than the previous LLC system, (2) design a polymer/monomer blend material that is more tactile and allows for more dexterity than LLC/BR composite materials, and (3) generate a composite co-cross-linked polymer material that still exhibits high tolerance toward and rejection of toxic industrial chemical gases.

4.3.1. Use of gemini ammonium surfactants

The new gemini ammonium monomers, **4a** and **9**, utilized for this work were developed from inexpensive, commercially-available ammine-based precursors that require no synthetic work to produce. The new monomers can be produced via a straight-forward, high-yield S_N2 reaction between 14-bromo-1,3-diene tails and these commercial diamines. The cost benefit of using gemini ammonium-based LLC monomers over analogous phosphonium monomers was previously discussed in Chapter 3.

Monomer **4a** was initially chosen because of its ability to form a robust bicontinuous cubic phase in water. The goal is to form a Q_I LLC phase in the presence of water and v-EPDM, and a good starting point is to begin with a monomer that forms a Q_I phase in the solvent of interest and then add in small amounts of co-polymer, hoping not to disrupt the LLC phase.

4.3.2. Choice of v-EPDM as cross-linkable co-polymer

v-EPDM was chosen as the co-polymer because it is one of the few commercially available elastomers that is radically cross-linkable, due to its pendant vinyl groups with a density that can be tailored during synthesis[14]. When cast and cross-linked into a neat membrane, v-EPDM (depending on its pendant vinyl group density) affords the kind of tactility and dexterity that is required for sensitive work, such as working with toxic industrial chemicals.

4.3.3. Water vapor transport results for 4a/v-EPDM composite

Using the above described method, three different membranes were tested to determine the effect of LLC/v-EPDM architecture on water vapor transport rate vs. that demonstrated by the uncoated Solupor® support and neat v-EPDM. The porous, pristine Solupor® support

membrane exhibited an exceptionally high water vapor transport rate (or flux) of 2.54 x 10^4 g m^{-2} day^{-1}, whereas the hydrophobic polymer v-EPDM demonstrated water vapor flux that was below the lower detection limit of the experimental apparatus (< 4.00 g m^{-2} day^{-1}). Under identical experimental conditions, the membrane fabricated from a mixture of 42/7.5/50/0.5 (w/w/w/w) LLC/H_2O/v-EPDM/photo-initiator on a Solupor® support exhibited a water vapor flux of 5.72 x 10^3 g m^{-2} day^{-1}, a value which is within the experimental error range found for the previous system (see Table 4.1). A summary of these results can be found in Table 4.2.

Table 4.2. Water vapor flux results for the membranes fabricated from pure v-EPDM and Solupor®, as well as a comparison of results between the current **4a**/v-EPDM and **3b**/BR composite systems.

Membrane	Water Vapor Flux
Pure EPDM	<4.00 g m^{-2} day^{-1}
Solupor®	2.54 x 10^4 g m^{-2} day^{-1}
3b/BR Composite	5.90 x 10^3 g m^{-2} day^{-1}
4a/EPDM Composite	5.72 x 10^3 g m^{-2} day^{-1}

Analysis of the above results shows that the membrane consisting of pure hydrophobic v-EPDM acted as a nearly impermeable barrier to water vapor under standard cross-flow conditions, while the pristine Solupor® support membrane exhibited the highest water vapor transport rate of any of the trials, due to its structured, open microporous architecture. The composite membrane of **4a**/v-EPDM/H_2O exhibited a water vapor flux that is nearly four times the accepted value for a breathable protective material based on U.S. Army guidelines[4].

Although the new composite system had a mixed LLC phase, it performed as well as the previous system that was based on the co-cross-linked Q_I-phase gemini phosphonium polymerizable LLC monomer **3b** and BR composite in terms of water vapor transport rate. This

rather surprisingly result can be attributed to several factors. First, the co-polymers used in each study are both extremely hydrophobic, leaving very little room for differentiation between these variables in each system. Likewise, utilizing hydrophilic domains (i.e., porous architectures where the nanopores are filled with H_2O) that are formed from LLC monomers are employed in both systems. Fabricating a membrane with the same type of porous domain leads to the same mechanism of transport for water vapor. Two variables that are harder to analyze under this scenario are the roles played by effective pore size of the membrane, as well as the comparative compositions of LLC : H_2O : co-polymer. Pore size should be seen to have a dramatic effect on water transport, as is evident by the difference in these values between RO and NF membranes[15], as well as between a supported membrane fabricated from **4a** and one from **3b**.[12] In this study and the previous study, it was not possible to determine the pore size of the composite membrane, because not enough data was provided. We can, however, begin to make assumptions as to the role that component compositions play in these composite systems. The previous membrane that was fabricated from a complex mixture consisting of 73.9/9.0/16.2/0.9 (w/w/w/w) **3b**/BR/H_2O/photo-initiator contained a higher overall proportion of hydrophobic polymer than did the 42/7.5/50/0.5 (w/w/w/w) LLC/H_2O/v-EPDM/photo-initiator composite system. However, the percentage of co-polymer in each composite should not be seen to affect the water vapor transport rate, because it should be contained in the hydrophobic domains of the membrane, not the hydrophilic domains (through which the water vapor is actually transported), unless it changes the pore size of the material.

4.3.4. TICs vapor transport results for 4a/v-EPDM composite

The toxic chemical vapor rejection ability of the composite membrane of **4a/**v-EPDM towards certain TICs and chemical agent simulants was performed at TDA Research, Inc. Unfortunately, the types of TICs and challenge vapors tested, as well as the vapor transport rate results are restricted from open publication because of International Trade in Arms Regulations (ITAR) considerations associated with the Department of Defense grant that funded this work. The only generalization about the results that we can include in this thesis chapter is that the test membranes showed excellent water vapor fluxes, while simultaneously acting as an excellent toxic organic chemical barrier. Additional results are available to U.S. government persons by referencing Army SBIR contract # W911NF-09-C-0108.

4.4. Summary

In summary, blended specimens consisting of new LLC monomer/H_2O/v-EPDM were evaluated at ambient conditions for their LLC characteristics. It was found that only one sample, 60.3/10.6/28.4/0.7 (w/w/w/w) **4a**/H_2O/v-EPDM/photo-initiator, exhibited a distinguishable LLC phase (hexagonal), but it was not possible to reproduce this data point upon further analysis. All other samples appeared to be phase-separated/heterogeneous upon thorough mixing. Representative supported composite membranes were fabricated from **4a** and v-EPDM, in which the composition of LLC:H_2O was kept consistent, and the amount of v-EPDM in the composite was varied systematically. These composite membranes showed water vapor transport characteristics that lay between those observed in the support membrane by itself, and a supported pure v-EPDM membrane. All membranes were tested rejection of a toxic industrial chemical under varying relative humidity conditions, and it was seen that the membrane that

performed the best consisted of 42.5/7.50/49.0/1.0 (w/w/w/w) **4a**/H_2O/v-EPDM/photo-initiator. This membrane showed an intermediate thickness-normalized water vapor flux, which was still higher than the U.S. Army guidelines for a breathable barrier membrane, as well as the best toxic agent rejection. This material should be seen as a promising membrane for selective vapor transport for protection from and remediation of toxic industrial chemicals.

4.5. References

1. Abbott, N. J. *Coatings Technology Handbook, 2nd Ed*. Satas, D.; Tracton, A. A., Eds.; Marcel Dekker: New York, 2001; pp 819.

2. Kresge, E.; Wang, H.C. *Kirk-Othmer Encyclopedia of Chemical Technology, 4th Ed*. Wiley: New York, 1993; pp 934.

3. Nagano, H. *Exxon Butyl Rubber Compounding and Applications*, Exxon Chemical Japan Polymers Technical Center, Yokohama, Japan, 2001.

4. Wartell, M. A.; Kleinman, M. T.; Huey, B. H.; Duffy, L. M. *Strategies to protect the health of deployed U.S. forces: Force protection and decontamination*, National Academy Press: Washington, DC, **1999**; pp 67.

5. Schreder-Gibson, H.L.; Truong, Q.; Walker, J. E.; Owens, J.R.; Wander, J. D.; Jones, Jr., W. E. *MRS Bull*. **2003**, *28*, 574.

6. Jin, J.; Nguyen, V.; Gu, W.; Lu, X.; Elliott, B. J.; Gin, D. L. *Chem Mater*. **2005**, *17*, 224.

7. Elliott, B. J. *US Patent 7090788*, **2006**.

8. Zhou, M.; Kidd, T. J.; Noble, R. D.; Gin, D. L. *Adv. Mater*. **2005**, *17*, 1850.

9. Fontell, K. *Colloid Polym. Sci.* **1990**, *268*, 264.

10. Mariani, P.; Luzzati, V.; Delacroix, J. *J. Mol. Biol.* **1988**, *204*, 165.

11. Pindzola, B. A.; Jin, J.; Gin, D. L. *J. Am. Chem. Soc*. **2003**, *125*, 2940.

12. Lu, X.; Nguyen, V.; Zhou, M.; Zeng, X.; Jin, J.; Elliott, B. J.; Gin, D. L. *Adv. Mater*. **2006**, *18*, 3294.

13. Pindzola, B. A.; Hoag, B. P.; Gin, D. L.; *J. Am. Chem. Soc.*, **2001**, *123*, 4617.

14. Budinski, K. G.; Budinski, M.; K. *Engineering Materials: Properties and Selection*, 7th ed.; Prentice Hall: Englewood Cliffs, 2002; pp 752.

15. Gin, D. L.; Bara, J. E.; Nobel, R. D.; Elliott, B. J. *Macromol. Rapid Commun*. **2008**, *29*, 367.

CHAPTER 5

A glycerol-based bicontinuous cubic lyotropic liquid crystal monomer system for the fabrication of thin-film membranes with uniform nanopores

(Manuscript published under the same title in *Chemistry of Materials* **2012,** *24,* 4005-4007, co-authored with Carter, B. M.; Hatakeyama, E. S.; Barton, J. L.; Noble, R. D.; Gin, D. L.)

Abstract

A glycerol-based, type I bicontinuous cubic lyotropic liquid crystal monomer system has been developed that allows facile solution fabrication of thin-film composite membranes with 3D-interconnected, ionic nanopores. These membranes have a ca. 3-μm-thick top layer with uniform, 0.96-nm-wide, cationic pores that size-exclude uncharged solutes from water. They also reject smaller hydrated salt ions near or at the level of reverse osmosis (RO) membranes (>98%) due to (cationic pore–metal ion) repulsive interactions, making this material quite unique in terms of its water purification performance. It also has a thickness-normalized pure water permeability comparable to active layer materials in RO membranes.

5.1. Introduction

Lyotropic liquid crystal (LLC) networks are nanoporous polymer materials formed by the in situ cross-linking of reactive amphiphiles (i.e., surfactants) that self-organize in water or other polar solvents into ordered, phase-separated assemblies.[1] They contain periodic, *uniform-size,* nanoscale solvent regions/pores (i.e., ≤1 to 10 nm) that have different possible geometries and are lined by the amphiphile headgroups, thus allowing for pore control and functionalization.[1]

Because of these features, LLC networks have been shown to be valuable for many applications.[1a,c]

One important application area where LLC networks have been found to have great potential is membrane-based water purification/desalination.[2] The ability of cross-linkable LLC systems to generate polymers with monodisperse, sub-1-nm, aqueous pores enables the removal of molecular contaminants from water (0.27 nm diameter) with high selectivity.[3] Also, the ability of LLCs to access different nanopore geometries and produce materials with high pore density is essential for high water filtration throughput (i.e., flux).[3] In particular, bicontinuous cubic (Q) LLC networks have been found to be the most desirable for this application.[2] In addition to high pore density, Q phases have 3D-interconnected nanopores that do not require alignment for high throughput, unlike those in lower-dimensionality LLC phases (i.e., the 1D cylindrical hexagonal (H) and 2D lamellar (L) phases).[2] Q phases are classified as type I (i.e., normal) or type II (i.e., inverted) depending on whether the hydrophilic-hydrophobic interface curves away or towards the water regions.[1]

Recently, we showed that water nanofiltration (NF) membranes based on cross-linked type I bicontinuous cubic (Q_I) phases can be formed. The first system was based on a gemini phosphonium monomer (**3b**) with water (0.75 nm pores),[4,5] while a second system was based on a more easily synthesized, gemini ammonium monomer with water (**4a**) (0.86 nm pores).[6] Both materials exhibit molecular-sieving capabilities; however, membrane fabrication was only possible via heating and pressing the Q_I monomer/water mixtures into a porous support, followed by radical photo-cross-linking to lock-in the phase.[4,6] This produces supported membranes with an active separation layer that is <u>completely infused</u> in the support material and thick as the support itself (ca. 40 μm[4–6] vs. the ≤0.1-μm-thick active layers of commercial reverse osmosis

(RO)[7] and NF membranes[8]), resulting in water fluxes too low to be practical. A thin separation layer is needed for high fluxes, since thicker layers have more resistance to flow. Attempts to make thinner Q_I films via solution-casting and related methods were unsuccessful due to the compositional sensitivity of the Q phases.[4] Evaporative water loss during processing and/or retention of residual casting solvent led to phase changes.[4]

As with composite RO and NF membranes, the ideal configuration for this type of system (especially for commercial application) is a thin-film composite (TFC) architecture (i.e., a very thin separation layer on top of a more porous support). This configuration yields the highest water flux while providing the mechanical stability needed to withstand the pressures required for passage through the separation layer.[7] TFC membranes have recently been formed using cubic *thermotropic* (i.e., solvent-free) LC monomers;[9] however, only one example of a TFC LLC membrane has been reported (i.e., a H_{II} system with non-aligned cylindrical nanopores and low flux).[10] In order to get the best LLC membrane performance, what is needed is a Q monomer phase with 3D nanopores that can be easily fabricated into a TFC configuration with retention of the desired phase composition and structure.

Herein, we present a new *imidazolium*-based gemini LLC monomer (**10**) that forms a cross-linkable Q_I-phase with the low volatility and environmentally benign solvent, glycerol, instead of water. This **10**/glycerol Q_I monomer phase can be readily fabricated into nanoporous TFC membranes via solution-casting from MeOH to form defect-free thin films on porous supports, with minimal glycerol loss and retention of the Q_I composition and nanostructure after MeOH evaporation and photopolymerization (Figure 5.1). After pre-filtration to exchange the glycerol in the pores with water, these TFC membranes were found to reject uncharged molecular solutes consistent with size-exclusion through uniform 0.96 nm pores but with

absolute water fluxes ca. 10 times greater than prior melt-infused Q_I membranes. The rejection of smaller hydrated salt ions was found to be at the high level of RO membranes (≥98%) due to (charged pore–charged solute) repulsive interactions.

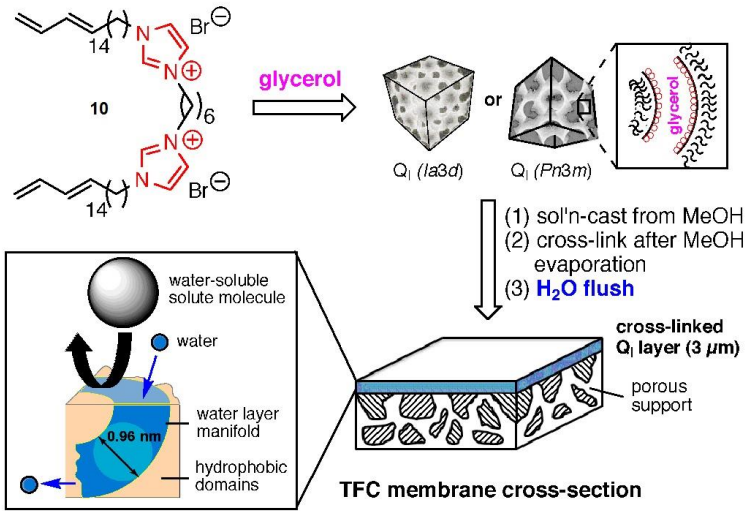

Figure 5.1. Monomer **10**, its Q_I phase with glycerol, and the formation of cross-linked Q_I-phase TFC membranes.

5.2. Results and discussion

To overcome the processing problems encountered in the earlier Q_I monomer systems, our approach was to substitute the water used for LLC phase formation with a lower volatility solvent. This alternative solvent should also be water-miscible (to enable facile flush-out) and non-toxic (in case traces remain in the membranes). Several polar organic solvents (formamide and its derivatives, *N*-methylsydnone, ethylene glycol (EG), glycerol, propylene carbonate)[11,12] and ionic liquids (ILs)[13,14] have been reported to form LLC phases (including Q phases) with select surfactants. Unfortunately, attempts to form LLC phases using 1 and 2 with many of these solvents were unsuccessful. To obtain better compatibility/LLC phase behavior with these solvents, a new gemini monomer (**10**) containing larger, more polarizable (i.e., "softer")

imidazolium headgroups was designed and synthesized (see the Supp. Info. for synthesis details). Initially, a series of six gemini imidazolium monomers with different 1,3-diene tails and headgroup spacers was synthesized and screened for LLC behavior in different solvents using the solvent penetration scan technique with polarized light microscopy (PLM).[15] Monomer **10** in this series was found to form Q phases with the broadest range of non-aqueous solvents (formamide, glycerol, and ethylammonium nitrate), in addition to pure water (see the Supporting Information.).

Since glycerol is a water-miscible, non-toxic solvent with low volatility (normal bp: 290 °C, vp @ 20 °C: <1 torr), the phase behavior of **10** with glycerol and water was studied in more detail. These studies showed that **10** forms a Q_I phase with pure glycerol, pure water, or a range of glycerol/water mixtures at 65 °C (see the Supporting Information for phase diagram). The Q_I phase appears as a viscous, optically transparent gel located on the solvent-rich side of the L phase of the phase diagram, with a black PLM optical texture and powder X-ray diffraction (PXRD) *d*-spacings in the ratio $1/\sqrt{6} : 1\sqrt{8}$, etc.[4,6] Bulk film photopolymerization studies using a water-free Q_I phase consisting of 79.7/19.8/0.5 (w/w/w) **10**/glycerol/2-hydroxy-2-methylpropriophenone (HMP, a radical photo-initiator) showed that this system can be cross-linked in the Q_I phase, as confirmed by retention of the PLM and PXRD features (Figure 5.2). The black PLM textures were unchanged, and the characteristic $1/\sqrt{6}$ and $1\sqrt{8}$ *d*-spacings showed very little change except for a slight increase in position after cross-linking, indicating a small unit cell expansion. FT-IR studies on the pre- and post-polymerized films showed > 90% diene conversion (see the Supporting Information).[4]

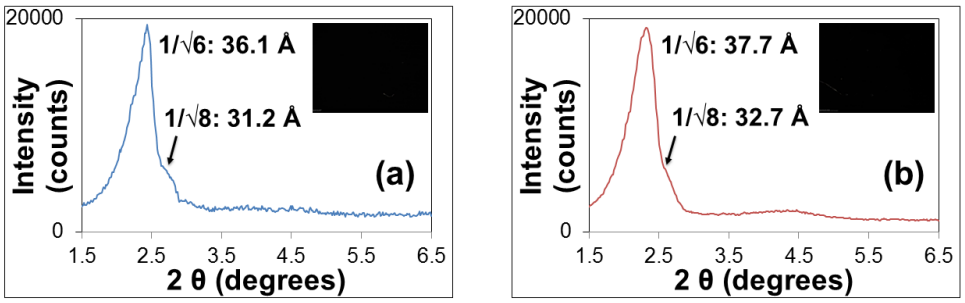

Figure 5.2. PXRD profiles of bulk Q_I-phase films of **10**/glycerol/HMP (79.7/19.8/0.5 (w/w/w)): (a) before, and (b) after photo-cross-linking. Inset: PLM optical textures (50x).

Given glycerol's properties, there should be minimal evaporative loss during thin-film solution processing if an appropriate volatile casting solvent is used. To prepare TFC membranes, a MeOH solution containing 60 wt% [79.7/19.8/0.5 (w/w/w)] **10**/glycerol/HMP was roll-cast onto the surface of porous, asymmetric poly(ether sulfone) (PES) support films using a wire-wound rod. After mild heating to evaporate off the MeOH and photo-cross-linking at 70 °C (see the Supp. Info. for details), scanning electron microscopy (SEM) indicated that the resulting membranes had defect-free coatings with an average thickness of 3 μm (Figure 5.3a). PXRD (Figure 5.3b) and FT-IR data (see the Supporting Information) confirmed that the TFC membranes had top layers with a Q_I structure and a high degree of polymerization.

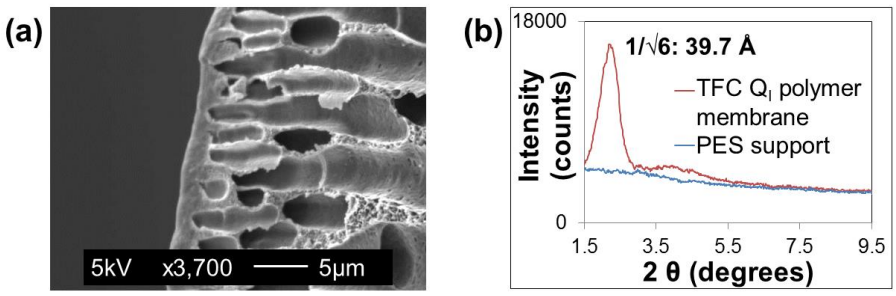

Figure 5.3. (a) Cross-sectional SEM photo and (b) PXRD profile of cross-linked Q_I TFC membrane prepared via MeOH solution roll-casting of **10**/glycerol/HMP (79.7/19.8/0.5 (w/w/w)).

After pre-filtering with pure water to remove the glycerol in the pores, the water filtration performance of these new TFC Q_I membranes was evaluated using dead-end filtration cells operating at 400 psi (27.6 bar) and aqueous solutions containing uncharged solutes and salts of varying molecular size (Table 1). Based on the rejection values of the uncharged organic solutes, the pore size of the TFC Q_I membranes was determined to be 0.96 nm using the Ferry pore size-exclusion model previously employed for Q_I membranes (see the Supporting Information).[4] Even though the pore size of the TFC Q_I membranes of **10** is larger than that of the prior melt-infused Q_I membranes of **3b** and **4a**,[4,6] its salt rejection performance is comparable or higher. This high salt rejection may be the result of the repulsive interactions between the new/different cationic headgroups in the pore walls and the approaching salt cations, or due to the new TFC configuration where the Q_I phase is a pure top layer instead of infused in the support.

Table 5.1. Water filtration performance of TFC Q_I membranes made from **10**/glycerol/HMP (3-μm-thick active layer).[a]

Test solute	Diameter (nm)	Rejection (%)[e]	Flux[f] (L m^{-2} h^{-1})[e]
Sucrose	0.94[b]	97 ± 1	0.26 ± 0.01
Glucose	0.73[b]	87 ± 4	0.29 ± 0.02
Glycerol	0.36[c]	45 ± 5	0.34 ± 0.03
EG	0.32[c]	24 ± 6	0.34 ± 0.03
NaCl	$Na^+_{(aq)}$: 0.72[d]	98 ± 1	0.52 ± 0.05
$MgCl_2$	$Mg^{2+}_{(aq)}$: 0.86[d]	99 ± 1	0.55 ± 0.03

[a]25-mm-I.D. stirred dead-end filtration cells; 400 psi; 2000 ppm aqueous feed solutions; 1 pass. [b]Ref. 16. [c]Ref. 17. [d]Ref. 18, diameter of $Cl^-_{(aq)}$ = 0.66 nm. [e]Average of ≥ 3 independent runs with std. dev. error ranges. [f]Pure water flux = 0.61 ± 0.05 L m^{-2} h^{-1} at the end of the filtration run.

The TFC Q_I membranes also have a pure water flux ca. 10 times higher than the prior melt-infused Q_I membranes[4,6] as a result of the much thinner active layer. Interestingly, the salt

filtration fluxes are ca. 1.5–2 times greater than the neutral solute filtrations (Table 5.1). We have found that aq. NaCl pre-treatment of the TFC Q_I membranes affords the same increased fluxes for neutral solute filtrations without altering rejection (see the Supporting Information). This beneficial effect is likely due to some sort of anion exchange or interaction between the salts and the ionic membrane pores/surface. We are currently investigating this phenomenon more fully.

Compared to commercial RO (Dow SW30HR) and NF (Dow NF-270) membranes tested under the same conditions,[5] the TFC Q_I membranes were found to have uncharged solute rejections higher than the NF membrane, but lower than the RO membrane (see the Supp. Info.). However, the salt rejection of the TFC Q_I membranes is much higher than that of NF-270 and on par with that of SW30HR. This dual-mode rejection behavior makes these new membranes quite unique in terms of their water purification performance. The thickness-normalized pure water permeability of the TFC Q_I membranes was found to be (6.6 ± 0.5) x 10^{-2} L m^{-2} h^{-1} bar^{-1} μm based on an average 3-μm-thick active layer. This value is comparable to that measured for SW30HR under the same conditions (8.0 x 10^{-2} L m^{-2} h^{-1} bar^{-1} μm),[5] as well as to ranges reported for RO membranes [ca. (5.0–55) x 10^{-2} L m^{-2} h^{-1} bar^{-1} μm].[19]

5.3. Conclusions

In summary, a new glycerol-based LLC monomer system has been developed that enables facile fabrication of unprecedented TFC Q_I membranes that have molecular sieving capabilities, high salt rejection, and good water permeability. We are currently exploring methods to reduce the thickness of the **10**/glycerol layers to ≤0.3 μm and increase flux by optimizing roll-casting and support parameters, as well as by using other solution processing techniques (e.g., dip-,

spray-, and spin-coating). We are also exploring methods for varying the Q_I pore size, such as the use of co-surfactants, different anions, and mixtures of LLC solvents.

5.4. Supporting information

5.4.1. Materials and general procedures

Chromium (IV) oxide, pyridine, allyltrimethylsilane (98%), *sec*-butyl lithium (1.4 M in cyclohexane), aluminum oxide (activated, basic), 2-isopropoxy-4,4,5,5-tetramethyl-1,3,2-dioxaborolane (98%), hydrogen bromide (48% wt. % in H_2O), borane-tetrahydrofuran complex solution (1.0 M in THF), *p*-toluenesulfonyl chloride, diethylene glycol, 1,4-dibromobutane (99%), 1,6-dibromohexane (96%), sodium hydride (60 wt. % dispersion in mineral oil), imidazole, ω-pentadecalactone (98%), 11-bromo-1-undecanol (98%), 2-hydroxy-2-methylpropiophenone (HMP, 97%), ethylamine (70 wt. % in H_2O), nitric acid, formamide, and ethylene glycol (all ACS Reagents unless specified otherwise) were purchased from the Sigma-Aldrich Chemical Co., and used as received. Glycerol (ACS Reagent) was purchased from Mallinckrodt, and used as received. Sulfuric acid (ACS Reagent) was purchased from VWR, and used as received. Sodium hydroxide, sodium chloride, and magnesium chloride (all ACS Reagents) were purchased from Fisher Scientific, and used as received. Filtration through silica gel was performed using 230-400 mesh, normal-phase silica gel purchased from Sorbent Technologies. The water used in LLC phase formulation and water nanofiltration experiments was de-ionized, and had a resistivity of >12 MΩ cm^{-1}. Poly(ether sulfone) (PES) polymer (Ultrason E 6020 P) was donated by BASF. Polyester fabric (Hollytex 3329) was generously donated by Ahlstrom Filtration, LLC.

5.4.2. Instrumentation

^{1}H NMR spectra were obtained using a Bruker 300 Ultrashield^{TM} (300 MHz for ^{1}H) spectrometer. Chemical shifts are reported in ppm relative to deuterated solvent. Fourier-transform infrared spectroscopy (FT-IR) measurements of all of the new monomers synthesized were performed using a Matteson Satellite series spectrometer, as thin films on Ge crystals. All other FT-IR measurements were performed using a Thermo Scientific Nicolet 6700 spectrometer equipped with a PIKE MIRacle^{TM} single-reflection horizontal ATR accessory with a diamond crystal. HRMS analysis was performed by the Central Analytical Facility in the Dept. of Chemistry and Biochemistry at the University of Colorado, Boulder. Powder X-ray diffraction (PXRD) spectra were collected using an Inel CPS 120 diffraction system with a monochromated Cu K_α radiation source. This apparatus was equipped with a film holder to analyze membrane samples. All PXRD spectra were calibrated using a silver behenate diffraction standard (d_{100} = 58.4 ± 0.1 Å). PXRD measurements were all performed at ambient temperature (22 ± 1 °C), unless noted otherwise. Polarized light microscopy (PLM) was performed using a Leica DMRXP polarizing light microscope equipped with a Linkam LTS 350 thermal stage, a Linkam CI 94 temperature controller, and a Q-Imaging MicroPublisher 3.3 RTV digital camera. Automatic temperature profiling and image capture were accomplished using Linkam Linksys32 software. Radical photopolymerizations were conducted using a Spectroline XX-15A 365 nm UV lamp (1 mW cm^{-2} at the sample surface). UV light fluxes at the sample surface were measured using a Spectroline DCR-100X digital radiometer equipped with a DIX-365 UV-A sensor. Water filtration studies were performed using custom-designed, stainless-steel, stirred, dead-end filtration cells for 2.5-cm-diameter membrane samples. The ion conductivity of permeate solutions was measured using a VWR International electrical conductivity meter model 2052-B.

Total organic carbon (TOC) analysis of aqueous permeate solutions containing organic solutes was conducted using a Test N Tube TOC kit (Hach Company), a COD reactor (DRM 200, Hach Company), and an Agilent 9453 UV-visible spectrophotometer. The wire-wound, stainless-steel applicator rods used to solution roll-cast the TFC Q_I membranes were purchased from the Paul N. Gardner Company.

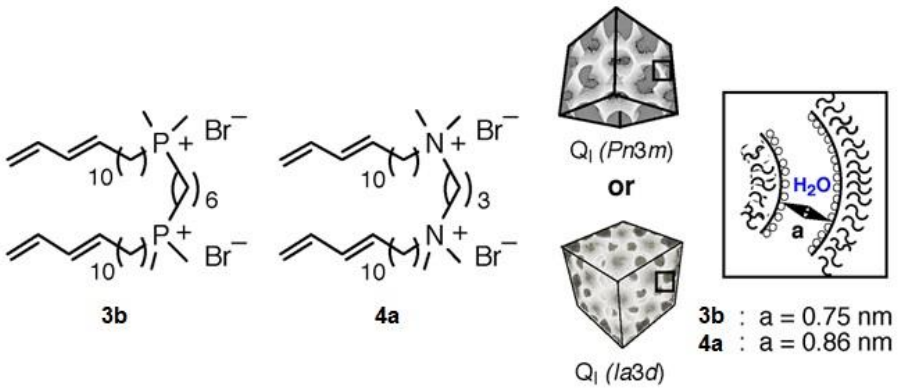

Figure 5.S1. Structures of prior gemini LLC monomers **3b** and **4a** used to form cross-linked Q_I-phase, melt-infused membranes for water purification that operate via a molecular sieving mechanism.[4,20]

5.4.3. New LLC monomer synthesis and characterization

Monomer **10** and five other homologues (**11–15**) were prepared as shown in Figure 5.S2 below. Detailed synthesis and structural characterization information on each of these monomers are also listed below.

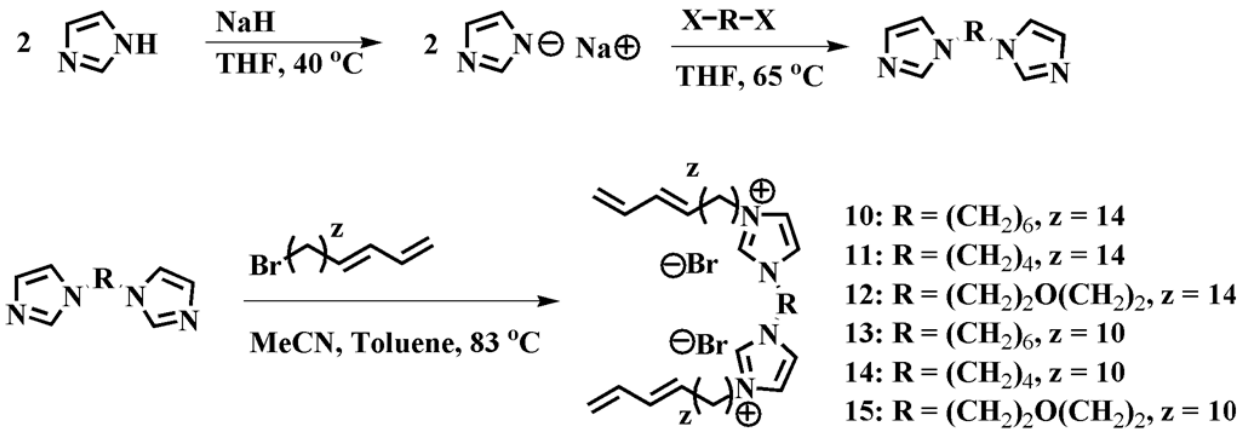

Figure 5.S2. General synthesis scheme for monomer **10** and several of its homologues that were tested for Q LLC phase formation in the presence of different solvents.

5.4.3.1. 15-Bromopentadecanoic acid.[21]

ω-Pentadecalactone (20.69 g, 86.09 mmol, 100 mol %) was stirred in 48% HBr (98 mL, 1.076 mmol, 1250 mol %) in a 250-mL round-bottom flask equipped with a stir bar and reflux condenser. H_2SO_4 (13 mL, 243.88 mmol, 283 mol %) was added dropwise to minimize exothermic activity, liquefying the solid lactone. The yellow emulsion was heated to 115 °C and stirred for 40 h. The resultant brown solution was extracted into $CHCl_3$ (200 mL), washed with de-ionized H_2O (3 x 100 mL) and brine (3 x 100 mL), dried over anhydrous $MgSO_4$. The resulting organic solution was reduced under rotary vacuum to afford a light yellow solid, which was then recrystallized from hot $CHCl_3$ and washed with cold hexanes to afford the product as a white, crystalline solid. Yield: 20.9 g (76%). Spectroscopic characterization and purity data for this compound matched published data.[21]

5.4.3.2. 15-Bromopentadecanol.[21]

Borane-THF complex solution (83 mL, 83 mmol, 210 mol %) was measured out into a 500-mL Schlenk flask equipped with a stir bar. 15-Bromo-1-pentadecanoic acid (12.70 g, 39.53 mmol, 100 mol%) was added slowly to minimize bubbling, and the light yellow solution turned clear over the course of 40 h of stirring. The reaction solution was then quenched with DI H_2O (10 mL) dropwise, extracted into Et_2O (50 mL), and washed with de-ionized H_2O (3 x 50 mL) and brine (3 x 50 mL), dried over anhydrous $MgSO_4$, and evaporated to afford the product as a white solid. Yield: 39.4 g (99%). Spectroscopic characterization and purity data for this compound matched published data.[21]

5.4.3.3. 15-Bromopentadecanal.[21]

15-Bromopentanol (6.69 g, 21.78 mmol, 100 mol %) was dissolved in CH_2Cl_2 (200 mL) in a 500-mL round-bottom flask equipped with a stir bar. To the clear, slightly yellow solution was added PCC on alumina (39.76 g, 37.48 mmol, 172 mol %) with vigorous stirring. The slurry was stirred at room temperature for 40 h. Reduction of the CH_2Cl_2 via rotary vacuum produced a dark brown solid that was stirred in diethyl ether and filtered through a pad of SiO_2, washing with diethyl ether (700 mL). Concentration of the diethyl ether under rotary evaporation afforded the product as a white solid. Yield: 21.1 g (92%). Spectroscopic characterization and purity data for this compound matched published data.[21]

5.4.3.4. 14-Bromotetradeca-1,3-diene.[21]

Synthesized as described in the literature.[21] Spectroscopic characterization and purity data for this compound matched published data.[21]

5.4.3.5. 18-Bromooctadeca-1,3-diene.[21]

Synthesized as described in the literature.[21] Spectroscopic characterization and purity data for this compound matched published data.[21]

5.4.3.6. 1,1'-(1,4-Butanediyl)bisimidazole.[22]

Synthesized as described in the literature.[22] Spectroscopic characterization and purity data for this compound matched published data.[22]

5.4.3.7. 1,1'-(1,6-Hexanediyl)bisimidazole.[22]

Synthesized as described in the literature.[22] Spectroscopic characterization and purity data for this compound matched published data.[22]

5.4.3.8. 1,1'-(Oxydi-2,1-ethanediyl)bisimidazole.[22]

Synthesized as described in the literature.[22] Spectroscopic characterization and purity data for this compound matched published data.[22]

5.4.3.9. 1,6-Bis(octadeca-15,17-dienylimidazolium)hexane dibromide (10).

18-Bromooctadeca-1,3-diene (4.25 g, 12.90 mmol, 204 mol %) and 1,1'-(1,6-hexanediyl)bisimidazole (1.38 g, 6.32 mmol, 100 mol %) were dissolved in acetonitrile (70 mL) in a 250-mL round-bottom flask equipped with a stir bar and reflux condenser. The clear, light yellow solution was stirred at 84 °C for 100 h. Concentration of the reaction solvent via rotary evaporation produced an off-white solid, which was stirred in hexanes (3 x 200 mL) and filtered

to afford the product as a white, crystalline solid. Yield: 5.2 g (93%). ^{1}H NMR (300 MHz, $CDCl_3$): δ 10.46 (s, 2H), 7.98 (s, 2H), 7.25 (s, 2H), 6.30 (dt, *J* = 10.1, 16.8, 2H), 6.03 (dd, *J* = 10.4, 15.1, 2H), 5.71 (dd, *J* = 7.3, 14.8, 2H), 5.07 (d, *J* = 16.7, 2H), 4.94 (d, *J* = 10.1, 2H), 4.46 (t, *J* = 7.3, 4H), 4.28 (t, *J* = 7.4, 4H), 2.00 (m, 12H), 1.32 (m, 58H). ^{13}C NMR (300 MHz, DMSO-d_6): δ 24.78, 25.50, 28.35, 28.58, 28.60, 28.84, 28.94, 28.99, 29.03, 29.31, 31.87, 48.62, 48.81, 115.03, 122.42, 130.84, 135.23, 135.95, 137.19. IR (thin film, MeOH): 3073, 3004, 2920, 2851, 1651, 1563, 1467, 1168, 1003, 949, 919 cm^{-1}. HRMS (ES) calcd. for $C_{48}H_{84}BrN_4$ ($M^+M^+Br^-$): 795.5897; observed: 795.5874.

5.4.3.10. 1,4-Bis(octadeca-15,17-dienylimidazolium)butane dibromide (11).

1,1'-(1,4-Butanediyl)bisimidazole (0.40 g, 2.10 mmol, 100 mol %) and 18-bromooctadeca-1,3-diene (1.47 g, 4.45 mmol, 212 mol %) were dissolved in acetonitrile (20 mL) and toluene (5 mL) in a 100 mL round bottom flask equipped with a stir bar and reflux condenser. The clear, light yellow solution was stirred at 86 °C for 196 h. Upon cooling to room temperature, the mixture was concentrated via rotary vacuum to afford a crude, off-white solid, which was stirred in hexanes (4 x 100 mL) and filtered to afford the product as a white, crystalline solid. Yield: 1.5 g (82%). ^{1}H NMR (300 MHz, DMSO-d_6): δ 9.25 (s, 2H), 7.81 (m, 4H), 6.28 (m, 2H), 6.03 (ddd, *J* = 0.6, 10.7, 11.7, 2H), 5.72 (dd, *J* = 7.3, 14.8, 2H), 5.08 (m, 2H), 4.95 (dd, *J* = 1.9, 10.1, 2H), 4.17 (m, 8H), 2.04 (q, *J* = 7.0, 4H), 1.77 (m, 8H), 1.25 (m, 44H). ^{13}C NMR (300 MHz, DMSO-d_6): δ 25.54, 26.06, 28.39, 28.58, 28.61, 28.85, 28.97, 28.99, 29.04, 29.33, 31.88, 48.06, 48.88, 115.09, 122.41, 122.54, 130.87, 135.27, 136.01, 137.22. IR (thin film, MeOH): 3070, 3005, 2920, 2851, 1656, 1568, 1468, 1338, 1165, 1004, cm^{-1}. HRMS (ES) calcd. for $C_{46}H_{80}BrN_4$ (M^+M^+Br): 767.5536; observed: 767.5561.

5.4.3.11. 1,1'-(Oxydi-2,1-ethanediyl)bis[3-(octadeca-15,17-dienyl)imidazolium] dibromide (12).

18-Bromooctadeca-1,3-diene (1.05 g, 3.18 mmol, 214 mol %) and 1,1-(oxydi-2,1-ethanediyl)bisimidazole (0.31 g, 1.49 mmol, 100 mol %) were dissolved in acetonitrile (20 mL) and toluene (10 mL) in a 50-mL round-bottom flask equipped with a stir bar and reflux condenser. The clear, light yellow solution was stirred at 86 °C for 100 h. Upon cooling to room temperature the reaction was concentrated under rotary vacuum to produce an off-white solid, which was stirred in hexanes (3 x 100 mL) and filtered to afford the product as a white, crystalline solid. Yield: 1.0 g (78%). ^{1}H NMR (300 MHz, DMSO-d_6): δ 9.24 (s, 2H), 7.79 (m, 2H), 7.71 (m, 2H), 6.29 (dt, *J* = 10.2, 16.8, 2H), 6.03 (dd, *J* = 10.5, 15.3, 2H), 5.72 (dd, *J* = 7.4, 14.7, 2H), 5.08 (d, *J* = 16.9, 2H), 4.95 (d, *J* = 10.1, 2H), 4.36 (d, *J* = 4.1, 4H), 4.18 (d, *J* = 7.6, 4H), 3.78 (s, 4H), 2.03 (t, *J* = 7.0, 4H), 1.77 (m, 4H), 1.23 (m, 44H). ^{13}C NMR (300 MHz, DMSO-d_6): δ 25.56, 28.43, 28.59, 28.61, 28.86, 28.89, 29.01, 29.05, 29.45, 31.89, 48.66, 48.81, 68.01, 115.08, 122.11, 122.80, 130.87, 135.26, 136.27, 137.21. IR (thin film, MeOH): 3078, 3010, 2922, 2850, 1658, 1565, 1468, 1163, 1124, 1003, 950 cm^{-1}. HRMS (ES) calcd. for $C_{46}H_{80}BrN_4$ ($M^+M^+Br^-$): 783.5535; observed: 783.5510.

5.4.3.12. 1,6-Bis(tetradeca-11,13-dienylimidazolium)hexane dibromide (13).

1,1-(1,6-Hexanediyl)bisimidazole (1.07 g, 4.89 mmol, 100 mol %) was dissolved in acetonitrile (15 mL) in a 100-mL round-bottom flask equipped with a stir bar and reflux condenser. Addition of 14-bromotetradeda-1,3-diene (2.70 g, 9.90 mmol, 203 mol %) produced a clear, light yellow solution that was stirred at 86 °C for 96 h. Upon cooling to room

temperature, solvent was concentrated under rotary vacuum to afford an off-white, waxy solid that was stirred in hexanes (3 x 50 mL) and filtered to afford the product as a white, crystalline solid. Yield: 3.1 g (82%). ^{1}H NMR (300 MHz, DMSO-d_6): δ 9.25 (s, 2H), 7.81 (ds, J = 1.4, 4H), 6.29 (dt, J = 10.2, 16.9, 2H), 6.03 (dd, J = 10.4, 15.2, 2H), 5.71 (m, 2H), 5.09 (dd, J = 1.7, 17.0, 2H), 4.95 (dd, 2H), 4.16 (t, J = 7.1, 8H), 2.04 (q, J = 6.7, 4H), 1.78 (m, 8H), 1.24 (m, 32H). ^{13}C NMR (300 MHz, DMSO-d_6): δ 25.29, 25.96, 28.80, 29.05, 29.08, 29.28, 29.34, 29.53, 29.79, 32.35, 49.12, 49.30, 115.56, 122.90, 131.34, 135.72, 136.43, 137.67. IR (thin film, MeOH): 3081, 3008, 2928, 2858, 1647, 1567, 1463, 1164, 1003, 953, 896 cm^{-1}. HRMS (ES) calcd. for $C_{40}H_{68}BrN_4$ ($M^+M^+Br^-$): 683.4622; observed: 683.4642.

5.4.3.13. 1,4-Bis(tetradeca-11,13-dienylimidazolium)butane dibromide (14).

14-Bromo-tetradeac-1,3-diene (0.912 g, 3.36 mmol, 213 mol %) and 1,1'-(1,4-butanediyl)bisimidazole (0.30 g, 1.58 mmol, 100 mol %) were dissolved in acetonitrile (25 mL) and toluene (10 mL) in a 100-mL round-bottom flask equipped with a stir bar and reflux condenser. The clear, light yellow solution was stirred at 86 °C for 70 h. Cooling to room temperature and concentration of the solvent under rotary evaporation afforded a light brown solid which was stirred in diethyl ether (4x50 mL) and filtered to afford the product as a white, crystalline solid. Yield: 0.7 g (57%). ^{1}H NMR (300 MHz, $CDCl_3$): δ 10.39 (s, 2H), 8.09 (s, 2H), 7.19 (s, 2H), 6.31 (dt, J = 10.2, 17.0, 2H), 6.04 (dd, J = 10.4, 15.2, 2H), 5.70 (m, 2H), 5.08 (dd, J = 1.2, 16.9, 2H), 4.95 (d, J = 10.1, 2H), 4.61 (t, 4H), 4.25 (m, 4H), 2.23 (t, 4H), 2.07 (q, J = 6.9, 4H), 1.98–1.75 (m, 4H), 1.30 (d, J = 20.8, 28H). ^{13}C NMR (300 MHz, $CDCl_3$): δ 26.43, 26.63, 29.08, 29.29, 29.46, 29.53, 30.33, 32.67, 48.98, 50.38, 114.73, 121.31, 123.85, 130.98, 135.70, 136.85, 137.48. IR (thin film, MeOH): 3070, 3012, 2924, 2851, 1652, 1564, 1464,

1165, 1004, 897 cm^{-1}. HRMS (ES) calcd. for $C_{38}H_{64}BrN_4$ ($M^+M^+Br^-$): 655.4321; observed: 655.4310.

5.4.3.14. 1,1'-(Oxydi-2,1-ethanediyl)bis[3-(tetraadeca-11,13-dienyl)imidazolium] dibromide (15).[23]

Synthesized as described in the patent literature.[23] Spectroscopic characterization and purity data for this compound matched published data.[23]

5.4.3.15. Ethylammonium nitrate.

Synthesized as described in the literature.[24] Spectroscopic characterization and purity data for this compound matched published data.[24]

5.4.4. Qualitative screening of LLC phase behavior with different solvents using the PLM-based penetration scan technique.[15]

To quickly and qualitatively determine the LLC phase behavior of homologues of monomer **10** (see Table 5.S1) with a specific solvent, the PLM penetration scan technique was employed.[15] This technique is a solvent-amphiphile gradient assay using PLM that quickly (i.e., in minutes) determines qualitatively what phases can be formed by a certain amphiphile and solvent pair at a specific temperature. This technique was performed by taking the solid monomer and pressing it in-between a microscope slide a cover slip. The sample was then placed on the PLM thermal stage and annealed to its melting temperature or up to 90 °C, whichever came first. The sample was then slowly cooled back down to room temperature. A small amount (<30 μL) of the chosen solvent was added to the edge of the cover slip and the solvent was drawn via capillary action into contact with the solid monomer, creating a concentration

gradient. The specimen was then heated to 95 °C at a rate of 5 °C/min with digital image capture. The differences in optical texture and intensity were used to determine the potential LLC phases formed. Since Q_I phases are black (i.e., isotropic) under PLM and are typically found between birefringent lamellar (L) and hexagonal (H_I) phases, a dark isotropic band between two birefringent LLC phases indicates a potential Q_I phase. The six gemini imidazolium bromide monomer homologues were tested with water, glycerol, formamide, ethylene glycol, and ethylammonium nitrate. Out of the six homologues analyzed, only monomer **10** had clear potential Q_I phases with multiple non-aqueous solvents tested. From qualitative analysis of the penetration scan PLM optical textures, monomer **10** showed evidence of Q_I phase formation with the non-aqueous solvents glycerol, formamide, and ethylammonium nitrate (e.g., see Figure 5.S3). Based on this initial study, only monomer **10** was chosen for more detailed LLC phase behavior characterization with glycerol as the LLC solvent.

Table 5.S1. The gemini imidazolium bromide monomer homologues synthesized, and a summary of their qualitative Q phase formation behavior between 22 °C and 95 °C with different solvents from PLM penetration scan screening studies.

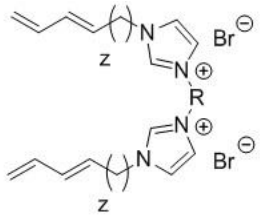

			Potential Q phase formation via penetration scan studies				
Monomer	**R**	**z**	**water**	**glycerol**	**formamide**	**ethylene glycol**	**ethylammonium nitrate**
10	$(CH_2)_6$	14	Yes	Yes	Yes	No	Yes
11	$(CH_2)_4$	14	Yes	No	No	No	No
12	$(CH_2)_2O(CH_2)_2$	14	No	Yes	No	No	No
13	$(CH_2)_6$	10	Yes	No	No	No	No
14	$(CH_2)_4$	10	Yes	No	No	No	No
15	$(CH_2)_2O(CH_2)_2$	10	Yes	No	No	No	No

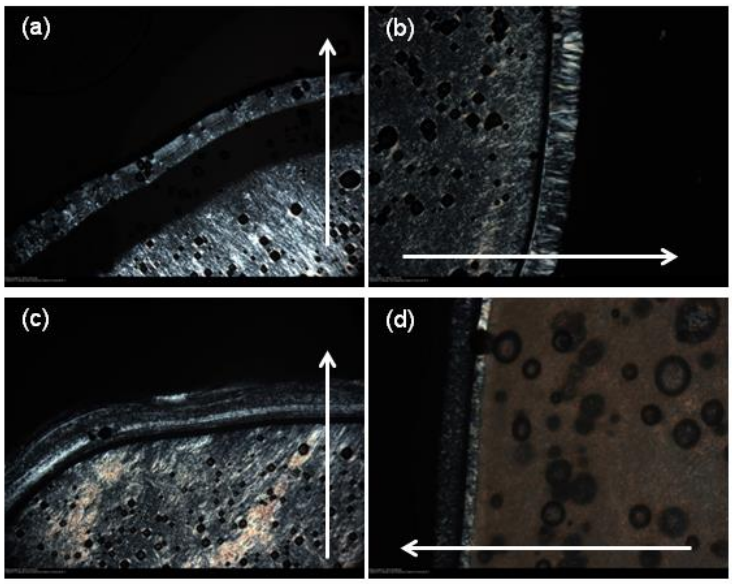

Figure 5.S3. Representative PLM images (magnification: 50x) of solvent penetration scans of **10** with (a) water at 68 °, (b) glycerol at 65 °C, (c) formamide at 55 °C, and (d) ethylammonium nitrate at 44 °C. The black (pseudo-isotropic) region between two bright, anisotropic LLC regions is indicative of the presence of a potential Q phase. The arrows in the PLM images point in the direction of increasing solvent concentration.

5.4.5. Preparation of LLC samples, determination of LLC phase behavior, and elucidation of LLC phase diagrams.

LLC samples of specific composition were made by adding an appropriate amount of monomer and solvent to custom-made glass vials. A photo-initiator, 2-hydroxy-2-methylpropiophenone (HMP), was added if required, and the vials were sealed with Parafilm™. LLC samples were mixed by alternately hand-mixing and centrifuging (2800 rpm) until completely homogenous. It should be noted that the LLC samples are sensitive to water loss or gain, depending on the solvent system. Special attention was taken to keep the samples sealed as much as possible during sample mixing and transferring to minimize composition drift.

For samples with low-viscosity solvent systems (e.g., water), LLC samples of specific composition were prepared by adding the desired amount of monomer to custom-made glass

vials, followed by the addition of an appropriate amount of solvent via pipette. Photo-initiator was then added if required. The vials were sealed with Parafilm™ and centrifuged at 2800 rpm. Samples were then alternately hand-mixed and centrifuged until homogeneous.

For samples with high viscosity solvent systems (e.g., glycerol), LLC samples of specific composition were prepared by adding the desired amount of solvent to custom-made glass vials, followed by the addition of an appropriate amount of monomer via spatula. Photo-initiator was then added if required. The vials were sealed with Parafilm™ and centrifuged at 2800 rpm. Samples were then alternately hand-mixed and centrifuged until homogeneous.

The composition and temperature range of the LLC phase was determined using variable-temperature PLM. Specimens at various concentrations were prepared and then pressed between a microscope slide and microscope cover-slip. The assembly was then placed on the PLM thermal stage and annealed past its isotropic temperature or up to 90 °C (whichever came first). The sample was slowly cooled and allowed to come back to its room temperature phase. The sample was then heated to 95 °C at a rate of 5 °C/min with digital image capture and continuous recording of the light intensity. Images were captured at 50x magnification. Changes in optical texture and light intensity were used to determine changes in the LLC phase of the mixture.

The identity of each observed phase was then confirmed with PXRD by analyzing a point in each distinct phase region as elucidated by PLM analysis. PXRD spectra of the samples were taken either by using a film holder apparatus for room temperature spectra or with a heated stage for higher temperature spectra. In the film holder, a sample was placed between Mylar sheets with an appropriate spacer, annealed, placed in the film holder, and then examined. On the heated stage, a sample was placed in an aluminum PXRD pan and a piece of Mylar was used to cover the sample. The *d* spacing pattern of the PXRD peaks is used to determine the LLC phase.

Using the combined PLM and PXRD data, a partial phase diagram of the **10**/glycerol/water system was created as a function of system composition and temperature. The minimum temperature for Q_I phase formation in this ternary system was found to be 65 °C. Above 65 °C, the Q_I phase typically remained up to 95 °C. A partial phase diagram of **10**/glycerol/water at 65 °C is shown in Figure 5.S4.

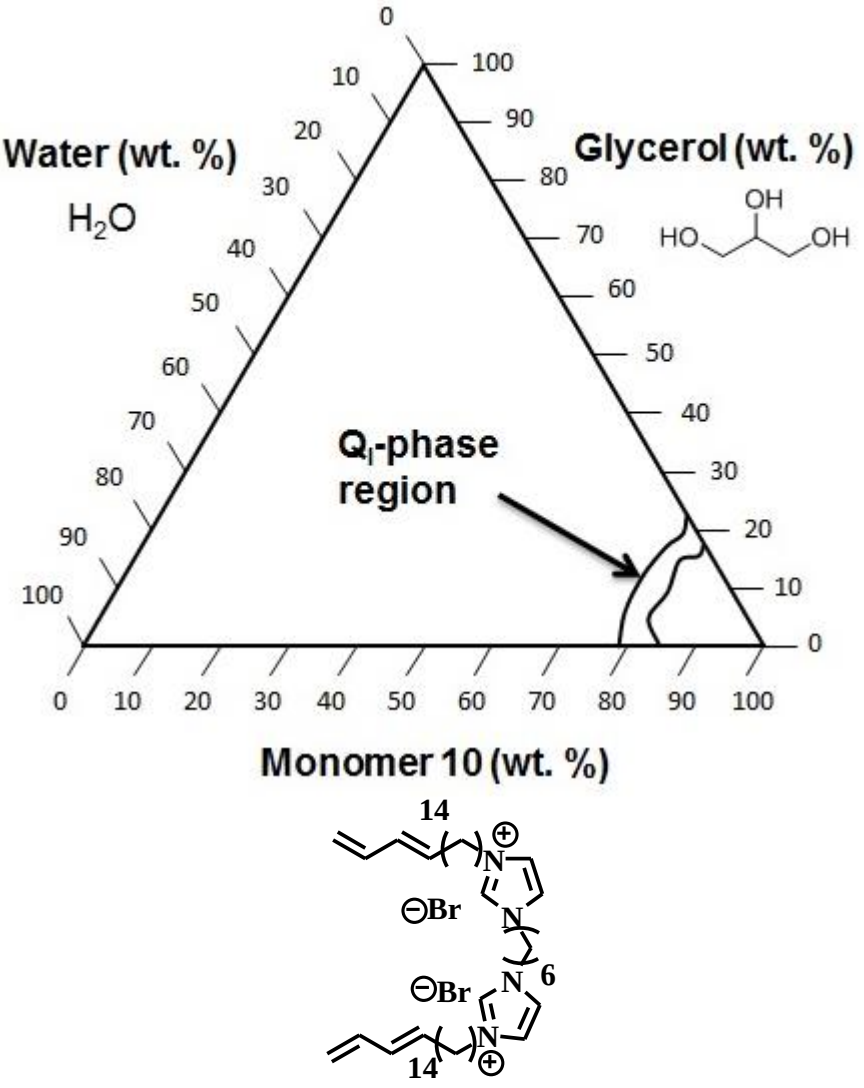

Figure 5.S4. Elucidated partial phase diagram highlighting the position of the Q_I phase for the **10**/water/glycerol system at 65 °C. (Other non-cubic LLC phases were also observed outside of the Q_I-phase region, but these have not been rigorously identified yet.)

5.4.6. Preparation of bulk Q_I-phase films of 10/glycerol/HMP and cross-linking with LLC phase retention.

Bulk LLC samples of the desired composition with HMP photo-initiator were prepared as described in the "Preparation of LLC samples" section. The Q_I phase monomer mixtures were then sandwiched between two pre-cut pieces of Mylar. The samples were clamped in-between two quartz plates and heated to 70 °C to form the Q_I phase. After 5 min, the samples were irradiated with 365 nm light (1 mW cm^{-2}) for 1 h. The quartz plates and Mylar sheets were carefully removed to afford thick, free-standing Q_I polymer films. PLM and PXRD analysis of the polymerized samples show that the Q_I-phase nanostructure is retained (see Figure 2 in main manuscript).

5.4.7. Comparison of the relative degree of order in the Q_I phases of 3b/water, 4a/water, and 10/glycerol by PXRD analysis.

Comparison of the PXRD profiles of the bulk cross-linked Q_I phases of **3b**/water,[21] **4a**/water,[20] and **10**/glycerol systems set to the same x-axis (i.e., 2θ (degrees)) range shows that the three Q_I phase systems have a similar degree of overall order. As can be seen in Figure S5, all three have 2 principal PXRD *d*-spacing peaks: a very pronounced first diffraction peak that indexes to $1/\sqrt{6}$, and a secondary, less intense peak/shoulder that indexes to $1/\sqrt{8}$. A weak, very broad peak can also be seen in some of the spectra that corresponds to either the $1/\sqrt{20}$[21] or $1\sqrt{22}$[20] *d*-spacing peaks of a Q_I phase.[25,26] The possible $1/\sqrt{20}$ and $1\sqrt{22}$ peaks do not correspond to hexagonal or lamellar phase PXRD peaks.[15] The $1/\sqrt{8}$ peak for the Q_I phase of **3b**/water is a bit better resolved from the main peak than the other two systems, but this may be due to the presence of additional heavier atoms (i.e., phosphorus) – and thus more electron density contrast – at the water/organic interface in the **3b**/water system compared to the other two. With their

PXRD profiles scaled to the same 2θ x-axis range, the three different cross-linked Q_I systems have similar widths for their principal (i.e., 1/√6) diffraction peak. The 1/√6 diffraction peak full width at half max for all three systems is approximately 0.5 degrees. The only major difference between the cross-linked Q_I phases of the three systems is the position of the *d*-spacings, indicating different unit cell sizes.

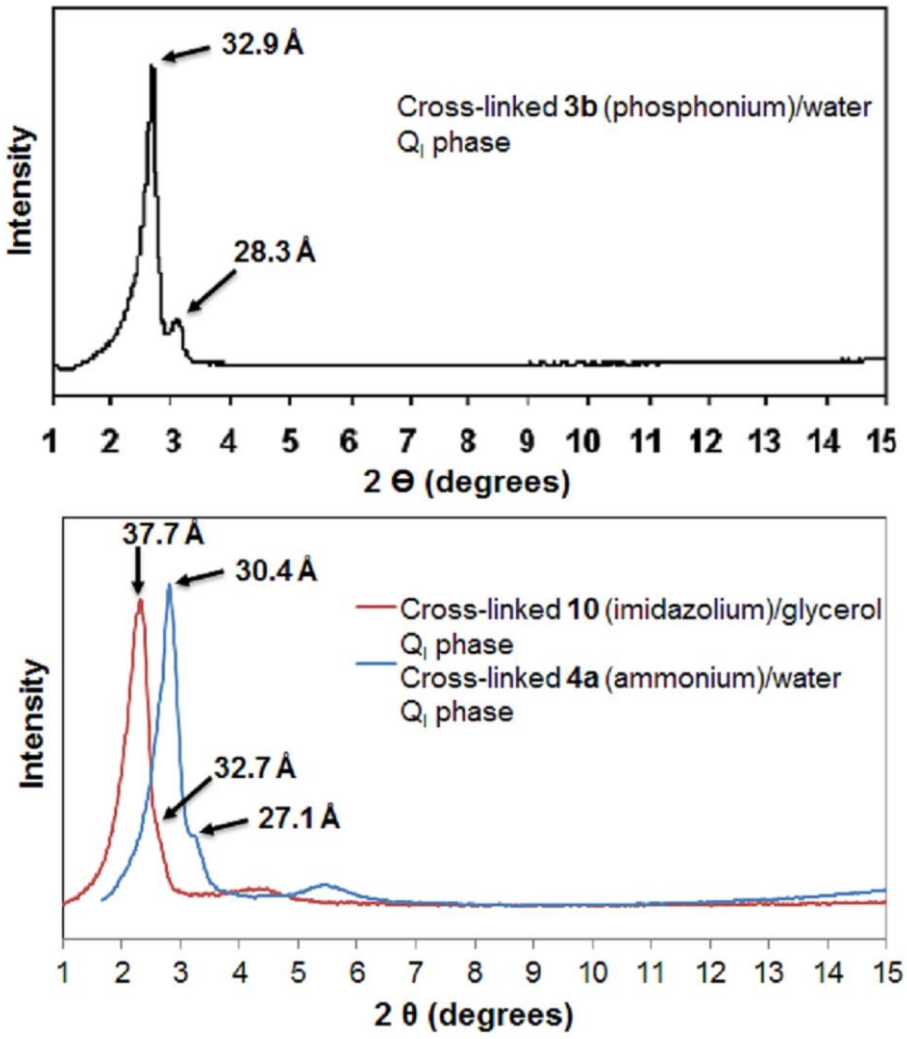

Figure 5.S5. PXRD profiles of the bulk cross-linked Q_I phases of the **3b**/water,[21] **4a**/water,[20] and **10**/glycerol systems shown to the same 2θ (x-axis) scale. The PXRD profile of the bulk cross-linked Q_I phase of **3b**/water is taken from Ref. 4, Figure S9. The data for the PXRD profile for the bulk cross-linked Q_I phase of **4a**/water is from Ref. 22.

5.4.8. Determination of degree of conversion for the radical photopolymerization of the 10/glycerol/HMP bicontinuous cubic (Q_I) phases.

Bulk samples of **10**/glycerol/HMP with the desired composition were prepared that form a Q_I phase when heated above 65 °C as described in previous sections. The Q_I phase monomer mixture was then placed on the ATR plate of the FT-TR spectrometer, and FT-IR spectra were collected. The Q_I phase monomer mixture was then sandwiched between two pre-cut pieces of Mylar. The sample was clamped in-between two quartz plates and heated to 70 °C to form the Q_I phase. After 5 min, the samples were irradiated with 365 nm light (1 mW cm^{-2}) for 1 h. The quartz plates and Mylar sheets were carefully removed and the Q_I polymer film was placed on the ATR plate and the post-polymerization FT-IR spectra was collected. The 1004 cm^{-1} absorption band in the monomer samples comes from the C–H out-of-plane wagging from the 1,3-diene units located on the end of the tails of the monomer.[4,21] As seen in Figure S6, the attenuation of the 1004 cm^{-1} peak in the post-polymerized sample suggests > 90% conversion of the 1,3-diene units for the Q_I-phase LLC sample based on a static internal reference peak at 1160 cm^{-1}. PLM and PXRD analysis of the polymerized samples show that the Q_I-phase nanostructure is retained.

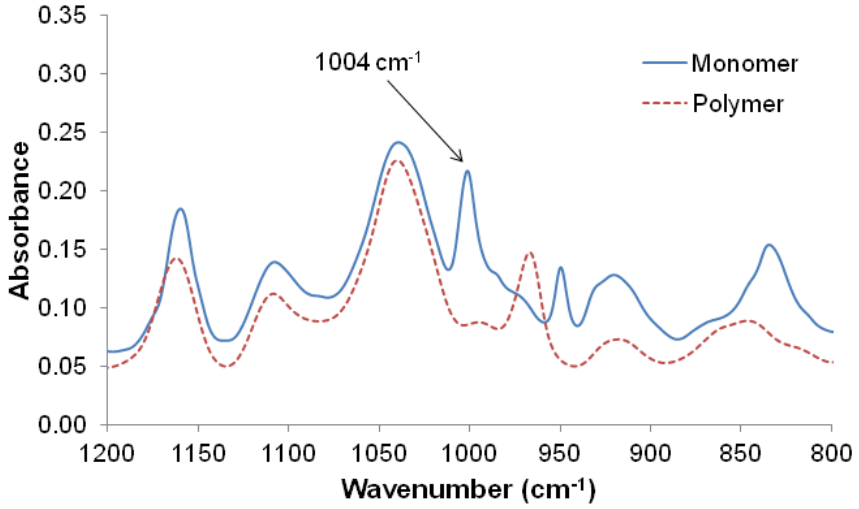

Figure 5.S6. FT-IR spectra of **10**/glycerol/HMP (79.7/19.8/0.5 (w/w/w)) Q_I-phase mixture: (a) before, and (b) after heating to 70 °C and polymerizing with 365 nm UV light (1 mW cm^{-2}) for 1 h. Attenuation of the 1004 cm^{-1} peak relative to the 1160 cm^{-1} internal reference peak suggests > 90% 1,3-diene group conversion.

5.4.9. Solution-casting and photo-cross-linking of a thin-film Q_I-phase of 10/glycerol/HMP on dense glass substrates to provide proof-of-concept for successful thin-film formation and cross-linking with LLC phase retention.

A trial casting solution was prepared by adding appropriate amounts of monomer **10**, glycerol, and HMP to a 10-mL glass vial and dissolving the components in the desired amount of methanol. A small amount of the casting solution (< 50 μL) was then pipette onto a glass slide and allowed to air dry for 10 min. After placing the glass slide on a temperature-controlled hot stage, the stage was warmed to 25 °C, and the temperature was gradually increased to 75 °C by heating at a rate of 5 °C/min and holding the temperature for 2 min every 10 °C up to 75 °C. This heating step removed excess methanol casting solvent from the mixture. A small portion of the sample was then scraped off the glass slide, placed on the ATR plate of the FT-IR spectrometer, and a pre-polymerization FT-IR spectrum was collected. The sample was then cooled to room temperature and placed in a specially designed photo-polymerization chamber

with an aluminum base and a Pyrex glass plate cover. The atmospheric O_2 in the chamber was removed by alternating vacuum (2000 mtorr) and Ar purge cycles three times. The Ar-filled polymerization chamber was then warmed to 70 °C by a hot stage with a temperature controller, and the chamber was irradiated with a 365 nm UV lamp (1 mW cm^{-2}) for 1 h. The glass slide was then removed from the chamber, and the sample was scraped from the slide with a razor blade. The resulting thin, free-standing film (ca. 10 μm thick) was placed on the ATR plate of the FT-IR spectrometer, and a post-polymerization FT-IR spectrum was collected. As seen in Figure S7, the absorbance attenuation of the peak at 1004 cm^{-1} suggests > 90% conversion for the solution-cast thin film Q_I phase. As shown in Figure S8, PLM and PXRD analysis of the polymerized thin-film sample show retention of the desired Q_I-phase structure.

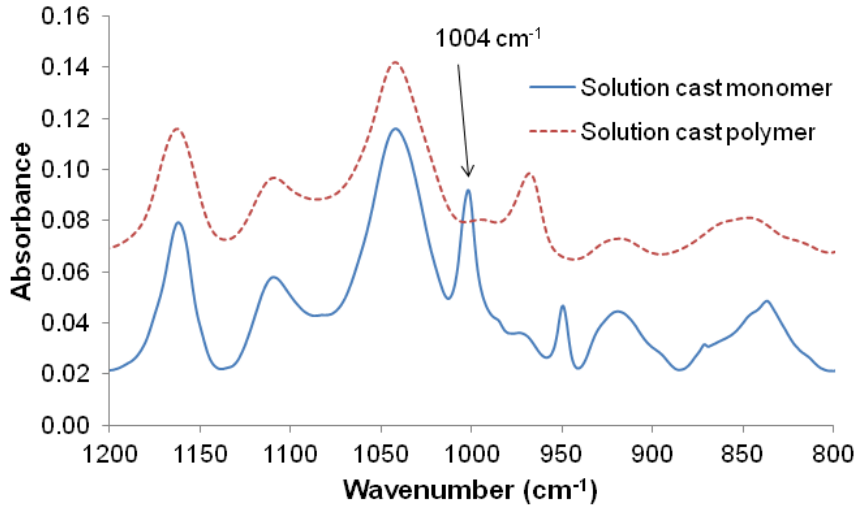

Figure 5.S7. FT-IR spectra of **10**/glycerol/HMP (79.6/19.7/0.7 (w/w/w)) before (dried solution-cast monomer mixture) and after (thin-film cross-linked Q_I polymer) heating to 70 °C and polymerizing with 365 nm UV light (1 mW cm^{-2}) for 1 h. Attenuation of the 1004 cm^{-1} peak suggests > 90% 1,3-diene group conversion.

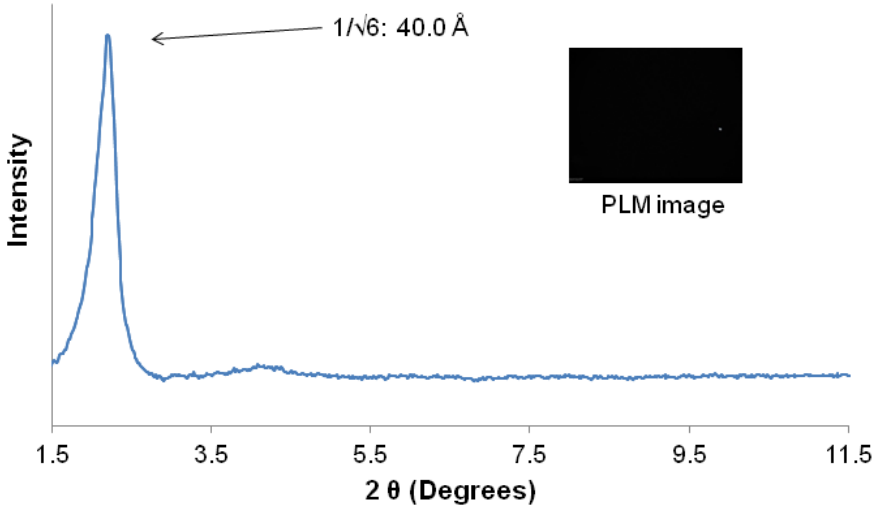

Figure 5.S8. PLM optical texture and PXRD spectrum of a thin film of **10**/glycerol/HMP (79.6/19.7/0.7 (w/w/w)) solution-cast from methanol onto glass, heated to 70 °C to remove the methanol, and photo-cross-linked with 365 nm UV light (1 mW cm^{-2}) for 1 h under Ar atmosphere.

5.4.10. Preparation of asymmetric, porous poly(ether sulfone) (PES) support membranes via phase-inversion processing.

The PES support membranes were prepared following guidelines described in the literature.[27] A 15 wt % solution of PES in dimethylformamide (DMF) was prepared by adding PES flakes to a small round-bottom flask containing a stir bar and the appropriate amount of DMF. The solution was stirred for 24 h under ambient conditions and then allowed to sit with no stirring for another 24 h to remove any bubbles from the solution. A piece of Hollytex 3329 fabric was cut and taped to a glass plate. A custom-made stainless-steel blade caster with a 250 µm gap was placed on the fabric swatch, and the PES solution was poured into the caster. The caster was then quickly drawn down the plate, and the plate was immediately transferred to a de-ionized water bath. The PES polymer immediately precipitated. After 30 min, the plate was transferred to a fresh water bath and allowed to soak overnight. The support membranes were then allowed to air dry for 24 h before use. As seen in Figure 5.S9, cross-section and top-view

scanning electron microscope (SEM) images of the support membranes demonstrate the desired asymmetric porous structure and a defect-free top surface.

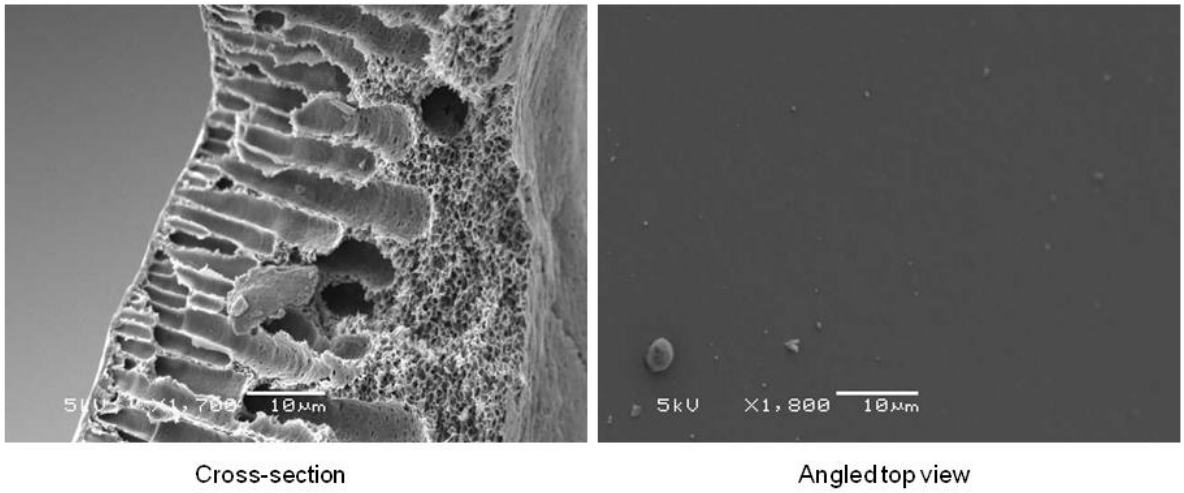

Figure 5.S9. Cross-section and angled top-view SEM images of the prepared PES support membranes.

5.4.11. Fabrication of PES-supported thin-film composite (TFC) Q_I polymer membranes of 10/glycerol/HMP (see Figure S10).

A Q_I-phase casting solution was prepared by adding appropriate amounts of monomer **10**, glycerol, and HMP to a 10 mL glass vial and dissolving the components in the desired amount of methanol. A PES support membrane was taped to a small glass plate along two edges and a small piece of aluminum foil was placed on top of one of the taped edges. A #3 wire-wound rod from the Paul N. Gardner Company was placed in the aluminum trough. The casting solution was pipette along the length of the trough and the rod was then immediately drawn at a slow constant speed across the support membrane. The membrane sample was allowed to air dry for 10 min and then placed on a temperature-controlled hot stage. The stage was warmed to 25 °C, and then the temperature was gradually increased to 75 °C by heating at a rate of 5 °C/min and holding the temperature for 2 min every 10 °C up to 75 °C. This gradual heating process is

performed to removes excess methanol casting solvent. The membrane sample was then cooled to room temperature. A portion of the sample was cut off and placed on the ATR plate of the FT-IR spectrometer and a pre-polymerization FT-IR spectrum of the solution-cast Q_I-phase monomer mixture on the PES support was collected. The membrane sample was then placed in a specially designed photo-polymerization chamber with an aluminum base and a Pyrex glass plate cover. The atmospheric O_2 in the chamber was removed by alternating vacuum (2000 mtorr) and Ar purge cycles three times. The Ar-filled polymerization chamber was then warmed to 70 °C by a temperature controller on a hot stage, and the chamber was irradiated with a 365 nm UV lamp (1 mW cm^{-2}) for 1 h. A portion of the membrane sample was cut off and placed on the ATR plate of the FT-IR spectrometer and a post-polymerization FT-IR spectrum of the final TFC Q_I membrane was collected. As seen in Figure 5.S11, the absorbance attenuation of the FT-IR band at 1004 cm^{-1} suggests a high degree of conversion for the TFC Q_I membrane.

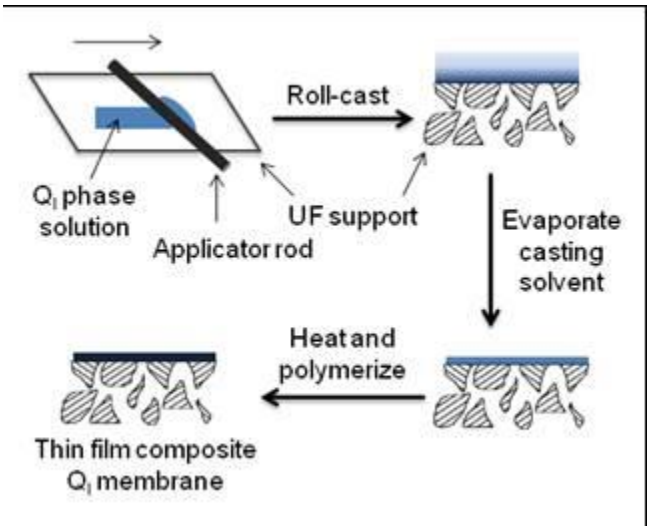

Figure 5.S10. Scheme for solution roll-casting and then cross-linking a thin Q_I-phase **10**/glycerol/HMP top layer on porous PES supports to prepare nanoporous TFC Q_I polymer membranes.

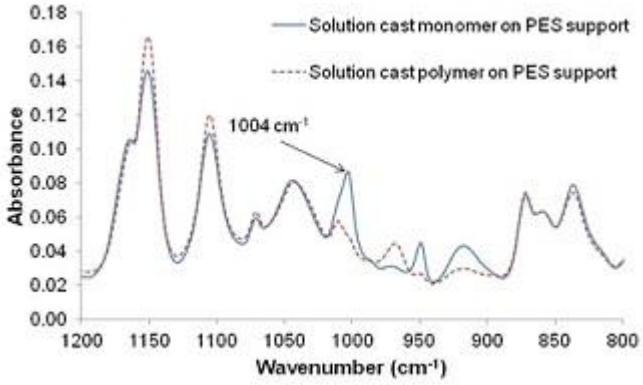

Figure 5.S11. FT-IR spectra of solution-cast **10**/glycerol/HMP (79.7/19.8/0.5 (w/w/w)) top layer (ca. 3 μm thick) on porous PES support before (blue trace) and after (red trace) heating to 70 °C and polymerizing with 365 nm UV light (1 mW cm^{-2}) for 1 h. Absorbance attenuation of the 1004 cm^{-1} peak suggests a high degree of 1,3-diene group conversion.

As seen in Figure 5.S12, a cross-section SEM image shows an average ca. 3-μm-thick coating on top of the porous PES support film. Retention of the desired Q_I-phase nanostructure of the coating was verified by PXRD analysis (see Figure 3 in the main manuscript). A picture of the resulting TFC Q_I polymer membrane made from **10**/glycerol/HMP is shown in Figure 5.S13.

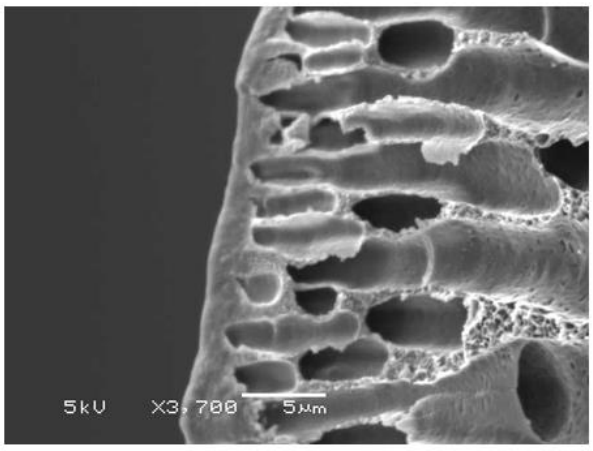

Figure 5.S12. Cross-sectional SEM image of a typical cross-linked TFC Q_I membrane fabricated by roll-casting a methanol solution of **10**/glycerol/HMP onto porous PES support.

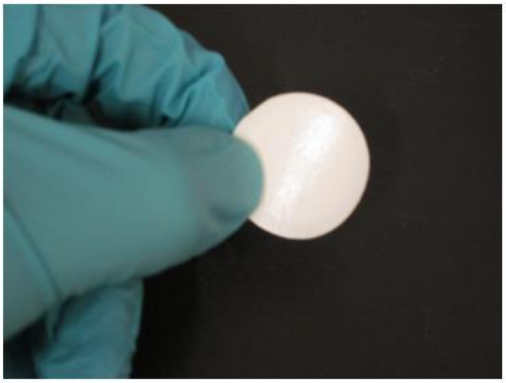

Figure 5.S13. Picture of the final TFC Q_I polymer membrane prepared from **10**/glycerol/HMP solution roll-cast on porous PES.

5.4.12. General water nanofiltration testing procedure.

Water nanofiltration experiments were performed using the same custom-made, stainless steel, stirred dead-end filtration cells used in previous studies.[4,20] The membrane holder of each cell has a 2.5 cm outer diameter, but only an effective filtration area of 3.8 cm[20] with the O-ring configuration. The nanofiltration experiments were performed using aqueous feed solutions containing a single solute at a concentration of 2000 ppm. Each dead-end filtration cell was loaded with 25 mL of the feed solution and pressurized until 4–5 mL of permeate was collected to wash out any of the previous permeate. The cell was then reloaded with the same feed solution and the next 3-4 mL of permeate was collected and analyzed to determine the flux and rejection.

For all of the filtration studies, the flux (J) was calculated as follows using Equation 5.S1:

$$J = \frac{\Delta V}{A \Delta t} \qquad \text{(Equation 5.S1)}$$

where ΔV is the permeate volume, A is the surface area of the membrane (3.8 cm^2), and Δt is the time needed to collect the permeate. The % rejection (R) was calculated using Equation 5.S2:

$$R = \left(1 - \frac{C_{permeate}}{C_{feed}}\right) \cdot 100 \qquad \text{(Equation 5.S2)}$$

where $C_{permeate}$ and C_{feed} are the concentration of the solute in the permeate and feed, respectively. All of the fluxes and rejections are averages of three different membrane samples in separate experiments. The reported error is the standard deviation from the three different membranes in separate experiments.

5.4.12.1. Permeate analysis

The concentrations of all the neutral organic solutions were determined using a TOC digestion kit with a modified procedure based on Hach method 10173 and subsequent UV-visible analysis. A calibration curve was made with standard solutions prior to each analysis. The concentrations of NaCl and $MgCl_2$ in the permeate solution were determined using an electrical conductivity meter. A calibration curve was made for each salt using aqueous standard solutions of each salt.

5.4.13. Water nanofiltration testing of uncoated PES support membranes as controls.

Membrane discs (2.5 cm in diameter) of the prepared porous PES support membrane were punched out from sheets using a sharpened circular die. The membrane discs were soaked in de-ionized water for 30 min at ambient temperature and then carefully loaded into the custom-made, stainless-steel, stirred dead-end filtration cells. The cells were filled with 25 mL of de-ionized water and pressurized to 50 psi (3.4×10^5 Pa) with N_2 pressure as the driving force at ambient temperature (22 ± 1 °C). The first 5 mL of permeate from each test cell was collected and discarded. This first filtration was to ensure the integrity of the membranes and clean out any

contaminants that might remain in the membranes after processing. The general water filtration procedure was then followed.

Analysis of all of the permeates showed the porous PES support membranes had < 10% rejection for all of the solutes tested (sucrose, glucose, glycerol, ethylene glycol, NaCl, and $MgCl_2$). This is to be expected, since the PES support membrane should have comparable performance to a conventional ultrafiltration (UF) membrane. The pure water flux of the uncoated PES support membrane was measured to be $(1.4 \pm 0.1) \times 10^2$ L m^{-2} h^{-1}.

5.4.14. Water nanofiltration testing of TFC Q_I polymer membranes made from 10/glycerol/HMP.

Membrane discs (2.5 cm in diameter) of the TFC Q_I polymer membranes of **10**/glycerol/HMP were punched out from small sheets using a sharpened circular die. Membrane discs were then soaked in de-ionized water for 1 hour at ambient temperature. After soaking, the membrane discs were carefully loaded into the custom-made, stainless-steel, stirred, dead-end filtration cells. All nanofiltration experiments were performed with 400 psi (2.76×10^6 Pa) of N_2 pressure as the driving force at ambient temperature (22 ± 1 °C). The cells were then filled with de-ionized water that was filtered through the membranes until at least 5 mL of permeate was collected in each cell. This first filtration was to ensure the integrity of the membranes and clean out any unreacted monomer, glycerol, or other contaminants that might remain in the membranes after processing. The cells were then reloaded with de-ionized water and filtered until another 5 mL of permeate was collected and analyzed for any residual organic carbon. All permeate samples had < 15 ppm of total organic carbon (detection limit of analysis), confirming virtually all of the glycerol had been removed from the TFC Q_I membrane pores. The general water

nanofiltration procedure was then followed, with the following order of solutes tested: sucrose, glucose, glycerol, ethylene glycol, NaCl, and $MgCl_2$. A final filtration was performed with pure water to determine the pure water flux at the end of the experiments.

5.4.15. Estimation of the effective pore size by fitting the neutral solute rejection data with the Ferry equation.

The original Ferry equation describes particle rejection through uniform-size pores as a function of effective solute particle size (r_{solute}) and effect pore size (r_{pore}).[28] This simple steric pore model assumes that the solutes are spherical and the membrane pores are uniform cylinders.[28] The Ferry equation has been used to describe a variety of porous membranes. The Ferry equation is shown as follows in Equation 5.S3:

$$R' = \left[1 - \left(1 - \frac{r_{solute}}{r_{pore}}\right)^2\right]^2 \cdot 100 \qquad \text{(Equation 5.S3)}$$

where *R'* is the rejection in percent based on pore size exclusion, r_{solute} is the solute diameter, and r_{pore} is the pore diameter. The Ferry equation has also been recently found to be also valid for earlier versions of Q_I-phase LLC polymer membranes with uniform slit pores with a uniform slit width that is equivalent to r_{pore}. (Figure 5.S14).[4]

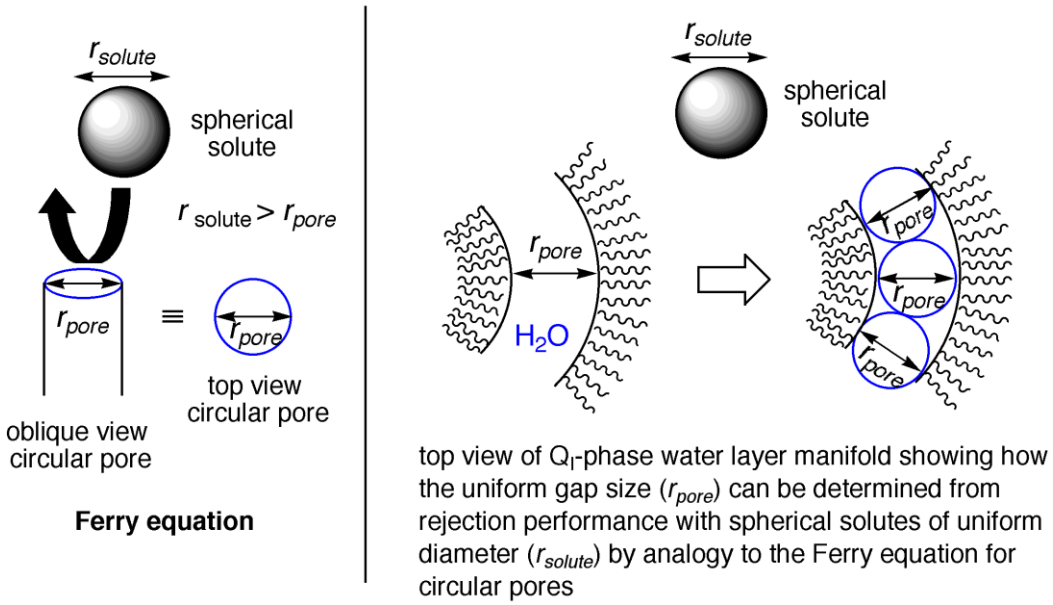

Figure 5.S14. Model for applying the Ferry equation for rejection performance of membranes with uniform circular pores to a Q_I-phase system with a uniform water layer manifold to determine layer gap spacing.[22]

The observed rejection data for the non-charged solutes of the TFC Q_I polymer membranes made from **10**/glycerol/HMP were fitted to the Ferry equation to estimate the effective pore size in the absence of pore wall and solute particle charge-charge effects. The neutral solute diameters used in this study are the same as the values used in two previous studies.[4,20] From fitting the uncharged solute rejection data to the Ferry model, it was found that the effective pore size of the TFC Q_I polymer membranes of **10**/glycerol/HMP is 0.96 nm. The Ferry Equation plot set to a uniform pore size of 0.96 nm is in excellent agreement with the experimental rejection data for the tested non-charged solutes (Figure 5.S15).

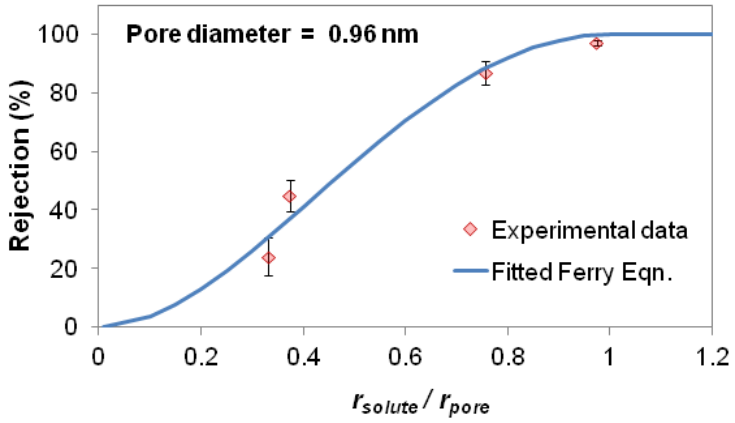

Figure 5.S15. Experimentally measured rejection data for the TFC Q_I membranes made from **10**/glycerol/HMP for several non-charged solute molecules, and the Ferry equation plot with a uniform pore size (r_{pore}) of 0.96 nm overlaid on these experimental data.

5.4.16. Preliminary studies showing the beneficial effect of aq. NaCl pre-treatment on the water flux of the TFC Q_I membranes for neutral solute filtrations without compromising rejection.

Membrane discs (2.5 cm in diameter) of the TFC Q_I polymer membranes made from **10**/glycerol/HMP were punched out from small sheets using a sharpened circular die. Membrane discs were then soaked in a 2000 ppm NaCl solution for 1 h at ambient temperature. After soaking, the membrane discs were carefully loaded into the custom-made, stainless-steel, stirred dead-end filtration cells. All nanofiltration experiments were performed with 400 psi (2.76×10^6 Pa) of N_2 pressure as the driving force at ambient temperature (22 ± 1 °C). The cells were then filled with de-ionized water that was then filtered through the membranes until at least 5 mL of permeate was collected in each cell. The cells were then reloaded with de-ionized water and filtered until another 5 mL of permeate was collected and analyzed for any residual organic carbon. All permeate samples had <15 ppm of total organic carbon (detection limit of analysis), confirming that virtually all of the glycerol had been removed from the TFC Q_I membrane pores.

The general water nanofiltration procedure was then followed. A final filtration was performed with de-ionized water to determine the pure water flux at the end of the experiment. As seen in Table S2, the rejection performance of the aq. NaCl pre-treated TFC Q_I polymer membranes is the same (within error) as that of the untreated TFC Q_I polymer membranes that were just soaked in de-ionized water before filtration (see Table 5.1). However, the fluxes of the aq. NaCl pre-treated TFC Q_I polymer membranes are virtually identical (within error) for all of the test solutes, whereas the untreated TFC Q_I membranes only showed a significant increase in the flux after contact with salt feed solutions (see Table 5.S2).

Table 5.S2. Rejection and water flux data for individually tested TFC Q_I polymer membranes pre-soaked in a 2000 ppm NaCl solution before conducting neutral solute filtration experiments.

Test solute	Hydrated diameter (nm)[a]	Rejection (%)	Flux (L m^{-2} h^{-1})
Sucrose	0.94	96 ± 2	0.7 ± 0.2
Glucose	0.73	78 ± 5	0.7 ± 0.2
Glycerol	0.36	37 ± 5	0.7 ± 0.2
Ethylene glycol	0.32	18 ± 3	0.7 ± 0.2
NaCl	0.72 (aq)	98 ± 1	0.7 ± 0.2
$MgCl_2$	0.86 (aq)	99.7 ± 0.1	0.7 ± 0.2

[a]Hydrated diameters of solute molecules and ions were obtained from the cited papers in Ref. 4.

PXRD analysis of the aq. NaCl pre-treated TFC Q_I membranes did not show any noticeable differences in the LLC nanostructure. We are currently investigating the nature of this beneficial effect on water flux (without compromising rejection performance) in more detail. More information on this phenomenon will be published in a more detailed follow-up publication.

5.4.17. Comparison of the performance of TFC Q_I membranes with commercial Dow SW30HR (RO) and DOW NF-270 (NF) membranes.

The water nanofiltration testing of SW30HR and NF-270 membranes under the same test conditions as the TFC Q_I membranes using the same custom-made, stainless-steel, stirred dead-end filtration cells is published in the literature.[5] Membrane discs (2.5 cm in diameter) were punched out from sheets using a sharpened circular die. The membrane discs were carefully loaded into separate custom-made, stainless-steel, stirred, dead-end filtration cells. All nanofiltration experiments were performed with 400 psi (2.76×10^6 Pa) of N_2 pressure as the driving force at ambient temperature (22 ± 1 °C). The cells were then filled with de-ionized water that was filtered through the membranes until at least 5 mL of permeate was collected in each cell. This first filtration was to ensure the integrity of the membrane and clean out any contaminants that might remain in the membrane after processing. Filtration experiments were then carried out using aqueous feed solution containing a single solute at 2000 ppm. Each stirred dead-end filtration cell was loaded with 25 mL of the feed solution and then pressurized. The first 1–2 mL of permeate was discarded. The next 2–4 mL of permeate was then collected and examined to determine rejection and flux. The neutral organic solute rejection, salt rejection, and water flux measurements were made as described in the previous sections.

As seen in Figure 5.S16, when compared to a high-performance RO membrane (Dow SW30HR) and a porous NF membrane with non-uniform pores (Dow NF-270) tested under the same conditions, the **10**/glycerol/HMP TFC Q_I membranes were found to have neutral solute rejections higher than the NF membrane but lower than the RO membrane for all of the solutes tested. However, the salt rejection performance of the TFC Q_I membrane is much higher than that of the NF membrane and comparable to that of the RO membrane. These rejection properties

make these new TFC Q_I membranes unique in terms of their water purification performance: They perform neutral solute separations better than a NF membrane (due to the uniform pore size distribution), but reject certain salts at a high level similar to that of a RO membrane. The TFC Q_I membranes operate in a performance regime between that of conventional NF and RO membranes. The pure water flux and thickness-normalized pure water permeability values of SW30HR, NF-270 and the TFC Q_I membranes measured under the same dead-end filtration conditions (25-mm-ID test cells; 400 psi applied pressure) are summarized in Table 5.S3 below.

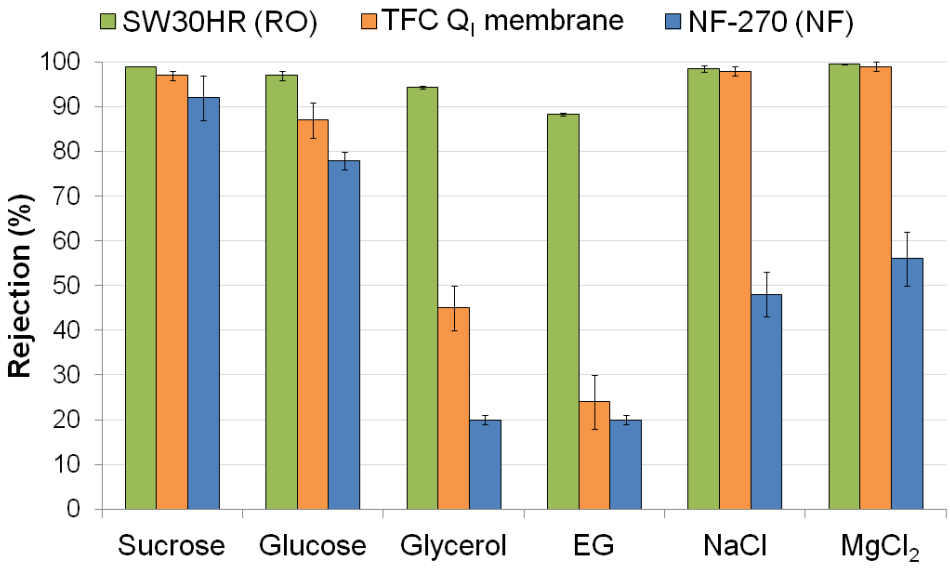

Figure 5.S16. Comparison of rejections of TFC Q_I, SW30HR, and NF-270 membranes (stirred dead-end filtration; 400 psi; 2000 ppm aq. feed solutions).

Table 5.S3. Comparison of pure water flux and thickness-normalized pure water permeability values for NF-270, SW30HR, and the TFC Q_I membranes of **10**/glycerol/HMP measured under the same dead-end filtration test conditions.

Membrane	**Active Layer Thickness (μm)**	**Pure Water Flux ($L\ m^{-2}\ h^{-1}$)**	**Thickness-normalized Pure Water Permeability ($L\ m^{-2}\ h^{-1}\ bar^{-1}\ \mu m$)**
NF-270	0.1[a]	250[a]	0.91[a]
SW30HR	0.1[a]	22[a]	0.080[a]
TFC Q_I membrane of 10/glycerol/HMP	3	0.61 ± 0.05	0.066 ± 0.005

(a) Data from Ref. 5.

As can be seen in Table 5.S3, the observed pure water flux of the TFC Q_I membranes is much lower than the commercial membranes. The low water flux can be attributed to the thicker active layer of the TFC Q_I membranes compared to SW30HR and NF-270 (i.e., 3 μm vs. ca. 0.1 μm). However, when normalized for active layer thickness, the nanoporous Q_I network separation material in the TFC Q_I membranes has a thickness-normalized pure water permeability that is comparable to that of the active material in SW30HR. This suggests if the Q_I separation material can be processed as thin as the commercial membranes, it may be possible to obtain fluxes comparable to that of an RO membrane.

5.5. References

1. For reviews of cross-linked LLC phases and their applications, see: (a) Gin, D. L.; Gu, W.; Pindzola, B. A.; Zhou, W.-J. *Acc. Chem. Res.* **2001**, *34*, 973. (b) Mueller, A.; O'Brien, D. F. *Chem. Rev.* **2002**, *102*, 727. (c) Gin, D. L.; Lu, X.; Nemade, P. R.; Pecinovsky, C. S.; Xu, Y.; Zhou, M. *Adv. Funct. Mater.* **2006**, *16*, 865.

2. Gin, D. L.; Bara, J. E.; Noble, R. D.; Elliott, B. J. *Macromol. Rapid Commun.* **2008**, *29*, 367.

3. For a recent overview of materials design for advanced membranes, see: Gin, D. L.; Noble, R. D. *Science* **2011**, *332*, 674.

4. Zhou, M.; Nemade, P. R.; Lu, X.; Zeng, X.; Hatakeyama, E. S.; Noble, R. D.; Gin, D. L. *J. Am. Chem. Soc.* **2007**, *129*, 9574.

5. Hatakeyama, E. S.; Gabriel, C. J.; Wiesenauer, B. R.; Lohr, J. L.; Zhou, M.; Noble, R. D.; Gin, D. L. *J. Mem. Sci.* **2011**, *366*, 62.

6. Hatakeyama, E. S.; Wiesenauer, B. R.; Gabriel, C. J.; Noble, R. D.; Gin, D. L. *Chem. Mater.* **2010**, *22*, 4525.

7. Fell, C. J. D. "Reverse Osmosis," In *Membrane Separations Technology. Principles and Applications*; Noble, R. D.; Stern, A. S.; Eds.; Elsevier Science: Amsterdam, 1995; Chapter 4.

8. Bhattacharya, A.; Ghosh, P. *Rev. Chem. Eng.* **2004**, *20*, 111.

9. Henmi, M.; Nakatsuji, K; Ichikawa, T.; Tomioka, H.; Sakamoto, T.; Yoshio, M.; Kato, T. *Adv. Mater*. **2012**, *24*, 2238.

10. Zhou, M.; Kidd, T. J.; Noble, R. D.; Gin. D. L. *Adv. Mater.* **2005**, *17*, 1850.

11. For an overview of LLC systems formed with organic solvents, see: Auvray, X.; Perche, T.; Petipas, C.; Anthore, R. *Langmuir* **1992**, *8*, 2671.

12. Kerr, R. L.; Miller, S. A.; Shoemaker, R. K.; Elliott, B. J.; Gin, D. L. *J. Am. Chem. Soc.* **2009**, *131*, 15972.

13. For a recent review of ILs as solvents for surfactant and LLC self-assembly, see: Greaves, T. L.; Drummond, C. J. *Chem. Soc. Rev.* **2008** *37*, 1709.

14. Shimura, H.; Yoshio, M.; Hoshino, K.; Mukai, Ohno, H.; Kato, T. *J. Am. Chem. Soc.* **2008**, *130*, 1759.

15. Tiddy, G. J. T. *Phys. Rep.* **1980**, *57*, 1.

16. Bowen, W. R.; Mohammad, A. W.; Hilal, N. *J. Mem. Sci.* **1997**, *126*, 91.

17. Kosutic, K.; Furac, L.; Sipos, L.; Kunst, B. *Sep. Purif. Technol.* **2004**, *42*, 137.

18. Nightingale, Jr., E. R. *J. Phys. Chem.* **1959**, *63*, 1381.

19. Bhattacharyya, D.; Williams, M. E. "Reverse Osmosis: Design," In *Membrane Handbook*; Ho, W. S.; Sirkar, K. K.; Eds.; Kluwer Academic: Boston, 2001.

20. Hatakeyama, E. S.; Wiesenauer, B. R.; Gabriel, C. J.; Noble, R. D.; Gin, D. L. *Chem. Mater.* **2010**, *22*, 4525.

21. Pindzola, B. A.; Hoag, B. P.; Gin, D. L. *J. Am. Chem. Soc.* **2001**, *123*, 4617.

22. Bara, J. E., Hatakeyama, E. S.; Zeng, X.; Noble, R. D.; Gin, D. L. *Liq. Cryst.* **2010**, *37*, 1587.

23. Gin, D. L.; Zhou, M.; Noble, R. D.; Bara, J. E.; Wiesenauer, B. R.; Kerr, R. L. U.S. Patent 20090173693, issued July 9, 2009.

24. Greaves, T. L; Weerawardena, A.; Fong, C.; Krodkiewska, I.; Drummond, C. J. *J. Phys. Chem. B.* **2006**, *110*, 22479.

25. Fontell, K. *Colloid Polym. Sci.* **1990**, *268*, 264.

26. Mariani, P.; Luzzati, V.; Delacroix, H. *J. Mol. Biol.* **1988**, *204*, 165.

27. Petersen, R. J. *J. Mem. Sci.* **1993**, *83*, 81.

28. Aimar, P.; Meireles, M.; Sanchez, V. *J. Mem. Sci.* **1990**, *54*, 321.

CHAPTER 6

Nanopore size-tuning of Q_I-phase lyotropic liquid crystal polymer membranes through the use of monomer blends

6.1. Introduction

Utilization of polymer-based membranes for molecular transport and filtration applications has been of great interest recently. In order to generate polymer membranes for these types of applications, some elements that must be considered are (a) forming mechanically stable and robust materials, (b) designing easily processed and scalable materials, and (c) fabrication of high surface-area, defect-free thin films.[1] Each of these characteristics is necessary for a membrane to perform chemical separations and also for the highest possible throughput of the generated material.[1] The two broad classes for membranes that can perform chemical separation and molecular transport are dense and nanoporous membranes.[2-7]

Dense polymer membranes are typically amorphous, rubbery polymer membranes with no structured porous morphology, where molecular transport occurs through the interchain voids of the polymers in a solution-diffusion (S-D) mechanism.[8] In S-D, partial pressure differential across a polymeric membrane causes a solute transport driving force, and in turn, a distinct solute permeability (P). Permeability is a function of the diffusivity (D) and the solubility (S) of each solute as it transports through the membrane. Solute transport occurs once the solute adsorbs onto the upstream face of the membrane, diffuses through the dense membrane, and finally desorbs from the membrane at the downstream surface. This mechanism is affected by the unique solubility and diffusivity properties of the polymeric membrane material. Solute

separation can be achieved through the aforementioned differences between solute particles to yield a permselectivity (α), which represents the ratio of permeabilities between solutes through the membrane material. Larger differences in diffusivities and/or solubilities between two solutes will result in larger differences in P and therefore better solute separation.

In contrast, nanoporous membranes have discreet, ordered pores on the order of 1–10 nm in diameter to enable separation of molecular- and macromolecular-size substrates via a size-exclusion mechanism.[8] This mechanism involves permeate particulates or molecules that are larger than the effective pore size to be prevented from passing through the membrane, while smaller compounds are allowed to permeate. Therefore, the separation capability of a nanoporous membrane is limited by the pore size distribution and pore density of the material. Dense polymer-based membranes are more easily fabricated because little consideration needs to be paid to membrane alignment or controlling membrane architecture. Unfortunately, when it comes to generation of nanoporous polymer membranes, there are several characteristics that are necessary for consideration. Any efficient nanoporous membrane needs the pores to be aligned in the direction of molecular transport, would have a high degree of porosity, and requires a uniformity of pore size such that separations are consistent across membranes. The difficulty in fabricating nanoporous polymer membranes stems from the lack of natural or commercially available building blocks and methods for easily producing and controlling pore architectures on this size regime. Only about a dozen methods exist in the literature for generating nanoporous materials with uniform, sub-1-nm pores for membrane-based molecular transport or filtration applications.[9-24] Methods to generate materials with sub-1-nm pores include use of carbon nanotubes,[9,10] deposition to reduce pore size of commercial organic polymers,[11,12] use of macrocyclic compounds,[13-15] self-organization of thermotropic liquid crystals,[16] mixed-matrix

systems,[17] inorganic- and zeolite-based systems,[18-20] and via track-etching of polymer and copolymer materials.[21-24] Within these broad methods for designing polymer-based membranes with uniform pore sizes, there are very few experimental techniques known that allow the researcher to systematically tune the nanopores that are generated. In terms of tuning of nanopores in inorganic materials, the methods that have been evaluated include modulating anionic character of titanium silicate molecular sieves,[25] using solvent manipulations to tune mesopore structure of TiO_2[26] and ZrO_2,[27] tuning the porosity of bimetallic structures via soft templating,[28] and manipulation of pores in silica-based materials[29-33]. Attempts have been made to modulate the pore size of organic polymer materials via deposition experiments,[34,35] plasticization with high pressure CO_2,[36] mechanical manipulations,[37] adjusting the conditions of the microemulsion that generated these polymers,[38-40] hydrogel functionalization of pores,[41,42] addition of sugars to pore-forming surfactant systems,[43] and changing temperature and salt concentration of surfactant systems.[44-48]

In this work, a new method for modulating the effective pore size of type I bicontinuous cubic (Q_I)-phase lyotropic liquid crystal (LLC)-based polymer membranes for water nanofiltration (NF) was explored. As described in prior chapters and cited papers, Q_I-phase LLC membranes based on amphiphilic gemini monomers **3b**, **4a**, and **10** have 3D-interconnected solvent-filled (i.e., water or glycerol) uniform pores in the 0.75-0.96 nm size scale that allow them to do molecular sieving separations of aqueous or gas mixtures.[49-51] This new method involves blending amphiphilic co-monomers with established Q_I-phase-forming monomers to attempt to subtly alter the resulting overall Q_I phase curvature, interfacial energy, and hopefully annular pore size. This new method was explored because prior work has shown that structural variation to the tail length, headgroup spacer length of established Q_I-phase forming monomers

did not afford any control/variation of Q_I phase pore size.[49-51] In fact, in some cases these monomer structure alterations disrupted the ability of the monomer to form a Q_I phase.[49]

Monomer **10** was used as the base monomer for all of the following LLC monomer blending experiments to adjust the Q_I-phase pore size because its non-aqueous phase formation and membrane fabrication has been well-established.[49] Systematic variation of the amount of the monomeric dopants (**11**, **12**, **16**, **18**, and **19**; see Figure 6.1) added to the base LLC monomer system, we were able to probe the LLC phase character of each blended monomer system in the low-volatility solvent glycerol. In order to fabricate these LLC monomer blends into usable NF membranes, it is necessary to perform thin-film processing techniques on the material, to cast as thin of a film as is possible. Along with LLC phase structure analysis, MeOH-casting of one of these blends was attempted.

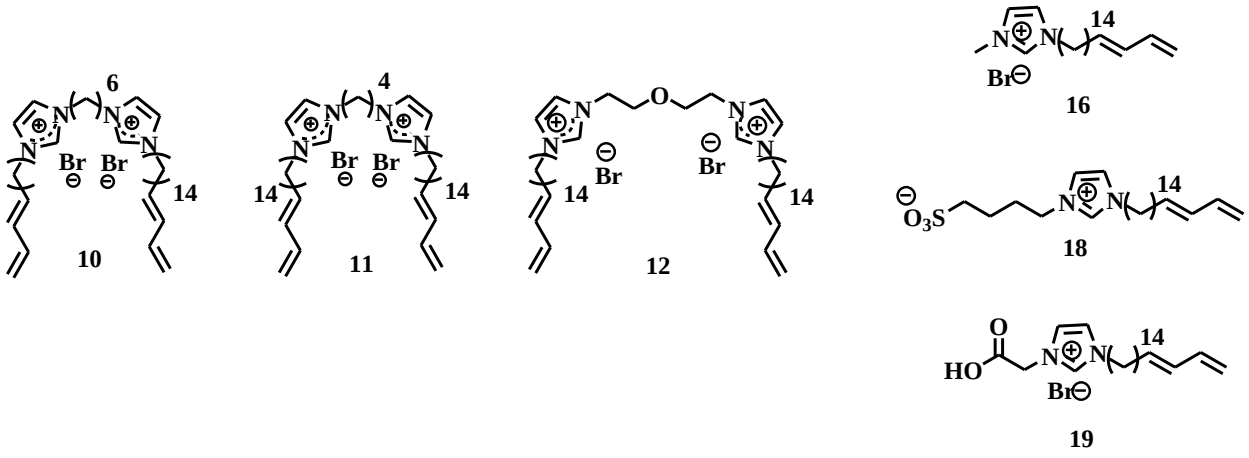

Figure 6.1. Structure of all LLC monomers analyzed for this work. LLC **10** was used as the base monomer for all of the blending studies. Small amounts (5, 10, 15 wt%) of the other monomers were added systematically, and the LLC phase behavior in glycerol was observed.

6.2. Experimental

6.2.1 Materials

Chromium (IV) oxide, pyridine, allyltrimethylsilane (98%), *sec*-butyl lithium (1.4 M in cyclohexane), aluminum oxide (activated, basic), 2-isopropoxy-4,4,5,5-tetramethyl-1,3,2-dioxaborolane (98%), hydrogen bromide (48 wt% in H_2O), borane-tetrahydrofuran complex solution (1.0 M in THF), *p*-toluenesulfonyl chloride, diethylene glycol, 1,4-dibromobutane (99%), 1,6-dibromohexane (96%), sodium hydride (60 wt.% dispersion in mineral oil), imidazole, ω-pentadecalactone (98%), 2-hydroxy-2-methylpropiophenone (HMP, 97%), 1-methylimidazole, 2-bromoacetic acid, and ethylene glycol (all ACS Reagents unless specified otherwise) were purchased from the Sigma-Aldrich Chemical Co., and used as received. Glycerol (ACS Reagent) was purchased from Mallinckrodt, and used as received. Sulfuric acid (ACS Reagent) was purchased from VWR, and used as received. Sodium hydroxide, sodium chloride, and magnesium chloride (all ACS Reagents) were purchased from Fisher Scientific, and used as received. 1,4-butanesultone was purchased from TCI America and used without further purification. Filtration through silica gel was performed using 230-400 mesh, normal-phase silica gel purchased from Sorbent Technologies.

6.2.2. Instrumentation

^{1}H NMR and ^{13}C NMR spectra were obtained using a Bruker 300 Ultrashield^{TM} (300 MHz for ^{1}H) spectrometer. Chemical shifts are reported in ppm relative to deuterated solvent. Fourier-transform infrared spectroscopy (FT-IR) measurements of all of the new monomers synthesized were performed using a Matteson Satellite series spectrometer, as thin films on Ge crystals. All other FT-IR measurements were performed using a Thermo Scientific Nicolet 6700

spectrometer equipped with a PIKE MIRacle^{TM} single-reflection horizontal ATR accessory with a diamond crystal. HRMS analysis was performed by the Central Analytical Facility in the Dept. of Chemistry and Biochemistry at the University of Colorado, Boulder. Powder X-ray diffraction (XRD) spectra were collected using an Inel CPS 120 diffraction system with a monochromated Cu K_α radiation source. This apparatus was equipped with a film holder to analyze membrane samples. All powder XRD spectra were calibrated using a silver behenate diffraction standard (d_{100} = 58.4 ± 0.1 Å). Powder XRD measurements were all performed at ambient temperature (22 ± 1 °C), unless noted otherwise. Polarized light microscopy (PLM) was performed using a Leica DMRXP polarizing light microscope equipped with a Linkam LTS 350 thermal stage, a Linkam CI 94 temperature controller, and a Q-Imaging MicroPublisher 3.3 RTV digital camera. Automatic temperature profiling and image capture were accomplished using Linkam Linksys32 software. Radical photopolymerizations were conducted using a Spectroline XX-15A 365 nm UV lamp (1 mW cm^{-2} at the sample surface). UV light fluxes at the sample surface were measured using a Spectroline DCR-100X digital radiometer equipped with a DIX-365 UV-A sensor.

6.2.3. New monomer synthesis and characterization

The new single-tailed monomer additives **16**, **18**, and **19** were prepared via the method seen in Figure 6.2 below. Detailed synthetic procedures, as well as structural analysis and characterization information on each new monomer synthesized will follow.

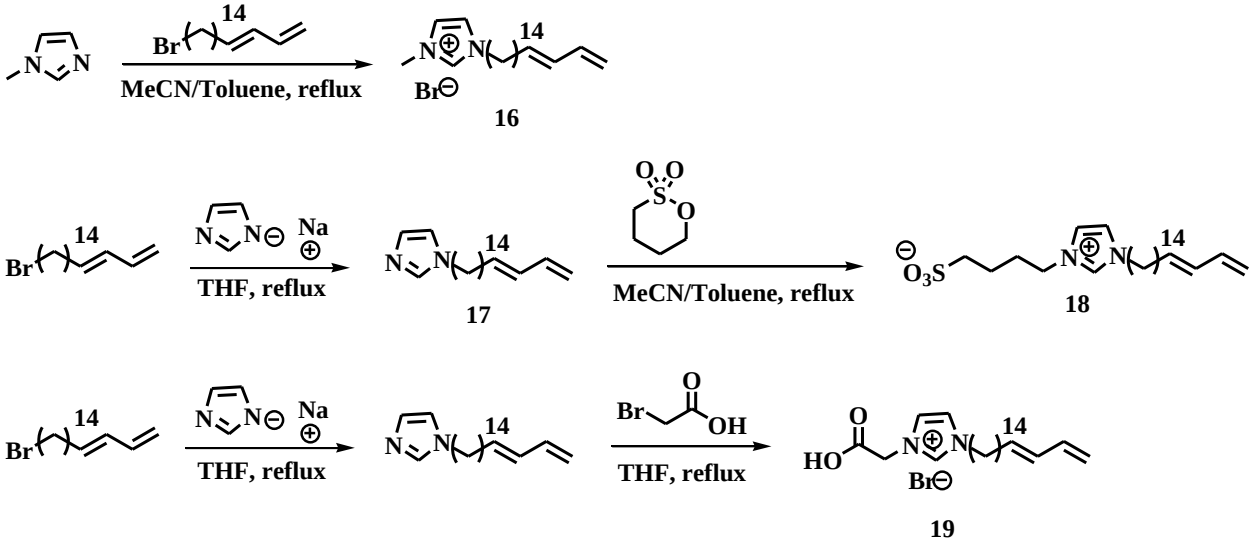

Figure 6.2. Schemes for the synthesis of new single-tailed and functionalized monomers **16**, **18** and **19**.

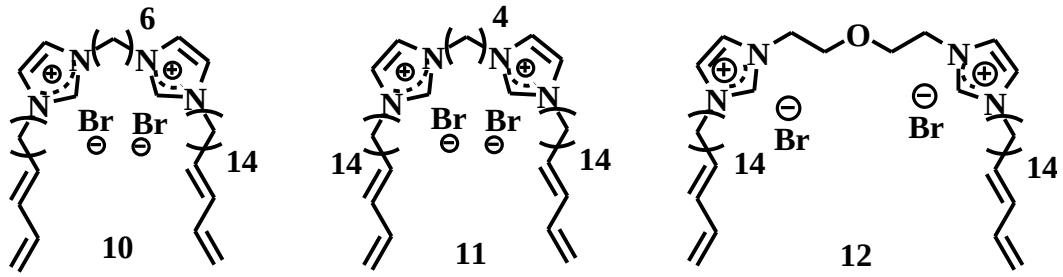

Figure 6.3. Structures of previously prepared gemini monomers used in the blending studies.

6.2.3.1. 1,6-Bis(octadeca-15,17-dienylimidazolium)hexane dibromide (10).

Synthesized as described in the literature.[49] Spectroscopic characterization and purity data for this compound matched published data.[49]

6.2.3.2. 1,4-Bis(octadeca-15,17-dienylimidazolium)butane dibromide (11).

Synthesized as described in the literature.[49] Spectroscopic characterization and purity data for this compound matched published data.[49]

6.2.3.3. 1,1'-(Oxydi-2,1-ethanediyl)bis[3-(octadeca-15,17-dienyl)imidazolium] dibromide (12).

Synthesized as described in the literature.[49] Spectroscopic characterization and purity data for this compound matched published data.[49]

6.2.3.4. 1-(octadeca-15,17-dienyl)imidazole (17).

Sodium imidazolate (1.495 g, 16.60 mmol, 100 mol%) was dried *in vacuo* in a 250-mL round-bottom flask equipped with a stir bar and reflux condenser with gentle heating, before the addition of THF (70 mL). The slurry was heated to 70 °C with stirring while 18-bromooctadeca-1,3-diene (6.072 g, 18.44 mmol, 111.1 mol%) dissolved in THF (20 mL) was added dropwise over the course of 3 h. Reaction solution was stirred at reflux for 20 h. Upon cooling to RT, the solids that had formed were filtered off, followed concentration of the filtrate via rotatory vacuum (30 mmHg). The residual oil was crystallized from hexanes (- 40 °C), providing an off-white solid that was filtered and washed with cold hexanes (- 40 °C). The filtrate was crystallized again, followed by the same filtration procedure. Solids from both crops were transferred to a round bottom flask and dried in vacuo to afford the pure product as a white, powdery solid. Yield: 5.223 g (70%). ^{1}H NMR (300 MHz, $CDCl_3$) δ 7.45 (t, *J* = 1.1 Hz, 1H), 7.05 (t, *J* = 1.1 Hz, 1H), 6.90 (t, *J* = 1.3 Hz, 1H), 6.29 (dd, *J* = 17.0, 10.2 Hz, 1H), 6.12 – 5.96 (m, 1H), 5.80 – 5.62 (m, 1H), 5.08 (ddt, *J* = 17.0, 1.9, 0.7 Hz, 1H), 4.95 (ddt, *J* = 10.1, 1.8, 0.6 Hz, 1H), 3.92 (t, *J* = 7.1 Hz, 2H), 2.14 – 2.00 (m, 2H), 1.77 (t, *J* = 7.2 Hz, 2H), 1.58 (s, 2H), 1.48 – 1.10 (m, 22H).

6.2.3.5. 3-methyl-1-(octadeca-15,17-dienyl)imidazolium bromide (16).

18-Bromooctadeca-1,3-diene (3.191 g, 9.688 mmol, 100 mol%) and 1-methylimidazole (0.902 g, 11.0 mmol, 113 mol%) were fully dissolved in MeCN (12 mL) and toluene (12 mL) in a 250-mL round-bottom flask equipped with a stir bar and reflux condenser. The clear, colorless solution was heated to reflux and stirred for 72 h. Upon cooling to RT, reaction solution was concentrated via rotatory vacuum (30 mm Hg) to yield a white, powdery solid as crude product. This crude product was stirred in Et_2O (3 x 150 mL), and the solvent was decanted. The resulting white solid was further concentrated under rotatory vacuum (30 mm Hg), followed by further drying in vacuo afforded the product as a pure white, powdery solid. Yield: 3.4 g (85%). ^{1}H NMR (300 MHz, DMSO-d_6) δ 9.20 – 9.06 (m, 1H), 7.84 – 7.74 (m, 1H), 7.74 – 7.63 (m, 1H), 6.29 (dt, *J* = 17.0, 10.2 Hz, 1H), 6.04 (dd, *J* = 15.3, 10.4 Hz, 1H), 5.73 (dd, *J* = 14.8, 7.3 Hz, 1H), 5.09 (dd, *J* = 17.1, 1.9 Hz, 1H), 4.95 (dd, *J* = 10.1, 1.9 Hz, 1H), 4.25 – 4.05 (m, 2H), 3.84 (s, 3H), 2.04 (d, *J* = 7.0 Hz, 2H), 1.78 (d, *J* = 7.2 Hz, 2H), 1.24 (d, *J* = 4.4 Hz, 22H). ^{13}C NMR (300 MHz, DMSO-d6) δ 138.24, 137.50, 135.81, 130.93, 123.30, 121.65, 114.68, 50.39, 36.92, 32.69, 29.77, 29.75, 29.72, 29.71, 29.63, 29.50, 29.35, 29.32, 29.12, 26.40. IR (thin film, MeOH): 3062, 2920, 2852, 1640, 1568, 1472, 1176, 1012, 951, 920 cm^{-1}. HRMS (ES) calcd. for $C_{22}H_{39}BrN_2$ ($2A^+Br^-$): 741.5394; observed: 741.5404.

6.2.3.6. 1-carboxymethyl-3-(octadeca-15,17-dienyl)imidazolium bromide (19).

1-(Octadeca-15,17-dienyl)imidazole (2.107 g, 6.657 mmol, 100 mol%) was fully dissolved in THF (70 mL) in a 250-mL round-bottom flask equipped with a stir bar and reflux condenser. 2-Bromoacetic acid (1.147 g, 8.255 mmol, 124 mol%) was added followed by heating the solution to 71 °C and stirring the clear, light yellow solution for 48 h. Overnight, a fine, off-

white precipitate formed. Upon cooling to RT, reaction solution was placed at 0 °C to drive precipitation of product. The white, powdery solid was filtered off, followed by washing with cold THF (3 x 50 mL). Solid was transferred to a round bottom flask and dried in vacuo to afford a white, powder as pure product. Yield: 5.59 g (84%). ^{1}H NMR (300 MHz, DMSO-d6) δ 9.05 – 8.94 (m, 1H), 7.65 (t, *J* = 1.8 Hz, 1H), 7.60 (t, *J* = 1.7 Hz, 1H), 6.36 – 6.14 (m, 1H), 6.06 – 5.92 (m, 1H), 5.76 – 5.63 (m, 1H), 5.14 – 4.97 (m, 3H), 4.92 (d, *J* = 10.2 Hz, 1H), 4.14 (t, *J* = 6.9 Hz, 2H), 2.00 (d, *J* = 7.0 Hz, 2H), 1.74 (s, 2H), 1.18 (s, 22H). ^{13}C NMR (300 MHz, DMSO-d6) δ 169.11, 138.17, 138.05, 136.25, 131.82, 124.85, 122.90, 116.04, 50.69, 49.87, 32.83, 30.30, 29.98, 29.88, 29.79, 29.55, 29.28, 26.38. HRMS (ES) calcd. for $C_{23}H_{39}BrN_2O_2$ (A^+): 375.3005; observed: 375.3011.

6.2.3.7. 3-(octadeca-15,17-dienyl)-1-(4-sulfobutyl)imidazolium (18).

1,4-Butanesultone (0.605 g, 4.45 mmol, 105 mol%) and 1-(octadeca-15,17-dienyl)imidazole (1.340 g, 4.233 mmol, 100 mol%) were fully dissolved in MeCN (10 mL) and toluene (10 mL) in a 100-mL round-bottom flask equipped with a stir bar and reflux condenser. The light yellow, clear solution was heated to 81 °C and stirred for 70 h. Upon cooling to RT, a powdery, off-white solid began to precipitate. Reaction solvent was decanted, followed by stirring in hexanes (2 x 100 mL) and Et_2O (3 x 100 mL), each followed by decantation of the solvent. Solid was transferred to a round-bottom flask and the solvent was concentrated under rotatory vacuum (30 mm Hg), then further dried in vacuo to afford a white, powdery solid as product. Yield: 1.801 g (94%). ^{1}H NMR (300 MHz, $CDCl_3$) δ 10.09 (s, 1H), 7.30 (d, *J* = 1.8 Hz, 1H), 7.14 (t, *J* = 1.6 Hz, 1H), 6.31 (dt, *J* = 17.0, 10.3 Hz, 1H), 6.04 (dd, *J* = 15.3, 10.3 Hz, 1H), 5.71 (dd, *J* = 14.7, 7.3 Hz, 1H), 5.16 – 5.01 (m, 1H), 4.94 (d, *J* = 10.6 Hz, 1H), 4.41 (t, *J* = 7.0 Hz, 2H), 4.23 (t, *J* = 7.5

Hz, 2H), 2.94 (t, *J* = 7.1 Hz, 2H), 2.28 – 2.00 (m, 4H), 2.00 – 1.78 (m, 4H), 1.49 – 0.98 (m, 22H). ^{13}C NMR (300 MHz, $CDCl_3$) δ 138.45, 137.72, 136.02, 131.16, 121.60, 114.90, 50.90, 50.51, 49.95, 32.91, 30.54, 30.00, 29.99, 29.95, 29.86, 29.73, 29.58, 29.55, 29.36, 26.67. HRMS (ES) calcd. for $C_{25}H_{44}N_2O_3S$ (MH^+): 453.3142; observed: 453.3151.

6.2.4. General procedures

6.2.4.1. Preparation of monomer blend samples for PLM analysis

In order to adequately mix the monomer blends into a homogeneous powder, with the appropriate weight percentage compositions, the powders were weighed out into a 50-mL round-bottom flask, then dissolved in CH_2Cl_2 (10 mL). After 1 h of stirring, the solvent was removed under rotatory vacuum (30 mmHg) then further removed in vacuo to afford the monomer blends as fine, powdery solids. The monomer blends that were analyzed in this study have been summarized in Table 6.1 below.

Table 6.1. The monomer blends and compositions that were studied for this work.

Monomer Blend	Wt% 10	Wt% 16	Wt% 18	Wt% 19	Wt% 12	Wt% 11
1016A	90	10	-	-	-	-
1018A	95	-	5	-	-	-
1018B	90	-	10	-	-	-
1018C	85	-	15	-	-	-
1019A	95	-	-	5	-	-
1019B	90	-	-	10	-	-
1019C	85	-	-	15	-	-
1012A	95	-	-	-	5	-
1012B	90	-	-	-	10	-
1012C	85	-	-	-	15	-
1011A	95	-	-	-	-	5
1011B	90	-	-	-	-	10
1011C	85	-	-	-	-	15

6.2.4.2. Screening of LLC phase behavior with glycerol using the PLM-based penetration scan technique.[52]

The PLM-based penetration scan technique[52] is a method used to quickly and qualitatively survey the LLC phase behavior monomer mixtures of both gemini/gemini blends, and gemini/single-tailed blends in glycerol (see Table 6.4). This technique is a solvent-amphiphile gradient assay utilizing PLM to quickly (i.e., in minutes) and qualitatively determine examine a solvent/amphiphile system for the possible phases in exhibits by varying the temperature of the system. This technique was performed by taking the solid, powdery monomer and placing it between a microscope slide and cover slip. The sample was then placed on the PLM thermal stage and annealed to 85 °C at a rate of 30 °C/min. The sample was held at this temperature, and a small amount (<30 μL) of glycerol was added to the edge of the cover slip.

Capillary action drew the solvent into contact with the solid sample, generating a concentration gradient throughout the specimen, which was held at this elevated temperature for 8 min. The sample was slowly cooled down to room temperature before gradually heating to 85 °C at a rate of 5 °C, capturing images digitally along the way.

6.2.4.3. LLC phase characterization of monomer blend 1016A in glycerol

PLM penetration scan analysis showed that there was a potential bicontinuous cubic phase in the monomer blend containing 90/10 (w/w) **10**/**16**, using glycerol as the solvent at elevated temperature. Samples were prepared for phase diagram work by placing an amount of glycerol into custom-made glass vials and centrifuging such that the glycerol was located at the bottom of the vials (3000 rpm, 15 min). The appropriate mass of the **1016A** monomer blend was added to the vial, followed by another round of centrifuging (3000 rpm, 15 min). Thorough hand-mixing produced a homogeneous LLC paste that was the specimen analyzed at each composition of interest. Each prepared LLC sample was run through the same heating/cooling cycle as prescribed above and the phase character was observed visually.

6.2.4.4. Polymerization of thin films of Q-phase 1016A in glycerol

A custom-made glass vial was prepared with the appropriate ratio of glycerol : **1016A** as prescribed above, with no photo-initiator added. The first polymerization attempt was run without photo-initiator because it was hypothesized that with this very small Q-phase composition window, the addition of a photo-initiator could cause the mixture to lose its desired phase. The composition of interest was determined to be 82/18 (w/w) **1016A** : glycerol, an LLC : solvent mixture composition that is in the middle of the Q-phase composition window. The

thoroughly mixed sample was then dissolved as a 60 wt% solution in MeOH before pipette-casting onto a glass slide. The glass slide was left at RT and ambient conditions for 45 min, in order to allow the MeOH to completely evaporate. The sample on the glass slide was transferred to a hot plate and heated to 85 °C, where it was held for 5 min before rapidly cooling to RT. This annealed sample was then slowly heated to 53 °C and equilibrated at that temperature for 5 min before irradiating with 365 nm light (1 mW cm^{-2}) for 1 h. After peeling the polymerized film off of the glass slide, it was taken for PLM and powder XRD analysis.

6.2.4.5. Polymerization of thin film of 1016A in glycerol under ambient and air-free conditions

The LLC mixture prepared in a custom-made glass vial with a mixture of 81.7/17.3/1 (w/w/w) **1016A**/glycerol/photo-initiator, in a manner similar to what was described above. A tiny aliquot of the mixture was kept aside, to determine via PLM whether the mixture will form a Q phase in the bulk (see Figure 6.4). The remaining LLC specimen was dissolve as a 60 wt% solution in MeOH and pipette-cast onto a glass slide, before allowing 45 min for the casting solvent would evaporate completely. The solvent-casted specimen was then transferred to a hot plate and ramped to 85 °C, where it was held to equilibrate for 5 min, followed by rapid cooling to RT. Sample was then slow heated to 55 °C and held for 5 min before irradiating with 365 nm light (1 mW cm^{-2}) for 1 h.

6.2.4.6. Air-free polymerization of 1016A in glycerol

Sample preparation was performed as described in section 6.2.4.2 above. A small aliquot of the prepared sample was saved for PLM observation before performing the MeOH-casting

process. The LLC specimen was dissolved in MeOH as a 60 wt% solution and pipette-casted onto a glass slide, before allowing 45 min for the solvent to fully evaporate. The sample was ramped to 85 °C and held for 5 min, before rapidly cooling to RT. After the sample had been given sufficient time to equilibrate to RT, the glass slide was transferred to an air-free polymerization cell. The air-free cell was purged of air using a high-vacuum line (500 mtorr), and filled with $Ar_{(g)}$, a process that was repeated 3 times to ensure no air remained. This cell was then placed on a hot plate, under a UV lamp and slowly heated to 55 °C before irradiating the sample with 365 nm light (1 mW cm^{-2}) for 1 h. The polymerized sample was peeled off of the glass slide and observed under PLM for LLC phase analysis.

6.2.4.7. LLC phase characterization for monomer blend 1011B in glycerol

PLM penetration scan analysis showed that there was a potential bicontinuous cubic phase in the monomer blend containing 90/10 (w/w) **10**/**11**, using glycerol as the solvent at elevated temperature. Samples were prepared for phase diagram work by placing an amount of glycerol into custom-made glass vials and centrifuging such that the glycerol was located at the bottom of the vials (3000 rpm, 15 min). The appropriate mass of the **1011B** blend was added to the vial, followed by another round of centrifuging (3000 rpm, 15 min). Thorough hand-mixing produced a homogeneous LLC paste that was the specimen analyzed at each composition of interest. Each prepared LLC sample was run through the same heating/cooling cycle as prescribed above and the phase character was observed visually.

6.2.4.8. LLC phase characterization for monomer blend 1011A in glycerol

PLM penetration scan analysis showed that there was a potential bicontinuous cubic phase in the monomer blend containing 95/5 (w/w) **10**/**11**, using glycerol as the solvent at elevated temperature. Samples were prepared for phase diagram work by placing an amount of glycerol into custom-made glass vials and centrifuging such that the glycerol was located at the bottom of the vials (3000 rpm, 15 min). The appropriate mass of the **1011A** blend was added to the vial, followed by another round of centrifuging (3000 rpm, 15 min). Thorough hand-mixing produced a homogeneous LLC paste that was the specimen analyzed at each composition of interest. Each prepared LLC sample was run through the same heating/cooling cycle as prescribed above and the phase character was observed visually.

6.3. Results and discussion

For this work, the use of different monomer blends with **10** was utilized to probe the ability tune the effective pore size of LLC-based polymeric NF membranes. Preliminary results were obtained for (a) monomer blends systems consisting of two gemini monomer amphiphiles in varying ratios and (b) gemini monomer **10** blended with single-tailed monomer species is varying compositions. Gemini LLC monomer **10** was chosen as the base monomer system, because its Q_I-phase-forming characteristics, effective pore size, and membrane fabrication processes have been well-defined and intensively studied in earlier work.[49]

6.3.1. PLM penetration scan analysis of phase character for all monomer blends

Potential LLC phases in the LLC/glycerol specimens were determined via examination of the differences in optical texture and intensity. Since Q phases are black (i.e., pseudo-

isotropic) under PLM and are typically found between birefringent (i.e., bright) lamellar (L) and hexagonal (H) phases, the presence of a dark isotropic band between two birefringent LLC phases indicates a potential Q phase. In this study, monomer **10** was blended in different proportions with both gemini monomers **11** and **12** (see Table 6.3), and single-tailed monomers **16**, **18**, and **19** in varying ratios (see Table 6.2), and the potential LLC phases were examined via PLM analysis, using glycerol as the solvent.

Table 6.2. Single-tailed/gemini monomer blends analyzed and their potential to form a bicontinuous cubic LLC phase.

Monomer Blend	Wt% 10	Wt% 16	Wt% 18	Wt% 19	Potential Q
1016A	90	10	-	-	Yes
1018A	95	-	5	-	No
1018B	90	-	10	-	No
1018C	85	-	15	-	No
1019A	95	-	-	5	Yes
1019B	90	-	-	10	No
1019C	85	-	-	15	No

Table 6.3. Gemini-based monomer blends that were analyzed, as well as their potential to form Q LLC phases.

Monomer Blend	Wt% 10	Wt% 11	Wt% 12	Potential Q
1011A	95	5	-	Yes
1011B	90	10	-	Yes
1011C	85	15	-	Yes
1012A	95	-	5	Yes
1012B	90	-	10	No
1012C	85	-	15	No

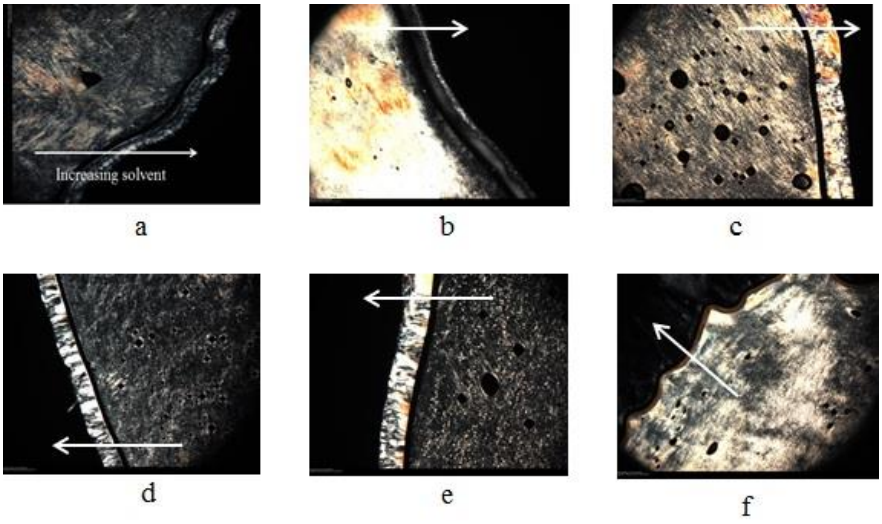

Figure 6.4. PLM images of penetration scans that exhibited a potential Q phase (mag = 50x). A black region between bright regions is indicative of a bicontinuous cubic phase. Solvent concentration increases in the direction of the arrow. Images are for monomer blends **1016A** (a), **1019A** (b), **1011A** (c), **1011B** (d), **1011C** (e), and **1012A** (f) in glycerol.

The most promising candidates based on this initial analysis were monomer blends involving gemini monomer **10** with gemini monomers **11** and **12**, as well as with single-tailed monomer **16**. In terms of gemini monomer blends with **10**, monomer **11** was selected for study because it exhibits more chemical similarity to **10** than **12** does. Monomer **16** was chosen

because of (a) its ease of synthesis was more amenable to this project, and (b) its lack of polar functional groups should allow it to incorporate better with monomer **10**.

6.3.2. Analysis of LLC monomer blends involving 10 and 16

Since PLM penetration scan observation suggested a robust Q_I phase for a 90/10 (w/w) **10**/**16** monomer blend, this composition was the initial target of observation. PLM analysis was performed on all compositions of monomer blend/glycerol that contained monomer blend percentages higher than those exhibiting the first appearance of the fluid isotropic phase (52 wt% **1016A**/48 wt% glycerol). The initial qualitative observations are recorded in the phase diagram and PLM images in Figure 6.5 below. Black PLM images were observed between 80 wt% and 83 wt% **1016A** monomer blend at elevated temperatures, with birefringent (i.e., bright) regions appearing on either side of the isotropic region. This observed Q_I-phase is somewhat narrower in comparison to previous Q_I LLC phases observed in monomer system designed in the Gin group (3 wt% vs. 5–7 wt%). These observations, as well as the optical transparency and stiffness of the LLC phase imply the presence of a bicontinuous cubic phase in the black region of the phase diagram.

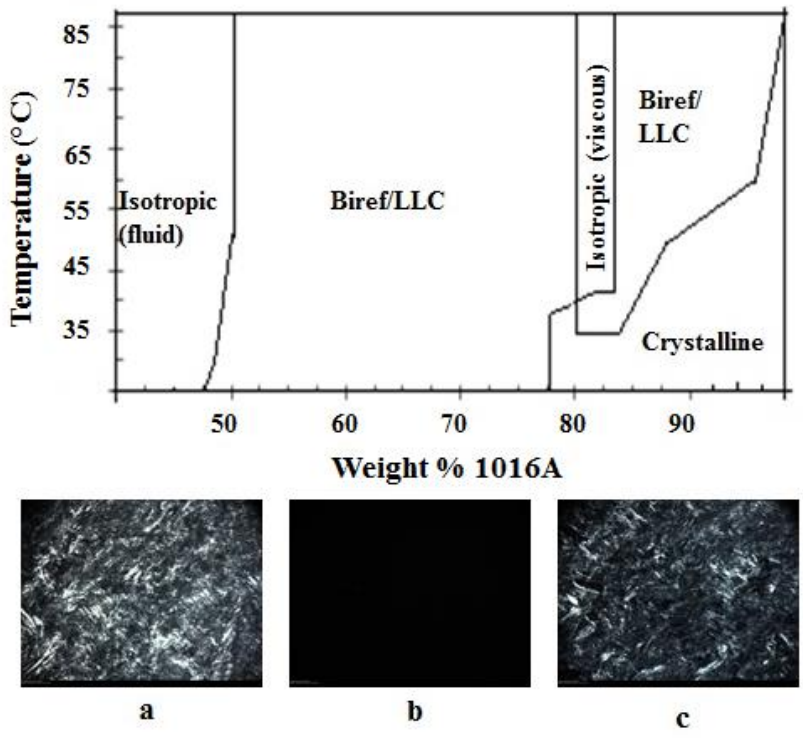

Figure 6.5. Phase diagram for the **1016A** monomer blend in glycerol (T = 22 ± 1 °C, P = 620 atm). The viscous, optically isotropic (i.e., black) phase as seen under PLM (b) between 80–83 wt% monomer can be interpreted as a Q phase, with anisotropic LLC phases on either side (a) and (c), and a crystalline phase at the same composition, but at lower temperatures (mag = 50x).

In order to confirm the LLC phase of the isotropic and optically clear phase outlined in the above phase diagram, XRD analysis is required. Powder XRD analysis of these LLC/glycerol mixtures must be performed on a polymer film, because in order to create a thin-film polymeric material out of these LLC monomer blends, they must retain phase character upon photo-polymerization. Visual inspection of the 82/18 (w/w) **1016A/**glycerol polymerized film showed a slightly cloudy film, which should imply an imperfect Q_I phase was formed, because a Q_I-phase material would be optically clear and completely transparent. The XRD analysis inferred that the polymer retained its Q-phase structure upon polymerization, while bright PLM textures imply that the sample must be a mixed LLC phase, not a pure Q_I phase (see Figure 6.6). The

powder XRD profile exhibited two principal *d*-spacing peaks (a very pronounced first diffraction peak that indexes to $1/\sqrt{6}$, and a secondary, less intense peak/shoulder that indexes to $1/\sqrt{8}$), which were indicative of a Q-phase material.[53,54] A weak, very broad peak can also be seen in some of the spectra that corresponds to either the $1/\sqrt{20}$ or $1\sqrt{22}$ *d*-spacing peaks of a Q_I phase.[53,54] The possible $1/\sqrt{20}$ and $1\sqrt{22}$ peaks do not correspond to H or L phase powder XRD peaks. The bright PLM images show that the material has some defect regions that did not maintain the Q phase upon polymerization. When comparing the XRD profiles (see Figure 6.7) of **10** in glycerol with **1016A** in glycerol, it is apparent that there are significant shifts in the *d*-spacing values, which indicates different unit cell sizes.

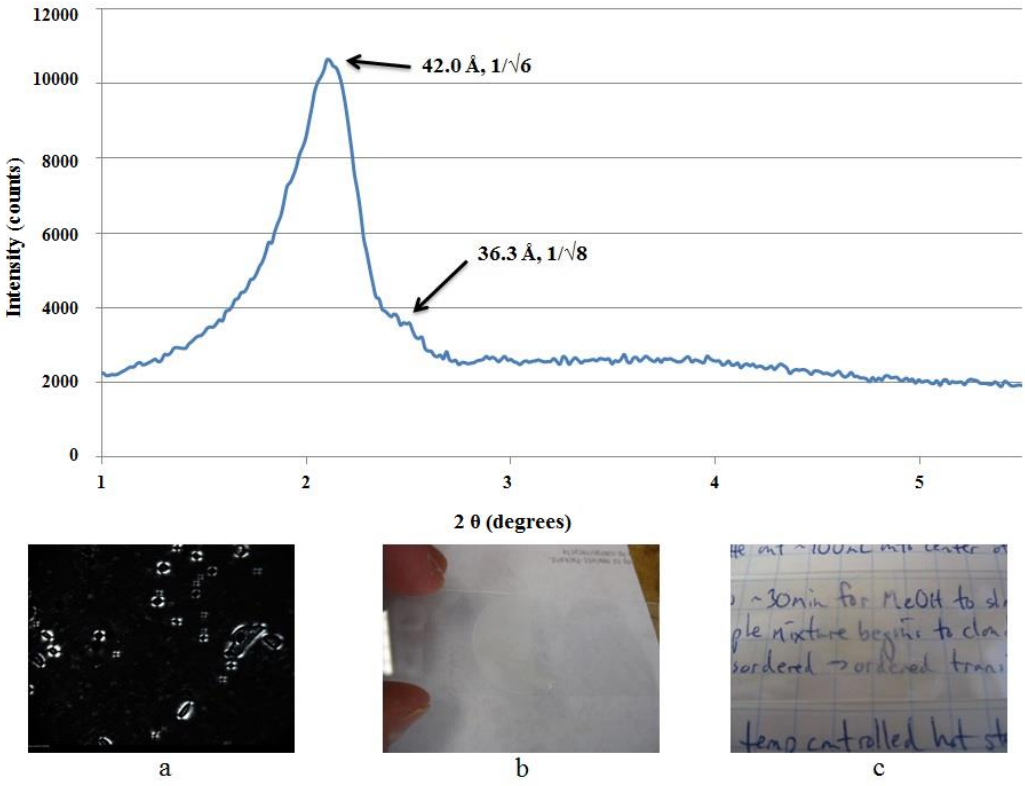

Figure 6.6. The powder XRD profile (top) shows the typical *d*-spacing peaks seen in a Q-phase material. The PLM image (a) shows bright characteristics that would indicate a phase other than bicontinuous cubic and visual inspection of the polymer films (b) and (c) shows a cloudy film that should be optically clear and transparent had a pure Q phase been present (mag = 50x).

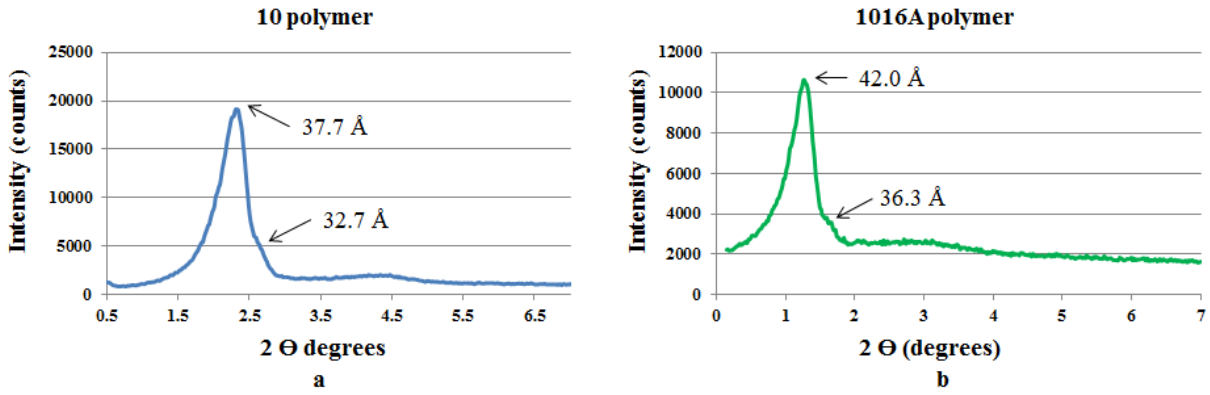

Figure 6.7. Powder XRD profiles of (a) a polymerized film of **10** and (b) a polymerized film of **1016A**. Profiles exhibit the dramatic differences in peaks indexing to $1/\sqrt{6}$ and $1/\sqrt{8}$ for each polymer film, indicating they have different unit cell sizes.

It was hypothesized that the reason the material did not appropriately retain its original LLC prior to photo-initiated radical cross-linking was that early on in the polymerization, discreet aggregates may have formed that did not form a Q_I phase. This aggregate formation could be enough to pull the material out of its bulk alignment and the resulting film would not be a Q_I-phase material. In order to overcome this situation, we attempted to polymerize the material in a more facile manner, hoping that by speeding up the polymerization, the formation of these aggregates would be minimal, and polymer formation would dominate. Addition of photo-initiator (2-hydroxy-2-methylpropiophenone) was utilized to increase the rate of polymerization. Sample was not analyzed by powder XRD, only PLM as an initial, cursory scan for phase retention. Figure 6.8 below shows PLM images of the bulk material that was black and inferred a Q_I phase was present, and the photo-cured sample, which had bright textures and did not exhibit a Q_I phase. This was seen as evidence that more care needs to be taken when polymerizing these samples.

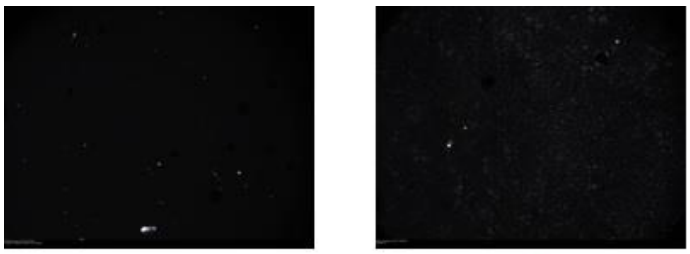

Figure 6.8. PLM images of bulk sample (a) and photo-initiated, polymerized sample (b) (mag = 50x). The bulk sample is completely black, indicating a cubic phase exists, whereas the polymerized sample has bright textures, indicating the loss of Q_I-phase architecture in the polymer film.

Because the polymerization using 1 wt% of photo-initiator apparently failed to stabilize the Q_I-phase that was seen in the bulk state of this material under ambient conditions, it was hypothesized that there could be some oxygen inhibition happening, leading to slower polymerization rates. Therefore, the same **1016A**/glycerol/photo-initiator composition was prepared, and systematically polymerized under an air-free, Ar-rich environment as described above. Prior to polymerization, a small aliquot was retained so that the bulk material properties could be compared to those of the polymerized thin-film sample. Figure 6.9 shows PLM images of the bulk, unpolymerized sample, as well as the polymerized film. The bulk sample was free of defects, optically transparent and elevated temperatures, and completely black under PLM. The photopolymerized film was mostly black under PLM, but showed numerous defect sites where birefringence was evident. This material, even when polymerized in an air-free environment, did not hold its bulk LLC architecture.

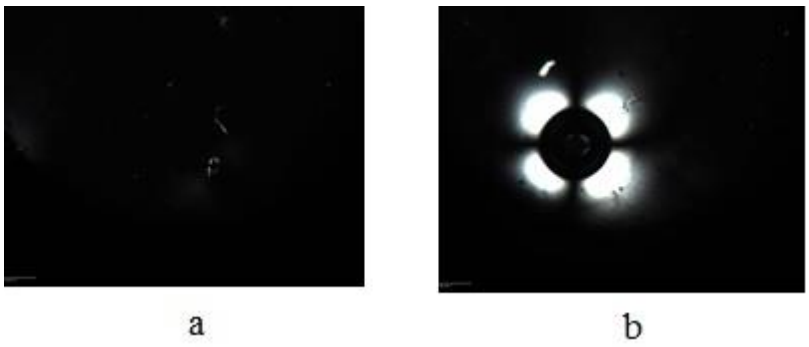

Figure 6.9. PLM images for (a) bulk, unpolymerized sample of air-free specimen, and (b) air-free polymerized film (mag = 50x). The bright regimes in PLM (b) appear to be defects. The majority of the sample was black. Because there were multiple defect sites, sample was not adequate to attempt membrane fabrication.

It appears that, though a Q-phase material can be isolated in the bulk state for the aforementioned monomer blends with **10**, three different attempts to stabilize this Q phase were all unsuccessful. Typically, O_2-rich polymerization conditions yielded a polymer film that was bright under PLM (indicating an optically anisotropic LLC phase instead of a Q phase), while a similarly prepared bulk sample was completely black. Utilization of 2-hydroxy-2-methylpropiophenone (i.e., a radical photo-initiator) for another attempted polymerization generated a polymer film that was also bright under PLM. The final air-free, $Ar_{(g)}$-rich polymerization attempt yielded a polymer film that was mostly black under PLM, while showing numerous areas of stress spots, whose edges appeared birefringent. In order to polymerize and "lock-in" a Q phase of this blended monomer material, more care must be taken, possibly using quickly initiating photo-initiators. These monomer blend systems were seen as possibly too chemically dissimilar to achieve the high initial 1,3-diene conversion needed to stabilize a Q-phase material. The next aim of this research was to study LLC monomer systems that were more chemically similar, in hopes that stabilization of any observed Q phase could be achieved in a more facile manner.

6.3.3. Analysis of gemini-gemini blend results

Two different monomer blends were analyzed for this work. The first, which exhibited a number of potential Q phases in glycerol, were blends involving **10** and **11**, while the other incorporated monomer **12** into monomer **10** in varying ratios and appeared to show less robust Q phases as determined by PLM observation (see Figure 6.4). By blending in monomer additives more similar to **10** but with different spacer groups in the charged region, this new gemini monomer-gemini monomer blend should provide the chemical compatibility not seen in the work discussed above, which should allow for the ability to stabilize any observed Q phases. These spacer changes in the headgroup will affect the change density of the pore walls in our nanoporous water desalination membranes. This effective change in charge density should have some effect on either (a) the size of the nanoporous regions of these materials or (b) the charge-charge repulsive interactions between these membranes and the inorganic solutes that are tested. The blended LLC monomer samples that exhibited potential Q-phase behavior via PLM analysis were blends of monomer **10** and **11** at compositions of 95 wt% : 5 wt%, 90 wt% : 10 wt%, and 85 wt% : 15 wt% respectively, as well as a blend of monomer **10** with **12** at 95 wt% : 5 wt%. Due to the large chemical similarity between **10** and **11**, these blends were analyzed initially, with particular attention paid to the 95/5 and 90/10 (w/w) **10**/**11** blends.

6.3.4. PLM analysis of 1011B blend

Preparation of the blended LLC mixture was performed via the CH_2Cl_2 dissolution method described above. Samples were prepared for PLM analysis as described above, and observed at weight percentages of **10**/**11** blend : glycerol starting at 97.5 wt% : 2.5 wt%, decreasing the wt%

of **1011B** blend by 2.5 wt%. Every specimen that contained between 97.5 wt% and 70 wt% **1011B** was analyzed by PLM. Some representative PLM images can be seen in Figure 6.10. By analyzing these PLM images, it can be ascertained that no Q phase lies at any of the **1011B** : glycerol compositions examined. All of the samples appeared bright under PLM over the entire analyzed temperature range from RT to 85 °C. The best explanations for this observation is that it is possible that a Q phase does in fact exist in this region, but the composition window is far too narrow (i.e., >2 wt%) to be isolated, or that the penetration scans of this blend were not representative of how this material behaves.

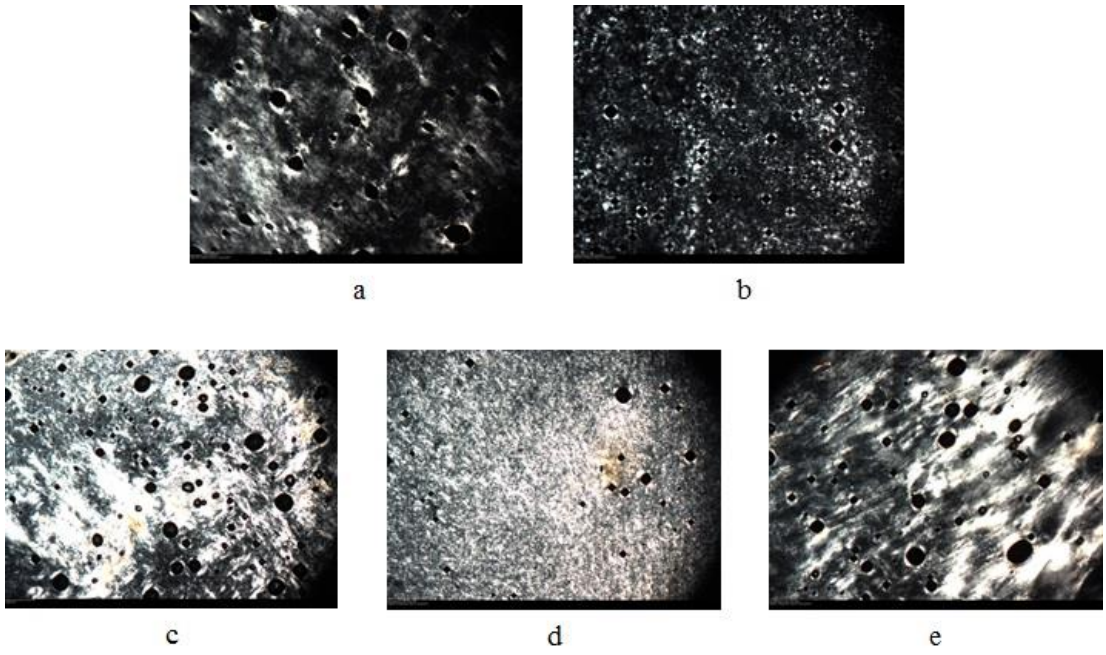

Figure 6.10. PLM images (mag = 50x) for 75/25 (w/w) sample at 75 °C (a), 80/20 (w/w) sample at 85 °C (b), 87.5/12.5 (w/w) sample at 45 °C (c). 82.5/17/5 (w/w) sample at 45 °C (d), and 90/10 (w/w) sample at 53 °C (e).

6.4. Conclusions

In this chapter, the design and use of amphiphilic monomer blends were explored for their ability to form Q_I LLC phases with potentially different pore sizes in glycerol over a given range of temperatures. Monomer **10** was chosen as the base Q_I-phase-forming monomer, and small percentages of both gemini and single-tailed surfactant monomers were doped into **10** to create a range of blended LLC monomer systems. It was observed that of the thirteen LLC monomer blends generated, six showed good potential to exhibit a Q phase in glycerol. The most promising included gemini monomer blends of **10** and **11** based on their inherent chemical compatibility, as well as blends of gemini monomer **10** and single-tailed monomer **16**. A full phase diagram of the blend **1016A** was completed, and it was found to exhibit a Q phase in the bulk state between 80 and 83 wt% monomer blend in glycerol. However, numerous attempts to photo-cross-link and trap the observed Q_I phase as a MeOH-cast thin film failed. We hypothesize that upon initiation of the added photo-initiator, small discreet, non-Q-phase aggregates of the monomers formed. Those aggregates preferred not to form the Q phase seen earlier in the bulk state, causing the system to relax back into an anisotropic LLC phase. More care, such as the use of a faster initiating cross-linking agent, will need to be taken with this material to generate a thin-film polymer. Monomer blends have also been generated utilizing gemini monomers **10** and **11**. Initial penetration scans of these materials showed potential Q phases at an array of composition intervals, however, full phase diagram characterization showed no Q phase was present, suggesting that the composition window for **1011B** in glycerol may be too narrow to identify in a reproducible fashion. More monomer blends are currently being analyzed at this time.

6.5. References

1. Gin, D. L.; Noble, R. D. *Science* **2011**, *332*, 674.

2. Tsuru, T. *J. Sol-Gel Sci. Technol*. **2008**, *46*, 349.

3. Schoenning, A. P. H. J.; Gonzalez-Lemus, Y. C.; Shishmanova, I. K.; Broer, D. J. *Liq. Cryst.* **2011**, *38*, 1627.

4. Jeon, G.; Yang, S. Y.; Kim, J. K. *J. Mater. Chem*. **2012**, *22*, 14814.

5. Martin, C. R. *Chem. Mater*. **1996**, *8*, 1739.

6. Pak, C.; Kang, S.; Suk, Y.; Chang, H. *J. Mater. Res*. **2010**, *25*, 2063.

7. Gawenda, M.; Sperschneider, A.; Schacher, F.; Krausch, G.; Müller, A.; Ulbricht, M. *Desalination* **2006**, *200*, 29.

8. Gin, D. L.; Bara, J. E.; Noble, R. D.; Elliott, B. J. *Macromol. Rapid Commun*. **2008**, *29*, 367.

9. Kim, S.; Chen, L.; Johnson, J. K.; Marand, E. *J. Mem. Sci*. **2007**, *294*, 147.

10. Hinds, B. J.; Chopra, N.; Rantell, T.; Andrews, R.; Gavalas, V.; Bachas, L. G. *Science* **2004**, *303*, 62.

11. Akthakul, A.; Salinaro, R. F.; Mayes, A. M. *Macromolecules* **2004**, *37*, 7663.

12. Xu, T.; Zhao, N.; Ren, F.; Hourani, R.; Lee, M. T.; Shu, J. Y.; Mao, S.; Helms, B. A. *ACS Nano* **2011**, *5*, 1376.

13. Yan, X.; Janout, V.; Hsu, J. T.; Regen, S. L. *J. Am. Chem. Soc*. **2002**, *124*, 10962.

14. Czaplewski, K. F.; Hupp, J. T.; Snurr, R. Q. *Adv. Mater*. **2001**, *13*, 1895.

15. Beginn, U.; Zipp, G.; Mourran, A.; Walther, P.; Möller, M. *Adv. Mater*. **2000**, *12*, 513.

16. Henmi, M.; Nakatsuji, K.; Ichikawa, T.; Tomioka, H.; Sakamoto, T.; Yoshio, M.; Kato, T. *Adv. Mater*. **2012**, *24*, 3338.

17. Jeong, B. H.; Hoek, E. M. V.; Yan, Y.; Subramani, A.; Huang, X.; Hurwitz, G.; Ghosh, A. K.; Jawor A. *J. Mem. Sci*. **2007**, *294*, 1.

18. Bae, T. H.; Lee, J. S.; Qiu, W.; Koros, W. J.; Jones, C. W.; Nair, S. *Angew. Chem. Int. Ed*. **2010**, *49*, 9863.

19. Bowen, T. C.; Noble, R. D.; Falconer, J. L. *J. Mem. Sci*. **2004**, *245*, 1.

20. Perez, E. V.; Balkus, Jr., K. J.; Ferraris, J. P.; Musselman, I. H. *J. Mem. Sci*. **2009**, *328*, 165.

21. Wolf, J. H.; Hillmyer, M. A. *Langmuir* **2003**, *19*, 6553.

22. Yang, S. Y.; Ryu, I.; Kim, H. Y.; Kim, J. K.; Jang, S. K.; Russell, T. P. *Adv. Mater*. **2006**, *18*, 709.

23. Jirage, K. B.; Hulteen, J. C.; Martin, C. R. *Science* **1997**, *278*, 655.

24. Liu, G.; Ding, J. *Adv. Mater*. **1998**, *10*, 69.

25. Lin, C. C. H.; Sawada, J. A.; Wu, L.; Haastrup, T.; Kuznicki, S. M. *J. Am. Chem. Soc*. **2009**, *131*, 609.

26. Wu, Q. L.; Subramanian, N.; Strzalka, J.; Jiang, Z.; Rankin, S. E. *Thin Solid Films* **2012**, *520*, 3558.

27. Li, X. Y.; Chen, L. H.; Li, Y.; Rooke, J. C.; Deng, Z.; Hu, Z. Y.; Liu, J.; Krief, A.; Yang, X. Y.; Su, B. L. *Micropor. and Mesopor. Mater.* **2012**, *152*, 110.

28. Lehoux, A.; Ramos, L.; Beaunier, P.; Uribe, D. B.; Dieudonné, P; Audonnet, F.; Etchberry, A.; Yacaman, M. J.; Remita, H. *Adv. Funct. Mater*. **2012**, *22*, 4900.

29. Chen, W.; Wu, J. S.; Xia, X. H. *ACS Nano* **2008**, *2*, 959.

30. Wang, J.; Gong, G.; Kanezashi, M.; Yoshioka, T.; Ito, K.; Tsuru, T. *Chem. Lett*. **2012**, *41*, 1663.

31. Chen, Y.; Chu, C.; Zhou, Y.; Ru, Y.; Chen, H.; Chen, F.; He, Q.; Zhang, Y.; Zhang, L.; Shi, J. *Small* **2011**, *7*, 2935.

32. Cabrera, S.; Haskouri, J. E.; Alamo, J.; Beltrán, A.; Beltrán, D.; Mendioroz, S.; Marcos, M. D., Amorós, P. *Adv. Mater*. **1999**, *11*, 379.

33. Telleria, I. A.; Requies, J.; Güemuz, M. B.; Arias, P. L. *Appl. Catal. B: Environ.* **2012**, *115-116*, 169.

34. Li, F.; Li, L.; Liao, X.; Wang, Y. *J. Mem. Sci*. **2011**, *385-386*, 1.

35. Xie, J.; Wang, X.; Deng, J.; Zhang, L. *Appl. Surf. Sci.* **2005**, *250*, 152.

36. Rouholamin, D.; Smith, P. J.; Ghassemieh, E. *J. Mater. Sci*. **2013**, *48*, 3254.

37. Kozak, D.; Anderson, W.; Trau, M. *Chem. Lett*. **2012**, *41*, 1134.

38. Liu, J.; Teo, W. K.; Chew, C. H.; Gan, L. M. *J. of Appl. Polym. Sci.* **2000**, *77*, 2785.

39. Li, T. D.; Gam, L. M.; Chew, C. H.; Teo, W. K.; Gan, L. H. *Langmuir* **1996**, *12*, 5863.

40. Nagarjuna, G.; Baghgar, M.; Labastide, J. A.; Algaier, D. D.; Barnes, M. D.; Venkataraman, D. *ACS Nano* **2012**, *6*, 10750.

41. Adrus, N.; Ulbricht, M. *J. Mem. Chem*. **2012**, *22*, 3088.

42. Zhao, Q.; Sun, J.; Ling, Q.; Zhou, Q. *Langmuir* **2009**, *25*, 3249.

43. Mariani, P.; Rustichelli, F.; Saturni, L.; Cordone, L. *Eur. Biophys. J*. **1999**, *28*, 294.

44. Han, S. H.; Kwon, H. J.; Kim, K. Y.; Seong, J. G.; Park, C. H.; Kim, S.; Doherty, C. M.; Thornton, A. W.; Hill, A. J.; Lozano, E.; Berchtold, K. A.; Lee, Y. M. *Phys. Chem. Chem. Phys*. **2012**, *14*, 4365.

45. Sanderson, P. W.; Lis, L. J.; Quinn, P. J.; Williams, W. P. *Biochim. Biophys. Acta* **1991**, *1067*, 43.

46. Vargas, R.; Mateu, L.; Romero, A. *Chem. Phys. Lipids* **2004**, *127*, 103.

47. Koynova, R.; Brankov, J.; Tenchov, B. *Eur. Biophys. J*. **1997**, *25*, 261.

48. Czeslik, C.; Winter, R.; Rapp, G.; Bartels, K. *Biophys. J.* **1995**, *68*, 1423.

49. Carter, B. M.; Wiesenauer, B. R.; Hatakeyama, E. S.; Barton, J. L.; Noble, R. D.; Gin, D. L. *Chem. Mater*. **2012**, *24*, 4005.

50. Hatakeyama, E. S.; Gabriel, C. J.; Wiesenauer, B. R.; Lohr, J. L.; Zhou, M.; Noble, R. D.; Gin, D. L. *J. Mem. Sci.* **2011**, *366*, 62.

51. Hatakeyama, E. S.; Wiesenauer, B. R.; Gabriel, C. J., Noble, R. D.; Gin, D. L. *Chem. Mater*. **2010**, *22*, 4525.

52. Tiddy, G. J. T. *Phys. Rep*. **1980**, *57*, 1.

53. Fontell, K. *Colloid Polym. Sci.* **1990**, *268*, 264.

54. Mariani, P.; Luzzati, V.; Delacroix, H. *J. Mol. Biol.* **1988**, *204*, 165.

CHAPTER 7

Conclusions and recommendations for future work

7.1. Overview of objectives

The overall objective of this thesis research project was the design and synthesis of new type I bicontinuous cubic- (Q_I) phase-forming, gemini-shaped lyotropic liquid crystal (LLC) monomers for the preparation of nanoporous polymer membrane materials. The goal was to design new Q_I-phase LLC monomers that overcome several shortcomings of previously developed Q-phase LLC monomers in the Gin research group, which include expensive and difficult synthesis, poor film processibility, and limited blendability with additives. Two separate applications have been examined to gauge how well they perform as molecular-size separation materials compared to existing Q_I LLC monomers.

One specific application of this research was the design of breathable barrier materials that overcome the disadvantages of the 1st-generation, gemini phosphonium-based Q_I monomer system devised in the Gin research lab in 2003. The goal was to (a) make the monomer system more easily produced and cost-effective, (b) provide the resulting polymerized material with the kind of tactility required for performing delicate chemical decontamination work, and (c) design a LLC/polymer blend that would afford a garment material that will allow the wearer to keep cool in humid, hot conditions while selectively rejecting toxic organic vapors. In general, using a nanoporous material to realize these goals is ideal in that it would allow good water vapor transport and simultaneously size-exclude larger organic contaminant molecules.

The second application-based goal of this thesis work was to design new nanoporous polymer membranes with uniform sub-1-nm pores for water nanofiltration applications. Current commercial water filtration membranes suffer from a series of issues, including requiring high pressures for performing filtration, containing a wide distribution of pore sizes, and low pore density. Development of a nanoporous polymeric membrane material with uniform, molecular-size pores would provide advantages over current water purification membranes. In this same vein, it would be desirable to be able to tune the size of the nanopores in these polymeric water nanofiltration membranes. The use of LLC monomer/monomer blends to change the curvature at the interface between the LLC monomer and solvent was an obvious starting point to explore research in this area.

7.2. Development of a new nanoporous, breathable protective garment material that selectively rejects toxic chemical vapors

7.2.1. Conclusions

For this research study, two new LLC monomers based on the gemini ammonium framework were designed, mixed with water, and blended with varying amounts of the commercially radically cross-linkable elastomer, v-EPDM. These LLC monomer/v-EPDM blends were analyzed via polarized light microscopy (PLM) to determine their ability to form LLC phases. A phase diagram of each monomer/water/v-EPDM blend was generated at 22 ± 1 °C and ambient pressure. From these results, a blend of **4a**/water/v-EPDM was investigated for its ability to form infused, supported polymer membranes. The resulting supported polymer membrane was tested for water vapor transport and toxic organic chemical vapor rejection, both at varying relative humidity (R.H.) conditions. It was observed that the **4a**/water/v-EPDM

composite polymer exhibited exceptionally high water vapor flux, while acting as an excellent toxic organic chemical vapor barrier material. However, permeability results are restricted from public disclosure or open publication because of ITAR restrictions stipulated in the Department of Defense grant that funded this work.

7.2.2. Recommendations for future work

Future studies in the area of nanoporous polymer membranes for breathable protective garments should focus on blends involving v-EPDM and any of the new gemini imidazolium monomers synthesized and discussed previously in this thesis work (monomers **10–15**). With the acquired knowledge that these monomers can form Q LLC phases in the presence of glycerol, it would be possible to generate thin-film composite (TFC) membranes via a solution-casting method, using **10–15** as the base monomers, so long as it is possible to find a high volatility organic solvent that can dissolve both the LLC/glycerol mixture and EPDM. This solution-casting method may be able to assist in homogenizing the LLC/glycerol/v-EPDM blends, thus reducing the need for the laborious hand-mixing steps currently required for generating blended samples.

If it were possible to eventually fabricate a TFC polymer membrane from these materials, this method would also improve the pure water vapor flux. A thinner membrane separating layer provides less resistance to flow of vapors passing through the membrane. Therefore, it would be possible to pass more water vapor out of the garment, thus making it a more effective chemical contaminant remediation device, so long as it still exhibits high rejection toward the chemical compounds of interest.

7.3. Design and synthesis of new Q_I-phase forming lyotropic liquid crystal monomers for deployment as water nanofiltration membranes

7.3.1. Conclusions

This second applications-based topic of research brought about several new monomer designs to our gemini LLC monomer platform.[1,2] The goal was to design new Q_I-phase forming LLC monomers that could be synthesized in a more facile and cost-effective fashion than the previous gemini phosphonium motif previously developed in the Gin research lab. It was also envisioned that one of these new monomer platforms would be able to form a bicontinuous cubic LLC phase in non-aqueous solvents, thus allowing for thin-film processing to be employed. Finally, it was hypothesized that by utilizing blends of these new LLC monomers, it might be possible to systematically tune or vary the size of the nanopores in the resulting cross-linked Q_I phases.

The first research aim in this area was to synthesize new LLC monomers based on a gemini ammonium headgroup platform. These monomers, which have headgroup units derived from commercially-available tertiary diamine starting materials dramatically reduced the cost of producing monomers, compared to the 1st-generation phosphonium-based materials. The reduction in cost allows for scale-up that is more amenable to industrial needs[1]. Likewise, no synthesis is involved in generating the phosphonium headgroups. By finding headgroup units that can be purchased and do not need to be synthesized, numerous synthesis and purification steps were reduced from the original 1st-generation monomer synthesis. These omitted steps were previously very expensive and involved a pyrophoric bis(phosphine) intermediate, whose presence dramatically limits the capability of these materials to be produced on a larger scale.

When evaluating the performance of polymeric materials derived by these gemini ammonium monomers, it was observed that the resulting Q_I membranes exhibited a slightly larger effective pore size than the 1st-generation phosphonium system, while having higher pure water flux values. This 2nd-generation Q_I monomer system was found to be also capable of forming melt-infused, robust polymers supported on Solupor®, a micropoous ultra-high molecular weight polyethylene fiber matte support, but no true commercial membrane fabrication techniques could be employed with this system. It was for this reason, that we devised a new LLC monomer platform, a 3rd-generation design based off of a gemini imidazolium headgroup system.[2]

Six new gemini imidazolium-based monomers were developed and synthesized, and their ability to form LLC phases in a variety of non-aqueous solvents was analyzed. PLM penetration scans (a visual screening technique to evaluate materials for potential Q and other LLC phases), determined that of the six new monomers of interest, only two formed potential Q phases in some of the non-aqueous solvents studied. The monomer chosen for further analysis was **10** because it exhibited Q_I phase formation with glycerol, formamide, and ethylammonium nitrate. A full ternary phase diagram for monomer **10**/water/glycerol was elucidated at 22 ± 1 °C and ambient pressure (620 mm Hg), and it was observed that the monomer formed a Q_I phase in pure glycerol, pure water, and a wide range of glycerol/water mixtures. For the purposes of TFC membrane fabrication, pure glycerol was determined to be the best solvent, because with its high normal b.p. (ca. 290 °C) and very low vapor pressure (≤20 mtorr) at ambient conditions, evaporative loss of solvent from a formed Q_I phase should be minimal upon processing and heating compared to water. Glycerol is also a water-soluble, inexpensive, and non-toxic natural product, making it ideal for processing and water-based filtration applications. Because glycerol

was used as the phase-forming solvent in place of water, a solution-cast method was devised where the **10**/glycerol gel was cast as a 60 wt% solution in MeOH onto a ultraporous poly(ether sulfone) support. Consequent UV irradiation in the presence of a radical photo-initiator generated a robust, cross-linked Q_I-phase TFC membrane with glycerol in the nanopores. Subsequent soaking of flushing of the resulting TFC membrane with pure glycerol afforded a cross-linked Q_I membrane with water-filled pores.

Analysis of this new TFC Q_I membrane showed the imidazolium-based material exhibited a slightly larger effective pore size when subjected filtering uncharged molecular solutes compared to both the 1st-generation and 2nd-generation Q_I LLC monomer systems. However, the new TFC Q_I membrane made from **10** showed pure water fluxes that were significantly higher than either of the previous systems due to its significantly thinner active layer film as part of the TFC membrane configuration. This material also exhibited exceptionally and surprisingly high inorganic salt rejection values. This collection of properties makes this new nanoporous Q_I polymer material unique for filtration applications, exhibiting neutral rejections better than commercial water nanofiltration (NF) membranes and salt rejections comparable to commercial reverse osmosis (RO) membranes.

One final aim of the research on water nanofiltration membranes performed in this work was the use of LLC monomer blends to explore potential tuning of the pore size of the polymeric matrix, for the purposes of performing specific separations. Thirteen different monomer/monomer blends using gemini imidazolium monomer **10** were prepared and analyzed. It was observed that six of these blends formed potential Q_I phases via the penetration scan technique. Of these six potential candidates, blends **1011B** and **1016A** were analyzed in greatest detail. A full phase diagram for **1016A** was elucidated at 22 ± 1 °C and ambient pressure (620

mm Hg), and a potential Q_I phase was observed in the bulk state between 83 wt% and 80 wt% of the monomer blend. However, subsequent attempts to UV photo-cross-link the Q_I phase of **1016A** in glycerol all failed. Some phase change/disruption was observed during polymerization in all cases.

7.3.2. Recommendations for future work

7.3.2.1. Future work toward systematic control of effective pore size

Future studies in this area should be focused on two distinct topics. The first topic should be the ability to systematically tune the size of nanopores in our Q_I LLC polymer water nanofiltration membranes. The second is the synthesis of gemini imidazolium LLC monomers that are more cost-effective and significantly more straight-forward to produce on a larger scale.

The first topic will be confronted from several different directions. The LLC monomer/monomer blend **1016A** previously described exhibited a Q_I phase nanostructure with a significant change in unit cell spacing based on powder X-ray diffraction analysis. However, subsequent attempts to polymerize a thin film that locked in that Q-phase architecture failed. It was hypothesized that upon initial polymerization, the gemini and single-tailed LLC monomers formed discreet aggregates, and the energy minimum for these aggregates leads to a relaxation out of that Q phase morphology. The addition of small amounts (>1 %) of additional step-growth cross-linking agent, such as a multi-functional thiol moiety, may help to stabilize the observed Q phase that was observed for this monomer/monomer blend. Small amounts of the external cross-linking agent are required because of the sensitivity of the composition of this Q phase. Any small change to the overall composition of the LLC mixture can significantly affect the phase of the material when the composition window is narrower than 5 wt%. Previously in

the Gin research group, a number of cross-linking agents have been employed in the fabrication of dense, thin-film materials,[3,4] but using these agents in the polymerization of nanoporous membranes has not been examined.

Thiol-ene radical step-growth polymerization chemistry is well-established[5-7], and the use of multi-functional thiol cross-linking agents has good precedent in the literature for use with polymers that have residual alkene moieties.[8] The ability to incorporate thiol-ene cross-linkers with our nanoporous Q phase LLC materials would be a novel application, and it has the potential capability to stabilize any sensitive Q phases that we discover (see Figure 7.1). This technology should be employed for use in our **1016A** LLC monomer/monomer to lock in the sensitive architecture. This may then give us the ability to systematically tune the size of the pores in nanoporous LLC-based Q-phase membranes.

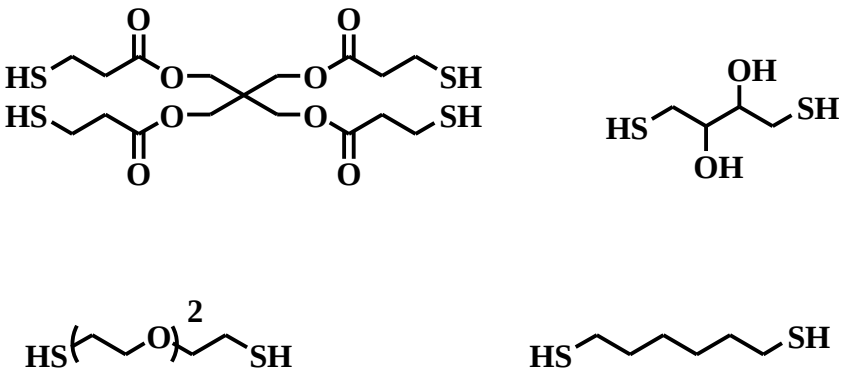

Figure 7.1. Structure of some possible thiol-functionalized cross-linking agents that may be able to help stabilize the Q LLC phase that is exhibited by **1016A**.

Another avenue that requires exploration to aid in tuning the pore size of nanoporous Q_I phases is the utilization of other monomer blends. It has been proven that a host of non-charged amphiphiles form Q LLC phases with water.[9] Most of these amphiphiles are comprised of an oligo(ethylene) glycol hydrophilic headgroup unit, with a normal long-chain alkyl tail as the

hydrophobic unit. Based on the surprisingly high rejections of inorganic salts observed under water nanofiltration conditions, as compared to the effective pore size of the TFC Q phase LLC membrane of **10**,[2] it was hypothesized that the charge density in the nanopores has a direct correlation to charged salt rejection. We also propose that small changes in the charge density of the pores may have an impact on neutral solute rejections. We plan on investigating this by synthesizing polymerizable, non-charged single-tailed LLC monomers, and generating blends by incorporating them into the base monomer **10** system in a systematic fashion (structures can be seen in Figure 7.2).

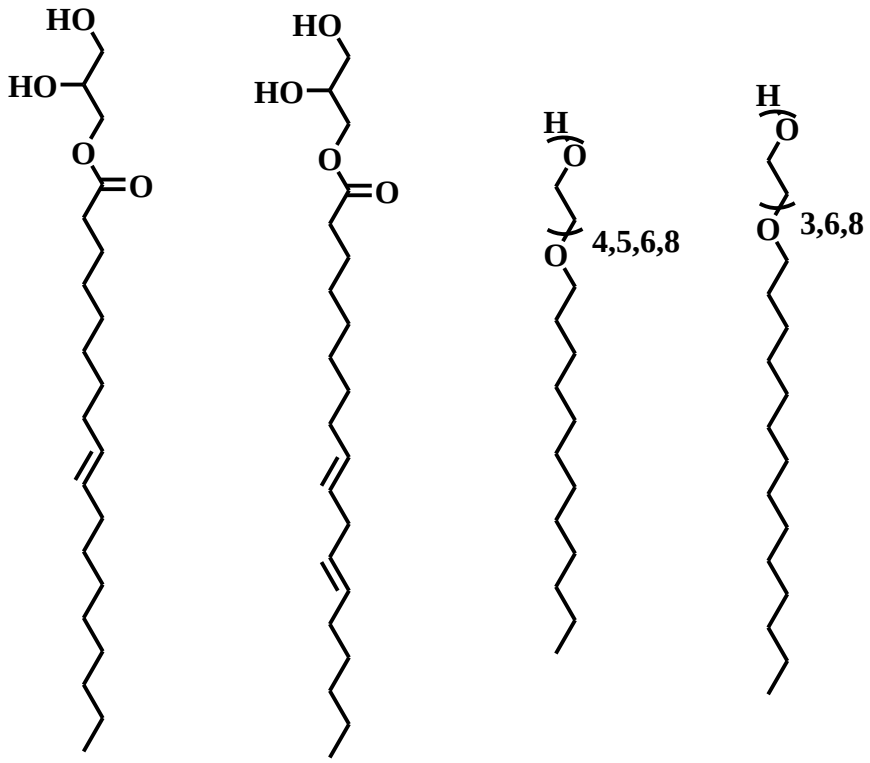

Figure 7.2. Structures of some non-charged amphiphiles that form Q LLC phases with water. From left to right: monoelaidin, monolinolein, and various amphilphiles with oligo(ethylene glycol) moieties.

The synthesis of derivatives of the above non-charged amphiphiles will follow a similar route to that used to synthesize the single-tailed imidazolium-based LLC monomers described in

Chapter 6. The headgroup materials, tetra(ethylene glycol) monomethyl ether and tri(ethylene glycol) monomethyl ether, are commercially available through a number of sources, and the synthesis of the diene tails is well-established in the literature.[2,3] The synthetic challenge then lies in linking these diene tails, to the oligo(ethylene glycol) headgroup units, but should be able to be completed through a standard Williamson ether synthesis reaction utilizing sodium hydride. The primary targets for this work are shown below in Figure 7.3.

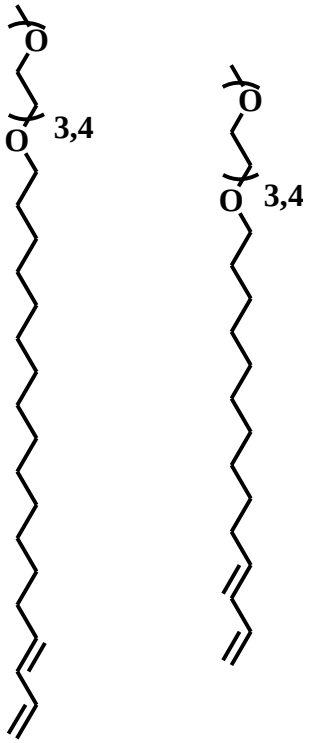

Figure 7.3. Structure of the initial polymerizable targets for generating non-charged amphiphiles that can blend with monomer **10** and form potential Q phases with water or glycerol. Terminal diene cross-linkable groups could be replaced by acrylate or methacrylate groups as well.

One more monomer blending study that should be investigated is the use of gemini imidazolium monomers with odd-numbered methylene carbon spacers in the headgroup to help affect the shape and packing relationships between monomer systems. A change in shape anisotropy would be expected when changing the monomer shape from a straight configuration

(i.e., having an even number of methylene carbons as a spacer in the headgroup) to a more bent configuration (i.e., having an odd number of methylene carbons as a spacer in the headgroup) These new bent-configuration monomer systems may be forced into different geometries than those with even-numbered methylene carbon spacer units, which would have an effect on how monomer blends containing small amounts of these monomers would order. Similar effects have been observed in thermotropic liquid crystal systems[10] but never for lyotropic liquid crystal systems to the best of our knowledge.

Another direction that can be taken with this research is the utilization of atomic layer deposition (ALD) to help vary and tune the size of the pores in our nanoporous water desalination membranes. ALD technology enables the functionalization of interior surfaces of nanoporous materials and pore size engineering at the atomic level by manipulating gas phase reactivity to deposit molecules onto the surface of a given material.[11] This method has already been used to decrease the pore size in a **3b**/H_2O polymer membrane, such that this material exhibits a five-fold improvement of H_2/N_2 selectivity in gas separation experiments.[12] This technique made it possible to reduce the effective pore size from 0.75 nm to <0.55 nm through the deposition of alumina particles. However, this type of effective pore size control has only been realized for gas separation applications using a melt-infused gemini phosphonium-based LLC membrane. It will need to be adapted to be compatible with (1) the new imidazolium-based Q_I-phase LLC polymer nanostructure, (2) glycerol, which is now being used as the phase-forming LLC solvent, and (3) the new supported TFC membrane architecture. ALD presents a unique procedure to dramatically decrease the pore sizes in our water nanofiltration membranes, and could allow for specific molecular-size separations to be achieved.

The final area of possible future work for systematic reduction of pore size is the utilization of solvent additives in order to increase or decrease the LLC interaction with glycerol at the solvent interface. Solutions of glycerol will be prepared with varying amounts of dopants such as inorganic salts (i.e., $MgSO_4$ and KCl), acids (i.e., HBr), oligo(ethylene glycol) derivatives (i.e., di(ethylene glycol), tri(ethylene glycol) and tetra(ethylene glycol)) and sugars (i.e., sucrose and glucose). The ability to use salts,[13] pH changes[14] and sugars[15-16] to affect pore size in nanoporous LLC systems is well-documented. By using small amounts of any of these dopants, it is should be possible to increase or decrease the effective pore size of our water filtration membranes. Systematic efforts will be taken to begin at a small amount (i.e., 5 wt%) of each dopant dissolved in glycerol and increase incrementally, visualizing LLC **10** by PLM penetration scans to examine whether potential Q phases exist. When Q phases are found, the goal would be to polymerize a TFC membrane of that material, then perform water filtration experiments with neutral solutes on the polymerized membranes. An effective pore size can be extrapolated from these experiments, and the effect of each dopant can then be qualified and generalized. This method would make it possible to deduce which dopant increases or decreases effective pore size, as well as to determine which direction the effective pore size moves with variances in the amount of the dopant used.

7.3.2.2. Future work toward synthesis of more cost-effective and scalable LLC monomer systems

One area of research that has already seen some progress is the synthesis of more cost-effective and easily produced LLC monomer systems centered around polymerizable acrylate- and methacrylate-based hydrophobic regions. Acrylate-based polymerizable tails have

previously been used in the Gin research group in the synthesis of **8**,[17] and it has been shown that this wedge-shaped LLC can form a Q_I phase with water. However, acrylate-based monomers systems utilizing the gemini platform have not been realized until now. Synthesis of the acrylate and methacrylate tails was completed by the common acid-catalyzed esterification protocol.[18] As of this writing, twelve different acrylate monomers and eight different methacrylate monomers were synthesized and their purity has been verified by nuclear magnetic resonance, infrared spectroscopy, and high-resolution mass spectrometry (Figure 7.4).

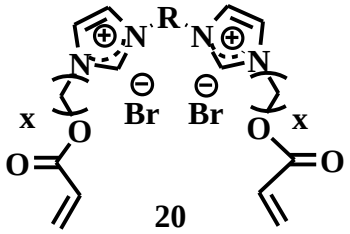

20

a : R = $(CH_2)_4$ x = $(CH_2)_{11}$ g : R = $(CH_2)_8$ x = $(CH_2)_{11}$
b : R = $(CH_2)_4$ x = $(CH_2)_{12}$ h : R = $(CH_2)_8$ x = $(CH_2)_{12}$
c : R = $(CH_2)_4$ x = $(CH_2)_{15}$ i : R = $(CH_2)_8$ x = $(CH_2)_{15}$
d : R = $(CH_2)_6$ x = $(CH_2)_{11}$ j : R = $(CH_2)_2O(CH_2)_2$ x = $(CH_2)_{11}$
e : R = $(CH_2)_6$ x = $(CH_2)_{12}$ k : R = $(CH_2)_2O(CH_2)_2$ x = $(CH_2)_{12}$
f : R = $(CH_2)_6$ x = $(CH_2)_{15}$ l : R = $(CH_2)_2O(CH_2)_2$ x = $(CH_2)_{15}$

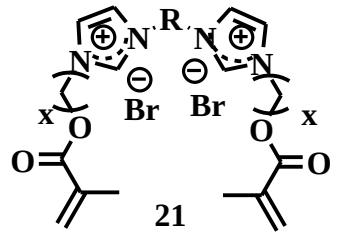

21

a : R = $(CH_2)_4$ x = $(CH_2)_{11}$ e : R = $(CH_2)_8$ x = $(CH_2)_{11}$
b : R = $(CH_2)_4$ x = $(CH_2)_{15}$ f : R = $(CH_2)_8$ x = $(CH_2)_{15}$
c : R = $(CH_2)_6$ x = $(CH_2)_{11}$ g : R = $(CH_2)_2O(CH_2)_2$ x = $(CH_2)_{11}$
d : R = $(CH_2)_6$ x = $(CH_2)_{15}$ h : R = $(CH_2)_2O(CH_2)_2$ x = $(CH_2)_{15}$

Figure 7.4. Structures of new acrylate- and methacrylate-derived LLC monomers synthesized thus far. All acrylate-based monomers have been analyzed by PLM penetration scans. All methacrylate-based monomers are still pending analysis.

PLM penetration scans have been performed for all of the acrylate-derived LLC monomers shown in Figure 7.5 and five of these have shown potential Q phases with glycerol. Table 7.1 details which of these monomers exhibited a potential Q phase with glycerol, and representative PLM images can be seen in Figure 7.5. At this time, no full phase diagrams have been elucidated for any of these acrylate or methacrylate gemini imidazolium LLC monomers, and no thin-film polymer membrane fabrication has been attempted. Also, only two of the methacrylate monomers have been analyzed via PLM penetration scan (**21g** and **21h**), neither of which showed a potential Q phase in glycerol. Future work for this project will include full phase diagram analysis for each acrylate monomer that exhibits a potential Q phase via penetration scan with glycerol, as well as PLM penetration scan observations of all derivatives of monomer **21**. This work should be fully finished within 4 months.

Table 7.1. List of acrylate-based polymerizable monomers synthesized and their potential to form Q phases with glycerol.

Monomer	20a	20b	20c	20d	20e	20f	20g	20h	20i	20j	20k	20l
Potential Q with glycerol	Yes	Yes	Yes	No	Yes	Yes	No	No	No	No	No	No

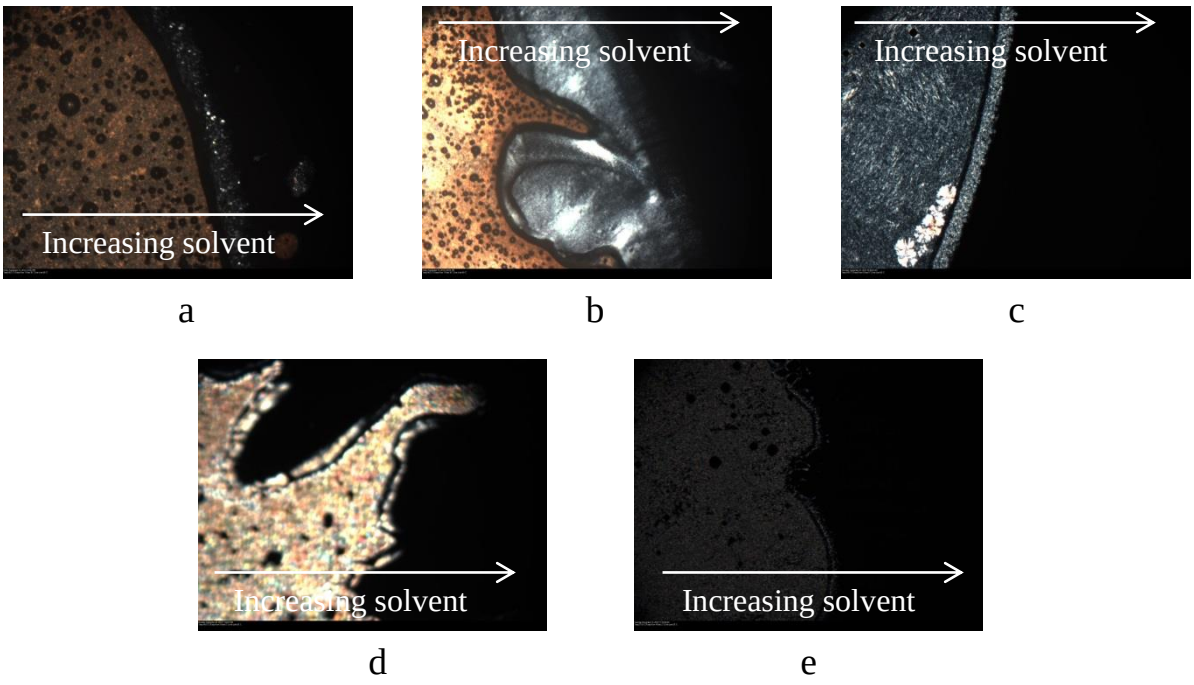

Figure 7.5. Representative PLM images of the acrylate-based monomers that appeared to exhibit a potential Q phase with glycerol. PLM penetration scan of **20a** at 75 °C (a). PLM penetration scan of **20b** at 80 °C (b). PLM penetration scan of **20c** at 64 °C (c). PLM penetration scan of **20e** at 49 °C (d). PLM penetration scan of **20f** at 52 °C (e).

7.4. References

1. Hatakeyama, E. S., Wiesenauer, B. R., Gabriel, C. J., Noble, R. D.; Gin, D. L. *Chem. Mater.* **2010**, *22*, 4525.

2. Carter, B. M.; Wiesenauer, B. R.; Hatakeyama, E. S.; Barton, J. L.; Noble, R. D.; Gin, D. L. *Chem. Mater*. **2012**, *24*, 4005.

3. Hatakeyama, E. S.; Ju, H.; Gabriel, C. J.; Lohr, J. L.; Bara, J. E.; Noble, R. D.; Freeman, B. D.; Gin, D. L. *J. Mem. Sci*. **2009**, *330*, 104.

4. Carlisle, T. K.; Nicodemus, G. D.; Gin, D. L.; Noble, R. D. *J. Mem. Sci*. **2012**, *397*, 24.

5. Hoyle, C. E.; Bowman, C. N. *Angew. Chem. Int. Ed*. **2010**, *49*, 1540.

6. Hoyle, C. E.; Lowe, A. B.; Bowman, C. N. *Chem. Soc. Rev*. **2010**, *39*, 1355.

7. Cramer, N. B.; Couch, C. L.; Schreck, K. M.; Carioscia, J. A.; Boulden, J. E.; Stansbury, J. W.; Bowman, C. N. *Dental Mater.* **2010**, *26*, 21.

8. Fairbanks, B. D.; Schwartz, M. P.; Halevi, A. E.; Nuttleman, C. R.; Bowman, C. N.; Anseth, K. S. A. *Adv. Mater*. **2009**, *21*, 5005.

9. Fontell, K. *Colloid Polym. Sci.* **1990**, *268*. 264.

10. Lalanne, J. R.; Lemaire, B.; Rouch, J.; Vaucamps, C.; Proutiere, A. *J. Chem. Phys*. **1980**, *73*, 1927-1932.

11. Detavernier, C.; Dendooven, J.; Sree, S. P.; Ludwig, K. F.; Martens, J. A. *Chem. Soc. Rev*. **2011**, *40*, 5242.

12. Liang, X.; Lu, X.; Yu, M.; Cavanagh, A. S.; Gin, D. L.; Weimer, A. W. *J. Mem. Sci*. **2010**, *349*, 1.

13. Vargas, R.; Mateu, L.; Romero, A. Chemistry of Physics and Lipids 2004, 127, 103.

14. Koynova, R.; Brankov, J.; Tenchov, B.. Eur. Biophys. J. 1997, 25, 261.

15. Mariani, P.; Rustichelli, F.; Saturni, L.; Cordone, L. *Eur. Biophys. J*. **1999**, *28*, 294.

16. Kulkarni, C. V.; Wachter, W.; Iglesias-Salto, G.; Engelskirchen, S.; Ahualli, S. *Phys. Chem. Chem. Phys*. **2011**, *13*, 3004.

17. Kerr, R. L.; Miller, S. A.; Shoemaker, R. K.; Elliott, B. J.; Gin, D. L. *J. Am. Chem. Soc.* **2009**, *131*, 15972.

18. Lal, J.; Green, R. *J. Org. Chem*. **1955**, *20*, 397.

BIBLIOGRAPHY

Abbott, N. J. *Coatings Technology Handbook, 2nd Ed*. Satas, D.; Tracton, A. A., Eds.; Marcel Dekker: New York, 2001; pp 819.

Abe, M.; Tsubone, K.; Koike, T.; Tsuchiya, K.; Ohkubo, T.; Sakai, H. Polymerizable cationic gemini surfactant. *Langmuir* **2006**, *22*, 8293.

Aimar, P.; Meireles, M.; Sanchez, V. A contribution to the translation of retention curves into pore size distributions for sieving membranes. *J. Mem. Sci.* **1990**, *54*, 321.

Akthakul, A.; Salinaro, R. F.; Mayes, A. M. Antifouling polymer membranes with subnanometer size selectivity. *Macromolecules* **2004**, *37*, 7663.

Anderson, D. M.; Ström, P. in *Polymer Association Structures*. El–Nokaly, M. A., Eds.; ACS Symposium Series 384; American Chemical Society: Washington, DC, 1989, pp 204–224.

Anderson, D. M.; Ström, P. Polymerized lyotropic liquid crystals as contact lens materials. *Physica A* **1991**, *176*, 151.

Adrus, N.; Ulbricht, M. Novel hydrogel pore-filled composite membranes with tunable and temperature-responsive size-selectivity. *J. Mem. Chem*. **2012**, *22*, 3088.

Auvray, X.; Perche, T.; Petipas, C.; Anthore, R. Influence of solvent-headgroup interactions on the formation of lyotropic liquid crystal phases of surfactants in water and nonaqueous protic and aprotic solvents *Langmuir* **1992**, *8*, 2671.

Bae, T. H.; Lee, J. S.; Qiu, W.; Koros, W. J.; Jones, C. W.; Nair, S. A high-performance gas-separation membrane containing submicrometer-sized metal-organic framework crystals. *Angew. Chem. Int. Ed*. **2010**, *49*, 9863.

Bara, J. E., Hatakeyama, E. S.; Wiesenauer, B. R.; Zeng, X.; Noble, R. D.; Gin, D. L. Thermotropic liquid crystal behavior of gemini imidazolium-based ionic amphiphiles. *Liq. Cryst.* **2010**, *37*, 1587.

Beginn, U.; Zipp, G.; Mourran, A.; Walther, P.; Möller, M. Membranes containing oriented supramolecular transport channels. *Adv. Mater*. **2000**, *12*, 513.

Bhattacharya, A.; Ghosh, P. Theory and application in separation of electrolytes. *Rev. Chem. Eng.* **2004**, *20*, 111.

Bhattacharyya, D.; Williams, M. E. "Reverse Osmosis: Design," In *Membrane Handbook*; Ho, W. S.; Sirkar, K. K.; Eds.; Kluwer Academic: Boston, 2001. 83.

Blanton, T. N.; Huang, T. C.; Toraya, H.; Hubbard, C. R.; Robie, S. B.; Louer, D.; Gobel, H. E.; Will, G.; Gilles, R.; Raftery, T. A possible low-angle X-ray diffraction calibration standard. *Powder Diffr.* **1995**, *10*, 91.

Bowen, T. C.; Noble, R. D.; Falconer, J. L. Fundamentals and applications of pervaporation through zeolite membranes. *J. Mem. Sci*. **2004**, *245*, 1.

Bowen, W. R.; Mohammad, A. W.; Hilal, N. Characterisation of nanofiltration membranes for predictive purposes - use of salts, uncharged solutes and atomic force microscopy. *J. Mem. Sci.* **1997**, *126*, 91.

Budinski, K. G.; Budinski, M.; K. *Engineering Materials: Properties and Selection*, 7th ed.; Prentice Hall: Englewood Cliffs, 2002; pp 752.

Cabrera, S.; Haskouri, J. E.; Alamo, J.; Beltrán, A.; Beltrán, D.; Mendioroz, S.; Marcos, M. D., Amorós, P. Surfactant-assisted synthesis of mesoporous alumina showing continuously adjustable pore sizes. *Adv. Mater*. **1999**, *11*, 379.

Caillier, L.; Taffin de Given, E.; Levy, R.; Vandenberghe, Y.; Geribaldi, S.; Guittard, F. Polymerizable semi-fluorinated gemini surfactants designed for antimicrobial materials. *J. Colloid Interfac. Sci.* **2009**, *332*, 201.

Carlisle, T. K.; Nicodemus, G. D.; Gin, D. L.; Noble, R. D. CO_2/light gas separation performance of cross-linked poly(vinylimidazolium) gel membranes as a function of ionic liquid loading and cross-linker content. *J. Mem. Sci*. **2012**, *397*, 24.

Carter, B. M.; Wiesenauer, B. R.; Hatakeyama, E. S.; Barton, J. L.; Noble, R. D.; Gin, D. L. Glycerol-based bicontinuous cubic lyotropic liquid crystal monomer system for the fabrication of thin-film membranes with uniform nanopores. *Chem. Mater*. **2012**, *24*, 4005.

Chen, L., Phillip, W. A., Cussler, E. L.; Hillmyer, M. A. Robust nanoporous membranes templated by a doubly reactive block copolymer. *J. Am. Chem. Soc.* **2007**, *129*, 13786.

Chen, W.; Wu, J. S.; Xia, X. H. Porous anodic alumina with continuously manipulated pore-cell size. *ACS Nano* **2008**, *2*, 959.

Chen, Y.; Chu, C.; Zhou, Y.; Ru, Y.; Chen, H.; Chen, F.; He, Q.; Zhang, Y.; Zhang, L.; Shi, J. Reversible pore-structure evolution in hollow silica nanocapsules: Large pores for siRNA delivery and nanoparticle collecting. *Small* **2011**, *7*, 2935.

Clapper, J. D.; Guymon, C. A. Physical behavior of cross-linked PEG hydrogels photopolymerized within nanostructured lyotropic liquid crystalline templates. *Macromolecules* **2007**, *40*, 1101.

Cramer, N. B.; Couch, C. L.; Schreck, K. M.; Carioscia, J. A.; Boulden, J. E.; Stansbury, J. W.; Bowman, C. N. Investigation of thiol-ene and thiol-ene-methacrylate based resins as dental restorative materials. *Dental Materials* **2010**, *26*, 21.

Czaplewski, K. F.; Hupp, J. T.; Snurr, R. Q. Molecular squares as molecules sieves: Size-selective transport through porous-membrane-supported thin-film materials. *Adv. Mater*. **2001**, *13*, 1895.

Czeslik, C.; Winter, R.; Rapp, G.; Bartels, K. Temperature- and pressure-dependent phase behavior of monoacylglycerides monoolein and monoelaidin. *Biophysical Journal* **1995**, *68*, 1423.

DePierro, M. A., Carpenter, K. G.; Guymon, C. A. Influence of polymerization conditions on nanostructure and properties of polyacrylamide hydrogels templated from lyotropic liquid crystals. *Chem. Mater.* **2006**, *18*, 5609.

Detavernier, C.; Dendooven, J.; Sree, S. P.; Ludwig, K. F.; Martens, J. A. Tailoring nanoporous materials by atomic layer deposition. *Chem. Soc. Rev*. **2011**, *40*, 5242.

Elliott, B. J. Nanoporous composites of polymerized lyotropic liquid-crystalline monomers and hydrophobic polymers *US Patent 7090788*, **2006**.

Fairbanks, B. D.; Schwartz, M. P.; Halevi, A. E.; Nuttleman, C. R.; Bowman, C. N.; Anseth, K. S. A versatile synthetic extracellular matrix mimic via thiol-norbornene photopolymerization. *Adv. Mater*. **2009**, *21*, 5005.

Fell, C. J. D. "Reverse Osmosis," in *Membrane Separations Technology. Principles and Applications*; Noble, R. D.; Stern, A. S.; Eds.; Elsevier Science: Amsterdam, 1995; Chapter 4.

Ferry, J. D. Ultrafilter membranes and ultrafiltration. *Chem. Rev.* **1936**, *18*, 373.

Fontell, K. Cubic phases in surfactant and surfactant-like lipid systems. *Colloid Polym. Sci.* **1990**, *268*, 264.

Forney, B. S.; Guymon, C. A. Fast deswelling kinetics of nanostructured poly(N-isopropylacrylamide) photopolymerized in lyotropic liquid crystal templates. *Macromol. Rapid Commun.* **2011**, *32*, 765.

Fuller, S.; Shinde, N. N.; Tiddy, G. J. T.; Attard, G. S.; Howell, O. Thermotropic and lyotropic mesophase behavior of amphitropic diammonium surfactants. *Langmuir* **1996**, *12*, 1117.

Gawenda, M.; Sperschneider, A.; Schacher, F.; Krausch, G.; Müller, A.; Ulbricht, M. Toward nanoporous composite membranes with tailored block copolymers as selective layer. *Desalination* **2006**, *200*, 29.

Geens, J.; Boussu, K.; Vandecasteele, C.; Van der Bruggen, B. Modelling of solute transport in non-aqueous nanofiltration. *J. Mem. Sci.* **2006**, *281*, 139.

Gibbins, E.; D' Antonio, M.; Nair, D.; White, L. S.; Freitas dos Santos, L. M.; Vankelecom, I. F. J.; Livingston, A. G. Observations on solvent flux and solute rejection across solvent resistant nanofiltration membranes. *Desalination* **2002**, *147*, 307.

Gin, D. L.; Bara, J. E.; Noble, R. D.; Elliott, B. J. Polymerized lyotropic liquid crystal assemblies for membrane applications. *Macromol. Rapid Commun.* **2008**, *29*, 367.

Gin, D. L., Gu, W., Pindzola, B. P.; Zhou, W. J. Polymerized lyotropic liquid crystal assemblies for materials applications. *Acc. Chem. Res.* **2001**, *34*, 973.

Gin, D. L., Lu, X., Nemade, P. R., Pecinovsky, C. S., Xu, Y.; Zhou, M. Recent advances in the design of polymerizable lyotropic liquid crystal assemblies for heterogeneous catalysis and selective separations. *Adv. Funct. Mater.* **2006**, *16*, 865.

Gin, D. L.; Noble, R. D. Designing the next generation of chemical separation membranes *Science* **2011**, *332*, 674.

Gin, D. L., Pecinovsky, C. S., Bara, J. E.; Kerr, R. L. Functional lyotropic liquid crystal materials. *Struct. Bonding* **2008**, *128*, 181.

Gin, D. L.; Zhou, M.; Noble, R. D.; Bara, J. E.; Wiesenauer, B. R.; Kerr, R. L. U.S. Patent 20090173693, issued July 9, 2009.

Greaves, T. L.; Drummond, C. J. Ionic liquids as amphiphile self-assembly media. *Chem. Soc. Rev.* **2008**, *37*, 1709.

Greaves, T. L; Weerawardena, A.; Fong, C.; Krodkiewska, I.; Drummond, C. J. Protic ionic liquids: Solvents with tunable phase behavior and physicochemical properties. *J. Phys. Chem. B.* **2006**, *110*, 22479.

Han, S. H.; Kwon, H. J.; Kim, K. Y.; Seong, J. G.; Park, C. H.; Kim, S.; Doherty, C. M.; Thornton, A. W.; Hill, A. J.; Lozano, E.; Berchtold, K. A.; Lee, Y. M. Tuning microcavities in thermally rearranged polymer membranes for CO_2 capture. *Phys. Chem. Chem. Phys*. **2012**, *14*, 4365.

Hartmann, P. C.; Sanderson, R. S. Templating polymerization of dodecylammonium surfactants with polymerizable (meth)acrylate counter ions. *Macromol. Symp.* **2005**, *225*, 229.

Hatakeyama, E. S., Gabriel, C. J., Wiesenauer, B. R., Lohr, J. L., Zhou, M., Noble, R. D.; Gin, D. L. Water filtration performance of a lyotropic liquid crystal polymer membrane with uniform, sub-1-nm pores. *J. Mem. Sci.* **2011**, *366*, 62.

Hatakeyama, E. S.; Ju, H.; Gabriel, C. J.; Lohr, J. L.; Bara, J. E.; Noble, R. D.; Freeman, B. D.; Gin, D. L. New protein-resistant coatings for water filtration membranes based on quaternary ammonium and phosphonium polymers. *J. Mem. Sci*. **2009**, *330*, 104.

Hatakeyama, E. S., Wiesenauer, B. R., Gabriel, C. J., Noble, R. D.; Gin, D. L. Nanoporous, bicontinuous cubic lyotropic liquid crystal networks via polymerizable gemini ammonium surfactants. *Chem. Mater*. **2010**, *22*, 4525.

Henmi, M.; Nakatsuji, K; Ichikawa, T.; Tomioka, H.; Sakamoto, T.; Yoshio, M.; Kato, T. Self-organized liquid-crystalline nanostructured membranes for water treatment: Selective permeation of ions. *Adv. Mater*. **2012**, *24*, 2238.

Hentze, H. P.; Kaler, E. W. Polymerization of and within self-organized media. *Curr. Opin. Colloid Interface Sci.* **2003**, *8*, 164.

Hinds, B. J.; Chopra, N.; Rantell, T.; Andrews, R.; Gavalas, V.;; Bachas, L. G. Aligned multiwalled carbon nanotube membranes. *Science* **2004**, *303*, 62.

Hoag, B. P.; Gin, D. L. Cross-linkable liquid crystal monomers containing hydrocarbon 1,3-diene tail systems. *Macromolecules* **2000**, *33*, 8549.

Hoyle, C. E.; Bowman, C. N. Thiol-ene click chemistry. *Angew. Chem. Int. Ed*. **2010**, *49*, 1540.

Hoyle, C. E.; Lowe, A. B.; Bowman, C. N. Thiol-click chemistry: a multifaceted toolbox for small molecule and polymer synthesis. *Chem. Soc. Rev*. **2010**, *39*, 1355.

Ichikawa, T., Yoshio, M., Hamasaki, A., Kagimoto, J., Ohno, H.; Kato, T. 3D interconnected ionic nano-channels formed in polymer films: Self-organization and polymerization of thermotropic bicontinuous cubic liquid crystals. *J. Am. Chem. Soc.* **2011**, *133*, 2163.

Ichikawa, T.; Yoshio, M.; Hamasaki, A.; Mukai, T.; Ohno, H.; Kato, T. Self-organization of room-temperature ionic liquids exhibiting liquid-crystalline bicontinuous cubic phases: Formation of nano-ion channel networks. *J. Am. Chem. Soc.* **2007**, *129*, 10662.

In, M.; Zana, R. Phase behavior of gemini surfactants. *J. Dispersion Sci. Techno.* **2007**, *28*, 143.

Israelachvili, J. N. *Intermolecular and Surface Forces* Academic Press: Boston, 1992; p. 291.

Israelachvili, J. N., Mitchell, D. J.; Ninham, B. W. Theory of self-assembly of hydrocarbon amphiphiles into micelles and bilayers. *J. Chem. Soc. Faraday Trans. II* **1975**, *72*, 1525.

Jeon, G.; Yang, S. Y.; Kim, J. K. Functional nanoporous membranes for drug delivery. *J. Mater. Chem*. **2012**, *22*, 14814.

Jeong, B. H.; Hoek, E. M. V.; Yan, Y.; Subramani, A.; Huang, X.; Hurwitz, G.; Ghosh, A. K.; Jawor A. Interfacial polymerization of thin film nanocomposites: A new concept of reverse osmosis membranes. *J. Mem. Sci*. **2007**, *294*, 1.

Jeong, S. W.; O'Brien, D. F. Encapsulation and diffusion of water-soluble dendrimers in a bicontinuous cubic phase. *Langmuir* **2002**, *18*, 1073.

Jin, J.; Nguyen, V.; Gu, W.; Lu, X.; Elliott, B. J.; Gin, D. L. Cross-linked lyotropic liquid crystal-butyl rubber composites: Promising "breathable" barrier materials for chemical protection applications. *Chem Mater*. **2005**, *17*, 224.

Jirage, K. B.; Hulteen, J. C.; Martin, C. R. Nanotubule-based molecular-filtration membranes. *Science* **1997**, *278*, 655.

Kato, T. From nanostructured liquid crystals to polymer-based electrolytes. *Angew. Chem. Int. Ed.* **2010**, *49*, 7847.

Kerr, R. L., Miller, S. A., Shoemaker, R. K., Elliott, B. J.; Gin, D. L. New type of Li ion conductor with 3D-interconnected nanochannels via polymerization of a liquid organic electrolyte-filled lyotropic liquid-crystal assembly. *J. Am. Chem. Soc.* **2009**, *131*, 15972.

Kim, S.; Chen, L.; Johnson, J. K.; Marand, E. Polysulfone and functionalized carbon nanotube mixed matrix membranes for gas separation: Theory and experiment. *J. Mem. Sci*. **2007**, *294*, 147.

Kosutic, K.; Furac, L.; Sipos, L.; Kunst, B. Removal of arsenic and pesticides from drinking water by nanofiltration membranes. *Sep. Purif. Technol.* **2004**, *42*, 137.

Koynova, R.; Brankov, J.; Tenchov, B. Modulation of lipid phase behavior by kosmotropic and chaotropic solutes. *Eur. Biophys. J*. **1997**, *25*, 261.

Kozak, D.; Anderson, W.; Trau, M. Tuning particle velocity and measurement sensitivity by changing pore sensor dimensions. *Chem. Lett*. **2012**, *41*, 1134.

Kresge, E.; Wang, H.C. *Kirk-Othmer Encyclopedia of Chemical Technology, 4th Ed*. Wiley: New York, 1993; p. 934.

Kulkarni, C. V.; Wachter, W.; Iglesias-Salto, G.; Engelskirchen, S.; Ahualli, S. Monoolein: A magic lipid? *Phys. Chem. Chem. Phys*. **2011**, *13*, 3004.

Lal, J.; Green, R. The preparation of the cyclopentyl esters of acrylic, methacrylic, and crotonic acids. *J. Org. Chem*. **1955**, *20*, 397.

Lalanne, J. R.; Lemaire, B.; Rouch, J.; Vaucamps, C.; Proutiere, A. The even-odd effect in liquid crystals: A collective or intrinsic molecular property. *J. Chem. Phys*. **1980**, *73*, 1927-1932.

Lee, Y. S., Yang, J. Z., Sisson, T. M., Frankel, D. A., Gleeson, J. T., Aksay, E., Keller, S. L., Gruner, S. M.; O'Brien, D. F. Polymerization of nonlamellar lipid assemblies. *J. Am. Chem. Soc.* **1995**, *117*, 5573.

Lehoux, A.; Ramos, L.; Beaunier, P.; Uribe, D. B.; Dieudonné, P; Audonnet, F.; Etchberry, A.; Yacaman, M. J.; Remita, H. Tuning the porosity of bimetallic nanostructures by a soft templating approach. *Adv. Funct. Mater*. **2012**, *22*, 4900.

Lester, C. L, Smith, S. M.; Guymon, C. A. Acceleration of polyacrylamide photopolymerization using lyotropic liquid crystals. *Macromolecules* **2001**, *34*, 8587.

Lester, C. L., Smith, S. M., Jarrett, W. L.; Guymon, C. A. Effects of monomer organization on the photopolymerization kinetics of acrylamide in lyotropic liquid crystalline phases. *Langmuir* **2003**, *19*, 9466.

Li, F.; Li, L.; Liao, X.; Wang, Y. Precise pore size tuning and surface modifications of polymeric membranes using the atomic layer deposition technique. *J. Mem. Sci*. **2011**, *385-386*, 1.

Li, T. D.; Gam, L. M.; Chew, C. H., Teo, W. K.; Gan, L. H. Preparation of ultrafiltration membranes by direct microemulsion polymerization using polymerizable surfactants. *Langmuir* **1996**, *12*, 5863.

Li, X. Y.; Chen, L. H.; Li, Y.; Rooke, J. C.; Deng, Z.; Hu, Z. Y.; Liu, J.; Krief, A.; Yang, X. Y.; Su, B. L. Tuning the structure of a hierarchically porous ZrO_2 for dye molecule depollution. *Micropor. Mesopor. Mater.* **2012**, *152*, 110.

Liang, X.; Lu, X.; Yu, M.; Cavanagh, A. S.; Gin, D. L.; Weimer, A. W. Modification of nanoporous supported lyotropic liquid crystal polymer membranes by atomic layer deposition. J. Membr. Sci. 2010, 349, 1.

Lin, C. C. H.; Sawada, J. A.; Wu, L.; Haastrup, T.; Kuznicki, S. M. Anion-controlled pore size of titanium silicate molecular sieves. *J. Am. Chem. Soc*. **2009**, *131*, 609.

Liu, G.; Ding, J. Diblock thin films with densely hexagonally packed nanochannels. *Adv. Mater.* **1998**, *10*, 69.

Liu, S.; O'Brien, D. F. Cross-linking polymerization in two-dimensional assemblies: Effect of the reactive group site. *Macromolecules* **1999**, *32*, 5519.

Liu, S., Sisson, T. M.; O'Brien, D. F. Synthesis and polymerization of heterobifunctional amphiphiles to cross-link supramolecular assemblies. *Macromolecules* **2001**, *34*, 465.

Liu, J.; Teo, W. K.; Chew, C. H.; Gan, L. M. Nanofiltration membranes prepared by direct microemulsion copolymerization using poly(ethylene oxide) macromonomer as a polymerizable surfactant. *J. Appl. Polym. Sci.* **2000**, *77*, 2785.

Lu, X., Nguyen, V., Zeng, X., Elliott, B. J.; Gin, D. L. Selective rejection of a water-soluble nerve agent simulant using a nanoporous lyotropic liquid crystal–butyl rubber vapor barrier material: Evidence for a molecular size-discrimination mechanism. *J. Mem. Sci.* **2008**, *318*, 397.

Lu, X., Nguyen, V., Zhou, M., Zeng, X., Jin, J., Elliott, B. J.; Gin, D. L. Cross-linked bicontinuous cubic lyotropic liquid crystal–butyl rubber composites: Highly selective, breathable barrier materials for chemical agent protection. *Adv. Mater*. **2006**, *18*, 3294.

Mariana, P., Luzzati, V.; Delacroix, H. Cubic phases in lipid-containing systems: Structure analysis and biological implications. *J. Mol. Biol.* **1988**, *204*, 165.

Mariani, P.; Rustichelli, F.; Saturni, L.; Cordone, L. Stabilization of the monoolein *Pn*3*m* cubic structure on trehalose glasses. *Eur. Biophys. J*. **1999**, *28*, 294.

Martin, C. R. Membrane-based synthesis of nanomaterials. *Chem. Mater*. **1996**, *8*, 1739.

Meng, Y.; Gu, D.; Zhang, F.; Shi, Y.; Yang, H.; Li, Z.; Tu, B.; Zhao, D. Ordered mesoporous polymers and homologous carbon frameworks: Amphiphilic surfactant templating and direct transformation. *Angew. Chem. Int. Ed.* **2005**, *44*, 7053.

Menger, F. M.; Keiper, J. S. Gemini surfactants. *Angew. Chem. Int. Ed.* **2000**, *39*, 1906.

Miller, S. A., Ding, J. H.; Gin, D. L. Nanostructured materials based on polymerizable amphiphiles. *Curr. Opin. Colloid Interface Sci*. **1999**, *4*, 338.

Mueller, A.; O'Brien, D. F. Supramolecular materials via polymerization of mesophases of hydrated amphiphiles. *Chem. Rev.* **2002**, *102*, 727.

Nagano, H. *Exxon Butyl Rubber Compounding and Applications*, Exxon Chemical Japan Polymers Technical Center, Yokohama, Japan, 2001.

Nagarjuna, G.; Baghgar, M.; Labastide, J. A.; Algaier, D. D.; Barnes, M. D.; Venkataraman, D. Tuning aggregation of poly(3-hexylthiophene) within nanoparticles. *ACS Nano* **2012**, *6*, 10750.

Ndoni, S., Vigild, M. E.; Berg, R. H. Nanoporous materials with spherical and gyroid cavities created by quantitative etching of polydimethylsiloxane in polystyrenepolydimethylsiloxane block copolymers. *J. Am. Chem. Soc.* **2003**, *125*, 13366.

Nightingale, Jr., E. R. Phenomenological theory of ion solvation. Effective radii of hydrated ions. *J. Phys. Chem.* **1959**, *63*, 1381.

O'Brien, D. F., Armitage, B., Benedicto, A., Bennett, D. E., Lamparski, H. G., Lee, Y.- S., Srisiri, W.; Sisson, T. M. Polymerization of preformed self-organized assemblies. *Acc. Chem. Res.* **1998**, *31*, 861.

Pak, C.; Kang, S.; Suk, Y.; Chang, H. Nanomaterials and structures for the fourth innovation of polymer electrolyte fuel cell. *J. Mater. Res.* **2010**, *25*, 2063.

Perez, E. V.; Balkus, Jr., K. J.; Ferraris, J. P.; Musselman, I. H. Mixed-matrix membranes containing MOF-5 for gas separation. *J. Mem. Sci*. **2009**, *328*, 165.

Petersen, R. J. Composite reverse osmosis and nanofiltration membranes. *J. Mem. Sci.* **1993**, *83*, 81.

Pindzola, B. A., Jin, J.; Gin, D. L. Cross-linked normal hexagonal and bicontinuous cubic assemblies via polymerizable gemini amphiphiles. *J. Am. Chem. Soc.* **2003**, *125*, 2940.

Pindzola, B. A.; Hoag, B. P.; Gin, D. L. Polymerization of a phosphonium diene amphiphile in the regular hexagonal phase with retention of mesostructure. *J. Am. Chem. Soc.* **2001**, *123*, 4617.

Rouholamin, D.; Smith, P. J.; Ghassemieh, E. Control of morphological properties of porous biodegradable scaffolds processed by supercritical CO_2 foaming. *J. Mater. Sci*. **2013**, *48*, 3254.

Sanderson, P. W.; Lis, L. J.; Quinn, P. J.; Williams, W. P. The Hofmeister effect in relation to membrane lipid phase stability. *Biochim. Biophys. Acta* **1991**, *1067*, 43.

Schoenning, A. P. H. J.; Gonzalez-Lemus, Y. C.; Shishmanova, I. K.; Broer, D. J. Nanoporous membranes based on liquid crystalline polymers. *Liq. Cryst.* **2011**, *38*, 1627.

Schreuder-Gibson, H. L., Truong, Q., Walker, J. E., Owens, J. R., Wander, J. D.; Jones, Jr. W. E. Chemical and biological protection and detection in fabrics for protective clothing. *Mater. Res. Soc. Bull.* **2003**, *28*, 574.

Seddon, J. M. Structure of the inverted hexagonal (HII) phase, and non–lamellar phase transitions of lipids. *Biochim. Biophys. Acta.* **1990**, *1031*, 1.

Shimura, H.; Yoshio, M.; Hoshino, K.; Mukai, Ohno, H.; Kato, T. Noncovalent approach to one-dimensional ion conductors: Enhancement of ionic conductivities in nanostructured columnar liquid crystals. *J. Am. Chem. Soc.* **2008**, *130*, 1759.

Sisson, T. M., Srisiri, W.; O'Brien, D. F. Novel polymer architectures via the selective polymerization of lyotropic liquid crystals of heterobifunctional amphiphiles. *J. Am.Chem. Soc.* **1998**, *120*, 2322.

Srisiri, W., Benedicto, A.; O'Brien, D. F. Stabilization of a bicontinuous cubic phase from polymerizable monoacylglycerol and diacylglycerol. *Langmuir* **1998**, *14*, 1921.

Srisiri, W., Lamparski, H. G.; O'Brien, D. F. Synthesis of polymerizable monoacylglycerols and 1,2-diacyl-sn-glycerols. *J. Org. Chem.* **1996**, *61*, 5911.

Talmage, S. S., Watson, A. P., Hauschild, V., Munro, N. B.; King, J. Chemical warfare agent degradation and decontamination. *Curr. Org. Chem.* **2007**, *11*, 285.

Tate, M. W., Eikenberry, E. F., Turner, D. C., Shyamsunder, E.; Gruner, S. M. Nonbilayer phases of membrane lipids. *Chem. Phys. Lipids*, **1991**, *57*, 147.

Telleria, I. A.; Requies, J.; Güemuz, M. B.; Arias, P. L. Pore size tuning of functionalized SBA-15 catalysts for the selective production of furfural from xylose. *Appl. Catal. B: Environmental* **2012**, *115-116*, 169.

Tiddy, G. J. T. Surfactant-water liquid crystal phases. *Phys. Rep.* **1980**, *57*, 1.

Tsuru, T. Nano-subnano-tuning of porous ceramic membranes for molecular separation. *J. Sol-Gel Sci. Technol*. **2008**, *46*, 349.

Urbas, A. M.; Maldovan, M.; DeRege, P.; Thomas, E. L. Bicontinuous cubic block copolymer photonic crystals. *Adv. Mater.* **2002**, *14*, 1850.

Wang, J.; Gong, G.; Kanezashi, M.; Yoshioka, T.; Ito, K.; Tsuru, T. Pore-size tuning of highly selective organic-inorganic hybrid silica membranes by solid-phase post-treatment at low temperature. *Chem. Lett*. **2012**, *41*, 1663.

Wartell, M. A.; Kleinman, M. T.; Huey, B. H.; Duffy, L. M. *Strategies to Protect the Health of Deployed U.S. forces: Force Protection and Decontamination*, National Academy Press: Washington, DC, **1999**; p. 67.

Wolf, J. H.; Hillmyer, M. A. Ordered nanoporous poly(cyclohexylethylene). *Langmuir* **2003**, *19*, 6553.

Wu, Q. L.; Subramanian, N.; Strzalka, J.; Jiang, Z.; Rankin, S. E. Tuning the mesopore structure of 3D hexagonal thin films using butanol as a co-solvent. *Thin Solid Films* **2012**, *520*, 3558.

Vargas, R.; Mateu, L.; Romero, A. The effect of increasing concentrations of precipitating salts used to crystallize proteins on the structure of the lipidic Q^{224} cubic phase. *Chem. Phys. Lipids* **2004**, *127*, 103.

Xie, J.; Wang, X.; Deng, J.; Zhang, L. Pore size control of pitch-based activated carbon fibers by pyrolytic deposition of propylene. *Appl. Surf. Sci.* **2005**, *250*, 152.

Xing, R.; Liu, N.; Liu, Y.; Wu, H.; Jiang, Y.; Chen, L.; He, M.; Wu, P. Novel solid acid catalysts: Sulfonic acid group-functionalized mesostructured polymers. *Adv. Funct. Mater.* **2007**, *17*, 2455.

Xu, T.; Zhao, N.; Ren, F.; Hourani, R.; Lee, M. T.; Shu, J. Y.; Mao, S.; Helms, B. A. Subnanometer porous thin films by the co-assembly of nanotube subunits and block copolymers. *ACS Nano* **2011**, *5*, 1376.

Yan, X.; Janout, V.; Hsu, J. T.; Regen, S. L. A polymerized calix[6]arene monolayer having gas permeation selectivity that exceeds Knudsen diffusion. *J. Am. Chem. Soc*. **2002**, *124*, 10962.

Yang, D., O'Brien, D. F.; Marder, S. R. Polymerized bicontinuous cubic nanoparticles (cubosome) from a reactive monoacylglycerol. *J. Am. Chem. Soc.* **2002**, *124*, 13388.

Yang, S. Y.; Ryu, I.; Kim, H. Y.; Kim, J. K.; Jang, S. K.; Russell, T. P. Nanoporous membranes with ultrahigh selectivity and flux for the filtration of viruses. *Adv. Mater.* **2006**, *18*, 709.

Zana, R. Dimeric (gemini) surfactants: Effect of the spacer group on the association behavior in aqueous solution. *J. Colloid Interface Sci.* **2002,** *228*, 203.

Zhang, F.; Meng, Y.; Gu, D.; Yan, Y.; Yu, C.; Tu, B.; Zhao, D. A facile aqueous route to synthesize highly ordered mesoporous polymers and carbon frameworks with *Ia*$\bar{3}$*d* bicontinuous cubic structure. *J. Am. Chem. Soc.* **2005**, *127*, 13508**.**

Zhao, Q.; Sun, J.; Ling, Q.; Zhou, Q. Synthesis of macroporous thermosensitive hydrogels: A novel method of controlling pore size. *Langmuir* **2009**, *25*, 3249.

Zhou, M.; Kidd, T. J.; Noble, R. D.; Gin. D. L. Supported lyotropic liquid-crystal polymer membranes: Promising materials for molecular-size-selective aqueous nanofiltration**.** *Adv. Mater.* **2005**, *17*, 1850.

Zhou, M., Nemade, P. R., Lu, X., Zeng, X., Hatakeyama, E. S., Noble, R. D.; Gin, D. L. New type of membrane material for water desalination based on a cross-linked bicontinuous cubic lyotropic liquid crystal assembly. *J. Am. Chem. Soc.* **2007**, *129*, 9574.